UNIVERSITÀ DEGLI STUDI DI TRIESTE

Università Ca'Foscari Venezia

UNIVERSITÀ DEGLI STUDI DI TRIESTE
e
UNIVERSITÀ CA' FOSCARI DI VENEZIA

XXXVII CICLO DEL DOTTORATO DI RICERCA IN CHIMICA

NEW PHOTO- AND NANOCATALYTIC SYSTEMS FOR APPLICATION IN ORGANIC SYNTHESIS

Settore scientifico-disciplinare: **CHIM/06**

DOTTORANDO / A
MARTINA MAMONE

COORDINATORE
PROF. ENZO ALESSIO

SUPERVISORE DI TESI
PROF. MAURIZIO PRATO

CO-SUPERVISORE DI TESI
DR. GIACOMO FILIPPINI

ANNO ACCADEMICO 2023/2024

Table of Contents

Abbreviations

0D	Zero-Dimensional
1D	One-Dimensional
2D	Two-Dimensional
3D	Tri-Dimensional
A	Acceptor
AFM	Atomic Force Microscopy
Arg	L-arginine
ATRA	Atom Transfer Radical Addition
BCA	Bicinchoninic acid
BDA	1,4-Diaminobutane
BET	Back-Electron Transfer
CA	Citric acid
CB	Conduction Band
CDs	Carbon Dots
NCDs	Amine-rich Carbon Dots
CNMs	Carbon NanoMaterials
CQDs	Carbon Quantum Dots
D	Donor
DA	Diamine
DBU	1,5-diazabiciclo(5.4.0)undec-7-ene
DIPEA	N,N-Diisopropylethylamine
DMF	N,N-dimethylformamide
DMSO	Dimethylsulfoxide
DOSY	Diffusion Ordered Spectroscopy
E	Electrophile
E_{00}	Excitation Energy
EA	Electron Affinity
ED	Electron Donor
EDA	Electron Donor-Acceptor
EDAm	Ethylenediamine
EDG	Electron-Donating Group
EWG	Electron-Withdrawing Group
FT-IR	Fourier Transform Infrared spectroscopy
HA	Protic Acid
HAS	Homolytic Aromatic Substitution
HAT	Hydrogen Atom Transfer
HDA	1,6-Diaminohexane
HFIP	Hexafluoroisopropanol
HOMO	Highest Occupied Molecular Orbital

HPLC	High performance Liquid Chromatography
HRMS	High-resolution mass spectra
KT	Kaiser Test
LEDs	Light Emitting Diodes
Lys	L-lysine
LUMO	Lowest Unoccupied Molecular Orbital
MeCN	Acetonitrile
MW	Microwave
NaAsc	Sodium Ascorbate
NMR	Nuclear Magnetic Resonance
Nu	Nucleophile
PC	Photocatalyst
p-CDs	Phenol-rich Carbon Dots
PET	Photoinduced Electron Transfer
QY	Quantum Yield
SET	Single Electron Transfer
SOMO	Singly Occupied Molecular Orbital
TEM	Transmission Electron Microscopy
TEMPO	2,2,6,6-tetramethylpiperidine-1-oxyl
TGA	Thermogravimetric Analysis
Tyr	L-tyrosine
TLC	Thin Layer Chromatography
TMG	1,1,3,3-tetramethylguanidine
UV	Ultraviolet
UV-Vis	Ultraviolet-Visible
VB	Valence Band
XAT	Halogen Atom Transfer
XPS	X-ray Photoelectron Spectroscopy

Abstract

This thesis investigates innovative photo- and nanocatalytic systems that enhance sustainability and efficiency in various organic transformations. In doing so, the synthesis of new nanomaterials and the development of effective catalytic methods were promptly achieved under mild conditions to match the requirements of more sustainable chemical synthesis.

Chapter 1 introduces the general concepts of catalysis, emphasizing its role in promoting green chemistry principles. It aims to describe the underlying theory and operative mechanisms of key polar and radical organic reactions, with a particular focus on the application of nanomaterials in photo- and organocatalysis.

Chapter 2 discusses the synthesis of nitrogen-doped carbon dots (NCDs) from L-arginine and alkyl diamines. This process demonstrates how the rational design of NCDs enhances their aminocatalytic performances in various enamine and iminium ion activated model reactions.

Chapter 3 introduces phenol-rich carbon dots (*p*-CDs), which serve as metal-free and recyclable photocatalysts. These nanoparticles effectively catalyse challenging photochemical reactions, such as [3+2] cycloaddition reactions, showcasing significant yields of desired products.

Chapter 4 focuses on the development of a new protocol for metal-free homolytic aromatic substitution of indoles under visible light, utilizing electron-donor-acceptor complexes.

Finally, Chapter 5 investigates the photopermutation of indazoles to give benzimidazoles under direct excitation using UV light. In particular, a logical and in-depth study of the reaction was accomplished.

Riassunto

Questa tesi esplora innovativi sistemi (foto)nanocatalitici che migliorano la sostenibilità e l'efficienza di varie reazioni organiche. In questo contesto, la sintesi di nuovi nanomateriali e lo sviluppo di metodi catalitici efficaci sono stati prontamente raggiunti in condizioni sintetiche blande, per soddisfare i requisiti di una sintesi chimica più sostenibile.

Il Capitolo 1 introduce i concetti generali di catalisi, enfatizzando il suo ruolo nella promozione dei principi della chimica verde. Si propone di descrivere i principi di base e i meccanismi operativi delle principali reazioni organiche polari e radicaliche, con un'attenzione particolare sull'applicazione dei nanomateriali nella foto- e nell'organocatalisi.

Il Capitolo 2 discute la sintesi di dots di carbonio dopati all'azoto (NCDs) a partire da L-arginina e diammine alchiliche. Questo processo dimostra come la sintesi razionale dei NCDs migliori le loro prestazioni amminocatalitiche in varie reazioni modello attivate da enammina e ioni imminio.

Il Capitolo 3 introduce dots di carbonio ricchi di fenolo (*p*-CDs), che fungono da fotocatalizzatori riciclabili e privi di metallo. Queste nanoparticelle catalizzano efficacemente reazioni fotocatalitiche, come la reazione di cicloaddizione [3+2], mostrando rese elevate per i prodotti desiderati.

Il Capitolo 4 si concentra sullo sviluppo di un nuovo protocollo senza l'utilizzo di metalli per la sostituzione aromatica omolitica degli indoli, utilizzando luce visibile, promosso dall'uso di complessi di donatore-accettore di elettroni.

Infine, il Capitolo 5 indaga la fotopermutazione degli indazoli per dare benzimidazoli, sotto eccitazione diretta utilizzando luce UV. È stato quindi svolto uno studio logico e approfondito della reazione.

Chapter 1.

General Introduction

One of the most remarkable aspects of organic chemistry is its constant evolution, driven by the fundamental efforts of chemists. While new reactions may often be discovered accidentally, understanding and evaluating their significance is the work of organic chemists. In this context, catalysis stands out as a pivotal area of research. The field of catalysis serves as a primary tool for developing chemical processes across various fields, ranging from agrochemicals to energy storage or the pharmaceutical industry.[1–3]

In general, catalysis involves the use of a substance, known as catalyst, that increases the rate of a reaction without altering the overall thermodynamics of the process.[4,5] This substance works by lowering the activation energy of the rate-determining step(s) compared to the non-catalysed pathway. Figure 1 illustrates the potential energy profile of a generic reaction, and the reduced activation energy associated with the presence of a catalyst.

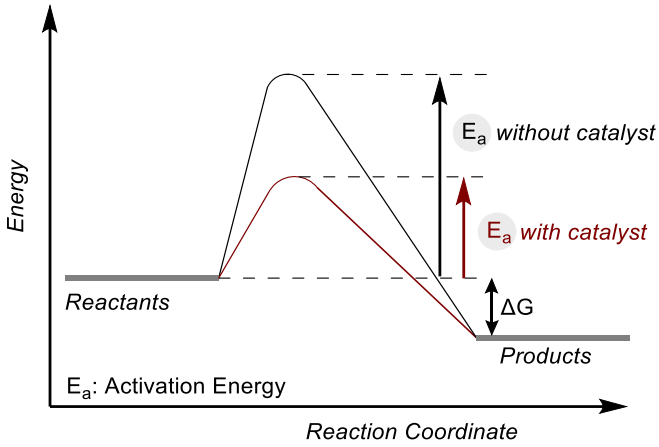

Figure 1.1 Simplified energy profiles of an uncatalyzed reaction (black line) versus a catalysed counterpart (red line). The actual profiles may be more sophisticated with different minima and maxima.

A catalytic approach presents numerous benefits for sustainability and economics, including cost saving, reduced time, energy consumption, and waste minimization.[6] Indeed, catalysis is one of the twelve principles of green chemistry, which aims to maximize efficiency and minimize the negative impact of chemistry on the effects of human health and the environment. Unsurprisingly, the growing interest in academia and industry in developing novel catalytic sustainable approaches is driving extensive research in this field.[7]

1.1 Organocatalysis

The discovery of new organocatalytic reactions is of fundamental importance for addressing challenging problems in organic chemistry.[8] Specifically, organocatalysis involves the use of small organic molecules as catalysts to drive relevant transformations. This field is now widely recognised as one of the main branches of the modern synthesis, which employs organocatalysts with bio-, metal- and photoredox systems.[9] Notably, in early 2000, the organic chemistry community witnessed an incredible rise in literature focused on the development of catalytic enantioselective reactions promoted by chiral small organic molecules.[10] This branch is particularly significant as enantiomers play a primary role in chiral environments, such as in biological systems.[11,12] Historically, organic reactions promoted by catalytic amounts of metal complexes with chiral ligands represented significant milestones in this field, culminating in the 2001 Nobel Prize awarded to K. Barry Sharpless for the Ti-tartrate catalytic asymmetric epoxidation of allylic alcohols and to Ryoji Noyori for the (2,2'-bis(diphenylphosphino)-1,1'-binaphthyl)-Ru catalytic asymmetric hydrogenation of ketones.[13,14] Furthermore, the importance of organocatalysis has been recently recognized with the awarding of the 2021 Nobel Prize to Prof. B. List and Prof D. MacMillan for their outstanding contribution to the development of asymmetric organocatalysis.[15]

The success of organocatalysis as a reliable platform for reaction engineering can be attributed to the discovery and development of new generic modes of activation. Specifically, the formation of a reactive catalytic intermediate results from the interaction between the organocatalyst and a specific substrate in a highly organized and predictable manner, ultimately leading to the formation of the desired product. Consequently, generic activation modes can be employed as valuable tools to design new syntheses in a relatively straightforward way. Based on the nature of this interaction, the activation modes can be classified into covalent and non-covalent.[12] In the first case, the catalyst forms a covalent bond with the substrate during the catalytic cycle. In the latter case, non-covalent interactions, such as hydrogen-bond donor catalysis, activate the molecule for the catalytic transformations.

Regarding the covalent activation techniques, aminocatalysis is the most widely used class of catalytic activation.[16] It relies on the use of primary or secondary amines to activate a carbonyl compound through the reversible formation of an enamine, iminium ion, ammonium enolate, or a three-electron system, known as SOMO catalysis.[10,16–18] Additionally, *N*-heterocyclic carbene (NHC) catalysis has been exploited to access acyl anion equivalents, unlocking polarity-driven reactivity.[19]

Generally, the strong interactions of covalent binding between catalyst and carbonyl compounds provided a reliable synthetic pathway for the functionalization of carbonyl compounds at α- or β-position.

On the other hand, non-covalent activation modes involve weaker, less directional and less distance-dependent interactions than their covalent counterparts.[20] Multiple hydrogen-bond donor moieties can work in concert to position the reaction partners in a highly organized transition state. Finally, another important non-covalent activation mode is the interaction of an ionic species combined with a chiral neutral, anionic, or cationic organocatalysts.[21] This area is referred as ion pairing catalysis, which is widely used in asymmetric synthesis.[21,22]

In the following sections, aminocatalytic activation modes, specifically iminium ion and enamine, will be discussed, as they have been studied during this PhD research.

1.1.1 Aminocatalysis

The use of simple amine molecules as organocatalyst was proposed for the first time in the early 1970s when Hajos and Parrish reported the proline-catalysed intramolecular aldol reaction for the asymmetric functionalization of carbonyl compounds.[23,24] However, it was only in 2000, with two groundbreaking studies, that the field of asymmetric aminocatalysis was established: the proline-catalysed intermolecular aldol reaction, reported by List, Lerner and Barbas, and the imidazolidinone asymmetric organocatalyzed Diels-Alder reaction, developed by MacMillan.[25,26] Since then, significant advances have been made in the implementation of aminocatalysis, opening new opportunities for the enantioselective functionalization of carbonyl compounds.[10,27] Both reports are based on the covalent intermediates transiently generated upon condensation of chiral cyclic secondary amines with carbonyl compounds (aldehydes and ketones). The condensation of a α,β-unsaturated carbonyl compound with a primary or secondary amine, in the presence of a protic acid, produces a positively charged iminium ion which lowers the Lowest Unoccupied Molecular Orbital (LUMO).[28,29] This intermediate greatly enhances the electrophilic character of the carbon at the β-position, favouring the attack of nucleophiles in reactions such as conjugated additions or pericyclic reactions (Figure 1.2a, right). For enolizable aldehydes or ketones, the LUMO-lowering effect increases the acidity of the *α*-protons inducing rapid tautomerization to the enamine reactive intermediates. This enamine is more nucleophilic than the corresponding enol resulting in more susceptibility to electrophilic attack.[30] This activation mode is referred as Highest Occupied Molecular Orbital (HOMO) raising and it enables the functionalization of the α-position of carbonyl

compounds with different electrophiles (Figure 1.2a, left).[31] Subsequently, the group of MacMillan introduced the concept of Single Occupied Molecular Orbital (SOMO) activation, which arises from single electron oxidation of the transiently generated enamine.[17] The resulting open-shell intermediate offers a pathway to access unconventional reactivity, leading to the formation of the respective products.

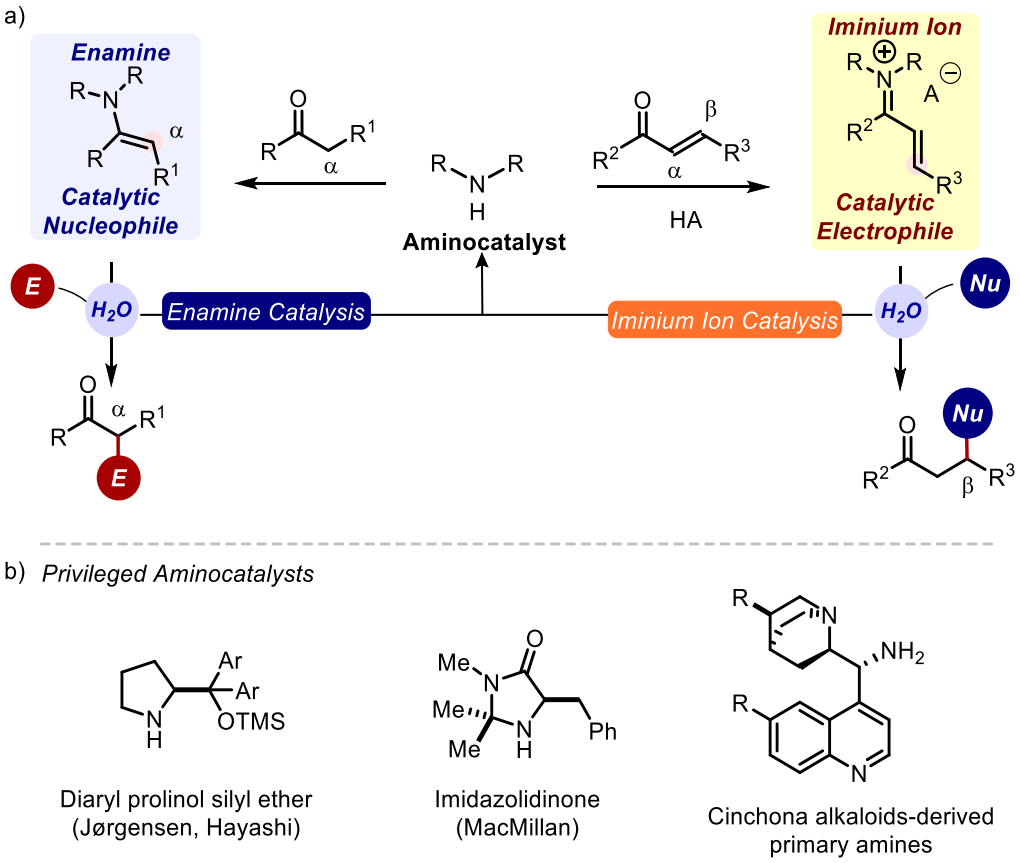

Figure 1.2 (a) Iminium ion and enamine activation of carbonyl compounds. HA = protic acid, Nu = nucleophile, E = electrophile (b) Some of the most used "privileged aminocatalysts".

In most reports, aminocatalytic reactions were conducted using bio-mimicking scaffolds providing a library of catalysts, such as aminoacids or cinchona alkaloids-derived primary amines, ureas among others, known as "privileged aminocatalysts" (Figure 1.2b).[32–34]

Remarkably, aminocatalysis has exhibited large applicability in organic synthesis, from total synthesis of drugs to biochemistry using enzimes.[35] The advantages of organocatalysis over organometallic chemistry contributed to its widespread use, particularly its cost-effectiveness, readily available from the natural chiral pool, usually non-toxic, tolerant to moisture and air, and environmentally friendly. Additionally, organocatalytic methods are particularly appealing for the large-scale production of

pharmaceutical compounds in industrial settings due to the absence of contaminants from transition metals. Nevertheless, several limitations are associated with these catalytic techniques. For instance, a long reaction time is usually required, as well as relatively high catalyst loading (5 to 30 mol%), and catalyst recyclability is quite variable. Despite these aspects, organocatalysis has become a popular research area and a widely used strategy in synthetic chemistry.

In this thesis, the iminium ion and enamine activation modes have been employed to initiate different aminocatalytic reactions. Specifically, nanomaterials rich in amines, namely carbon dots, were used as aminocatalysts. A comprehensive discussion of these findings can be found in Chapter 2.

1.2 Direct photochemistry and Photocatalysis

1.2.1 From Photochemistry to Photoredox Catalysis

Photochemistry is the branch of chemistry that deals with chemical changes promoted by the absorption of light.[4] In these chemical transformations, the energy required to convert the starting materials into the final products is provided by photons. From this perspective, sunlight is a remarkable natural source of energy. One of the most significant challenges of the twenty-first century was the necessity of considering alternative energy sources to move from the limited supply of fossil fuels.[36] Giacomo Ciamician was among the first scientists to pay attention to the energy problem. In his study "The Photochemistry of the Future" published in 1912, Giacomo Ciamician highlighted the necessity to switch from fossils to renewable energy sources.[37] Nowadays, photochemistry is an established strategy for driving many transformations not achievable using traditional methodologies.

Upon light absorption, a chemical species reaches an electronically excited-state, which differs from the corresponding ground state in terms of energy content and chemical and physical properties.[38] The study of this phenomenon has led to the discovery of numerous novel reactions and preparative methodologies. The twentieth century harnessed UV light as a powerful source of energy for the construction of organic molecules. Subsequently, an increasing number of research groups adopted visible-light-mediated synthetic transformations to avoid the harsh conditions associated with UV light.

Nevertheless, a basic impediment in the use of visible light, which has limited its growth for decades, relies on the inability of most organic molecules to absorb visible light.[39] In the past decade, the

independent efforts of MacMillan,[9] Yoon,[40] Stephenson,[41] and other contributors allowed to circumnavigate this problem, thus opening the way to a new field of research, namely visible-light photocatalysis.[42,43] This approach is based on the ability of light-absorbing metal-based complexes to generate reactive radicals from suitable precursors under visible light irradiation. In particular, when the light-excited photocatalysts can act as photo-oxidants or photo-reductants towards a reaction component, the described approach is known as photoredox catalysis.[44] In fact, it made possible the development of radical chemistry for synthetic purposes by accessing the generation of highly reactive open-shell species in very mild conditions.[42] The foundation of photoredox catalysis lies in the effectiveness and versatility of transition metal chromophores (mainly Ru, Ir and Cu) for a wide range of photochemical transformations under visible light irradiation.[39,44,45] However, several issues have rendered transition-metal-based photocatalysts less interesting nowadays. Specifically, their toxicity, limited abundance, relatively high cost and difficult recyclability have prompted researchers to seek more environmentally friendly photocatalytic alternatives.[46,47] In the last years, metal-free organic chromophores, with optical and redox properties, have become increasingly common to meet more sustainable demands.[48] These more affordable and long-lasting photocatalytic systems have emerged as promising photocatalytic platforms for innovative green synthetic methodologies.[49]

Specifically, this thesis addresses the utilization of photo-active metal-free nanomaterial, namely carbon dots, to trigger synthetically relevant transformations under visible light irradiation. These results are depicted in Chapter 3. We also reported the visible-light absorbing Electron-Donor Acceptor (EDA) complexes capable of generating open-shell species to undergo relevant catalytic-free reactions (Chapter 4). Considering the extensive study about reactions promoted by UV-visible light, it is essential to discuss the general mechanistic aspects leading to the formation of key radical species upon light absorption. This is the main aim of the following sections.

1.2.2 Light Absorption and Excited-State Deactivation Pathways

Light absorption is the element that connects all the photochemical transformations. This event is crucial in the light-matter interaction because it allows the formation of electronically excited-state species starting from ground-state compounds. The phenomenon of the absorption of a monochromatic photon by an absorber species in solution is governed by the Beer-Lambert law (*eq*. 1):

$$A = log(\frac{I_0}{I}) = \varepsilon lc \qquad (eq.\ 1)$$

where *A* is the absorbance, *I* the intensity of the transmitted light, I_0 the intensity of the incident light, ε the molar absorption coefficient, *l* the optical path length and *c* the concentration of the absorber solution.

Compounds that absorb light contain antennae groups, known as chromophores, which are responsible for light absorption. The energy of the absorbed photons triggers the transition of one electron from the HOMO to the LUMO. This implies that the molecule passes from the ground electronic state to an electronically excited-state, respectively described by the wave functions Ψinitial and Ψfinal. The feasibility of the electronic transition is determined by the matching between the energy of the photons ($h\nu$) and the energy of a pair of electronic energy levels Ψ in the absorber (*eq*. 2):

$$h\nu = E_f - E_i \qquad (eq.\ 2)$$

where E_f and E_i are the energies of the excited-state Ψ_f and the ground state Ψ_i. Moreover, the magnitude of the electronic transition relies on the selection rules, that indicate which transitions are allowed or forbidden, considering the symmetry of the orbitals involved and their spin multiplicity.[38]

After the electronic transition, the excited-state species may release its energy content or undergo chemical reactions. In general, a photochemical reaction can be initiated by (*i*) direct excitation of the substrates or reaction intermediates (direct photochemistry), or by (*ii*) the ability of structures to absorb light and then activate the non-absorbing substrates. If the absorbing compounds are regenerated during the catalytic cycle, they are called photocatalysts. Figure 1.3 schematized the processes of an excited-state species and their interaction mode with the reaction components.

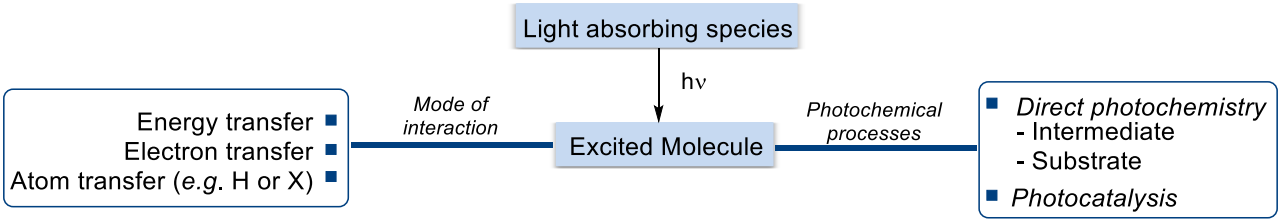

Figure 1.3 The light absorption produces an excited-state molecule that can undergo various deactivation pathways.

In some cases, the absorbing substrate directly undergoes a chemical transformation, such as photochemical rearrangements. While the mechanisms of the interaction of the photoexcited species with other reaction components may be classified in (*i*) energy transfer, (*ii*) photo induced electron transfer or (*iii*) atom transfer (*e.g.*, hydrogen atom transfer or halogen atom transfer). Detailed information about these common pathways is described in the next sections. Instead, the energy-releasing pathways can be classified as radiative (transitions to lower states involving light emission, *i.e.* fluorescence and phosphorescence) and non-radiative (transitions involving the release of heat, i.e. internal conversion and vibrational relaxation). While ground-state compounds are indefinitely stable, excited-states are transient and short-lived species. Their lifetime (τ) depends on the rate of the abovementioned deactivation processes.[50] In addition, the excited-state intermediate can participate in numerous inter- and intramolecular processes that lead to a change in the chemical composition of the species involved.

1.2.3 Direct Substrate Photoexcitation and Electron Donor-Acceptor (EDA) Complexes

In the field of synthetic photochemistry, photochemical processes are driven by harvesting the energy of the incident photons.[51] As anticipated in Section 1.2.2, a reaction substrate (S) directly absorbs the light leading to the formation of the product (P). Traditionally, these reactions were conducted using UV light due to its higher source of energy associated with UV wavelengths. In the twenty-first century, the focus on photochemistry has shifted towards visible light to avoid the harsh conditions associated with UV irradiation.[52] However, the traditional view of UV wavelengths as the primary drivers of photochemical transformations is evolving. A novel trend has emerged, aiming to achieve efficient synthetic methods with a high level of mechanistic understanding.[53] Previously, the use of UV light was often linked to low selectivity due to its high energy and complex reaction setups (*e.g.,* quartz tubes as reaction vessels and apparatus such as Xe or Hg lamps).[54] Today, however, conducting a photochemical reaction under UV light can be as straightforward as using visible-light sources.

An elegant example of direct photoexcitation involves the UV light absorption of an aldehyde, in the Paternò-Büchi reaction, and subsequently reaction with an olefin to yield the corresponding oxetane (Figure 1.4a).[55] Other studies investigated the [2+2] photocycloadditions, which represent a common method to access carbocyclic products, through UV light irradiation of strained nonconjugated alkenes[56] or the alkylation of transient photo-enols, *via* unconventional Michael-type

addition, through direct irradiation at 320 nm.[57] Recently, Leonori and co-workers reported the photoexcitation of nitroarenes under purple light irradiation to use them as ozone in various reactivities, such as cycloadditions with alkenes or dearomatization (Figure 1.4a).[58–60]

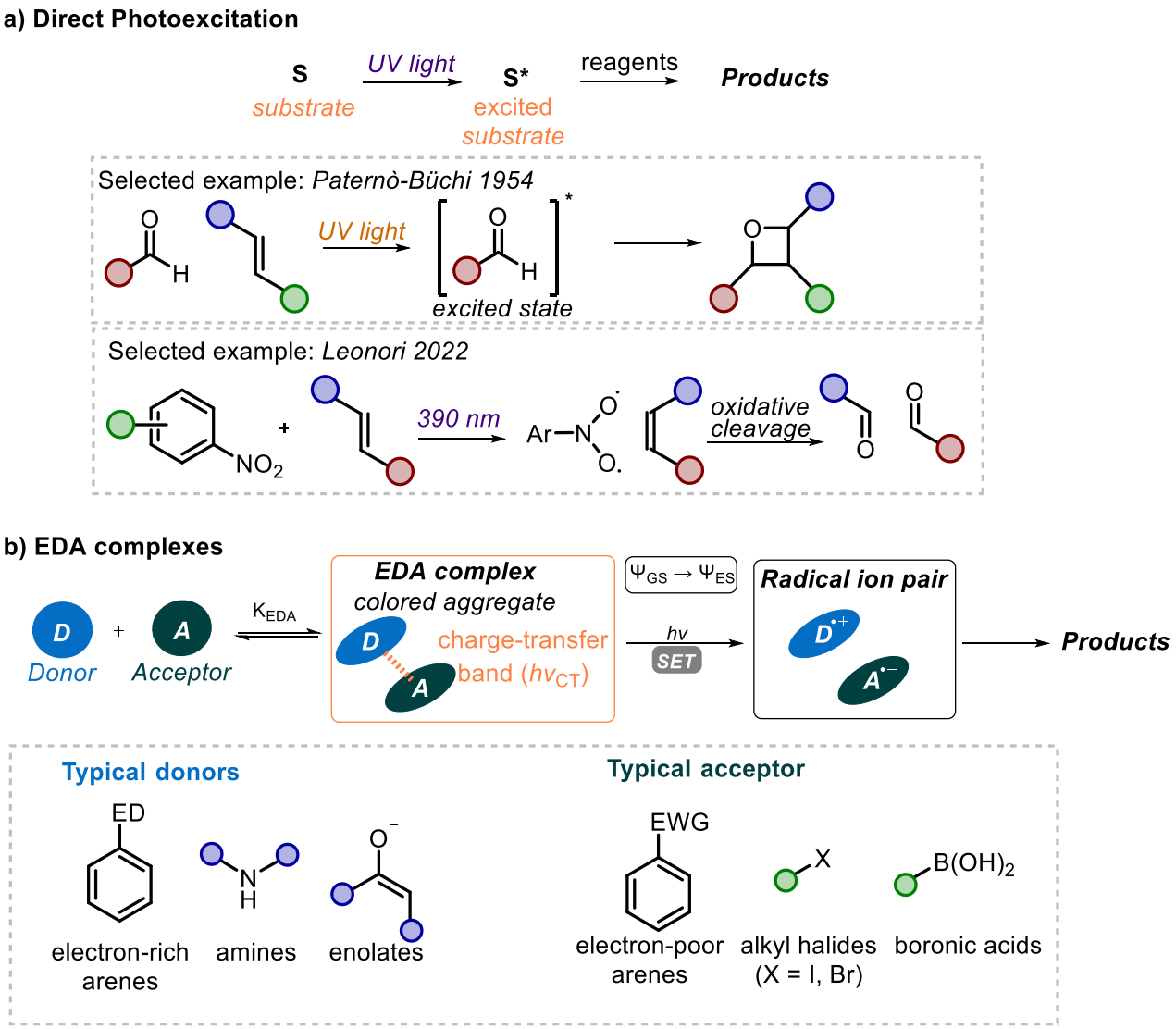

Figure 1.4 (a) Ground-state species that can harvest the energy of incident photons to undergo photochemical reactions. Example of Paternò-Büchi. Example of the direct irradiation of nitroarenes for the oxidative cleavage of alkenes. (b) Irradiation of an electron donor-acceptor complex (EDA) complex to generate radical ion pair species. Examples of typical donors and acceptors employed in this approach. ED = electron-donating group. EWG = electron-withdrawing group.

Alternative catalytic-free approaches include the formation of coloured molecular associations between two or more species, which are transiently generated in the ground state, to drive diverse reactivity.[61] The appearance of vivid colours when two colourless organic compounds are combined was observed 40 years ago. Hildebrand investigated the different coloured solutions formed when iodine is mixed with various solvents.[62] Eventually, spectroscopic investigations showed that

benzene and mesitylene form 1:1 stable complexes with iodine.[63] In 1952, Robert Mulliken proposed a quantum mechanical theory to explain the formation of these complexes.[64] According to the Mulliken charge-transfer theory, the aggregation of an electron-rich substrate (a donor D with a low ionization potential, IP) with an electron-accepting molecule (an acceptor A with a high electronic affinity, EA) can trigger the formation of a new complex in the ground state, known as EDA complex (Figure 1.4b, K_{EDA} being the association constant for the complex formation).[61] New molecular orbitals are formed from the electronic coupling of the D and A frontier orbitals (HOMO/LUMO), resulting in physical properties for the EDA complex that differ from those of the separated substrates.[65] This new chemical entity is characterized by the appearance of a new absorption band, the charge transfer band ($h\nu_{CT}$), associated with an $\Psi_{GS} \rightarrow \Psi_{ES}$ electronic transition (Ψ is the wave function, associated with ground and excited-states). In many cases, the energy of this transition lies within the visible range. Upon excitation of the EDA complex (orange box in Figure 1.4b), the Ψ_{ES} is populated, leading to the transfer of an electron (PET) from the HOMO of the D to the LUMO of the A to generate a radical ion pair characterized by a net charge separation. This complex may ultimately furnish reactive radicals that then evolve through the formation of the desired products.

Thanks to the EDA complex, it is possible to activate compounds under visible-light irradiation that would not normally absorb in the visible spectrum.[64,66] Thereafter, a variety of examples of the utilization of coloured EDA complexes in synthetic photochemistry have been reported, providing new opportunities in this field.[67] In the most relevant case studies, the donors are typically electron-rich arene, amines, enamines or enolates, while the acceptors are generally electron-poor arenes, alkyl halides, boronic acids, iminium ions and so on.[68–71]

To better understand the formation of the EDA complexes, efforts have focused on their photophysical characterization. The section 1.3 will examine some essential techniques to investigate the EDA complex and generally the common photochemical transformations.

1.2.4 Photocatalytic Transformations

Besides direct photochemistry, different photocatalytic activation modes can be in play. Firstly, the energy transfer (EnT) phenomenon, commonly referred to as photosensitization, enables the indirect excitation of a molecule that cannot directly absorb incident photons.[72] The EnT mechanism occurs frequently in nature, playing a pivotal role in processes like photosynthesis.[73] By exciting an acceptor in its ground-state, the energy transfer process involves the deactivation of the excited-state photocatalyst (PC*). Energy transfer can occur through two distinct modes (Figure

1.5a). The first is Förster resonance energy transfer, where the photoexcited donor D* triggers the excitation of the ground state acceptor A *via* Coulombic interactions. However, in the context of reactions in solution, particularly in the majority of laboratory synthetic photocatalysis, a second mode of EnT is more appropriate.[72] This mode is referred to as Dexter energy transfer, where D* excites an acceptor molecule A through an intermolecular exchange of ground state and excited-state electrons.[74]

Beyond energy transfer, the photocatalyst (PC) can participate in the electron transfer pathway. The photoinduced electron transfer (PET) mechanism provides a straightforward method for producing reactive open-shell species. This mechanism serves as the basis for photoredox catalysis, in which a PC, used in sub-stoichiometric quantities, harnesses the energy to reach its excited-state (PC*).[42,48,75] This excited species exploits its high energy to promote the photochemical reaction by interacting bimolecularly with the substrate in the ground state. Depending on the properties of both the PC and the substrate, three mechanistic approaches can be considered: electron transfer, energy transfer, and atom transfer.[45] In the electron transfer event, PC* can interact in either an oxidative or reductive quenching cycle. In the oxidative quenching cycle, PC* acts as a reductant, transferring an electron to an appropriate electron acceptor (A) via PET. This step generates the radical anion of the acceptor ($A^{\bullet-}$) and the oxidized photocatalyst ($PC^{\bullet+}$). Conversely, when PC* acts as an oxidant, taking an electron from a donor (D), the reduced photocatalyst is formed ($PC^{\bullet-}$). The catalytic cycle is then closed by a second SET event from a redox-active species, either a sacrificial donor/acceptor or an open-shell intermediate (Figure 1.5a). This approach is valuable for constructing new synthetically useful chemical bonds.[76]

In literature, the most popular metal-based visible light-absorbing PCs consist of Ru and Ir.[42,77] When the related polypyridyl complexes are in their excited-state, they can function as strong oxidant or reducing agents towards suitable donors or acceptors[78,79] (Figure 1.5a).

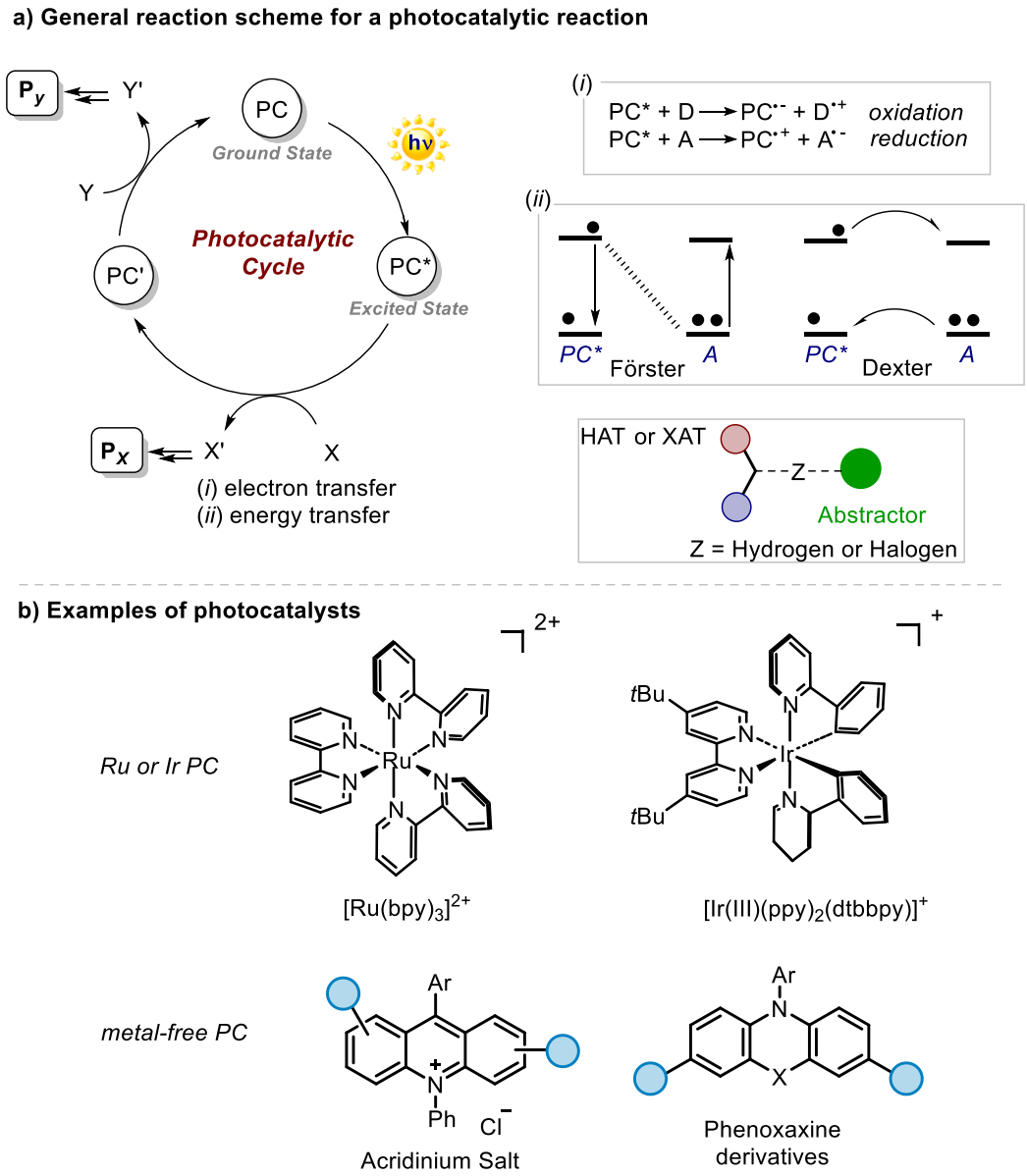

Figure 1.5 (a) General photocatalytic cycle for a photocatalytic reaction. (b) Some examples of the most employed metal-based and metal-free photocatalysts.

Given that ligands significantly influence the redox activity of these PCs, therefore they can be finely tuned to impart the desired properties to the photoactive catalysts. Customized photoredox properties can also be achieved through substituent modifications. For instance, incorporating bulky or long alkyl chain substituents can reduce unwanted outer sphere SET and modulate catalyst aggregation.[74] When the electron density of the metal centre rises, the oxidative power of the complex decreases while, its reductive power simultaneously increases.[76,77]

Over the last few years, major efforts have been devoted to the development of metal-free organic PCs.[80] The most employed organic PCs feature a highly functionalized aromatic core that provides

them the desired features, such as a strong absorption in the visible region and pronounced redox character. Besides being a more economical and sustainable option compared to metal-based PCs, organic PCs offer an increasing number of modular scaffolds that are characterized by peculiar and tunable physicochemical features.[49,81] Examples of rational modifications include doping with heteroatoms or the incorporation of electron-donating or electron-withdrawing substituents on the PC scaffold.[81] Common organic dyes employed as PCs are acridinium salts, phenoxaxine derivatives, xanthenes (Figure 1.5b).[82] Along with the abovementioned advantages of visible-light-absorbing PCs, the field of organic photoredox catalysis plays an important role in the development of novel photochemical transformations such as C-C and C-X couplings, C-H functionalizations or cycloadditions.[40,45,83]

Other commonly used reaction pathways involve the formation of open-shell species via hydrogen or halogen atom transfer (HAT or XAT) from ground-state compounds. HAT is characterized by the simultaneous transfer of a proton and an electron from the C-H bond of the substrate, referred to as hydrogen donor, to an accepting species in a single kinetic step (Figure 1.5a).[84] This mode of catalysis is commonly observed in certain families of aromatic ketones, polyoxometalates, and uranyl cations when they function as photocatalysts.[85] Whereas, XAT-based activation involves the direct homolytic abstraction of the halogen atom by an appropriate abstractor radical. This method offers an attractive tool for developing densely functionalised compounds, as many XAT agents exhibit great chemo selectivity, reacting preferentially with halide groups.[86]

1.2.5 Photoinduced Electron Transfer

The most relevant excited-state deactivation pathways in synthetic photochemistry are indisputably electron. Regarding the first interaction mode, electron transfer occurs when a light-excited molecule can donate or accept an electron by interacting with suitable redox-active compounds. Specifically, the photoinduced electron transfer (PET) is defined from IUPAC as “electron transfer resulting from an electronic state produced by the resonant interaction of electromagnetic radiation with matter”. Remarkably, the high energy content of the excited-state species influences its electron transfer ability, making it both a better oxidant and reductant than the corresponding ground-state compound.[50]

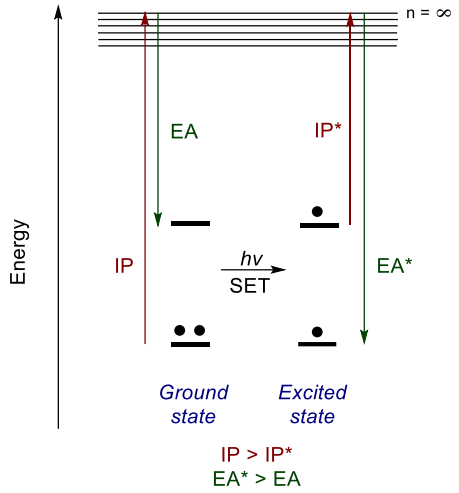

Figure 1.6 The ionization potential (IP) and electron affinity (EA) of an excited-state species that explains why it is a better oxidant and reductant than its corresponding ground-state.

To explain this phenomenon in depth, is necessary to consider the whole photochemical process from a thermodynamic point of view. In fact, upon excitation of the absorbing molecule, one electron populates the antibonding orbital, which is positioned at a greater separation distance from the nucleus. For this reason, the energy required for a single-electron ejection process (also called ionization potential) is lower with respect to the ground-state species. On the other hand, the presence of a half-filled orbital near the nucleus increases the amount of energy released during a single-electron addition process (known as electron affinity), compared to the ground-state species (Figure 1.6).[47] Consequently, the energy level of the excited-state enhances the capacity for electron transfer, rendering it a more effective oxidizing and reducing agent.

PET event that involves an excited-state species and a ground-state molecule can occur in two different circumstances (*eq*. 3-4):

$$D^* + A \rightarrow D^+ + A^- \qquad (eq.\ 3)$$

$$D + A^* \rightarrow D^+ + A^- \qquad (eq.\ 4)$$

where D* and A* are respectively the excited-state donor and acceptor. Indeed, the Gibbs free energy variation of the process (ΔG^0_{et}) depends on the difference between $E^0_{D^+/D^*}$ and E^0_{A/A^-} and the term C which describes the interaction between the charged species formed and the solvation effects. The ΔG^0_{et} associated to the PET must include the excitation energy (E_{00}) and can be calculated through the Rehm-Weller equation.[87,88] For the case of an excited donor (D*) that reacts with a ground-state acceptor (A, *eq*. 5-7):

$$\Delta G^0_{et} = (E^0_{D^+/D^*} - E^0_{A/A^-}) + C \quad (eq.\ 5)$$

$$E^0_{D^+/D^*} = E^0_{D^+/D} - E_{00} \quad (eq.\ 6)$$

$$\Delta G^0_{et} = (E^0_{D^+/D} - E^0_{A/A^-} - E_{00}) + C \quad (eq.\ 7)$$

where $E^0_{D^+/D^*}$ is the reduction potential of the donor in the excited-state (D*). This value is expected to be smaller than the reduction potential of the donor ($E^0_{D^+/D}$), since D* is a better reducing agent than D. While the redox potential of the ground-state species can be easily accessed through cyclic voltammetry measurements, the excitation energy (E_{00}) may be spectroscopically estimated. Specifically, it can be derived from the position of the long wavelength tail of the absorption spectrum of the electron donor (D) or, alternatively, from the position of the short wavelength tail of the emission spectrum of D.[38] An analogous discussion may be done to evaluate the magnitude of ΔG^0_{et} for a PET between an excited acceptor (A*) and a ground-state donor (D). It is evident that the use of the Rehm-Weller equation is fundamental to evaluate the excited-state potential of light-absorbing species. In this way, it is possible to predict the feasibility of a productive PET for synthetic purposes.[67]

On the other hand, single-electron transfer is the key concept of redox chemistry, where one reaction partner loses electrons (oxidation) while the other gains electrons (reduction). The definition of SET from IUPAC consists of "a reaction mechanism characterized by the transfer of a single electron between the species occurring on the reaction coordinate of one of the elementary steps".

Specifically, a single-electron transfer (SET) from a donor (D) to an acceptor (A) may thermodynamically occur when the $E^0_{D^+/D}$ is lower than the reduction potential of the acceptor (E^0_{A/A^-}) in the ground state. In this case, the Gibbs free energy variation of the process (ΔG^0_{et}) depends on the difference between these two values and the term C. (*eq*. 8-9).[89]

$$D + A \rightarrow D^+ + A^- \quad (eq.\ 8)$$

$$\Delta G^0_{et} = (E^0_{D^+/D} - E^0_{A/A^-}) + C \quad (eq.\ 9)$$

1.3 Mechanistic Techniques for Investigating Photochemical Transformations

Mechanistic investigations are crucial for guiding the development of photochemical transformations.[67] In every photochemical reaction, the first event that occurs is the absorption of light from a ground-state photoactive structure leading to an electronically excited-state. This section briefly discusses primary mechanistic experiments commonly conducted when studying light-driven reactions, with particular attention to those featured in this thesis.

Initial studies often focus on the ground state of the absorbers by using UV-Vis spectroscopy. This analysis allows for the identification of the chromophore and accurate selection of the appropriate irradiation wavelength to excite the photoactive target. Regarding the EDA complex, it is important to carry out the absorption analysis of both the individual component and the EDA complex. In fact, taken individually, D and A usually are colourless, and the characteristic new band appears only in their associated form.

In addition, cyclic voltammetry can be employed to ascertain the electrochemical characteristics of the chromophore. As a result, by understanding its redox potential value, it is feasible to select the reaction partners that are required to build the photochemical process.

As previously mentioned, examining the radiative deactivation of the excited-state through fluorescence or phosphorescence spectroscopy can provide valuable mechanistic insights. Specifically, the excitation energy (E_{00}) can be spectroscopically estimated using the Rehm-Weller theory for an initial thermodynamic characterization of the process. Another fundamental method for elucidating the interaction between excited-state species and other components of the reaction is the Stern Volmer quenching analysis, which can be conducted using a straightforward spectrofluorometer. Notably, a reduction in the intensity of emission (quenching) occurs when an excited-state molecule is deactivated upon collision with another species (quencher). Even if this approach may not distinguish between processes involving energy transfer and electron transfer, it does offer valuable clues for elucidating the mechanism of a photochemical reaction.

For identifying and characterizing ground state aggregates, such as EDA complexes or assemblies *via* non-covalent interactions, additional techniques can be exploited. Thanks to the stability of the transiently generated aggregates, they can be also studied by nuclear magnetic resonance (NMR) titration experiments or computational calculations. The NMR titration is a unique tool for investigating the kinetics of the EDA complex formations; as the donor compound is gradually added

to a solution containing the acceptor, changes in the chemical shifts of atoms near the EDA interaction can be detected. In this way, the stoichiometry and the association constant (K_{EDA}) of these complexes can be evaluated *via* a Job's plot analysis.[90] Occasionally, it is even possible to isolate the bench-stable EDA complexes and determine their exact structure by X-ray diffraction.[66,69] In conclusion, UV light has been exploited to promote the photochemical rearrangement of valuable compounds.

1.4 Nanocatalysis

1.4.1 Carbon-based Nanomaterials

Carbon-based nanomaterials (CNMs) have been essential to the field of nanotechnology. A significant turning point in nanomaterial research occurred with the discovery of fullerenes in 1985, particularly fullerene C60 the first molecular CNM made entirely of a specific number of carbon atoms.[91,92] This discovery paved the way for the development of other carbon-based nanostructures, including carbon nanotubes,[93] graphene,[94] and more recently, carbon dots.[95,96] These materials can be categorized by their dimensional classes: 0D (*e.g.,* fullerenes and carbon dots), 1D materials (*e.g.,* carbon nanotubes), 2D materials (*e.g.,* graphene), and 3D materials (*e.g.,* graphite), depicted in Figure 1.7.[97,98] Due to their diverse designs and morphologies, along with their distinctive physicochemical properties, CNMs have attracted significant attention from the scientific community in recent years. Nevertheless, a primary limitation of pristine CNMs is their difficult manipulation and a strong tendency to aggregate when exposed to certain solvents.[99] The fundamental requirements of nanoscience include the control and determination of functional properties. Importantly, the characteristics of these carbon-based nanostructures can be easily tailored through chemical modifications of their surfaces.

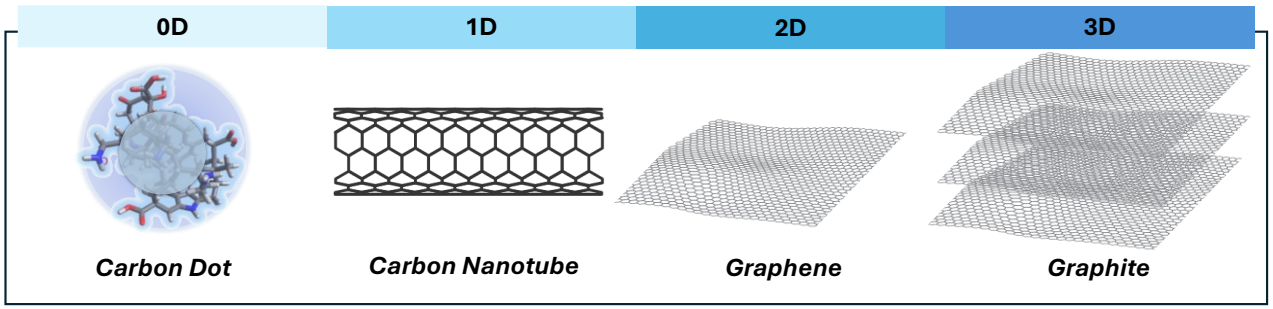

Figure 1.7 Classification of the most common carbon nanoforms based on their dimensionality.

These fine-tuning alterations enhance their desirable features making them applicable across various technological domains, ranging from catalysis, optoelectronics, and nanomedicine.[100–102] In the early 2000s, traditional catalysis often felt short of meeting the demands for tunability of the catalyst and strict process control.[103–105] The introduction of functionalised materials to enhance the control of catalytic chemical transformations, opened a broad and fruitful research area known as nanocatalysis.[105]

The utilization of catalysts at the nanoscale typically refers to dimensions from 1 to 100 nanometers.[106] Today, functionalized and/or post-synthetically modified carbon-based nanomaterials are actively involved in catalytic cycles through diverse chemical interactions occurring between their surface functionalities and the components of the reaction.[97] Furthermore, the development of metal-free nanocatalytic systems has been encouraged by the growing emphasis on sustainable and environmentally friendly approaches in chemistry.[107–109] Consequently, the application of such materials in catalysis relies on their rational design, careful surface derivatizations and in-depth characterization of their surface groups.[110] Thus, both polar and light-driven radical processes of synthetical importance can currently be conducted using carbon-based nanocatalysts.[98]

1.4.2 Nano-organocatalysis

In recent years, there has been a notable increase in the publication of research focused on metal-free, carbon-based nanostructured catalysts. Many of these studies focused on the introduction of functional groups onto the surfaces of inert carbon nanomaterials (CNMs). The instalment of specific moieties of carbon-based nanostructures is a well-established and effective strategy in materials science, particularly in the field of nanocatalysis (Figure 1.8).[111] For example, amino-functionalized CNMs are widely employed in catalytic applications due to their properties such as enhanced dispersion and solubilization of materials as well as the high chemical reactivity of amine groups which can promote aminocatalytic reactions.[112] It is important to note that the specific properties and applications of amino-functionalized CNMs can vary depending on factors such as the methods used for their functionalization and the type of carbon-based nanostructure (*e.g.,* carbon nanotubes, graphene, or fullerenes).

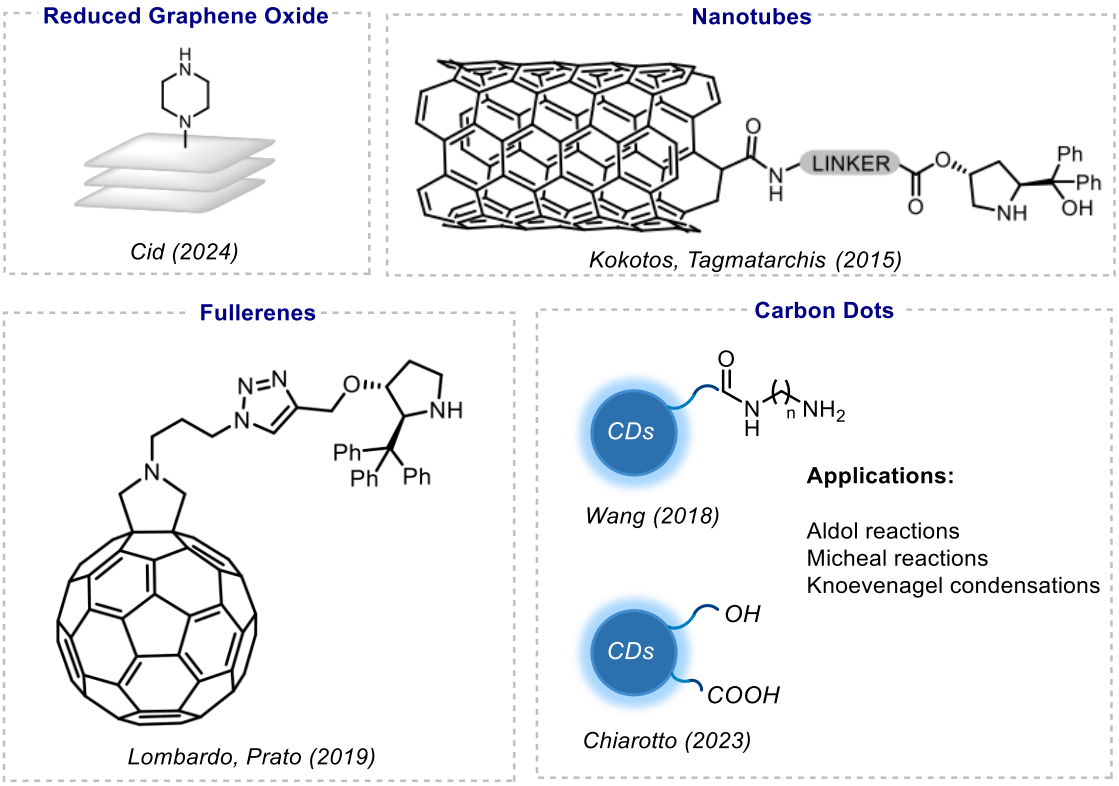

Figure 1.8 Selected examples of carbon-based nano-organocatalysts for the most common organocatalytic transformations.

Among them, carbon dots (CDs) serve as an intriguing example in the field of nano-organocatalysis.[111] These nanomaterials consist of carbon cores surrounded by shells containing numerous polar groups. The precursors and operating conditions used during the CD synthesis significantly influence their chemical-physical properties.[113] Consequently, the choice of the precursors plays a crucial role in the catalytic features of the final material. In fact, the functional groups of the starting materials end up on the surface of nanoparticles during the synthesis. Exploiting their surface groups, CDs can catalyse the formation of valuable organic compounds under mild and green operating conditions using classical polar reactivities.[114,115] Consequently, the popularity of these nanoparticles is rising due to their straightforward and rapid preparation from inexpensive raw materials, including waste and naturally renewable sources, as well as their scalability for large-scale operations and customizable surfaces. Amino-functionalized carbon dots have been successfully employed in various organocatalytic reactions, including aldol condensation, Michael addition, and Knoevenagel reactions,[110] even in enantioselective fashion, by following the general activation modes described in Section 1.1. However, despite their significant potential, these applications remain largely exploratory in the context of nano-organocatalysts.

To this aim, Chapter 2 discusses the synthesis of nitrogen-doped CDs to develop highly catalytically active nanocatalysts for enamine and iminium ion transformations, focusing on the optimization of their synthesis.

1.4.3 Nano-photocatalysis

CNMs are becoming an attractive trend not only as organic catalysts but also in the field of photocatalysis. They are emerging as promising nano-photocatalytic platforms for light-driven transformations across a wide range of radical reactions. Several classes of modified CNMs exhibit excellent optoelectronic properties, along with low toxicity, easy preparation and potential recyclability.[116] Specifically, efficient CNMs that function as semiconductor-like materials, typically show strong light absorption. This event causes the excitation of electrons from the valence band (VB) to the conduction band (CB), resulting in charge separation and the formation of electrons and holes (Figure 1.9a). Depending on the energy positions of the VB and CB, the considered photocatalysts can provide sufficiently high redox potential and abundant surface sites to drive the desired transformations.[117,118] Notably, solid-phase semiconductor-like photocatalysts are capable of generating both oxidizing and reducing species at the same time. This characteristic makes them suitable for application in organic synthesis through oxidative or reductive pathways.[119]

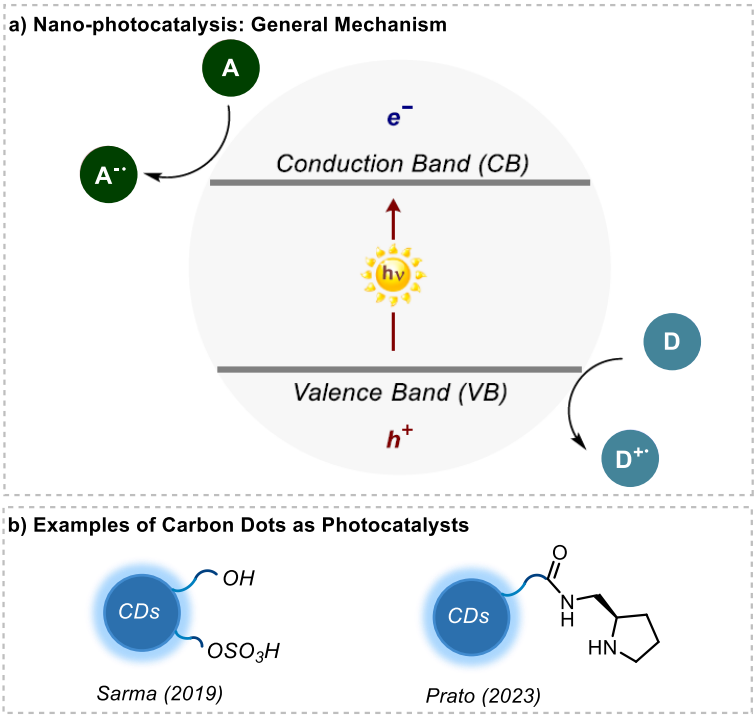

Figure 1.9 (a) General photocatalytic mechanism of heterogeneous nano-photocatalysts. (b) Examples of CDs as nano-photocatalysts.

As an example, CDs have drawn increasing attention as a viable alternative to traditional photocatalysts.[120] In addition to the aforementioned properties, CDs typically exhibit excitation wavelength-dependent emission, high photostability, great up-conversion ability, and excellent redox properties.[121] When exposed to a proper UV-Vis light, CDs can reach an excited-state (CDs*), dissipating the excess energy through either fluorescence or the initiation of radical processes. Moreover, the doping of the nanoparticles plays an important role in determining their overall photochemical reactivity.[122,123] Various heteroatom-doped CDs have the potential to be applied in different photoredox transformations (Figure 1.9b).[111] Nevertheless, the research involving these materials in synthetic photochemistry is still in its early stages.[121] In this regard, photoactive CDs, with tailored functional groups on their surfaces, have been employed to trigger valuable reactions under light irradiation. These results are described in Chapter 3.

1.5 References Chapter 1

(1) Armor, J. N. A History of Industrial Catalysis. *Catalysis Today* **2011**, *163* (1), 3–9. https://doi.org/10.1016/j.cattod.2009.11.019.

(2) Busacca, C. A.; Fandrick, D. R.; Song, J. J.; Senanayake, C. H. The Growing Impact of Catalysis in the Pharmaceutical Industry. *Advanced Synthesis & Catalysis* **2011**, *353* (11–12), 1825–1864. https://doi.org/10.1002/adsc.201100488.

(3) Schlögl, R. Catalysis 4.0. *ChemCatChem* **2017**, *9* (4), 533–541. https://doi.org/10.1002/cctc.201700026.

(4) *The IUPAC Compendium of Chemical Terminology: The Gold Book*, 4th ed.; Gold, V., Ed.; International Union of Pure and Applied Chemistry (IUPAC): Research Triangle Park, NC, 2019. https://doi.org/10.1351/goldbook.

(5) Jencks, W. P. *Catalysis in Chemistry and Enzymology*; Courier Corporation, 1987.

(6) Centi, G.; Ciambelli, P.; Perathoner, S.; Russo, P. Environmental Catalysis: Trends and Outlook. *Catalysis Today* **2002**, *75* (1), 3–15. https://doi.org/10.1016/S0920-5861(02)00037-8.

(7) Michaudel, Q.; Ishihara, Y.; Baran, P. S. Academia–Industry Symbiosis in Organic Chemistry. *Acc. Chem. Res.* **2015**, *48* (3), 712–721. https://doi.org/10.1021/ar500424a.

(8) Dalko, P. I.; Moisan, L. In the Golden Age of Organocatalysis. *Angew. Chem. Int. Ed.* **2004**, *43* (39), 5138–5175. https://doi.org/10.1002/anie.200400650.

(9) Nicewicz, D. A.; MacMillan, D. W. C. Merging Photoredox Catalysis with Organocatalysis: The Direct Asymmetric Alkylation of Aldehydes. *Science* **2008**, *322* (5898), 77–80. https://doi.org/10.1126/science.1161976.

(10) Melchiorre, P.; Marigo, M.; Carlone, A.; Bartoli, G. Asymmetric Aminocatalysis—Gold Rush in Organic Chemistry. *Angew. Chem. Int. Ed.* **2008**, *47* (33), 6138–6171. https://doi.org/10.1002/anie.200705523.

(11) Seayad, J.; List, B. Asymmetric Organocatalysis. *Org. Biomol. Chem.* **2005**, *3* (5), 719–724. https://doi.org/10.1039/B415217B.

(12) Introduction: Organocatalysis – From Biomimetic Concepts to Powerful Methods for Asymmetric Synthesis. In *Asymmetric Organocatalysis*; John Wiley & Sons, Ltd, 2005; pp 1–8. https://doi.org/10.1002/3527604677.ch1.

(13) Katsuki, T.; Sharpless, K. B. The First Practical Method for Asymmetric Epoxidation. *J. Am. Chem. Soc.* **1980**, *102* (18), 5974–5976. https://doi.org/10.1021/ja00538a077.

(14) Ohkuma, T.; Ooka, H.; Hashiguchi, S.; Ikariya, T.; Noyori, R. Practical Enantioselective Hydrogenation of Aromatic Ketones. *J. Am. Chem. Soc.* **1995**, *117* (9), 2675–2676. https://doi.org/10.1021/ja00114a043.

(15) Ooi, T.; Crudden, C. 2021 Nobel Laureates Recognized in Organocatalysis. *ACS Catal.* **2021**, *11* (24), 15234–15234. https://doi.org/10.1021/acscatal.1c05384.

(16) Bertelsen, S.; Jørgensen, K. A. Organocatalysis—after the Gold Rush. *Chem. Soc. Rev.* **2009**, *38* (8), 2178–2189. https://doi.org/10.1039/B903816G.

(17) Beeson, T. D.; Mastracchio, A.; Hong, J.-B.; Ashton, K.; Macmillan, D. W. C. Enantioselective Organocatalysis Using SOMO Activation. *Science* **2007**, *316* (5824), 582–585.

(18) Gaunt, M. J.; Johansson, C. C. C. Recent Developments in the Use of Catalytic Asymmetric Ammonium Enolates in Chemical Synthesis. *Chem. Rev.* **2007**, *107* (12), 5596–5605. https://doi.org/10.1021/cr0683764.

(19) Bugaut, X.; Glorius, F. Organocatalytic Umpolung: N-Heterocyclic Carbenes and Beyond. *Chemical Society Reviews* **2012**, *41* (9), 3511–3522. https://doi.org/10.1039/C2CS15333E.

(20) Taylor, M. S.; Jacobsen, E. N. Asymmetric Catalysis by Chiral Hydrogen-Bond Donors. *Angew. Chem. Int. Ed.* **2006**, *45* (10), 1520–1543. https://doi.org/10.1002/anie.200503132.

(21) Brak, K.; Jacobsen, E. N. Asymmetric Ion-Pairing Catalysis. *Angew. Chem. Int. Ed.* **2013**, *52* (2), 534–561. https://doi.org/10.1002/anie.201205449.

(22) Mahlau, M.; List, B. Asymmetric Counteranion-Directed Catalysis: Concept, Definition, and Applications. *Angew. Chem. Int. Ed.* **2013**, *52* (2), 518–533. https://doi.org/10.1002/anie.201205343.

(23) Hajos, Z. G.; Parrish, D. R. Asymmetric Synthesis of Bicyclic Intermediates of Natural Product Chemistry. *J. Org. Chem.* **1974**, *39* (12), 1615–1621. https://doi.org/10.1021/jo00925a003.

(24) Eder, U.; Sauer, G.; Wiechert, R. New Type of Asymmetric Cyclization to Optically Active Steroid CD Partial Structures. *Angew. Chem. Int. Ed.* **1971**, *10* (7), 496–497. https://doi.org/10.1002/anie.197104961.

(25) List, B.; Lerner, R. A.; Barbas, C. F. Proline-Catalyzed Direct Asymmetric Aldol Reactions. *J. Am. Chem. Soc.* **2000**, *122* (10), 2395–2396. https://doi.org/10.1021/ja994280y.

(26) Ahrendt, K. A.; Borths, C. J.; MacMillan, D. W. C. New Strategies for Organic Catalysis: The First Highly Enantioselective Organocatalytic Diels−Alder Reaction. *J. Am. Chem. Soc.* **2000**, *122* (17), 4243–4244. https://doi.org/10.1021/ja000092s.

(27) Donslund, B. S.; Johansen, T. K.; Poulsen, P. H.; Halskov, K. S.; Jørgensen, K. A. The Diarylprolinol Silyl Ethers: Ten Years After. *Angew. Chem. Int. Ed.* **2015**, *54* (47), 13860–13874. https://doi.org/10.1002/anie.201503920.

(28) Lelais, G.; MacMillan, D. W. C. Modern Strategies in Organic Catalysis: The Advent and Development of Iminium Activation. *Aldrichimica Acta* **2006**, *39* (3), 79–87.

(29) Erkkilä, A.; Majander, I.; Pihko, P. M. Iminium Catalysis. *Chem. Rev.* **2007**, *107* (12), 5416–5470. https://doi.org/10.1021/cr068388p.

(30) Melchiorre, P. Cinchona-Based Primary Amine Catalysis in the Asymmetric Functionalization of Carbonyl Compounds. *Angew. Chem. Int. Ed.* **2012**, *51* (39), 9748–9770. https://doi.org/10.1002/anie.201109036.

(31) Mukherjee, S.; Yang, J. W.; Hoffmann, S.; List, B. Asymmetric Enamine Catalysis. *Chem. Rev.* **2007**, *107* (12), 5471–5569. https://doi.org/10.1021/cr0684016.

(32) Vetica, F.; Figueiredo, R. M. de; Orsini, M.; Tofani, D.; Gasperi, T. Recent Advances in Organocatalytic Cascade Reactions toward the Formation of Quaternary Stereocenters. *Synthesis* **2015**, *47*, 2139–2184. https://doi.org/10.1055/s-0034-1378742.

(33) Bernardi, L.; Fochi, M.; Franchini, M. C.; Ricci, A. Bioinspired Organocatalytic Asymmetric Reactions. *Org. Biomol. Chem.* **2012**, *10* (15), 2911–2922. https://doi.org/10.1039/C2OB07037E.

(34) Doyle, A. G.; Jacobsen, E. N. Small-Molecule H-Bond Donors in Asymmetric Catalysis. *Chem. Rev.* **2007**, *107* (12), 5713–5743. https://doi.org/10.1021/cr068373r.

(35) Alemán, J.; Cabrera, S. Applications of Asymmetric Organocatalysis in Medicinal Chemistry. *Chemical Society Reviews* **2013**, *42* (2), 774–793. https://doi.org/10.1039/C2CS35380F.

(36) Armaroli, N.; Balzani, V. The Future of Energy Supply: Challenges and Opportunities. *Angew. Chem. Int. Ed.* **2007**, *46* (1–2), 52–66. https://doi.org/10.1002/anie.200602373.

(37) Ciamician, G. The Photochemistry of the Future. *Science* **1912**, *36* (926), 385–394. https://doi.org/10.1126/science.36.926.385.

(38) Balzani, V.; Ceroni, P.; Juris, A. *Photochemistry and Photophysics: Concepts, Research, Applications*; John Wiley & Sons, 2014.

(39) Marzo, L.; Pagire, S. K.; Reiser, O.; König, B. Visible-Light Photocatalysis: Does It Make a Difference in Organic Synthesis? *Angew. Chem. Int. Ed.* **2018**, *57* (32), 10034–10072. https://doi.org/10.1002/anie.201709766.

(40) Ischay, M. A.; Anzovino, M. E.; Du, J.; Yoon, T. P. Efficient Visible Light Photocatalysis of [2+2] Enone Cycloadditions. *J. Am. Chem. Soc.* **2008**, *130* (39), 12886–12887. https://doi.org/10.1021/ja805387f.

(41) Narayanam, J. M. R.; Tucker, J. W.; Stephenson, C. R. J. Electron-Transfer Photoredox Catalysis: Development of a Tin-Free Reductive Dehalogenation Reaction. *J. Am. Chem. Soc.* **2009**, *131* (25), 8756–8757. https://doi.org/10.1021/ja9033582.

(42) Shaw, M. H.; Twilton, J.; MacMillan, D. W. C. Photoredox Catalysis in Organic Chemistry. *J. Org. Chem.* **2016**, *81* (16), 6898–6926. https://doi.org/10.1021/acs.joc.6b01449.

(43) Ravelli, D.; Fagnoni, M.; Albini, A. Photoorganocatalysis. What For? *Chem. Soc. Rev.* **2012**, *42* (1), 97–113. https://doi.org/10.1039/C2CS35250H.

(44) Prier, C. K.; Rankic, D. A.; MacMillan, D. W. C. Visible Light Photoredox Catalysis with Transition Metal Complexes: Applications in Organic Synthesis. *Chem. Rev.* **2013**, *113* (7), 5322–5363. https://doi.org/10.1021/cr300503r.

(45) Fagnoni, M.; Dondi, D.; Ravelli, D.; Albini, A. Photocatalysis for the Formation of the C−C Bond. *Chem. Rev.* **2007**, *107* (6), 2725–2756. https://doi.org/10.1021/cr068352x.

(46) Crisenza, G. E. M.; Melchiorre, P. Chemistry Glows Green with Photoredox Catalysis. *Nat Commun* **2020**, *11* (1), 803. https://doi.org/10.1038/s41467-019-13887-8.

(47) Pitre, S. P.; McTiernan, C. D.; Scaiano, J. C. Understanding the Kinetics and Spectroscopy of Photoredox Catalysis and Transition-Metal-Free Alternatives. *Acc. Chem. Res.* **2016**, *49* (6), 1320–1330. https://doi.org/10.1021/acs.accounts.6b00012.

(48) Romero, N. A.; Nicewicz, D. A. Organic Photoredox Catalysis. *Chem. Rev.* **2016**, *116* (17), 10075–10166. https://doi.org/10.1021/acs.chemrev.6b00057.

(49) Amos, S. G. E.; Garreau, M.; Buzzetti, L.; Waser, J. Photocatalysis with Organic Dyes: Facile Access to Reactive Intermediates for Synthesis. *Beilstein J. Org. Chem.* **2020**, *16* (1), 1163–1187. https://doi.org/10.3762/bjoc.16.103.

(50) Grampp, G. G. J. Kavarnos: Fundamentals of Photoinduced Electron Transfer, VCH, Weinheim, New York, 1993, ISBN 3-527-27856-1, 359 Seiten, Preis: DM 132,—. *Berichte der Bunsengesellschaft für physikalische Chemie* **1994**, *98* (10), 1349–1349. https://doi.org/10.1002/bbpc.19940981031.

(51) Albini, A.; Germani, L. Photochemical Methods. In *Handbook of Synthetic Photochemistry*; John Wiley & Sons, Ltd, 2009; pp 1–24. https://doi.org/10.1002/978352AMI7628193.ch1.

(52) *Solar Synthesis: Prospects in Visible Light Photocatalysis*. https://doi.org/10.1126/science.1239176.

(53) Goti, G.; Manal, K.; Sivaguru, J.; Dell'Amico, L. The Impact of UV Light on Synthetic Photochemistry and Photocatalysis. *Nat. Chem.* **2024**, *16* (5), 684–692. https://doi.org/10.1038/s41557-024-01472-6.

(54) Roth, H. D. The Beginnings of Organic Photochemistry. *Angew. Chem. Int. Ed. in English* **1989**, *28* (9), 1193–1207. https://doi.org/10.1002/anie.198911931.

(55) Büchi, G.; Inman, C. G.; Lipinsky, E. S. Light-Catalyzed Organic Reactions. I. The Reaction of Carbonyl Compounds with 2-Methyl-2-Butene in the Presence of Ultraviolet Light. *J. Am. Chem. Soc.* **1954**, *76* (17), 4327–4331. https://doi.org/10.1021/ja01646a024.

(56) Poplata, S.; Tröster, A.; Zou, Y.-Q.; Bach, T. Recent Advances in the Synthesis of Cyclobutanes by Olefin [2 + 2] Photocycloaddition Reactions. *Chem. Rev.* **2016**, *116* (17), 9748–9815. https://doi.org/10.1021/acs.chemrev.5b00723.

(57) Dell'Amico, L.; Fernández-Alvarez, V. M.; Maseras, F.; Melchiorre, P. Light-Driven Enantioselective Organocatalytic β-Benzylation of Enals. *Angew. Chem. Int. Ed.* **2017**, *56* (12), 3304–3308. https://doi.org/10.1002/anie.201612159.

(58) Sánchez-Bento, R.; Roure, B.; Llaveria, J.; Ruffoni, A.; Leonori, D. A Strategy for Ortho-Phenylenediamine Synthesis via Dearomative-Rearomative Coupling of Nitrobenzenes and Amines. *Chem* **2023**, *9* (12), 3685–3695. https://doi.org/10.1016/j.chempr.2023.10.008.

(59) Ruffoni, A.; Hampton, C.; Simonetti, M.; Leonori, D. Photoexcited Nitroarenes for the Oxidative Cleavage of Alkenes. *Nature* **2022**, *610* (7930), 81–86. https://doi.org/10.1038/s41586-022-05211-0.

(60) Mykura, R.; Sánchez-Bento, R.; Matador, E.; Duong, V. K.; Varela, A.; Angelini, L.; Carbajo, R. J.; Llaveria, J.; Ruffoni, A.; Leonori, D. Synthesis of Polysubstituted Azepanes by Dearomative Ring Expansion of Nitroarenes. *Nat. Chem.* **2024**, *16* (5), 771–779. https://doi.org/10.1038/s41557-023-01429-1.

(61) Foster, R. Electron Donor-Acceptor Complexes. *J. Phys. Chem.* **1980**, *84* (17), 2135–2141. https://doi.org/10.1021/j100454a006.

(62) Hildebrand, J. H.; Glascock, B. L. THE COLOR OF IODINE SOLUTIONS. *J. Am. Chem. Soc.* **1909**, *31* (1), 26–31. https://doi.org/10.1021/ja01931a005.

(63) Benesi, H. A.; Hildebrand, J. H. A Spectrophotometric Investigation of the Interaction of Iodine with Aromatic Hydrocarbons. *J. Am. Chem. Soc.* **1949**, *71* (8), 2703–2707. https://doi.org/10.1021/ja01176a030.

(64) Mulliken, R. S. Molecular Compounds and Their Spectra. II. *J. Am. Chem. Soc.* **1952**, *74* (3), 811–824. https://doi.org/10.1021/ja01123a067.

(65) Lima, C. G. S.; De M. Lima, T.; Duarte, M.; Jurberg, I. D.; Paixão, M. W. Organic Synthesis Enabled by Light-Irradiation of EDA Complexes: Theoretical Background and Synthetic Applications. *ACS Catal.* **2016**, *6* (3), 1389–1407. https://doi.org/10.1021/acscatal.5b02386.

(66) Yuan, Y.; Majumder, S.; Yang, M.; Guo, S. Recent Advances in Catalyst-Free Photochemical Reactions via Electron-Donor-Acceptor (EDA) Complex Process. *Tetrahedron Letters* **2020**, *61* (8), 151506. https://doi.org/10.1016/j.tetlet.2019.151506.

(67) Buzzetti, L.; Crisenza, G. E. M.; Melchiorre, P. Mechanistic Studies in Photocatalysis. *Angew. Chem. Int. Ed.* **2019**, *58* (12), 3730–3747. https://doi.org/10.1002/anie.201809984.

(68) Davies, J.; Booth, S. G.; Essafi, S.; Dryfe, R. A. W.; Leonori, D. Visible-Light-Mediated Generation of Nitrogen-Centered Radicals: Metal-Free Hydroimination and Iminohydroxylation Cyclization Reactions. *Angew. Chem. Int. Ed.* **2015**, *54* (47), 14017–14021. https://doi.org/10.1002/anie.201507641.

(69) Cao, Z.-Y.; Ghosh, T.; Melchiorre, P. Enantioselective Radical Conjugate Additions Driven by a Photoactive Intramolecular Iminium-Ion-Based EDA Complex. *Nat Commun* **2018**, *9* (1), 3274. https://doi.org/10.1038/s41467-018-05375-2.

(70) Wu, J.; He, L.; Noble, A.; Aggarwal, V. K. Photoinduced Deaminative Borylation of Alkylamines. *J. Am. Chem. Soc.* **2018**, *140* (34), 10700–10704. https://doi.org/10.1021/jacs.8b07103.

(71) Sandfort, F.; Strieth-Kalthoff, F.; Klauck, F. J. R.; James, M. J.; Glorius, F. Deaminative Borylation of Aliphatic Amines Enabled by Visible Light Excitation of an Electron Donor-Acceptor Complex. *Chemistry* **2018**, *24* (65), 17210–17214. https://doi.org/10.1002/chem.201804246.

(72) Strieth-Kalthoff, F.; James, M. J.; Teders, M.; Pitzer, L.; Glorius, F. Energy Transfer Catalysis Mediated by Visible Light: Principles, Applications, Directions. *Chem. Soc. Rev.* **2018**, *47* (19), 7190–7202. https://doi.org/10.1039/C8CS00054A.

(73) Govindjee; Shevela, D.; Björn, L. O. Evolution of the Z-Scheme of Photosynthesis: A Perspective. *Photosynth Res* **2017**, *133* (1), 5–15. https://doi.org/10.1007/s11120-016-0333-z.

(74) Mandigma, M. J. P.; Kaur, J.; Barham, J. P. Organophotocatalytic Mechanisms: Simplicity or Naïvety? Diverting Reactive Pathways by Modifications of Catalyst Structure, Redox States and

Substrate Preassemblies. *ChemCatChem* **2023**, *15* (11), e202201542. https://doi.org/10.1002/cctc.202201542.

(75) Escudero, D. Revising Intramolecular Photoinduced Electron Transfer (PET) from First-Principles. *Acc. Chem. Res.* **2016**, *49* (9), 1816–1824. https://doi.org/10.1021/acs.accounts.6b00299.

(76) Twilton, J.; Le, C. (Chip); Zhang, P.; Shaw, M. H.; Evans, R. W.; MacMillan, D. W. C. The Merger of Transition Metal and Photocatalysis. *Nat Rev Chem* **2017**, *1* (7), 1–19. https://doi.org/10.1038/s41570-017-0052.

(77) Chan, A. Y.; Perry, I. B.; Bissonnette, N. B.; Buksh, B. F.; Edwards, G. A.; Frye, L. I.; Garry, O. L.; Lavagnino, M. N.; Li, B. X.; Liang, Y.; Mao, E.; Millet, A.; Oakley, J. V.; Reed, N. L.; Sakai, H. A.; Seath, C. P.; MacMillan, D. W. C. Metallaphotoredox: The Merger of Photoredox and Transition Metal Catalysis. *Chem. Rev.* **2022**, *122* (2), 1485–1542. https://doi.org/10.1021/acs.chemrev.1c00383.

(78) Juris, A.; Balzani, V.; Barigelletti, F.; Campagna, S.; Belser, P.; von Zelewsky, A. Ru(II) Polypyridine Complexes: Photophysics, Photochemistry, Eletrochemistry, and Chemiluminescence. *Coordination Chemistry Reviews* **1988**, *84*, 85–277. https://doi.org/10.1016/0010-8545(88)80032-8.

(79) Juris, A.; Gandolfi, M. T.; Manfrin, M. F.; Balzani, V. Electron and Energy Transfer Mechanisms in the Quenching of the Tris(2,2'-Bipyridine)Ruthenium(II) Luminescence by Cyanide Complexes. *J. Am. Chem. Soc.* **1976**, *98* (4), 1047–1048. https://doi.org/10.1021/ja00420a046.

(80) Schweitzer-Chaput, B.; Horwitz, M. A.; de Pedro Beato, E.; Melchiorre, P. Photochemical Generation of Radicals from Alkyl Electrophiles Using a Nucleophilic Organic Catalyst. *Nature Chem* **2019**, *11* (2), 129–135. https://doi.org/10.1038/s41557-018-0173-x.

(81) Vega-Peñaloza, A.; Mateos, J.; Companyó, X.; Escudero-Casao, M.; Dell'Amico, L. A Rational Approach to Organo-Photocatalysis: Novel Designs and Structure-Property Relationships. *Angew. Chem. Int. Ed.* **2021**, *60* (3), 1082–1097. https://doi.org/10.1002/anie.202006416.

(82) Nicewicz, D. A.; Nguyen, T. M. Recent Applications of Organic Dyes as Photoredox Catalysts in Organic Synthesis. *ACS Catal.* **2014**, *4* (1), 355–360. https://doi.org/10.1021/cs400956a.

(83) Yoon, T. P.; Ischay, M. A.; Du, J. Visible Light Photocatalysis as a Greener Approach to Photochemical Synthesis. *Nature Chem* **2010**, *2* (7), 527–532. https://doi.org/10.1038/nchem.687.

(84) Capaldo, L.; Ravelli, D. Hydrogen Atom Transfer (HAT): A Versatile Strategy for Substrate Activation in Photocatalyzed Organic Synthesis. *European Journal of Organic Chemistry* **2017**, *2017* (15), 2056–2071. https://doi.org/10.1002/ejoc.201601485.

(85) Capaldo, L.; Ravelli, D.; Fagnoni, M. Direct Photocatalyzed Hydrogen Atom Transfer (HAT) for Aliphatic C–H Bonds Elaboration. *Chem. Rev.* **2022**, *122* (2), 1875–1924. https://doi.org/10.1021/acs.chemrev.1c00263.

(86) Juliá, F.; Constantin, T.; Leonori, D. Applications of Halogen-Atom Transfer (XAT) for the Generation of Carbon Radicals in Synthetic Photochemistry and Photocatalysis. *Chem. Rev.* **2022**, *122* (2), 2292–2352. https://doi.org/10.1021/acs.chemrev.1c00558.

(87) Rehm, D.; Weller, A. Kinetics of Fluorescence Quenching by Electron and H-Atom Transfer. *Israel Journal of Chemistry* **1970**, *8* (2), 259–271. https://doi.org/10.1002/ijch.197000029.

(88) Farid, S.; Dinnocenzo, J. P.; Merkel, P. B.; Young, R. H.; Shukla, D.; Guirado, G. Reexamination of the Rehm–Weller Data Set Reveals Electron Transfer Quenching That Follows a Sandros–Boltzmann Dependence on Free Energy. *J. Am. Chem. Soc.* **2011**, *133* (30), 11580–11587. https://doi.org/10.1021/ja2024367.

(89) Marcus, R. A. Electron Transfer Reactions in Chemistry. Theory and Experiment. *Rev. Mod. Phys.* **1993**, *65* (3), 599–610. https://doi.org/10.1103/RevModPhys.65.599.

(90) Job, P. Formation and stability of inorganic complexes in solution. *Ann. Chim. Appl.* 1928, *9*, 113-203.

(91) Kroto, H. W.; Heath, J. R.; O'Brien, S. C.; Curl, R. F.; Smalley, R. E. C60: Buckminsterfullerene. *Nature* **1985**, *318* (6042), 162–163. https://doi.org/10.1038/318162a0.

(92) Yan, Q.-L.; Gozin, M.; Zhao, F.-Q.; Cohen, A.; Pang, S.-P. Highly Energetic Compositions Based on Functionalized Carbon Nanomaterials. *Nanoscale* **2016**, *8* (9), 4799–4851. https://doi.org/10.1039/C5NR07855E.

(93) Tasis, D.; Tagmatarchis, N.; Bianco, A.; Prato, M. Chemistry of Carbon Nanotubes. *Chem. Rev.* **2006**, *106* (3), 1105–1136. https://doi.org/10.1021/cr050569o.

(94) Novoselov, K. S.; Geim, A. K.; Morozov, S. V.; Jiang, D.; Zhang, Y.; Dubonos, S. V.; Grigorieva, I. V.; Firsov, A. A. Electric Field Effect in Atomically Thin Carbon Films. *Science* **2004**, *306* (5696), 666–669. https://doi.org/10.1126/science.1102896.

(95) Xu, X.; Ray, R.; Gu, Y.; Ploehn, H. J.; Gearheart, L.; Raker, K.; Scrivens, W. A. Electrophoretic Analysis and Purification of Fluorescent Single-Walled Carbon Nanotube Fragments. *J. Am. Chem. Soc.* **2004**, *126* (40), 12736–12737. https://doi.org/10.1021/ja040082h.

(96) Zhu, S.; Zhang, J.; Qiao, C.; Tang, S.; Li, Y.; Yuan, W.; Li, B.; Tian, L.; Liu, F.; Hu, R.; Gao, H.; Wei, H.; Zhang, H.; Sun, H.; Yang, B. Strongly Green-Photoluminescent Graphene Quantum Dots for Bioimaging Applications. *Chem. Commun.* **2011**, *47* (24), 6858–6860. https://doi.org/10.1039/C1CC11122A.

(97) Campisciano, V.; Gruttadauria, M.; Giacalone, F. Modified Nanocarbons for Catalysis. *ChemCatChem* **2019**, *11* (1), 90–133. https://doi.org/10.1002/cctc.201801414.

(98) Campisciano, V.; Gruttadauria, M.; Giacalone, F. Modified Nanocarbons as Catalysts in Organic Processes. In *Catalyst Immobilization*; John Wiley & Sons, Ltd, 2020; pp 77–113. https://doi.org/10.1002/9783527817290.ch3.

(99) Vázquez, E.; Giacalone, F.; Prato, M. Non-Conventional Methods and Media for the Activation and Manipulation of Carbon Nanoforms. *Chem. Soc. Rev.* **2013**, *43* (1), 58–69. https://doi.org/10.1039/C3CS60164A.

(100) Martín, N. Carbon Nanoforms for Photovoltaics: Myth or Reality? *Advanced Energy Materials* **2017**, *7* (10), 1601102. https://doi.org/10.1002/aenm.201601102.

(101) Reina, G.; González-Domínguez, J. M.; Criado, A.; Vázquez, E.; Bianco, A.; Prato, M. Promises, Facts and Challenges for Graphene in Biomedical Applications. *Chem. Soc. Rev.* **2017**, *46* (15), 4400–4416. https://doi.org/10.1039/C7CS00363C.

(102) Semeniuk, M.; Yi, Z.; Poursorkhabi, V.; Tjong, J.; Jaffer, S.; Lu, Z.-H.; Sain, M. Future Perspectives and Review on Organic Carbon Dots in Electronic Applications. *ACS Nano* **2019**, *13* (6), 6224–6255. https://doi.org/10.1021/acsnano.9b00688.

(103) Lai, X.; Goodman, D. W. Structure–Reactivity Correlations for Oxide-Supported Metal Catalysts: New Perspectives from STM. *Journal of Molecular Catalysis A: Chemical* **2000**, *162* (1), 33–50. https://doi.org/10.1016/S1381-1169(00)00320-4.

(104) Günter, M. M.; Ressler, T.; Jentoft, R. E.; Bems, B. Redox Behavior of Copper Oxide/Zinc Oxide Catalysts in the Steam Reforming of Methanol Studied by *in Situ* X-Ray Diffraction and Absorption Spectroscopy. *Journal of Catalysis* **2001**, *203* (1), 133–149. https://doi.org/10.1006/jcat.2001.3322.

(105) Schlögl, R.; Abd Hamid, S. B. Nanocatalysis: Mature Science Revisited or Something Really New? *Angew. Chem. Int. Ed.* **2004**, *43* (13), 1628–1637. https://doi.org/10.1002/anie.200301684.

(106) Philippot, K.; Serp, P. Concepts in Nanocatalysis. In *Nanomaterials in Catalysis*; John Wiley & Sons, Ltd, 2013; pp 1–54. https://doi.org/10.1002/9783527656875.ch1.

(107) Simon, M.-O.; Li, C.-J. Green Chemistry Oriented Organic Synthesis in Water. *Chem. Soc. Rev.* **2012**, *41* (4), 1415–1427. https://doi.org/10.1039/C1CS15222J.

(108) Egorova, K. S.; Ananikov, V. P. Which Metals Are Green for Catalysis? Comparison of the Toxicities of Ni, Cu, Fe, Pd, Pt, Rh, and Au Salts. *Angew. Chem. Int. Ed.* **2016**, *55* (40), 12150–12162. https://doi.org/10.1002/anie.201603777.

(109) Horváth, I. T. Introduction: Sustainable Chemistry. *Chem. Rev.* **2018**, *118* (2), 369–371. https://doi.org/10.1021/acs.chemrev.7b00721.

(110) Gentile, G.; Mamone, M.; Rosso, C.; Amato, F.; Lanfrit, C.; Filippini, G.; Prato, M. Tailoring the Chemical Structure of Nitrogen-Doped Carbon Dots for Nano-Aminocatalysis in Aqueous Media. *ChemSusChem* **2023**, *16* (7), e202202399. https://doi.org/10.1002/cssc.202202399.

(111) Rosso, C.; Filippini, G.; Prato, M. Carbon Dots as Nano-Organocatalysts for Synthetic Applications. *ACS Catal.* **2020**, *10* (15), 8090–8105. https://doi.org/10.1021/acscatal.0c01989.

(112) Jeon, I.-Y.; Noh, H.-J.; Baek, J.-B. Nitrogen-Doped Carbon Nanomaterials: Synthesis, Characteristics and Applications. *Chemistry – An Asian Journal* **2020**, *15* (15), 2282–2293. https://doi.org/10.1002/asia.201901318.

(113) Filippini, G.; Amato, F.; Rosso, C.; Ragazzon, G.; Vega-Peñaloza, A.; Companyó, X.; Dell'Amico, L.; Bonchio, M.; Prato, M. Mapping the Surface Groups of Amine-Rich Carbon Dots Enables Covalent Catalysis in Aqueous Media. *Chem* **2020**, *6* (11), 3022–3037. https://doi.org/10.1016/j.chempr.2020.08.009.

(114) Corti, V.; Bartolomei, B.; Mamone, M.; Gentile, G.; Prato, M.; Filippini, G. Amine-Rich Carbon Dots as Novel Nano-Aminocatalytic Platforms in Organic Synthesis. *European Journal of Organic Chemistry* **2022**, *2022* (41), e202200879. https://doi.org/10.1002/ejoc.202200879.

(115) Kang, Z.; Lee, S.-T. Carbon Dots: Advances in Nanocarbon Applications. *Nanoscale* **2019**, *11* (41), 19214–19224. https://doi.org/10.1039/C9NR05647E.

(116) Gisbertz, S.; Pieber, B. Heterogeneous Photocatalysis in Organic Synthesis. *ChemPhotoChem* **2020**, *4* (7), 456–475. https://doi.org/10.1002/cptc.202000014.

(117) Liu, G.; Zhen, C.; Kang, Y.; Wang, L.; Cheng, H.-M. Unique Physicochemical Properties of Two-Dimensional Light Absorbers Facilitating Photocatalysis. *Chemical Society Reviews* **2018**, *47* (16), 6410–6444. https://doi.org/10.1039/C8CS00396C.

(118) Hutton, G. A. M.; Martindale, B. C. M.; Reisner, E. Carbon Dots as Photosensitisers for Solar-Driven Catalysis. *Chem. Soc. Rev.* **2017**, *46* (20), 6111–6123. https://doi.org/10.1039/C7CS00235A.

(119) Friedmann, D.; Hakki, A.; Kim, H.; Choi, W.; Bahnemann, D. Heterogeneous Photocatalytic Organic Synthesis: State-of-the-Art and Future Perspectives. *Green Chemistry* **2016**, *18* (20), 5391–5411. https://doi.org/10.1039/C6GC01582D.

(120) Zdražil, L.; Cadranel, A.; Medved, M.; Otyepka, M.; Zbořil, R.; Guldi, D. M. Designing Carbon Dots for Enhanced Photo-Catalysis: Challenges and Opportunities. *Chem* **2024**, *10* (9), 2700–2723. https://doi.org/10.1016/j.chempr.2024.07.018.

(121) Sbacchi, M.; Mamone, M.; Morbiato, L.; Gobbo, P.; Filippini, G.; Prato, M. Shining Light on Carbon Dots: New Opportunities in Photocatalysis. *ChemCatChem* **2023**, *15* (16), e202300667. https://doi.org/10.1002/cctc.202300667.

(122) Wang, Y.; Wang, X.; Antonietti, M. Polymeric Graphitic Carbon Nitride as a Heterogeneous Organocatalyst: From Photochemistry to Multipurpose Catalysis to Sustainable Chemistry. *Angew. Chem. Int. Ed.* **2012**, *51* (1), 68–89. https://doi.org/10.1002/anie.201101182.

(123) Bartolomei, B.; Dosso, J.; Prato, M. New Trends in Nonconventional Carbon Dot Synthesis. *Trends in Chemistry* **2021**, *3* (11), 943–953. https://doi.org/10.1016/j.trechm.2021.09.003.

Chapter 2.

Tailoring the Chemical Structure of Nitrogen-Doped Carbon Dots for Nano-Aminocatalysis in Aqueous Media

Abstract

This Chapter discusses the development and production of novel and increasingly active amine-rich carbon dots (NCDs)-based catalysts capable of promoting a wide range of aminocatalytic transformations. Specifically, a new family of NCDs was prepared using amino acid *L-arginine* (Arg) along with different alkyl diamines with progressively longer carbon skeletons, as molecular precursors. The main objective of this project was to determine how the chemical nature of starting materials influences the catalytic performances of such nanoparticles in different enamine and iminium ion activated model reactions. The best performing NCDs, obtained by using 1,4-butanediamine (BDA) and Arg as starting materials, were employed to drive various organic reactions in water, including aldol reactions, Michael additions, Knoevenagel condensations, Mannich alkylations and Tandem Knoevenagel-Michael reactions.

This work was conducted in the carbon nanotechnology group at the University of Trieste. The project was supervised and conceived by *Prof. Maurizio Prato* and *Dr Giacomo Filippini. Dr Giuseppe Gentile*, *Dr Francesco Amato* and *Mrs Chiara Lanfrit* collaborated in the preparation of the NCDs. *Dr Cristian Rosso* helped to perform the catalytic experiments. A significant part of this work was published in 2023 under the title: "Tailoring the Chemical Structure of Nitrogen-Doped Carbon Dots for Nano-Aminocatalysis in Aqueous Media".[1] Besides, a concept article titled "Amine-Rich Carbon Dots as Novel Nano-Aminocatalytic Platforms in Organic Synthesis" published in 2022 served as a base for this chapter introduction.[2]

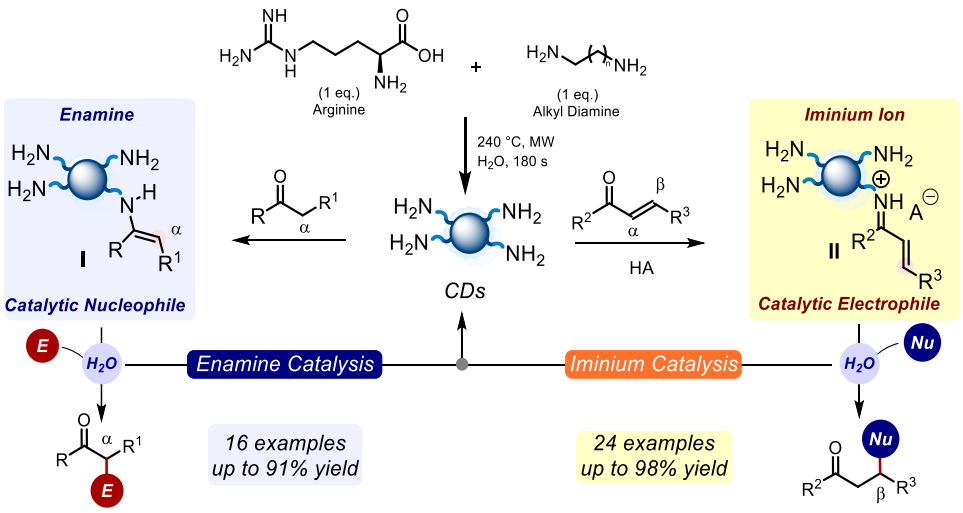

2.1 Introduction

2.1.1 Carbon Dots in Organocatalysis

Carbon dots (CDs) are fascinating core-shell quasi-spherical nanoparticles characterized by sizes below 10 nm and peculiar physicochemical properties.[3–5] Figure 2.1 illustrates the structure of CDs composed of a carbon core and a shell with different functional groups, such as carboxylic acids, alcohols, and amines, derived from the compounds employed in the synthesis.[2,6–8] Interestingly, their molecular-like behaviour can address CDs as the missing link between the molecular and nanoscale world. Numerous studies have highlighted the excellent luminescence and optical features, high chemical and photostability, low toxicity and good biocompatibility of CDs as well as their optimal dispersibility in aqueous and polar solvents.[9,10] These features make CDs highly versatile for applications ranging from bioimaging and electronics to catalysis.[11–14]

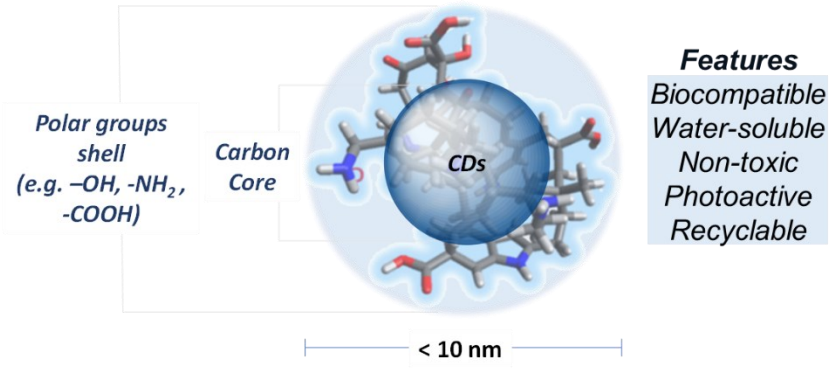

Figure 2.1 Schematic representation of CDs cores, surface functionalities, and main characteristics.

CDs can be synthesized through simple and robust *bottom-up* synthetic protocols from inexpensive and abundant molecular precursors.[15,16] The *bottom-up* approach is particularly versatile due to the wide array of available molecular precursors, vast choices of thermal treatments (*e.g.,* hydrothermal, pyrolysis, electrochemical) and relatively short reaction times.[5,17,18] Furthermore, the use of molecular precursors allows the structure and properties of the CDs to reflect those of the starting materials.[19–21] For example, functional groups contained in the starting materials might be present in the resulting CDs. As an example, incorporating heteroatom-containing compounds in the synthesis of CDs is a known strategy to enhance their photochemical and physical properties, finding application in energy storage, photocatalysis or bio-imaging.[22] In this regard, it was reported the *bottom-up* growth of nitrogen-doped carbon quantum dots (CQDs) from citric acid and

ammonia, resulting in enhanced quantum yield,[23] while glucose and *p*-sulfonic acid calix[4]arene have been used to produce sulfur-doped CQDs with excellent colloidal stability in aqueous media.[23] Moreover, post-functionalization treatments are often employed to achieve precise control over CDs' surface structure.[6,24] For instance, MacFarlane and colleagues reported the preparation in two steps of sulfonated CDs for photocatalytic purposes. The carbonaceous core of these nanoparticles was prepared by electrochemical ablation of graphite rods in water (15−60 V for 6 days). After their purification, the sulfur decoration was introduced using sulfuric acid in water (1:1 v/v, 60°C for 24 h) to afford CDs which bear hydrosulfate groups on their surface.[25]

However, a straight and precise control of CDs' surfaces during their synthesis remains a significant challenge. In catalysis, fine-tuning CDs' surface functionalities is crucial for achieving nano-catalytic platforms. In this field, CDs are therefore emerging as promising nanocatalytic platforms that fulfill the sustainability requirements of nontoxic, water-compatible, readily available, and potentially recyclable catalysts for green chemical production.[12,26] Most examples of CDs catalytic applications include the use of surface moieties as catalytic sites to promote organic reactions. For example, CDs bearing carboxylic moieties have been used to deliver *aza*-Michael adducts and quinazolinones derivatives.[27] Likewise, hydroxyl rich carbon quantum dots have catalysed multi-component condensation reactions between naphthols, aldehydes and malononitriles in micelles in water.[28] Additionally, amine-rich carbon dots (NCDs) have been reported to catalyse Knoevenagel condensation reactions between aldehydes and malononitriles.[29] In particular, the presence of primary and secondary amines on the NCD surfaces can activate a large number of carbonyl compounds. These nanostructures pave the way for the development of a novel class of nano catalytic material capable of driving different aminocatalytic reactions.

The next section will discuss various examples of the synthesis, characterization and application of CDs bearing surface amine groups for organocatalytic applications.

2.1.2 (Nano)Aminocatalysis

Aminocatalysis is a class, arguably the most studied, of organocatalysis. Thanks to the pioneering work of Benjamin List and David W.C. Mac Millan, who were awarded the Nobel Prize in Chemistry in 2021, the basis for two novel generic activation modes of carbonyl compounds was established.[30,31] Both methods involve covalent intermediates transiently generated upon condensation of amines with aldehydes or ketones.[32] In particular, one aminocatalytic intermediate,

namely enamine, consists of the condensation of an amine with an α-enolizable carbonyl compound followed by tautomeric equilibrium to generate its enamine derivative with increased nucleophilicity. Thus, the intermediate can react with an electrophile.[33] Conversely, an aminocatalyst can condense with an α,β-unsaturated carbonyl compound in acidic conditions to produce an iminium ion species. Consequently, a nucleophilic attack is favourite to the β-carbon of the iminium ion intermediate.[34]

Considering the broad potentialities of aminocatalysis to produce valuable compounds, some groups recently investigated the use of amine-rich CDs (NCDs) as nano-catalytic platforms for a wide range of organic reactions. In these cases, the surface amino groups can mimic the chemical behaviour of classical molecular aminocatalysts, thus paving the way for the application of harmless, easy-to-prepare, and potentially recyclable NCDs based catalysts in environmentally benign solvents. A few examples are highlighted below.

Kalhor and co-workers reported the use of nitrogen-doped CDs to catalyse organic reactions.[35] The nanoparticles NCDs-A were prepared from CA and L-lysine (Lys) that was selected because of its long carbon chain terminated with a primary amine. This aspect was supposed to increase the catalytic activity of NCDs-A because of the long chain which renders the primary amine more accessible for the substrate activation. More specifically, NCDs-A were employed in the nucleophilic substitution of urea with (hetero)aromatic and aliphatic amines at 60°C in choline chloride/urea as a deep eutectic solvent (DES) system (Figure 2.2a). The reaction scope with primary amines produced monosubstituted ureas in yields ranging from 45% to 93%.

In 2020, our group reported the use of NCDs-B to promote a series of aminocatalytic transformations in water media (Figure 2.2b).[19] The amine-rich nanoparticles were prepared following a hydrothermal microwave treatment using L-Arg and ethylenediamine (EDAm) in water. The amines on the surface of the NCDs-B were exploited to generate iminium ion intermediates to drive Michael addition reactions. Specifically, the reaction between α,β-unsaturated carbonyl compounds with different nucleophiles in the presence of benzoic acid in water afforded functionalised products from good to excellent yields. Furthermore, NCDs-B could activate isatine derivatives *via* enamine catalysis reacting with various ketones affording corresponding products in very good yields (up to 96%). Importantly, fluorine nuclear magnetic resonance (NMR) analysis was used for the detection of the iminium ion intermediates on the surface of NCDs-B, due to the high

sensitivity of the fluorine nucleus. Within this valuable technique, it is possible to identify and quantify the reactive intermediates on the NCDs-B, after the reaction between the fluorinated probe 4-fluorocinnamaldehyde and the surface primary amines on NCDs-B. Moreover, the asymmetric catalytic aldolic transformation was successfully performed using chiral NCDs-C. The corresponding product between the addition of acetone and isatine was obtained in 59% yield and 38% *ee* (Figure 2.2c). NCDs-C with chiral amines were obtained from L-Arg and (*S*,*S*)-1,2-cyclohexanediamine ((*S*,*S*)-CyHDA). This study represented one of the first examples of asymmetric synthesis using NCDs, conveying the chirality of the carbon-based nanoparticle to the desired products.[19]

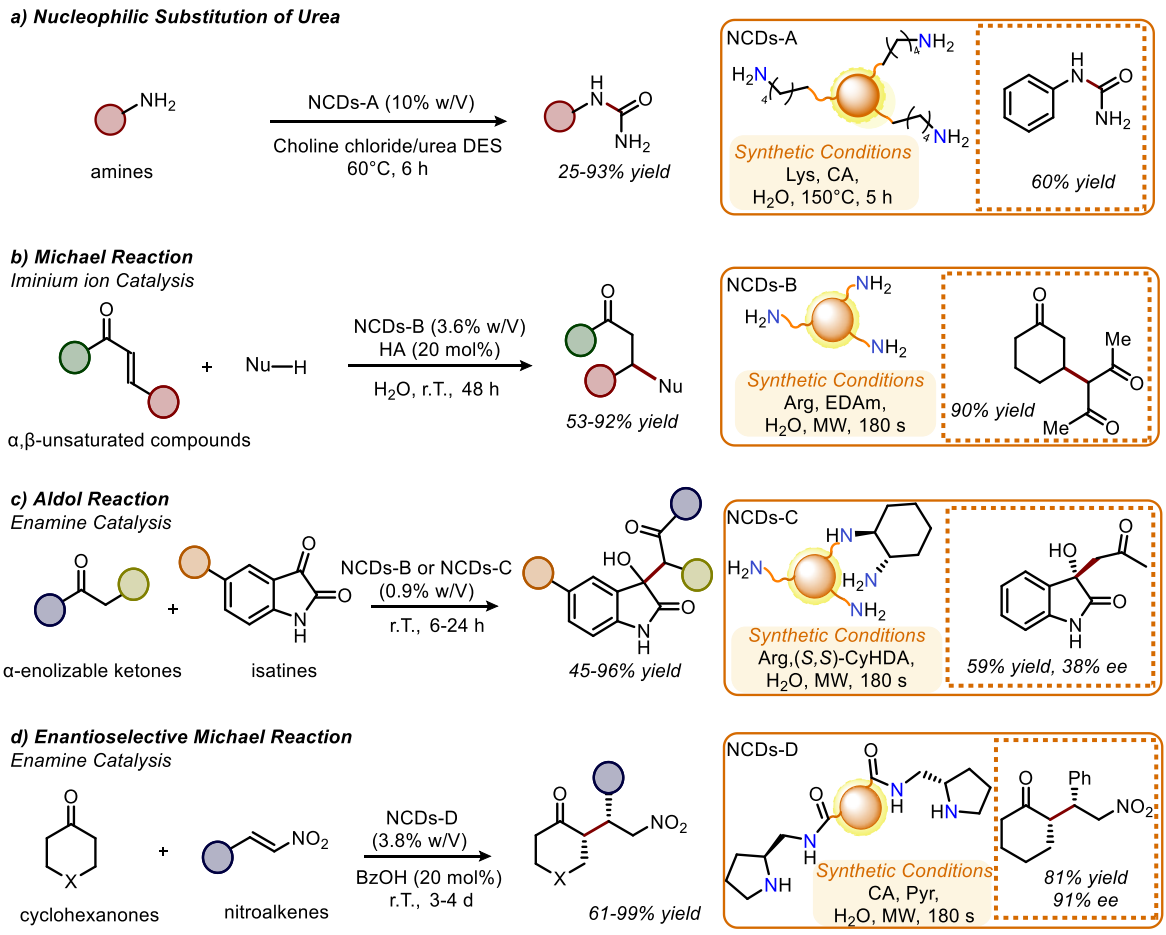

Figure 2.2 Examples of applications of NCDs as aminocatalysts: a) Nucleophilic Substitution of Urea, b) Michael Reaction, c) (Enantioselective) Aldol Reaction, d) Enantioselective Michael Reaction.

Recently, new chiral carbon-dots have been synthetized as multivalent catalysts by our group.[36] The nanoparticles (NCDs-D) were prepared from citric acid (CA) and (*S*)-2-(aminomethyl)-1-boc-pyrrolidine (Pyr). The secondary amine was chosen because the configurational stability of amine

would protect the stereochemical information during the synthetic process, thereby producing chiral nanoparticles. Additionally, a variety of chiral organocatalysts are reported to have the pyrrolidine scaffold. The number of secondary amines was quantified through a post-synthetic strategy using the reductive amination reaction. The functionalization of the NCDs-D using 3,5-bis(trifluoromethyl)benzaldehyde as a fluorinated probe in the presence of $NaCNBH_3$ allowed the formation of fluorinated nanoparticles. The quantification of the reactive surface amines utilizing ^{19}F-NMR and an internal standard, resulted to be around 300 µmol/g. The NCDs-D were applied for enantioselective aldol reaction between cyclohexanone and 4-nitrobenzaldehyde and Michael addition reaction of cyclohexanone and nitroalkenes affording desired products in good yields (Figure 2.2d).

2.2 Aim of the Project

In recent years, CDs have garnered significant attention in nanomaterials science. However, a clear understanding of the mechanistic process of carbon dots has yet to be achieved. To fill this gap, we aimed to establish a correlation between the synthetic design of CDs surface groups and their catalytic performances towards various aminocatalytic reactions.

Specifically, we prepared a library of amine-rich carbon dots (NCDs) using a *bottom-up* approach starting from amino acids along with different alkyl diamines (DAs) with progressively longer carbon skeletons. Different nanoparticles were obtained with customized features (*i.e.,* superficial amines on NCDs) depending on the changing factor in each synthesis (*i.e.,* the length of the carbon backbone of the diamine used).

It has been demonstrated that the accessibility of amine moieties on the nanoparticles is influenced by the dialkylamines, which are crucial for their catalytic applications. A comprehensive scope study was carried out to explore the catalytic relevance of these NCDs, exploiting iminium ion and enamine intermediates.

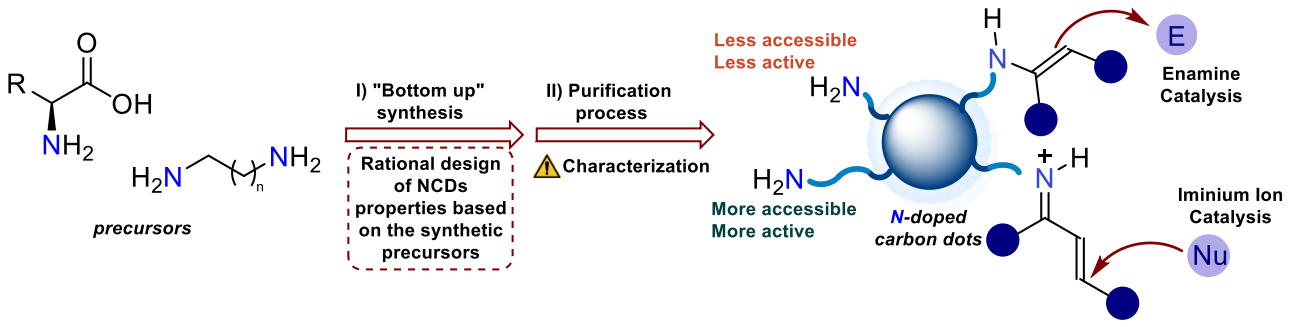

Figure 2.3 Illustration of the aim of the project on the synthesis and catalytic application of nitrogen-doped carbon dots.

2.3 Results and Discussion

2.3.1 Synthesis and Characterization of NCDs

The preparation of NCDs-**1**-**4** consists of a simple and robust synthetic methodology,[37] which can be schematized as follows: (*i*) microwave-assisted (MW) hydrothermal treatment of the molecular precursor/s at 240°C for 180 s; (*ii*) filtration of the crude reaction through a polytetrafluoroethylene (PTFE) membrane to eliminate large carbon particles and insoluble organic compounds (pore size of 0.1 µm); (*iii*) dialysis against milli-Q water to remove soluble molecular species; (*iv*) freeze-drying process to obtain the purified nanoparticles as yellowish solid materials.

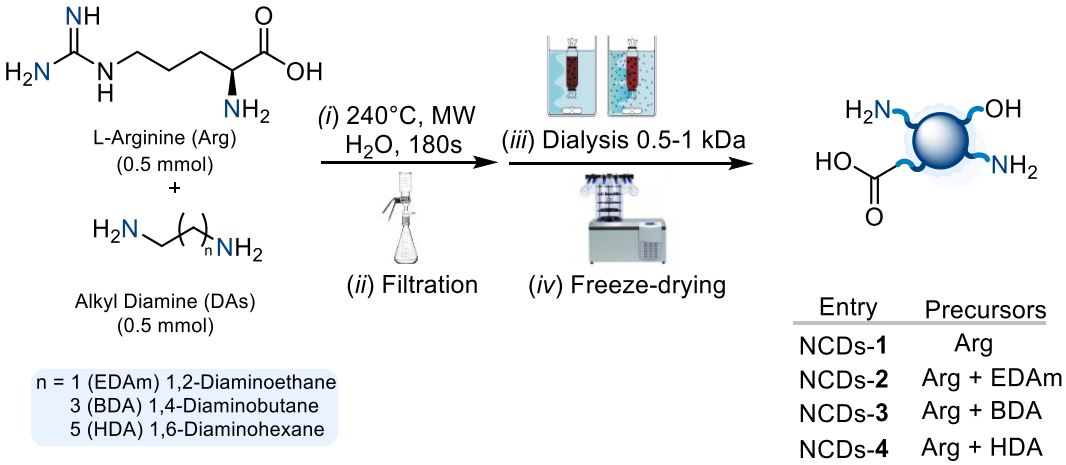

*Figure 2.4 Synthesis and purification of NCDs-**1**-**4** starting from L-arginine (Arg) and different alkyl diamines (DAs)*

In particular, NCDs-**1** were obtained from a mono-component synthetic procedure using Arg while NCDs-**2**-**4** were synthetised from Arg and different DAs (1:1 molar ratio), namely EDAm, BDA, and 1,6-diaminohexane (HDA), as nitrogen-doping agents (Figure 2.4). Specifically, we questioned which impact DAs might have on the amount and availability of amine surface groups. Arg was reported to

play a crucial role in templating the overall core-shell motifs, while diamines may mainly affect the chemical structure of external shells.[22,38]

The mass yields of the purified NCDs (calculated as the percentage of the weight of the starting materials retained in the purified NCDs) reveal half of the amount of the starting material (Arg) converted into NCDs-**1** while a decrease in the mass yields of NCDs-2-4 is shown for the bi-component synthesis (Figure 2.5a). A longer carbon chain of the DA in the synthesis progressively reduces the mass yields probably due to the correlation between the microwave heating and the less polarity of the reaction mixtures. Precisely, longer aliphatic DAs are low polar molecules with a lower dielectric constant. They decreased the efficiency of the heat transfer in the reaction vessel hindering the formation of the NCDs.[39]

Firstly, the removal of starting materials and by-products from the nanoparticles is a critical step during the purification process.[21,40] Consequently, the effective purification of the nanoparticles must be checked by NMR analysis.[41]

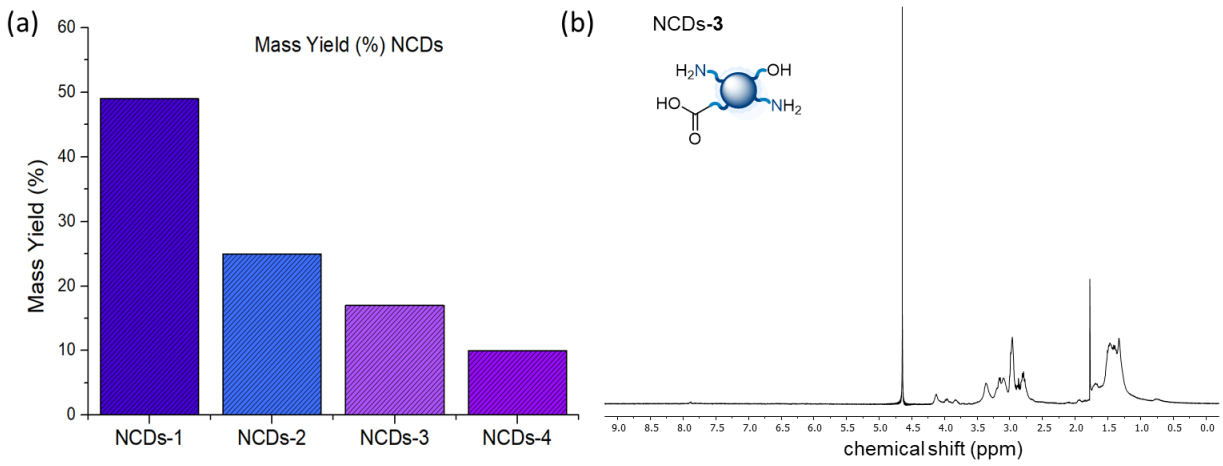

*Figure 2.5 a) Mass yield histogram for NCDs-**1**-**4**; b) ^{1}H-NMR recorded in D_2O of NCDs-**3**.*

Figure 2.5 shows the ^{1}H-NMR recorded in D_2O of NCDs-**3** as a representative example (^{1}H-NMR spectra of other NCDs are found in Figure 2.19). A set of broad signals established the formation of the nanomaterial without any molecular impurities, typically identified by sharp peaks. Hence, the ^{1}H-NMR spectrum evidences the successful purification of molecular species. At this point, a deep evaluation of the structures of the NCDs-**1**-**4** was complemented by extensive characterizations.

Information on NCDs-**1**-**4** was gathered by thermogravimetric analysis (TGA), atomic force microscopy (AFM) and attenuated total reflectance-Fourier-transform infrared spectroscopy (ATR-FTIR). TGA proved the largely amorphous nature of NCDs-**1**-**4**. In fact, around 90% of the total weight loss of NCDs-**2**-**4** was recorded under nitrogen at 600°C, while NCDs-**1** had slightly higher thermal stability (Figure 2.31, see section 2.5.3). AFM analysis confirmed the nano-scale dimensions of the NCDs-**1**-**4**, which range from 2 to 4 nm. In Figure 2.6b, AFM image of NCDs-**3** is presented as a model.

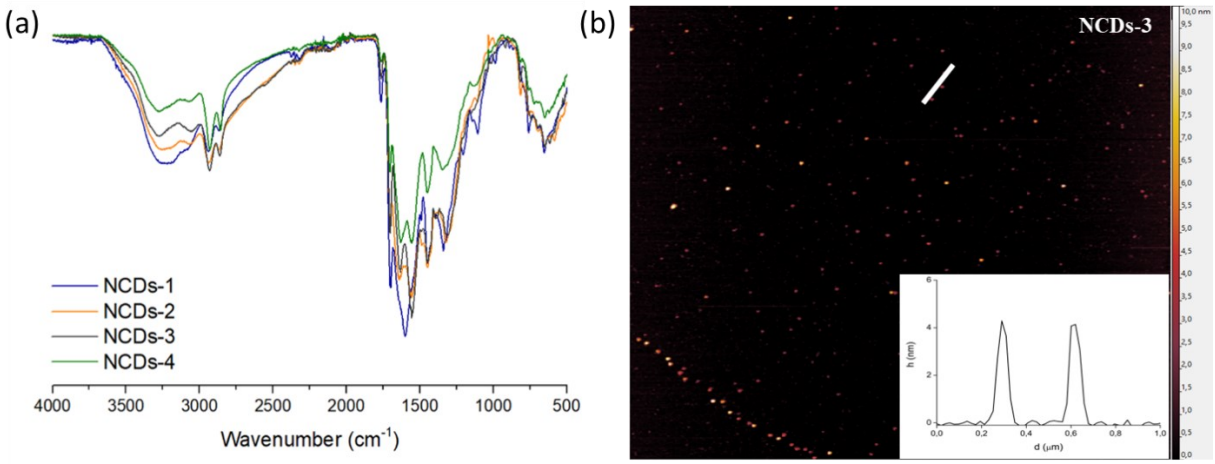

*Figure 2.6 a) Stacked ATR-FTIR spectra of NCDs-**1**-**4**; b) Tapping mode AFM of NCDs-**3** deposited on a mica substrate; inset: height profile along the white solid line.*

ATR-FTIR identified the N-H and O-H stretching from 3000 to 3400 cm^{-1} and a strong band at 1540 cm^{-1} which corresponds to the bending of the primary amide (Figure 2.6a). These bonds can be generated during the NCD synthesis through amines condensation with carboxylic acids. The quantification of these amide groups was delivered by Bicinchoninic acid essay, a widely used colorimetric method to determine the concentration of peptide bonds in a protein solution.[42] In this test, Cu (II) is reduced selectively, in an alkaline buffer, to Cu (I) by the amide bonds.[43] Subsequently, Cu(I) cations are chelated by two bicinchoninic acid moieties forming a tetrahedral complex that absorbs at around 562 nm. By knowing the molar extinction coefficient of the coloured metal complex formed, it is possible to quantify the concentration of amide bonds present on the NCDs. Interestingly, the number of amide bonds decreases when the DAs are introduced in the synthesis (Figure 2.7).

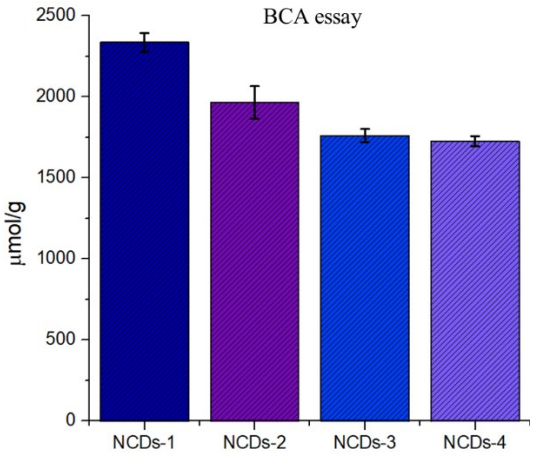

*Figure 2.7 BCA assay results for NCDs-**1**-**4**. BCA: Bicinchoninic acid*

Moreover, the number of amides goes from 2340±60 µmol/g for NCDs-**1** to 1720±30 µmol/g for NCDs-**4**. To further assess the surface moieties on the NCDs, the intrinsic pH of the water-soluble nanoparticles was evaluated by dissolving NCDs-**1**-**4** in milli-Q water (concentration of 2.5 mgmL^{-1}). For all NCDs the measured intrinsic pH was alkaline ranging from 9 up to 10. Notably, the alkalinity increased progressively from NCDs-**1** to NCDs-**4**.

Consequently, the quantification of the total number of acid/base sites was established by Gran Plot analysis, which involves the linearization of a pH back titration curve.

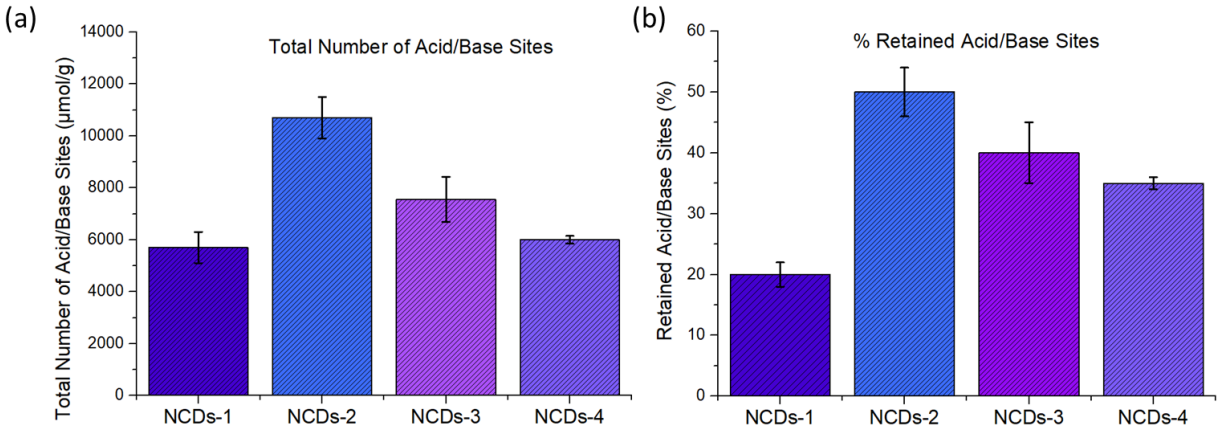

*Figure 2.8 a) Total number of acid/base sites obtained from back titration of NCDs-**1**-**4**; b) Retained percentage histogram of acid/base sites.*

The number of acid/base sites varies depending on the NCDs, from a minimum of 5700±600 µmol/g for NCDs-**1** to a maximum of 10700±800 µmol/g for NCDs-**2** (Figure 2.8a). Moreover, the percentage of acid/base sites retained on the NCDs surfaces from the initial precursors was calculated. Up to 50% of acid/base moieties of the starting materials are missing during the synthesis of the NCDs-**1**-

4 due to different phenomena such as decarboxylation reactions, dehydration, the formation of amide bonds and the appearance of molecular side-products. Generally, a sharp increase of the retained sites in the bicomponent synthesis was observed in comparison to the mono-component approach. Indeed, the absolute number of sites retained and their percentage decrease consistently with the increase in the length of the diamine carbon chain (Figure 2.8b). Interestingly, a clear correlation can be perceived between the total number of acid/base sites, the percentage of retained sites, and the length of the DA used. To get more information about the nature of the surface groups, agarose gel electrophoresis was carried out. The test in a citrate buffer (pH = 4) revealed the migration of NCDs-**1**-**4** toward the cathode in uniform blue emissive bands under UV-light irradiation indicating the positive charge of the nanoparticles. This result could be a further proof of the presence of protonated amino surface groups. Furthermore, the staining of the agarose gel with Coomassie brilliant blue dye gave the same outcome with the appearance of blue spots where NCDs were previously detected in the electrophoresis analysis (Figure 2.9).

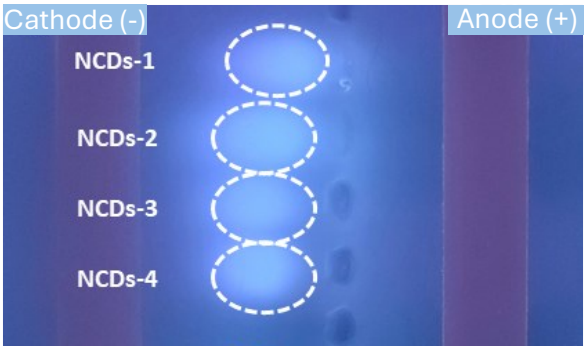

*Figure 2.9 Post-electrophoresis photograph taken under UV light (365 nm) of the gel at pH 4 for NCDs-**1**-**4**.*

Interested on the amino groups of NCDs, we detected and quantified these superficial moieties using the Kaiser test (KT). In this analysis, ninhydrin reacts with aliphatic primary amines on the surface of nanomaterials to form stoichiometric Ruhemann's purple dye that can be detected and quantified from its absorbance value recorded at 570 nm (detailed mechanism in Figure 2.20-30). Once added the KT reagents to our samples containing NCDs, the positive response for aliphatic amines was detectable by the rapid appearance of the characteristic purple colour.

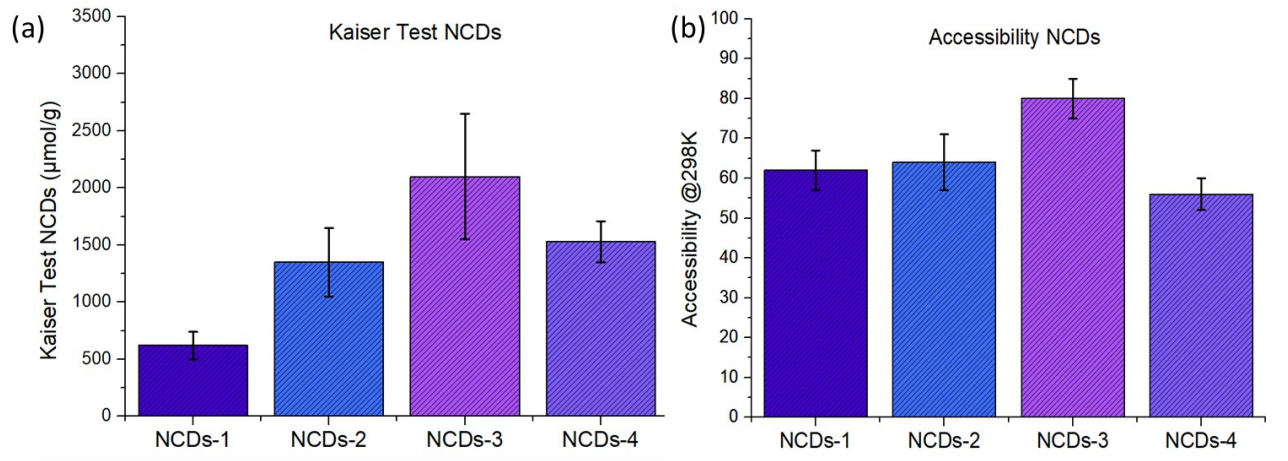

*Figure 2.10 a) Kaiser test (KT) of NCDs-**1**-**4** conducted at 393 K; b) Time-dependent (320 min) KT (accessibility) at 298 K for NCDs-**1**-**4**.*

After KT analysis, the outcome for NCDs-**1**, synthesized by Arg alone, revealed approximately 620±800 µmol/g of amines (Figure 2.10a). On the other hand, when the DAs were added to the starting materials, the number of surface amines increased remarkably. Interestingly, when the length of the diamine carbon chain was increased from 2 (NCDs-**2**) to 4 carbon atoms in NCDs-**3** the amines quantified by KT increased from 1350±300 µmol/g to 2100±550 µmol/g. Unexpectedly, the number of amines did not increase in NCDs-**4** when the longest diamine of the series was employed. This trend can be explained by considering that the low polarity of HDA contrasts the MW heat transfer, and thus the nanoparticle formation. In order to nearly all amines can react with ninhydrin, the standard temperature, at which the KT is performed, is 120°C. However, model organic reactions catalysed by NCDs are generally conducted at ambient temperature. Consequently, to assess the availability of primary aliphatic amines to react at ambient temperature, a time-dependent KT was carried out (Figure 2.10b). In this procedure, the KT at 120°C is set as the benchmark value and the time-dependent accessibility for 320 min is expressed as a percentage of this benchmark. The trend of KT at 120°C is in accordance with the accessibility at ambient temperature. Increasing the amines on NCDs from mono- to bi-component synthesis, NCDs-**3** show the highest accessibility value of 80%±5%.

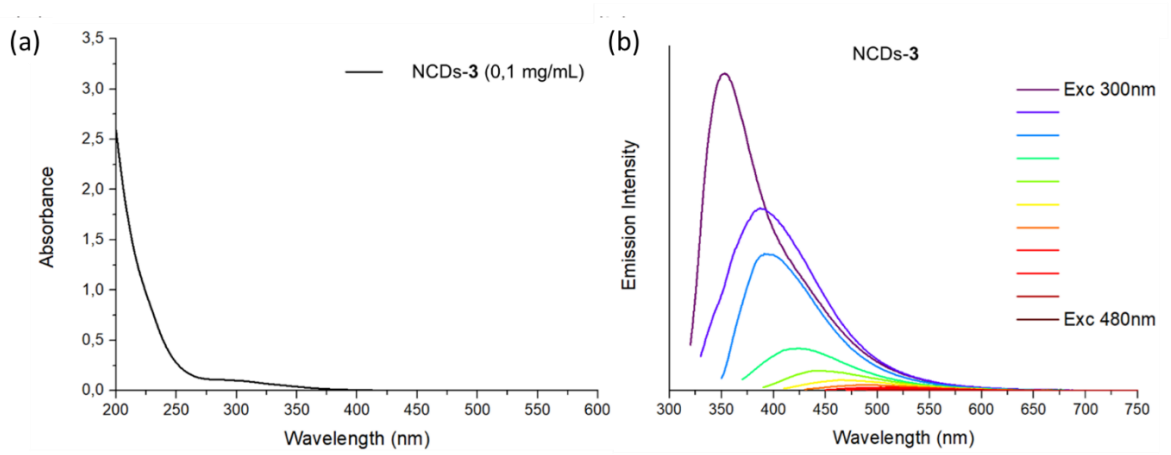

*Figure 2.11 UV-Vis (a) and emission spectra (b) of NCDs-**3** recorded at 0.1mgmL-1 in milli-Q water. For emission spectroscopy, the excitation wavelength changes from 300 to 480 nm every 20 nm.*

To acquire deeper information regarding the photophysical properties of the NCDs-**1**-**4**, they were investigated by absorbance and emission spectroscopies. UV-Vis spectroscopy displays broad absorption bands extending into the visible region up to 420 nm. Absorption of NCDs-**3** is shown in Figure 2.11a. Remarkably, the nanomaterial affords low-energy optical transitions in the visible region whereas none of the precursors absorbs more than 400 nm. The emissions of NCDs-**1**-**4** exhibit the typical excitation wavelength-dependent from 300 to 480 nm centering the maximum fluorescence band at around 350 nm as shown in Figure 2.11b for the NCDs-**3**. For UV-Vis and emission spectra of NCDs-**1**-**4**, see section 2.5.3 Figure 2.14-2.17.

2.3.2 Application of NCDs in Aminocatalytic Reactions

A benchmark aminocatalytic transformation was selected to evaluate the activity of NCDs-**1**-**4**. Specifically, acetone **1a** and *para*-nitro benzaldehyde **2a** were chosen to achieve the product **3a** using NCDs (3% w/V) in water.

*Table 2.1 Comparative study on the catalytic activity of NCDs-**1**-**5** and different free molecular amines in the aldol addition reaction between acetone **1a** and p-nitrobenzaldehyde **2a**.*

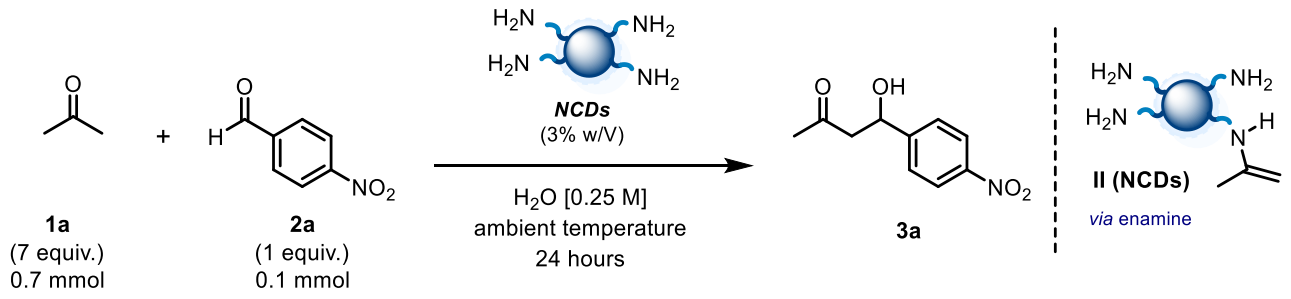

Entry	Catalyst	Precursors	Yield % [a]
1	-	-	0
2	NCDs-**1**	Arg	42±4
3	NCDs-**2**	Arg+EDAm	61±5
4	NCDs-**3**	Arg+BDA	75±3
5	NCDs-**4**	Arg+HDA	45±5
6	NCDs-**5**	Lys+BDA	66±5
7	Benzylamine[b]	-	7±3
8	Pyrrolidine[b]	-	0
9	Aniline[b]	-	0
10	Polyethyleneimine[c]	-	24±4
11	PAMAM 1.0 dendrimer[c]	-	14±2

[a] Yield determined by ^{1}H-NMR spectroscopy using 1,1,2-trichloroethene as the internal standard over five independent experiments. [b] Catalytic loading of 83 mol% calculated based on acid/base backtitration on NCDs-**3**. [c] Catalytic loading of 83 mol% calculated on the basis of Kaiser Test at 25°C on NCDs-**3**.

As expected, no reaction occurred in the absence of the NCDs, attesting the catalytic nature of the transformation (Table 2.1, Entry 1). Subsequently, NCDs-**1**, obtained solely from Arg, led to the formation of product **3a** in moderate yield (Table 2.1, Entry 2). In contrast, NCDs-**2** displayed better catalytic performances, affording **3a** in 61% yield (Table 2.1, Entry 3). Interestingly, the use of NCDs-**3**, produced from a longer carbon atom chain than EDAm, increased the reactivity up to 75% yield (Table 2.1, Entry 4). Lastly, **3a** was achieved in 45% yield using NCDs-**4**, evidencing that the use of HDA in the NCDs preparation reduced the reactivity of catalytic transformation. Therefore, NCDs-**3** have proven to be the best nano-aminocatalytic systems for the studied reaction. Notably, the total amount and accessibility of the surface amino moieties, both determined by the KT analysis of the materials, are compatible with our results. Indeed, NCDs-**3** displayed the highest number of primary amines as well as the best accessibility toward carbonyl compounds at room temperature.

To further investigate the role of Arg in the catalytical activity of NCDs, we synthesized NCDs-**5** starting from a different amino acid, namely *L*-lysine (Lys), and keeping the BDA as diamine (see section 2.5.2 for details). Interestingly, these nanoparticles yielded product **3a** in a lower chemical

yield (66%) than that provided by NCDs-**3** (Table 2.1, Entries 4 and 6). This result demonstrates the contribution of the amino acid in the production of active NCD-based catalysts.

To prove the advantages of NCDs-**3** in our model reaction in terms of catalytic performance, we tested easily accessible amine-bearing polymers and simple molecular amines to compare their catalytic effects. Specifically, benzylamine, pyrrolidine and aniline gave traces of product **3a** (Table 2.1, Entries 7-9). On the other hand, polyethyleneimine and poly(amidoamine) (PAMAM dendrimer) provided significantly lower quantity of **3a** than NCDs-**3** (Table 2.1, Entries 10-11). Importantly, NCDs-**3** confirmed their synthetic potential as nanocatalyst in this transformation.

Subsequently, we investigated the formation of aminocatalytic intermediates on the surface of NCDs-**3** to gain insight into the reaction mechanism. To do this, we exploited ^{19}F-NMR spectroscopy. The high sensitivity of fluorine nucleus led to recognise and quantify different functionalities without the overlaps of impurities that can usually affect ^{1}H-NMR or ^{13}C-NMR. Firstly, we selected model primary and secondary amines, including benzylamine, aniline, butylamine, and pyrrolidine, that could mimic the terminal moieties of the NCDs surfaces. These molecular amines reacted with appropriate fluorinated aldehydes, namely 4-fluorobenzaldehyde and 4-fluorophenylacetaldehyde, in deuterated dimethyl sulfoxide (DMSO-d_6) to generate the fluorinated imine and enamine species. Thus, the fluorinated products can be detected by ^{19}F-NMR analysis. Employing 4-fluorobenzaldehyde as alpha non enolizable probe, the related molecular imines were generated *in situ* and resonated between -108.6 and -110.5 ppm (Figure 2.12).

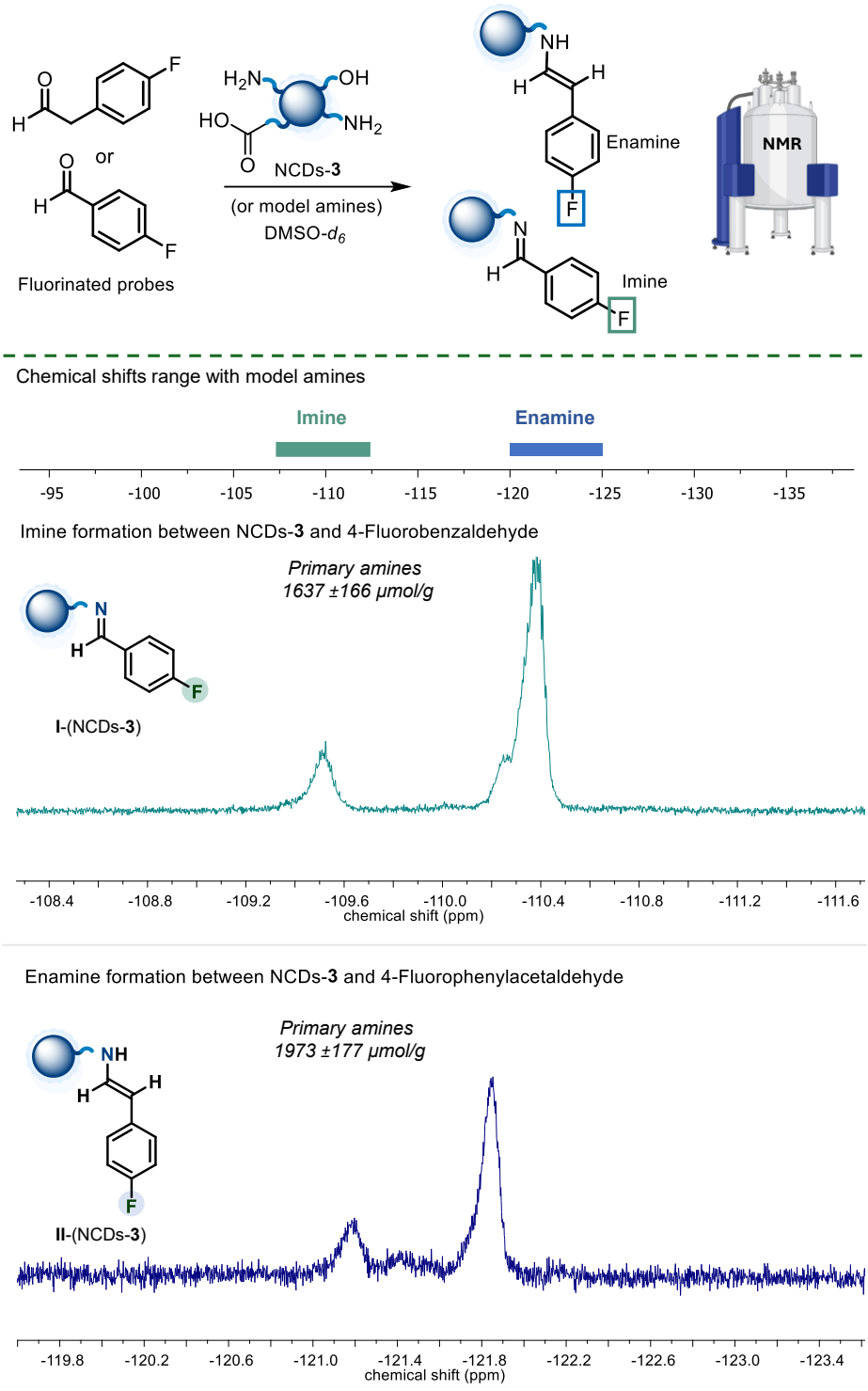

*Figure 2.12 Fluorinated imines and enamines formation from respectively 4-fluorobenzaldehyde and 4-fluorophenylacetaldehyde with model amines and NCDs-**3**. Chemical shift range for ^{19}F-NMR of model fluorinated imines and enamines. ^{19}F-NMR spectrum of imine, between NCDs-**3** and 4-fluorobenzaldehyde, and enamine, between NCDs-**3** and 4-fluorophenylacetaldehyde, in DMSO-d_6.*

Thereafter, the primary amines on carbon dots may easily condense with 4-fluorobenzaldehyde giving the corresponding imine intermediates **I**-(NCDs-**3**) on the NCDs-**3** surfaces corresponding to two new signals at around -109.4 and -110.6 ppm (Figure 2.12). These broad peaks suggested the formation of several surface imine moieties because of the different chemical environments. The

fluorine chemical shifts of the previously model imines and **I**-(NCDs-**3**) are both in the same ppm range confirming the formation of the imine functional groups on the surface of the nanoparticles. Accordingly, the same procedure was performed to study enamine intermediates. Model enamines, produced by condensation of molecular amines with 4-fluorophenylacetaldehyde, showed chemical shifts range between -120 and -122 ppm. Consequently, the formation of enamine **II**-(NCDs-**3**) was established by the occurrence of two broad signals closely related in terms of chemical shifts with the signals of molecular enamines (Figure 2.12). The formation of imines or enamines between the fluorinated aldehyde and various types of amine on the surface of NCDs-**3** can explain the presence of two broad peaks in the ^{19}F-NMR spectra. Verified the formation of amino intermediates on the NCDs-**3**, we sought to quantify the number of these catalytically active species on the NCDs-**3** by ^{19}F-NMR investigations. Within α,α,α-trifluorotoluene as internal standard, the number of superficial amines on NCDs-**3** was determined to be 1637±166 mmolg^{-1} for the detection through **I**-(NCDs-**3**), but it resulted in 1973±177 mmolg^{-1} when revealed using **II**-(NCDs-**3**) species. Since enamines may be generated on the NCDs-**3** surfaces from both primary and secondary amines, whereas imines can only be produced from primary amines, the number of enamines turned out to be higher than that of imines. These values are quite similar to the ones obtained from the KT at 25°C (1640±550 mmolg^{-1}).

Consequently, we employed NCDs-**3** as nano-aminocatalytic platforms for different transformations promoting a variety of transformations. Building on these premises, NCDs-**3** were employed in aldol additions, Mannich reactions, Knoevenagel condensations, Michael, and tandem Knoevenagel and Michael reactions (Schemes 1-5) to prove the generality of nanocatalysts. These transformations were conducted in aqueous solution.

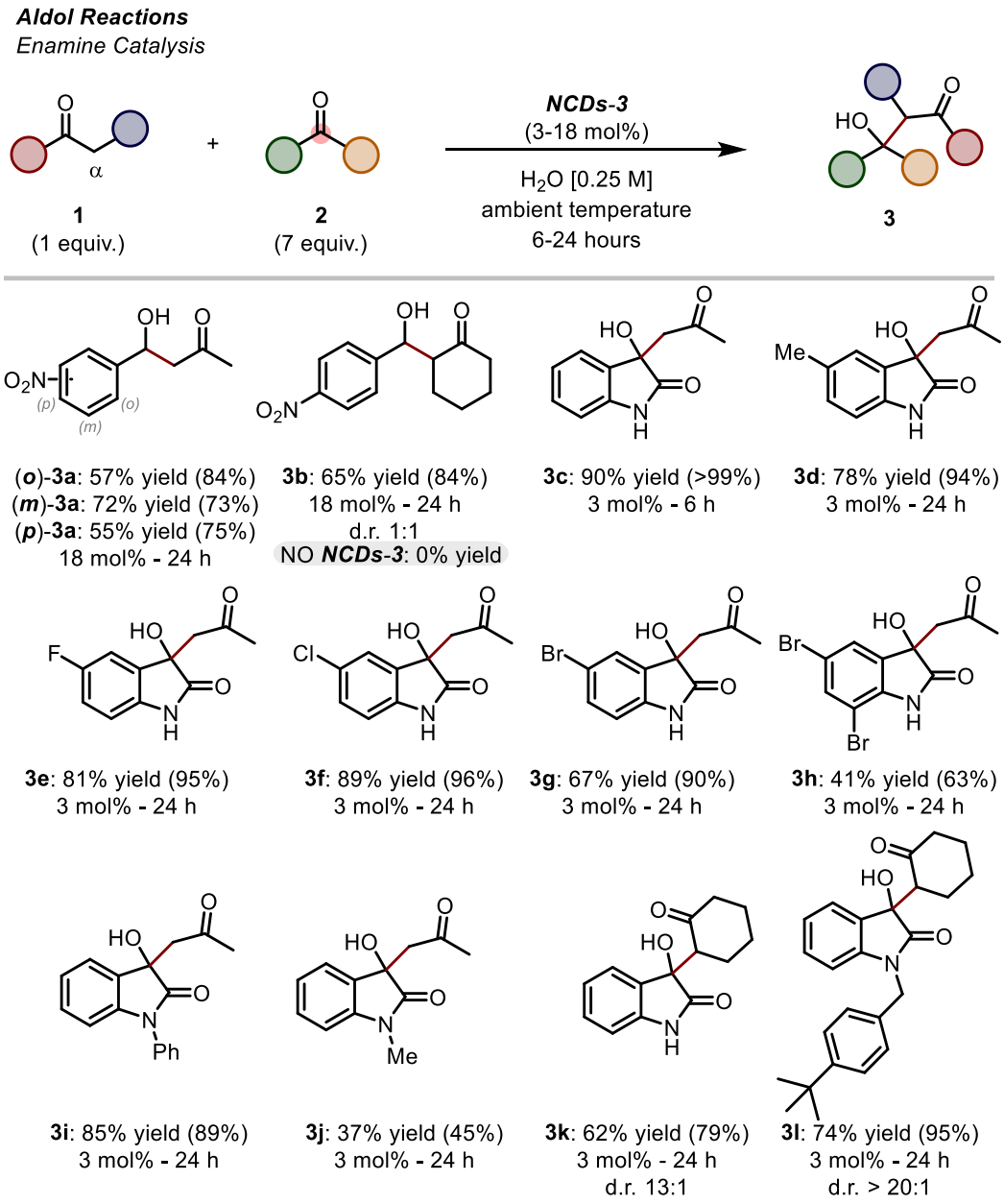

*Scheme 2.1 Reaction scope study for the aldol additions between α-enolizable carbonyl compounds **1** and electrophiles **2** using NCDs-**3** as nano-organocatalysts. Yields in parentheses were determined by ^{1}H-NMR analyses, using trichloroethylene as internal standard.*

First, we studied the scope of the aldol addition testing different α-enolizable carbonyl compounds **1** and electrophiles **2** to afford the products **3** *via* enamine catalysis (Scheme 2.1).

In particular, the addition of nitro-substituted aldehydes with acetone and cyclohexanone **2a**-**b** in the presence of NCDs-**3** (18 mol% of amine that is based on KT analysis at ambient temperature) delivered the corresponding β-hydroxy products **3a**-**b** in good isolated yields (up to 72%). Remarkably, a very low amount of catalyst (3 mol%) was necessary to yield products **3c**-**l**. In

particular, substituents in position five of the phenyl ring of the isatin did not reduce the reactivity of the transformation, affording products **3d**-**g** in excellent yields (up to 89%). Remarkably, when **2b** reacted with indole scaffold, very high diastereoselectivity and good yield were observed (**3k**-**l**, up to 74% yield and 20:1 diasteromeric ratio). Importantly, no formation of product **3b** in the absence of NCDs-**3** was detected.

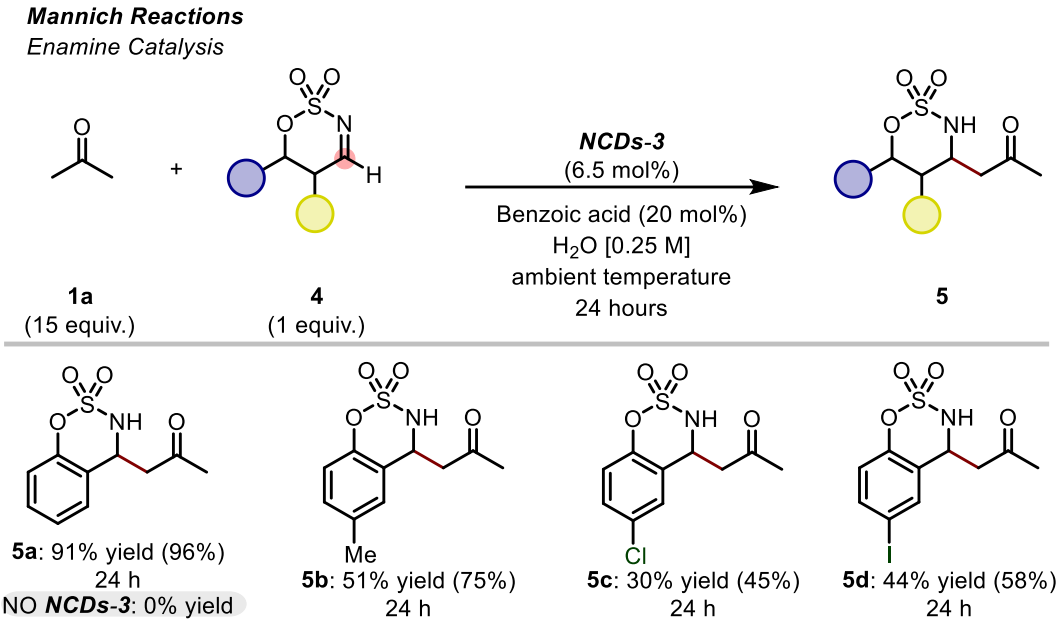

*Scheme 2.2 Reaction scope study for the Mannich reactions between acetone **1a** and imines **4** using NCDs-**3** as nano-organocatalysts. Yields in parentheses were determined by ^{1}H-NMR analyses, using trichloroethylene as internal standard.*

Acetone **1a** was also explored in the Mannich transformation with different imines **4**. Benzoic acid has been employed as co-catalyst (20 mol%) in combination with 6.5 mol% of NCDs-**3**. As shown in Scheme 2.2, various imines **4** bearing alkyl or halogen functionalities on the aromatic ring, allowed moderate to excellent product yields (up to 91%). The control experiment without NCDs-**3** did not produce any traces of compound **5a**.

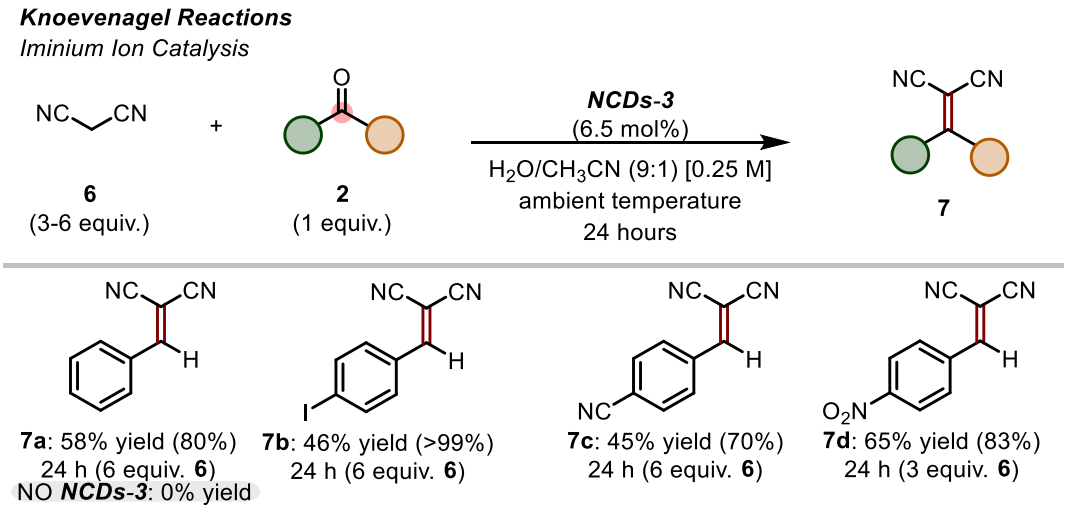

*Scheme 2.3 Reaction scope study for the Knoevenagel condensations between malononitrile **6** and electrophiles **2** using NCDs-**3** as nano-organocatalysts. Yields in parentheses were determined by ^{1}H-NMR analyses, using trichloroethylene as internal standard.*

We then turned our attention to the iminium ion catalysis. First, we evaluated the Knoevenagel condensation between malononitrile **6** and electrophiles **2** in a mixture of water/acetonitrile (9:1) as solvent (Scheme 2.3). The NCDs-**3** in combination with aldehydes **2** led to the formation of the iminium ion intermediates to trigger the nucleophilic attack of **6**. Importantly, no background reactivity in the absence of NCDs-**3** was detected. Different electron-withdrawing groups (EWGs) on **2** (-NO_2, -CN, -I) were well tolerated, delivering products **7** in excellent NMR yield (up to 99%). It is worth mentioning that the deterioration of the isolated yields for compounds **7a**-**d** should be attributed to degradative pathways during their purification.

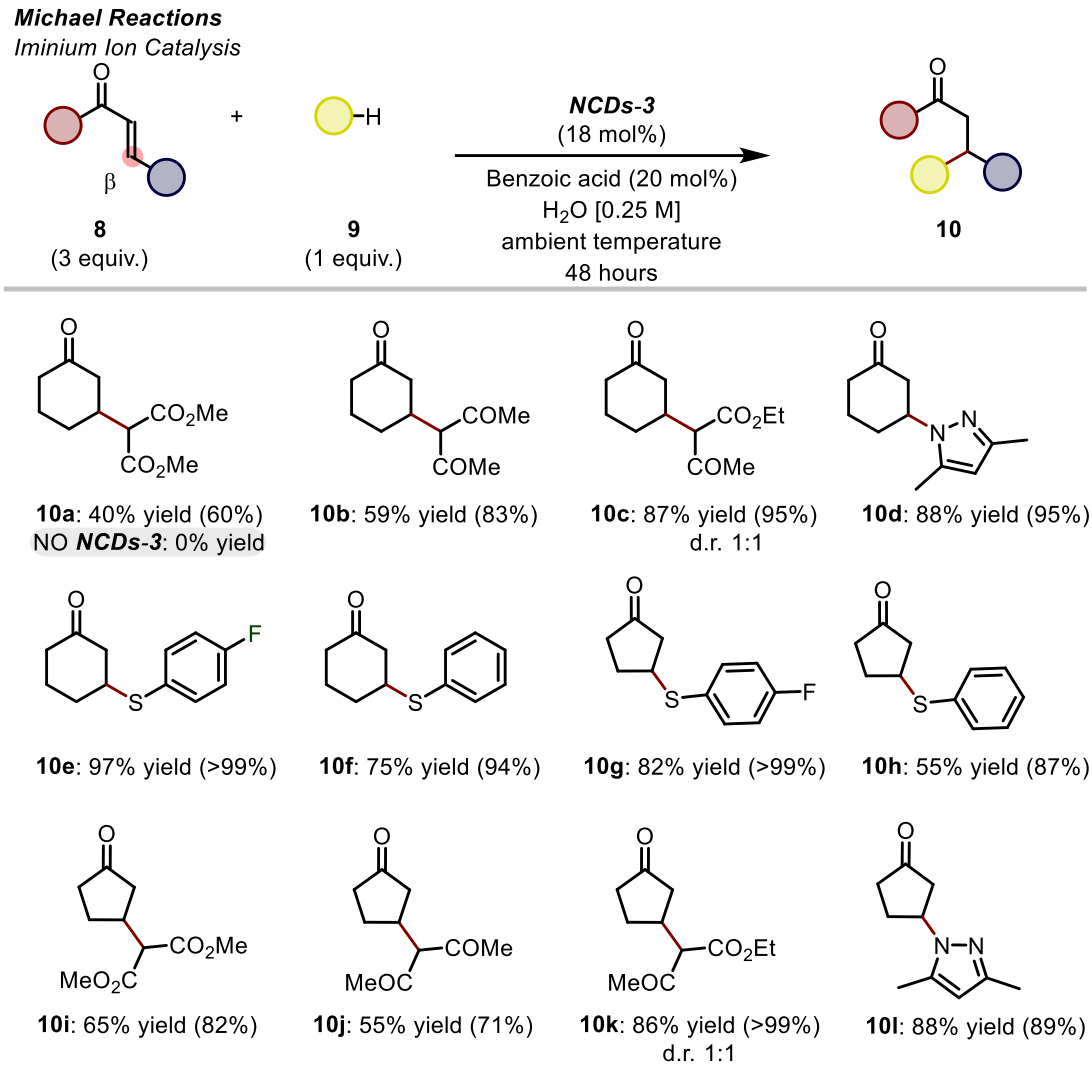

*Scheme 2.4 Reaction scope study for the Michael additions between α, β-unsaturated carbonyl compounds **8** and nucleophiles **9** using NCDs-**3** as nano-organocatalysts. Yields in parentheses were determined by ^{1}H-NMR analyses, using trichloroethylene as internal standard.*

Afterward, we moved to the Michael addition of nucleophiles **9** to α, β-unsaturated carbonyl compounds **8** (Scheme 2.4). The optimized reaction for 48 hours occurred with 18 mol% of NCDs-**3** and 20 mol% of benzoic acid. Importantly, no reaction took place in the absence of NCDs-**3**. A diverse set of C- and hetero-nucleophiles (*e.g.,* O, N, S) was well tolerated under the optimized operative conditions, affording the corresponding adducts **10a**-**l** in good to excellent isolated yields (up to 97%).

Lastly, we looked into the iminium ion activation of 1,3-dicarbonyl compounds **11** and aldehydes **2** using NCDs-**3** for the tandem Knoevenagel-Michael reactions (Scheme 2.5). Remarkably, low catalyst loading (3.3 mol%) and short reaction times (as low as 1 h) were used to access products **12a**-**f** in excellent yields (up to 98%).

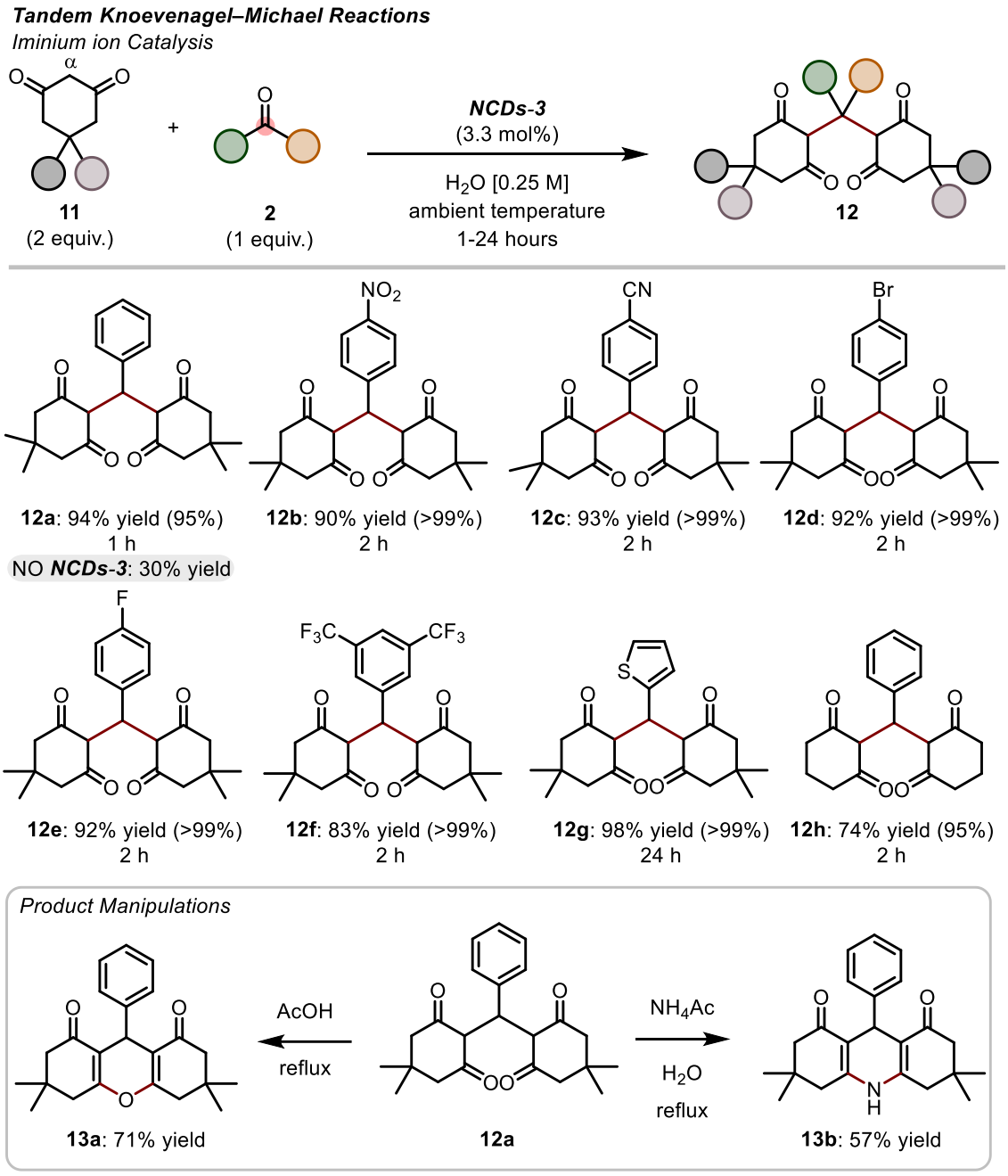

*Scheme 2.5 Reaction scope study for the Tandem Knoevenagel-Michael reactions between 1,3-dicarbonyl compounds **11** and electrophiles **2** using NCDs-**3** as nano-organocatalysts. Yields in parentheses were determined by ^{1}H-NMR analyses, using trichloroethylene as internal standard.*

In this case, a modest formation of product **12a** was observed without the use of NCDs-3 (30% yield), while a 93% yield was obtained by employing the nanocatalysts.

Different moieties at the *para* position of the aromatic ring of electrophiles **2** provided the corresponding products **12a**-**e** in very good yields (90-94% isolated yield). Indeed, heteroaromatic aldehyde **2g** reacted under the standard conditions to produce **12f** in an almost quantitative yield –

although an extended reaction time of 24 h was required. Finally, we demonstrated the synthetic utility of the developed methodology by performing a series of product manipulations on the tandem Knoevenagel-Michael adduct **12a**. In detail, introducing the oxygen or nitrogen source, acetic acid (AcOH) or ammonium acetate (NH_4Ac), the compounds xanthendione **13a** and acridindione derivatives **13b** were synthesized in reflux. These two redox-active molecules are exploited in the field of organic photocatalysis and biochemistry.[44–46]

2.4 Conclusion

This chapter provides a detailed experimental analysis of the relation between aminocatalytic activity and the structure of the amine-rich carbon dots. We synthetized a new family of NCDs by using L-arginine and different alkyl diamines as starting materials (NCDs-**1**-**4**) to test NCDs as aminocatalysts. Moreover, we carried out a discrimination of the critical parameters that determine the activity of these nanoparticles toward aminocatalytic reactions. Thus, a set of investigations on NCDs-**1**-**4** was conducted to compare and study their properties. Among different characterization techniques, KT analysis and ^{19}F-NMR provided important quantitative information about the number and the availability of the surface amino groups.

Lastly, aldol and Mannich reactions, which proceed *via* enamine intermediates, and iminium ion catalytic Knoevenagel, Michael and Tandel Knoevenagel-Michael transformations, were efficiently catalyzed by NCDs-**3** in water solution. To conclude, we believe that this work has the potential to inspire future rational design of NCD-based aminocatalysts for other organic reactions.

2.5. Experimental Section

2.5.1 General Information

The microwave synthesis was performed on a CEM Discover-SP instrument. UV-Vis measurements were carried out on Cary 5000 UV-Vis-NIR. All the spectra were recorded at room temperature using 10 mm path-length quartz cuvettes. Emission spectra and absolute Quantum Yield (QY) have been recorded utilizing FS5 Spectrofluorometer provided by Edinburgh Instruments Ltd equipped with a SC-30 Integrating Sphere. AFM images were obtained with a Nanoscope IIIa, VEECO Instruments. As a general procedure to perform AFM analyses, tapping mode with a HQ:NSC19/ALBS probe (80kHz; 0.6 N/m) (MikroMasch) from drop cast of samples in an aqueous or MeOH solutions (concentration in the order of μg/mL) on a mica substrate was performed. The AFM raw data were analyzed using S3 Gwyddion 2.35. TGA was performed with a TGA Q500 (TA instruments), under a flow of N_2 (25 mL/min), following a temperature program consisting of the equilibration of the sample at 100°C for

10 minutes followed by a ramp at 5°C/min up to 800°C. The sample aliquot ranged from 1 to 2 mg, exactly weighed. ATR-IR measurements were performed using a Spectrum 2000 FT-IR Instrument (Perkin Elmer). The NMR spectra were recorded on Varian 400 spectrometer (^{1}H-NMR: 400 MHz; ^{19}F-NMR: 376.0 MHz; ^{13}C-NMR: 101.0 MHz).

General procedures. All organocatalytic reactions were set up in glass vials, unless otherwise stated. Chromatographic purification of products was accomplished using flash chromatography on silica gel (35-70 mesh). For thin layer chromatography (TLC) analysis throughout this work, Merck pre-coated TLC plates (silica gel 60 GF254, 0.25 mm) were employed, using UV light as the visualizing agent (254 nm), basic aqueous potassium permanganate ($KMnO_4$) stain solution or iodine, and heat as developing agents. Organic solutions were concentrated under reduced pressure on a Büchi rotatory evaporator. Dialysis tubes Float-A-Lyzer® with molecular weight cutoff 0.5-1 KDa were bought from Spectrum Labs and used as stated by the manufacturer. The power supply for electrophoresis was bought from Consort (Model E844). Ultrapure fresh water obtained from a Millipore water purification system (>18 MΩ Milli-Q, Millipore) was used in all experiments.

Materials. Commercial reagents and solvents were purchased from Sigma-Aldrich, Fluka, Alfa Aesar, Fluorochem and VWR. They were used as received, without further purification, unless otherwise stated. Synthesis grade and anhydrous solvents were used as purchased.

2.5.2 General Procedure for the Synthesis of NCDs-1-5

For the synthesis of NCDs-**1**-**5**, the following experimental procedures have been followed, as previously reported in the literature.[3,19]

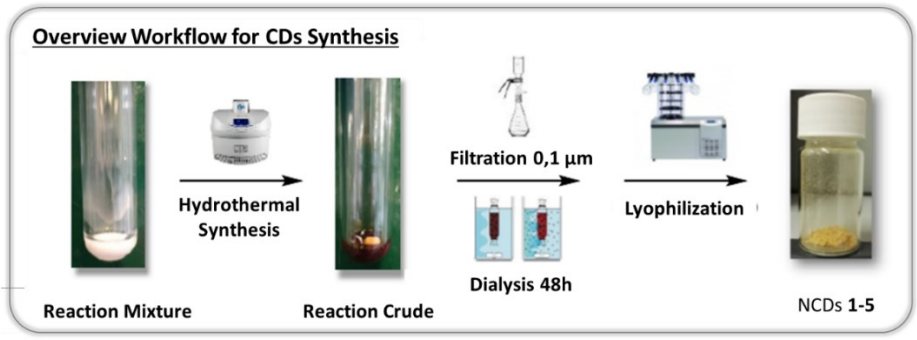

*Figure 2.13 Workflow of the synthesis of NCDs-**1**-**5***

Mono-component synthesis: Arg (87.0 mg, 0.5 mmol, 1 equiv.) and Milli-Q water (100.0 µL) were added into a sealable microwave reaction vessel and subsequently heated in a microwave reactor (200 W) at 240°C, 26 bar for 180 seconds.

Bi-component synthesis: Arg (87.0 mg, 0.5 mmol, 1 equiv.) or Lys (73.1 mg, 0.5 mmol, 1 equiv.), Milli-Q water (100.0 µL), along with one of the alkyl diamines selected for this experimental work (Figure S1), namely EDAm or BDA or HDA (0.5 mmol, 1 equiv.) were added into a sealable microwave reaction vessel and subsequently heated in a microwave reactor (200 W) at 240°C for 180 seconds.

The solution of the starting materials changes color from transparent to brown because of the formation of CDs. The solution was then diluted with water and filtered through a 0.1 µm PTFE microporous membrane. The crude so obtained was dialyzed against Milli-Q water through a dialysis membrane (0.5-1 kDa Cut-Off) Float-A-Lyzer® for 48 hours. The resulting aqueous solution of CDs was lyophilized resulting in an orange-to-yellow fluffy solid. The solid was collected and its weight was measured. To prevent the absorption of moisture the samples have been kept in a desiccator.

NCDs-**1**. L-arginine (87.0 mg, 0.5 mmol, 1 equiv.) and Milli-Q water (100.0 µL) were heated in a microwave reactor (200 W) at 240°C for 180 seconds. The aqueous solution of NCDs-8 was lyophilized giving a yellow solid (NCDs-**1**: 43.0 mg, 49% mass yield).

NCDs-**2**. L-arginine (87.0 mg, 0.5 mmol, 1 equiv.), 1,2-Diaminoethane (EDAm) (33.0 µL, 0.5 mmol, 1 equiv.) and Milli-Q water (100.0 µL) were heated in a microwave reactor (200 W) at 240°C for 180 seconds. The aqueous solution of NCDs-8 was lyophilized yielding an orange solid (NCDs-**2**: 29.4 mg, 25% mass yield).

NCDs-**3**. L-arginine (87.0 mg, 0.5 mmol, 1 equiv.), 1,4-Diaminobutane (BDA) (50.0 µL, 0.5 mmol, 1 equiv.) and Milli-Q water (100.0 µL) were irradiated into a microwave reactor (200 W) at 240°C for 180 seconds. The aqueous solution of CDs-3 was lyophilized resulting in a yellow solid (NCDs-**3**: 15.6 mg, 17% mass yield).

NCDs-**4**. L-arginine (87.0 mg, 0.5 mmol, 1 equiv.), 1,6-diaminohexane (HAD) (69.0 µL, 0.5 mmol, 1 equiv.) and Milli-Q water (100.0 µL) were irradiated into a microwave reactor (200 W) at 240°C for 180 seconds. The aqueous solution of CDs-3 was lyophilized resulting in a yellow solid (NCDs-**4**: 14.5 mg, 10% mass yield).

NCDs-**5**. L-Lysine (73.1 mg, 0.5 mmol, 1 equiv.), 1,4-Diaminobutane (BDA) (50.0 µL, 0.5 mmol, 1 equiv.) and Milli-Q water (100.0 µL) were heated in a microwave reactor (200 W) at 240°C for 180 seconds. The aqueous solution of CDs-7 was lyophilized giving a yellow solid (NCDs-**5**: 14.0 mg, 12% mass yield).

2.5.3 Characterization of NCDs-1-5

Physical-Chemical Analysis

UV-vis absorption and fluorescence spectra were recorded at a concentration of 0.1 mg/mL in Milli-Q water using a standard quartz cuvette with an optical path length of 1 cm.

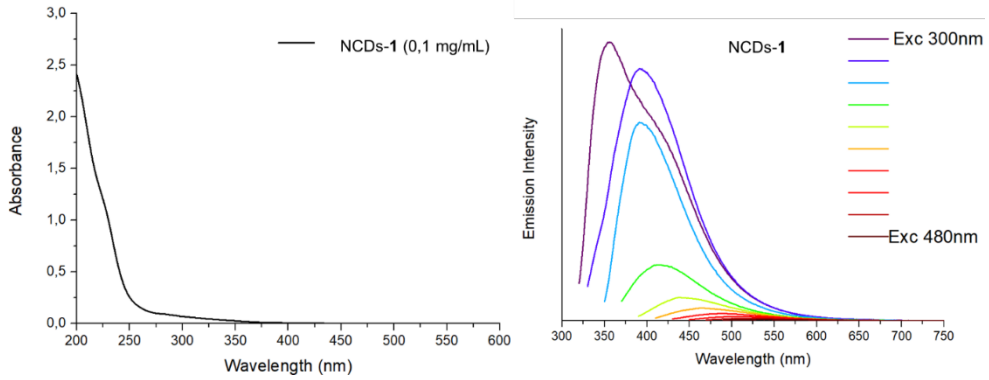

*Figure 2.14 UV-vis and Emission spectra of NCDs-**1**.*

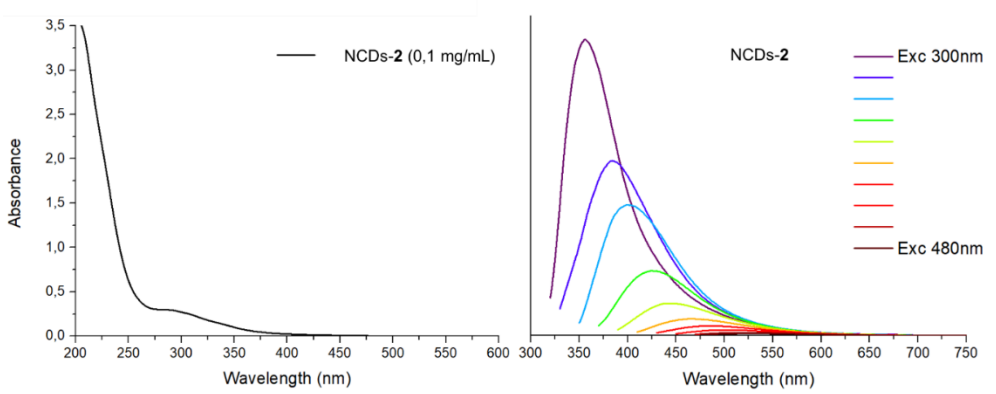

*Figure 2.15 UV-vis and Emission spectra of NCDs-**2**.*

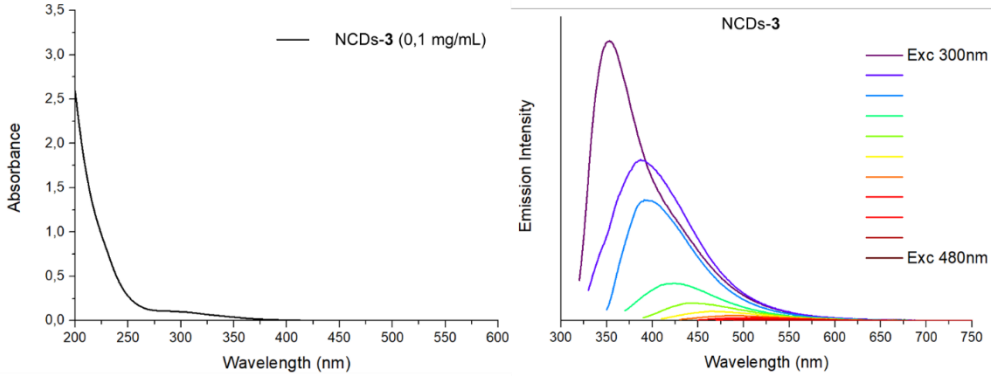

*Figure 2.16 UV-vis and Emission spectra of NCDs-**3**.*

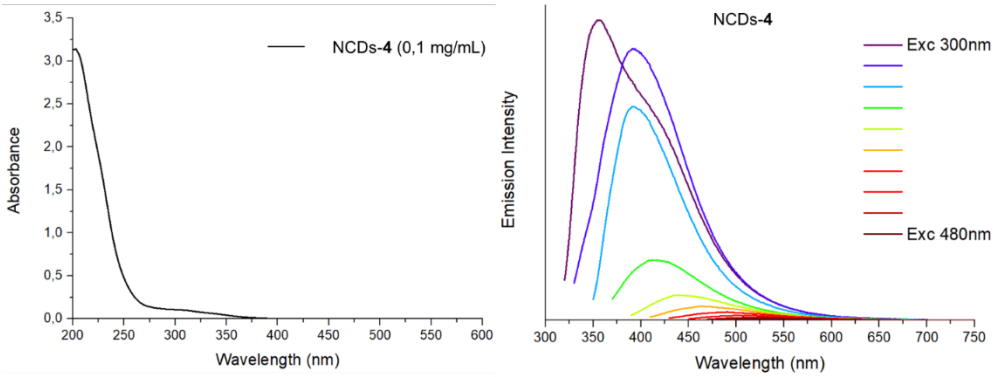

*Figure 2.17 UV-vis and Emission spectra of NCDs-**4**.*

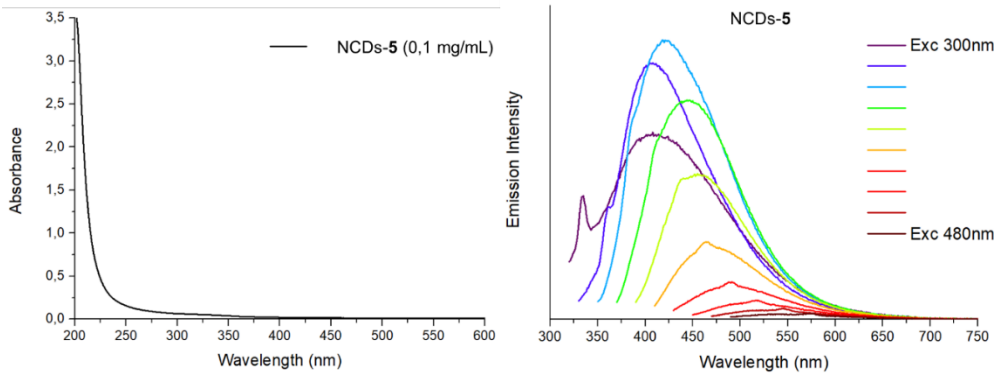

*Figure 2.18 UV-vis and Emission spectra of NCDs-**5**.*

^{1}H-NMR characterization. The ^{1}H-NMR spectra were recorded by dissolving 7 mg of NCDs-**1**-**5** into 700 µL of D_2O.

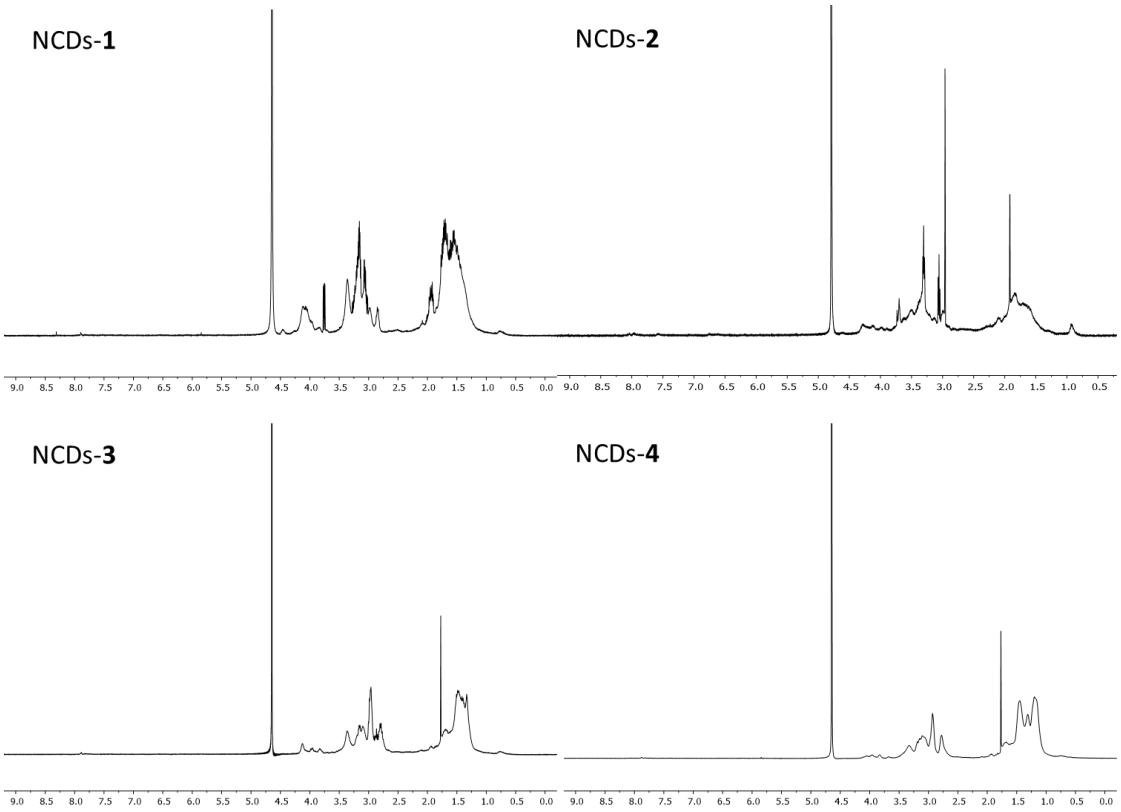

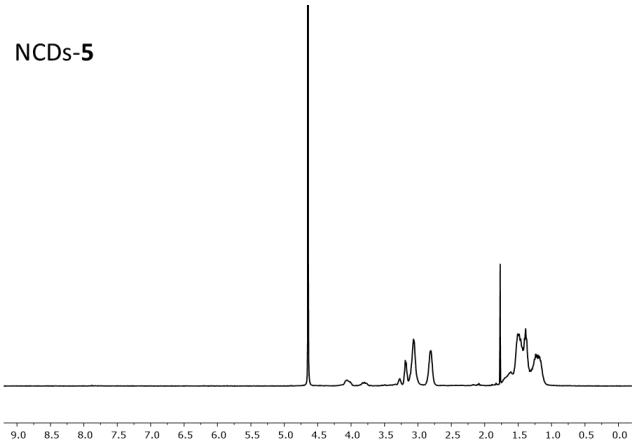

*Figure 2.19 ^{1}H-NMR of NCDs-**1**-**5**.*

Kaiser test procedure. Kaiser tests (KTs) were performed according to a modified protocol by employing a commercially available kit provided by Merck. Typically, about 1 mg of NCDs was placed in a test tube. Then, 75 µL of a phenolic solution in ethanol (Sol A), 100 µL of a KCN solution in pyridine/water (Sol B), and 75 µL of a ninhydrin solution in ethanol (Sol C) were added. The tube was sealed and the so obtained mixture was heated at 120 °C for 10 minutes. The resulting solution was diluted with ethanol in water (60% v/v, 1:18 dilution) and its absorption spectrum was recorded. A blank solution was also run to be used as reference. For each sample, at least three independent analyses were performed. Primary amines on the carbon dots surface were thus quantified from the absorbance value recorded at 570 nm, considering a molar absorption coefficient for the ninhydrin derivative of 15000 M^{-1} cm^{-1} (Ruhemann's purple). Equation 1 was used to determine the KT value.

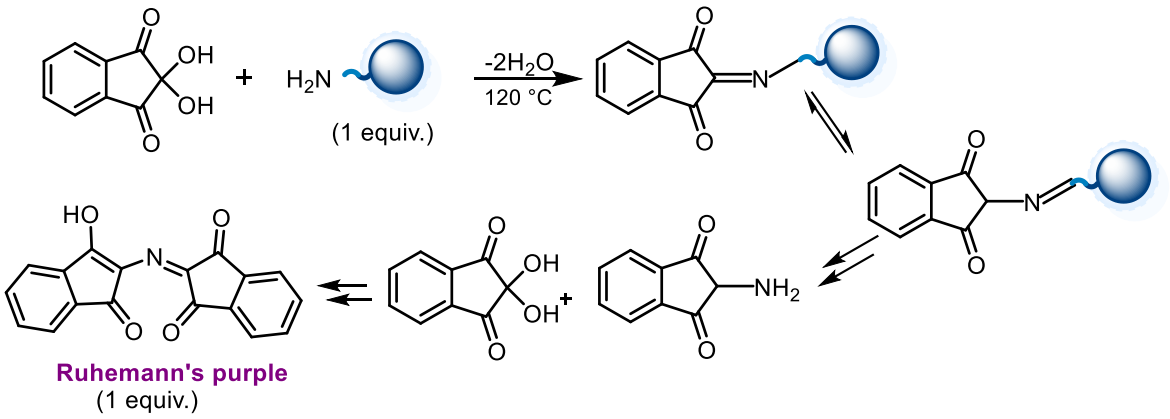

Figure 2.20 Schematization of Kaiser test molecular mechanism.

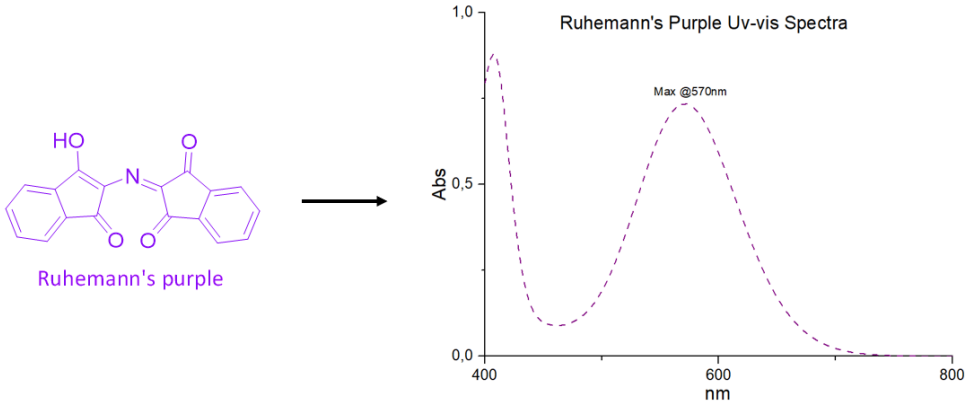

Figure 2.21 Visible spectra of Ruhemann's purple dye.

$$KT\ (^{\mu mol}/_{g}) = \frac{[Abs@570nm \times dil \times 10^{6}]}{\varepsilon \times Weight\ (mg)}$$

*Equation 1. Calculation of primary amines on NCDs-**1-5**.*

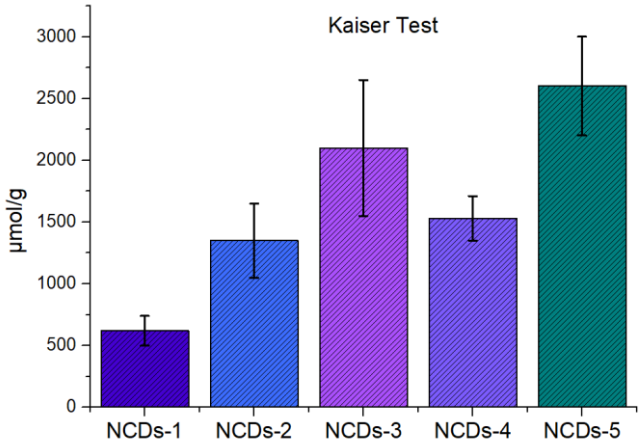

*Figure 2.22 Results of Kaiser test performed at 120°C on NCDs-**1-5**.*

Room Temperature Kaiser Test. In the accessibility experiments, the analyzed solution was kept at room temperature (r.t., 25°C) throughout the experiment. Therefore, to a known amount of NCDs (about 1 mg), the Kaiser test solutions (Sol A, B and C) were added as previously described. At a certain time, an aliquot (20 µL) was collected, diluted, and analyzed. The experiment was repeated in triplicate for each NCDs material. Equation 2 was used to determine the accessibility value.

$$Accessibility\ (\%) = \frac{KT\ (r.t)}{KT\ (120\ °C)} \times\ dil\ \times\ 100$$

Equation 2. Determination of the accessibility of the examined amines into the corresponding ninhydrin derivative.

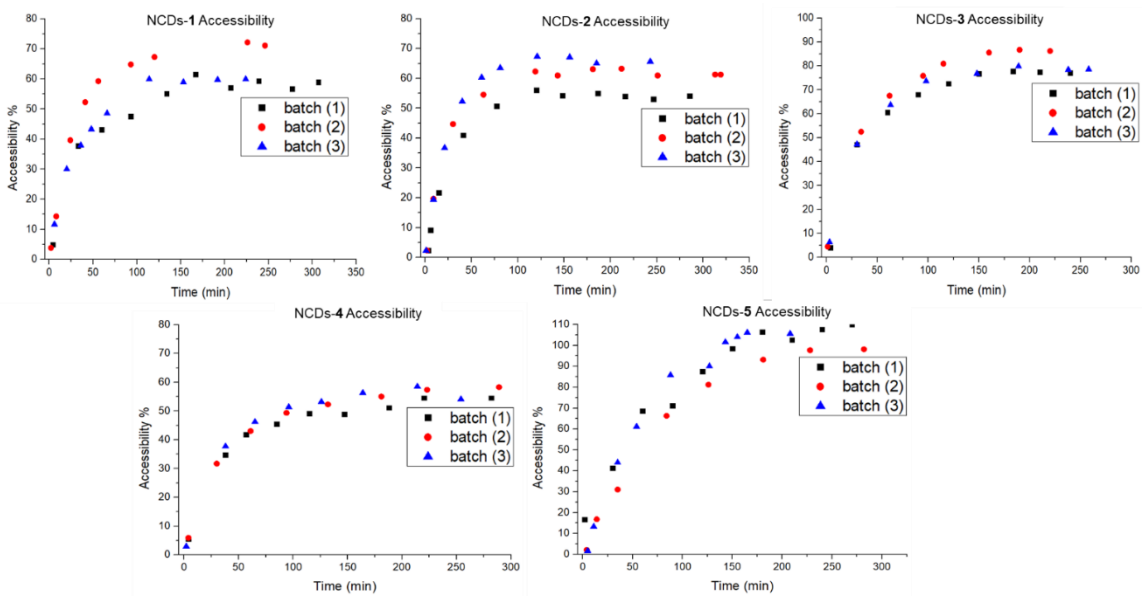

*Figure 2.23 Time-dependent Kaiser test performed at 25°C for NCDs-**1**-**5**.*

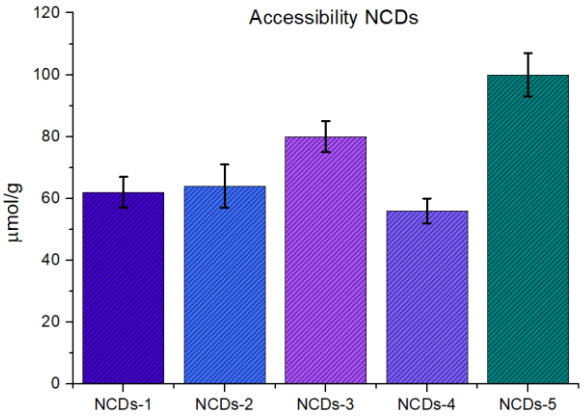

*Figure 2.24 Comparison between the Kaiser test values obtained at 25°C after 250 minutes for NCDs-**1**-**5**.*

Acid/base back titration. A known amount of NCDs (about 10 mg) was solubilized in 4 mL of milli-Q-water. Subsequently, 1 mL of NaOH 0.5 M (Titripur ®, Merck) was added and then the resulting solution was titrated with a 0.1 N or 1.0 N solution of HCl (Titripur ®, Merck).

For the quantification of acid/base sites, a Gran Plot analysis was performed.[4] By plotting the µmol of H^+ and OH- *vs*. the µmol of titrant), two linear regions were individuated. The resulting amounts of titrant at the equivalent point (μmol_{eq1} and μmol_{eq2}) were extrapolated through a linear fitting. Finally, the total number of acid/base active sites were calculated by subtracting μmol_{eq2} from μmol_{eq1} and dividing the resulting number by the amount of carbon dots analysed. Back titrations and Gran plot analysis were repeated in triplicate. A sample titration curve and the corresponding linearized plots for each NCDs are shown below (Figure 25-29). The intrinsic pH turned out to be 9.0 for NCDs-**1**, 9.2 for NCDs-**2**, 9.5 for NCDs-**3**, 9.8 for NCDs-**4**, and 9.5 for NCDs-**5**, respectively.

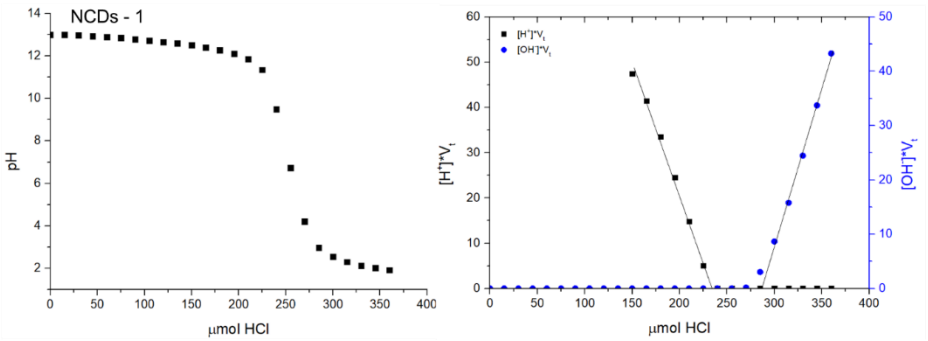

*Figure 2.25 Back titration of NCDs-**1** (left) and Gran plot linearization (right).*

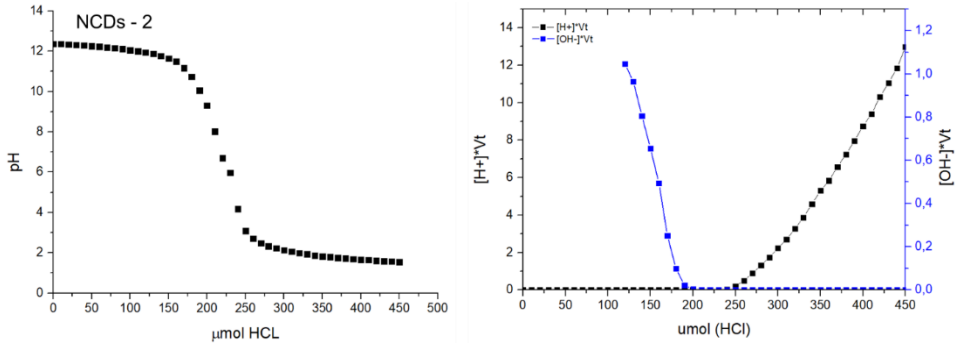

*Figure 2.26 Back titration of NCDs-**2** (left) and Gran plot linearization (right).*

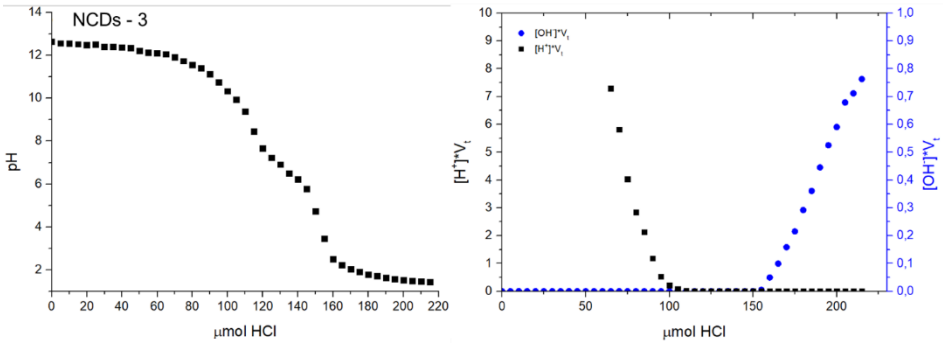

*Figure 2.27 Back titration of NCDs-**3** (left) and Gran plot linearization (right).*

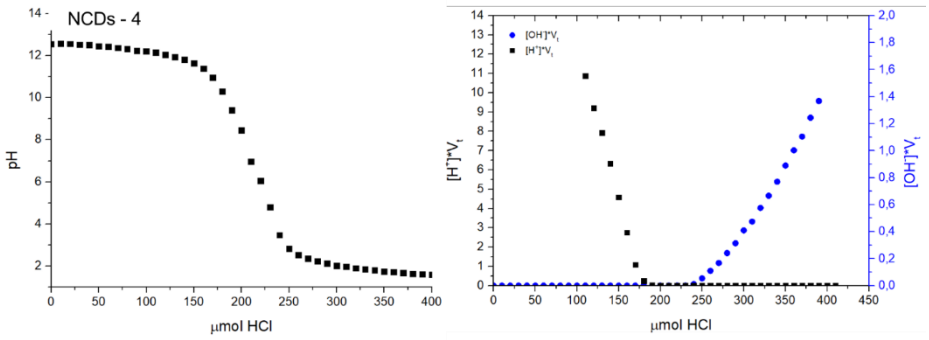

*Figure 2.28 Back titration of NCDs-**4** (left) and Gran plot linearization (right).*

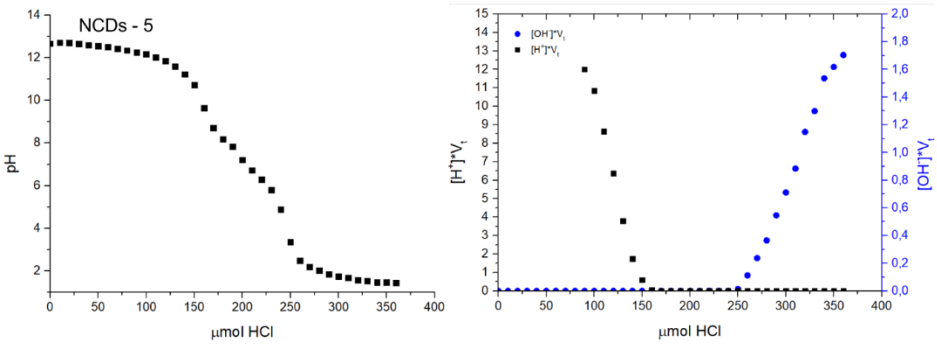

*Figure 2.29 Back titration of NCDs-**5** (left) and Gran plot linearization (right).*

ATR-FTIR analysis. NCDs-**1**-**5** were analyzed by infrared spectroscopy.

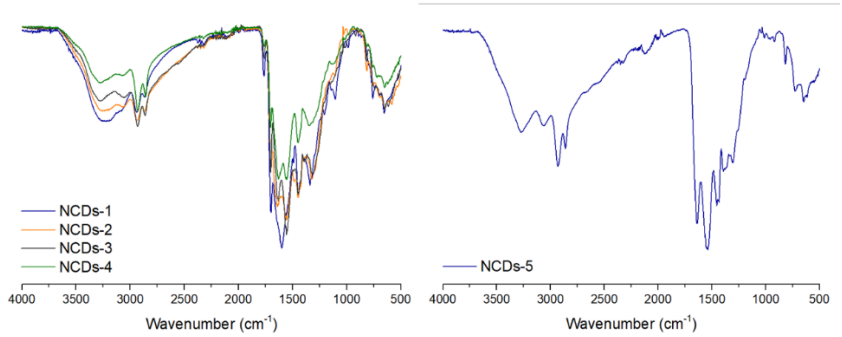

*Figure 2.30 ATR-FTIR spectra of NCDs-**1-4** (left) and NCDs-**5** (right).*

TGA analysis. NCDs-**1**-**5** were analyzed by Thermogravimetric analysis.

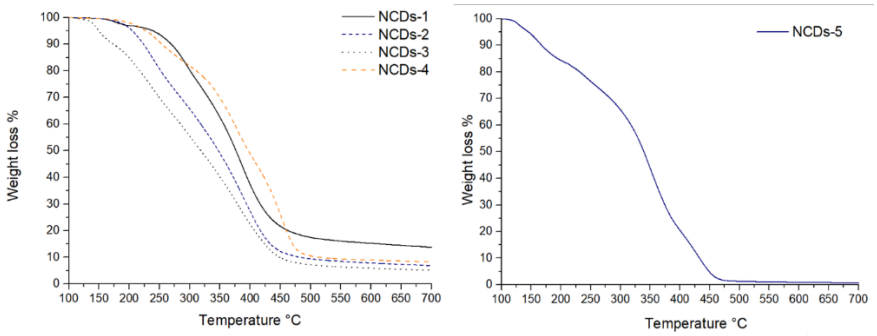

*Figure 2.31 Thermogravimetric analysis under nitrogen of NCDs-**1-4** (left) and NCDs-**5** (right).*

Biuret assay. To demonstrate the actual presence of amide groups on NCDs, Biuret test was performed. This assay is based on the ability of peptide bond to reduce Cu(II) ions to Cu(I) in alkaline aqueous solution. In alkaline solutions containing sodium potassium tartrate, Cu(I) ions complex with the peptide bonds of proteins forming a light blue to purple colored complex. The process is schematized in Figure 2.32.

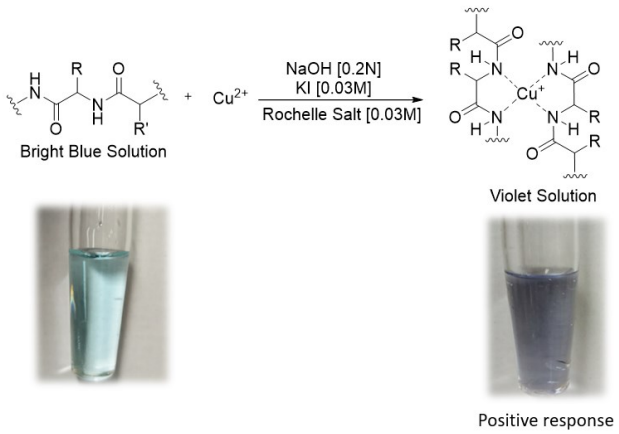

Figure 2.32 General schematization for Biuret assay.

Subsequently, a reagent solution was prepared by mixing 0.9% w/w sodium potassium tartrate (Rochelle salt), 0.5 %w/w copper sulphate pentahydrate and 0.5% w/w potassium iodide in a 0.2 N sodium hydroxide solution. To run the text, 2.5 mL of the reagent solution were transferred into a test tube along with 200 µL of 2 mg/mL NCDs solution in Milli-Q water. The test tube was subsequently sealed with a silicon lid and incubated at 37°C for 30 minutes. After the incubation time the NCDs produced from L-Lysine (NCDs-**5**) tested positive affording the characteristic violet colored copper complex, whereas no violet coloration was observed for the NCDs produced from L-arginine (NCDs-**1**-**4**). Figure 2.33 shows the UV-Vis afforded by a positive response to the biuret test. As known, L-arginine can interfere with standard Biuret test, therefore bicinchoninic acid (BCA) assay was performed to detect and quantify the superficial amide functionalities on NCDs-**1**-**5**.

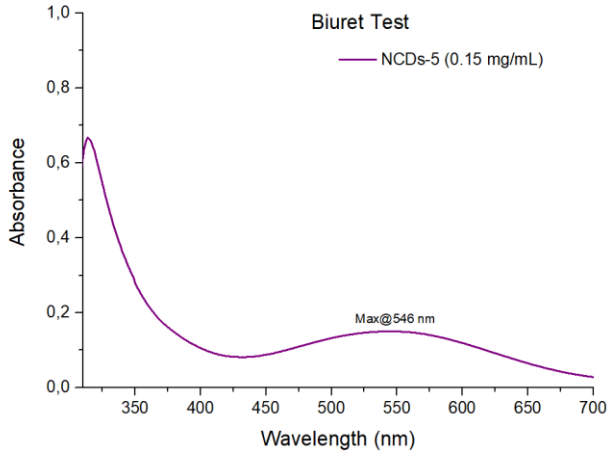

*Figure 2.33 UV-Vis spectra recorded on NCDs-**5** after Biuret assay (0.15 mg/mL in water).*

Bicinchoninic acid (BCA) assay. BCA assay is a biochemical assay routinely applied to determine the total concentration of protein in an aqueous media. After the reduction of copper Cu(II) ions to Cu(I)

in a basic aqueous buffer (pH: 11.25), the Cu(I) ion produced is chelated by two molecules of BCA^{2-} to form a colored copper complex with a characteristic maximum of absorption at 562 nm that can be easily detected by UV-Vis spectroscopy.

Initially the BCA Buffer solution was prepared (Sol A) accordingly with a well-established procedure. To Milli-Q water it has been added 1 %w/w BCA-Na_2 • H_2O, 2% w/w Na_2CO_3, 0.4% w/w NaOH and 0.95% w/w $NaHCO_3$. The buffer solution was adjusted to a pH = 11.25 dropwise with a NaOH 50% w/w solution. Moreover, a 4% w/w $CuSO_4$ • $5H_2O$ solution was prepared in Milli-Q water (Sol B). Finally, the working solution (WR-S) was obtained by mixing Sol A and Sol B in a 50:1 ratio.

To run the test, 1000 µL of the WR-S solution was added to an Eppendorf tube followed by 40 µL of NCDs-**1**-**4** derived from L-arginine and 80 µL of NCDs-**5** derived from L-Lysine. All NCDs solutions were at 2 mg/mL concentration. The Eppendorf tube was closed and incubated through a thermostatic water bath at 37°C for 30 minutes. Then, an aliquot (900 µL) of the sample was taken and diluted with an alkaline buffer solution adjusted at pH = 11.25 containing 2% Na_2CO_3, 0.4% NaOH and 0.95% $NaHCO_3$. UV-Vis spectra were recorded within 10 minutes (Figure 2.34).

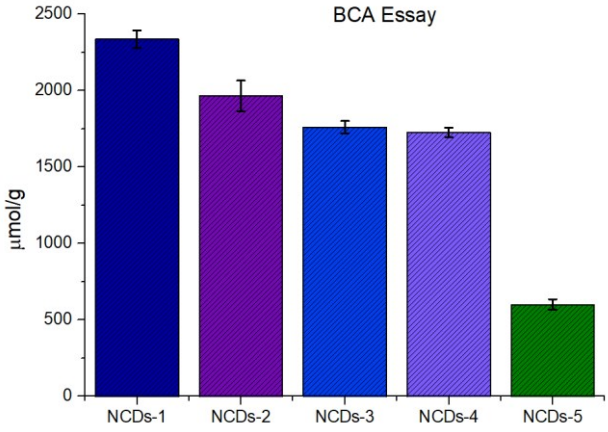

*Figure 2.34 BCA assay results for NCDs-**1-5**.*

To measure the molar extinction coefficient of the $[Cu\ (BCA)_2]^{3-}$ complex in the buffer solution, Na_2BCA • H_2O (23.30 mg, $6x10^{-5}$ mol) was added to a 20 mL volumetric flask along with $CuSO_4$ • $5H_2O$ (5.00 mg, $6x10^{-5}$ mol). Finally, ascorbic acid (5.30 mg, $3x10^{-5}$ mol) was introduced as reducing agent and the volume was finalized at 20 mL with the alkaline buffer.

The flask was incubated at 37°C for 30 minutes and subsequently aliquots were collected and diluted opportunely to a known concentration. UV-Vis spectra has been recorded. The plotted data and the corresponding linear fitting are shown in Figure 2.35. The molar extinction coefficient of the

$[Cu(BCA)_2]^{3-}$ complex was calculated at [6.800 x 10^3 L (mol Cu • cm)$^{-1}$]. The value fits with what reported in literature.

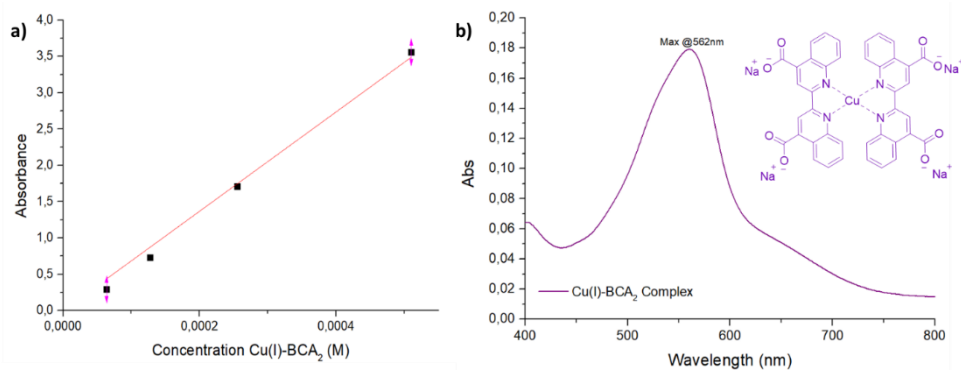

Figure 2.35 a) Linear fitting for molar extinction coefficient b) UV-Vis spectra and structure of $[Cu(BCA)_2]^{3-}$ complex.

Gel electrophoresis. For the electrophoresis studies, an agarose gel was prepared in a pH = 4 citrate buffer. The buffer was obtained by dissolving citric acid and trisodium citrate in milli-Q-water ($C_6H_8O_7$ 0.0330 M and $Na_3C_6H_5O_7$ 0.0170 M), providing a final pH equal to 4.0. The gel precursors employed for each electrophoresis experiment, were freshly obtained mixing agarose along with the buffer solution (2 wt%) and heated up at 100°C for 10 min. Therefore, the so-formed gel was allowed to cool into the electrophoresis chamber. (total volume = 200 µL, concentration = 50 mg/mL) were prepared in the citrate buffer.

In a typical electrophoresis experiment, 20 µL of NCDs solution were placed in the loading well of the gel and the chamber was filled with the buffer solution. Then, an electric current of 250 mA was applied recording a voltage of 60 V. UV light irradiation at 365 nm was used to visualize the fluorescent NCDs after the electrophoretic experiment.

Coomassie Brilliant Blue staining for gel electrophoresis. To prepare the staining solution 250 mg of Coomassie Brilliant Blue dye were solubilized in a mixture of 50 mL of glacial acetic acid, 250 mL of methanol and 200 mL of Milli-Q water affording a final dye concentration of 5.80 x 10^{-4} M The agarose gel containing the CDs particles was placed in the dye mixture for 45 min. Subsequently, the gel was removed from the coloring solution and rinsed three times with a washing solution composed by 30% methanol, 10% acetic acid and 60% Milli-Q water. The gel was then placed overnight in the washing solution.

2.5.4 General Procedures for the Synthesis of the Starting Materials

PREPARATION OF N-FUNCTIONALISED ISATIN (**2l**)

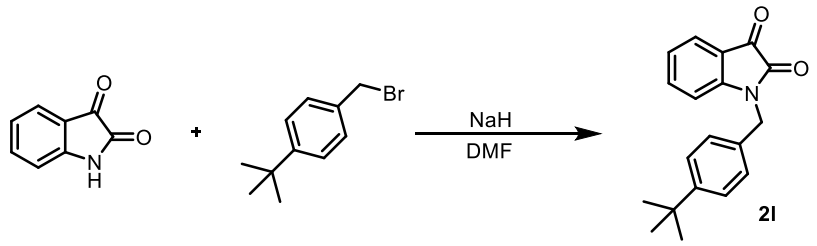

Prepared according to a modified literature procedure.[47] Isatin (1.0 mmol, 1.0 equiv., 165 mg) was dissolved in anhydrous DMF (2 mL, 0.5 M) at 0°C before the addition of sodium hydride (60% dispersion in mineral oil, 1.3 mmol, 1.3 equiv., 91 mg). The resulting mixture was stirred for 30 minutes at 0°C. 4-*tert*-butylbenzyl bromide (1.2 mmol, 1.2 equiv., 221 µL) was then added and the reaction was stirred for 5 hours at room temperature. At the end, the reaction was quenched with saturated aqueous NH_4Cl (50 mL) and extracted with EtOAc (3 x 100 mL). The combined organic layers were washed with water and brine, then dried over anhydrous sodium sulfate. The residue was purified by flash chromatography (Hex/EtOAc) to afford the corresponding product **2l** as red solid (125 mg, 43%).

Characterization Data

^{1}H-NMR (400 MHz, $CDCl_3$) δ 7.59 (dd, *J* = 7.5, 0.8 Hz, 1H), 7.49 (td, *J* = 7.8, 1.3 Hz, 1H), 7.38 – 7.33 (m, 2H), 7.28 (dd, *J* = 7.7, 5.7 Hz, 2H), 7.08 (td, *J* = 7.6, 0.7 Hz, 1H), 6.83 (d, *J* = 8.0 Hz, 1H), 4.89 (s, *J* = 12.3 Hz, 2H), 1.29 (s, *J* = 3.3 Hz, 9H). **^{13}C-NMR (101 MHz, $CDCl_3$)** δ 183.46, 158.34, 151.30, 150.97, 138.41, 131.57, 127.37, 126.04, 125.44, 123.87, 117.77, 111.15, 43.81, 34.67, 31.38. The characterization data matched with the reported one.[48]

PREPARATION OF CYCLIC IMINES (**4a**-**4d**)

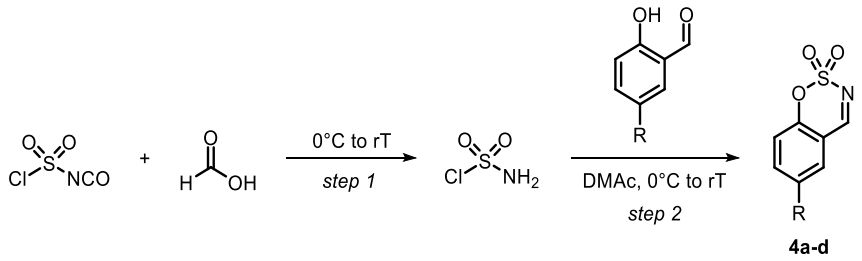

STEP 1, according to a modified literature procedure.[49] Anhydrous formic acid (10.0 mmol, 1 equiv., 377 µL) was added dropwise to neat chlorosulfonyl isocyanate (10.0 mmol, 1 equiv., 868 µL) at 0 °C with rapid stirring. Strong gas evolution was observed during the addition process. The resulting suspension was stirred at room temperature for 2 hours. The resulting white solid was immediately used in the following step.

STEP 2, according to a modified literature procedure.[49] To a solution of the appropriate salicylaldehyde (3.75 mmol, 1 equiv.) in *N,N*-dimethylacetamide (DMAc, 25 mL, 0.15 M) at 0 °C was carefully added the freshly prepared sulfamoyl chloride (10.0 mmol, 2.67 equiv., 1.16 g) in small portions, and the resulting solution was stirred for 18 hours at room temperature. The reaction was quenched carefully with ice-cold water (50 mL), and the mixture was extracted with EtOAc (3 x 100 mL). The combined organic layers were washed with saturated $NaHCO_3$ solution (100 mL), then dried over anhydrous sodium sulfate. The residue was purified by flash chromatography (Hex/EtOAc) to afford the corresponding cyclic imines **4a-4d** as solids.

Characterization Data

Benzo[*e*][1,2,3]oxathiazine 2,2-dioxide (4a)

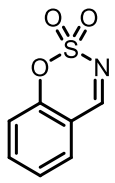

4a

4a was synthesized according to the general procedure from salicylaldehyde (398 µL, 3.75 mmol). The cyclic imine **4a** was obtained as a pale-yellow solid (652 mg, 95% yield).

^{1}H-NMR (400 MHz, $CDCl_3$) δ 8.68 (s, 1H), 7.80 – 7.68 (m, 2H), 7.43 (td, *J* = 7.6, 1.0 Hz, 1H), 7.30 – 7.24 (m, 1H). **^{13}C-NMR (101 MHz, $CDCl_3$)** δ 167.96, 154.21, 137.81, 131.03, 126.36, 118.60, 115.38. The characterization data matched with the reported one.[50]

6-methylbenzo[*e*][1,2,3]oxathiazine 2,2-dioxide (4b)

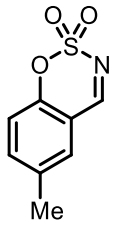

4b

4b was synthesized according to the general procedure from 2-hydroxy-5-methylbenzaldehyde (511 mg, 3.75 mmol). The cyclic imine **4b** was obtained as a pale-yellow solid (587 mg, 80% yield).

^{1}H-NMR (400 MHz, $CDCl_3$) δ 8.61 (s, 1H), 7.63 – 7.51 (m, 1H), 7.46 (d, *J* = 1.5 Hz, 1H), 7.26 (s, 1H), 7.17 (d, *J* = 8.5 Hz, 1H), 2.44 (s, 1H). **^{13}C-NMR (101 MHz, $CDCl_3$)** δ 167.91, 152.33, 138.54, 136.51, 130.75, 118.42, 115.25, 20.77. The characterization data matched with the reported one.[51]

6-chlorobenzo[*e*][1,2,3]oxathiazine 2,2-dioxide (4c)

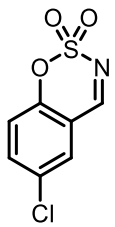

4c

4c was synthesized according to the general procedure from 5-chloro-2-hydroxybenzaldehyde (511 µL, 3.75 mmol). The cyclic imine **4c** was obtained as a pale-yellow solid (434 mg, 53% yield).

^{1}H-NMR (400 MHz, $CDCl_3$) δ 8.67 – 8.55 (m, 1H), 7.77 – 7.62 (m, 2H), 7.31 – 7.19 (m, 1H). **^{13}C-NMR (101 MHz, $CDCl_3$)** δ 166.50, 152.76, 137.48, 131.80, 130.07, 120.39, 116.22. The characterization data matched with the reported one.

6-iodobenzo[*e*][1,2,3]oxathiazine 2,2-dioxide (4d)

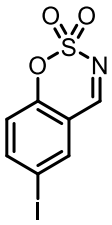

4d

4d was synthesized according to the general procedure from 2-hydroxy-5-iodobenzaldehyde (930 mg, 3.75 mmol). The cyclic imine **4d** was obtained as a pale-yellow solid (583 mg, 74% yield).

^{1}H-NMR (400 MHz, $CDCl_3$) δ 8.60 (s, 1H), 8.04 – 7.97 (m, 2H), 7.07 (d, *J* = 8.6 Hz, 1H).**^{13}C-NMR (101 MHz, $CDCl_3$)** δ 166.27, 154.07, 146.09, 139.07, 120.68, 117.05, 88.73. The characterization data matched with the reported one.[50]

PREPARATION OF 4-PHENYLACETALDEHYDE

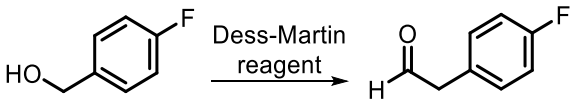

Prepared according to a modified literature procedure.[52] To a solution of the (4-fluorophenyl)methanol (1.0 mmol, 1 equiv., 125 µL) in dichloromethane (4 mL, 0.25 M) at 0 °C was carefully added the Dess-martin reagent (1.2 mmol, 1.2 equiv., 509 mg), and the resulting solution was stirred for 2 hours at room temperature. The reaction was filtered on celite. The residue was purified by flash chromatography (Hex/EtOAc) to afford the product as colorless liquid (33 mg, 24% yield).

Characterization Data

^{1}H-NMR (400 MHz, DMSO-d_6) δ 9.68 (t, *J* = 1.7 Hz, 1H), 7.31 – 7.22 (m, 2H), 7.22 – 7.13 (m, 2H), 3.78 (d, *J* = 1.2 Hz, 2H). **^{19}F-NMR (376 MHz, DMSO-d_6)** δ -116.19. The characterization data matched with the reported one.[52]

2.5.5 General Procedures for the Use of NCDs-3 as Nano-Organocatalysts

AMINOCATALYTIC ALDOL REACTIONS (**3a**-**3l**)

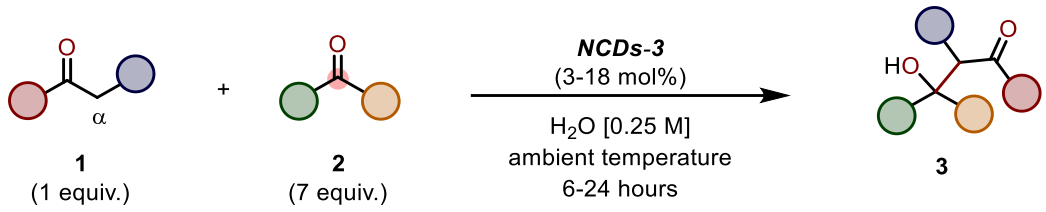

A 4 mL glass vial was charged with the appropriate nucleophile **2** (0.7 mmol, 7 equiv.), NCDs-**3** (3-18 mol%, 2.8-11 mg), the appropriate electrophile **1** (0.1 mmol, 1 equiv.) and water (final concentration: 0.25 M). The resulting mixture was stirred for the indicated time (generally 24 hours) at ambient temperature. The reaction crude was then extracted with EtOAc and the organic phase was filtered through sodium sulfate. The solvent was removed under reduced pressure and the residue was purified by column chromatography (eluent: Hex/EtOAc) to give the corresponding β-hydroxy carbonyl compounds **3**.

Characterization Data

4-hydroxy-4-(4-nitrophenyl)butan-2-one ((*p*)-3a) Prepared according to the general procedure using 4-nitrobenzaldehyde **2a** (0.1 mmol, 10 µL) and acetone **1a** (0.7 mmol, 50 µL). The product **(*p*)-3a** was obtained as yellowish solid (11 mg, 55% yield).

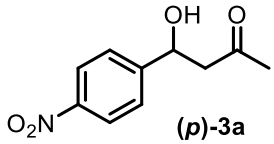

(*p*)-3a

^{1}H-NMR (400 MHz, $CDCl_3$) δ 8.27 – 8.11 (m, 2H), 7.63 – 7.42 (m, 2H), 5.26 (dd, *J* = 7.4, 4.5 Hz, 1H), 3.58 (s, 1H), 2.92 – 2.82 (m, 2H), 2.22 (s, 3H). **^{13}C-NMR (101 MHz, $CDCl_3$)** δ 208.62, 150.05, 126.55, 123.91, 69.06, 51.63, 30.85. **HRMS** calculated for $C_{13}H_{15}NO_4$ (M-Na): 232.0550, found: 232.0580. The characterization of the compound matches with the data reported in the literature.[53]

4-hydroxy-4-(2-nitrophenyl)butan-2-one ((*o*)-3a) Prepared according to the general procedure using 2-nitrobenzaldehyde **2b** (0.1 mmol, 10 µL) and acetone **1a** (0.7 mmol, 50 µL). The product **(*o*)-3a** was obtained as yellowish solid (12 mg, 57% yield).

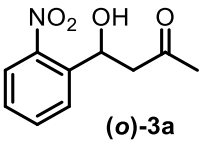

(*o*)-3a

^{1}H-NMR (400 MHz, $CDCl_3$) δ 7.96 (dd, *J* = 8.2, 1.2 Hz, 1H), 7.90 (dd, *J* = 7.9, 1.3 Hz, 1H), 7.67 (m, 1H), 7.48 – 7.40 (m, 1H), 5.68 (dd, *J* = 9.4, 1.9 Hz, 1H), 3.72 (s, 1H), 3.14 (dd, *J* = 17.8, 2.1 Hz, 1H), 2.72 (dd, *J* = 17.8, 9.4 Hz, 1H), 2.24 (s, 3H). **HRMS** calculated for $C_{13}H_{15}NO_4$ (M-Na): 232.0583, found: 232.0580. The characterization of the compound matches with the data reported in the literature.[54]

4-hydroxy-4-(3-nitrophenyl)butan-2-one ((*m*)-3a) Prepared according to the general procedure using 3-nitrobenzaldehyde **2c** (0.1 mmol, 10 µL) and acetone **1a** (0.7 mmol, 50 µL). The product **(*m*)-3a** was obtained as yellowish solid (15 mg, 72% yield).

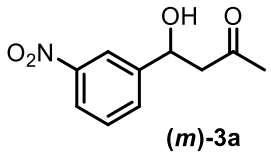

(*m*)-3a

^{1}H-NMR (400 MHz, $CDCl_3$) δ 8.24 (t, *J* = 1.9 Hz, 1H), 8.13 (ddd, *J* = 8.2, 2.2, 1.0 Hz, 1H), 7.75 – 7.61 (m, 1H), 7.53 (t, *J* = 7.9 Hz, 1H), 5.30 – 5.22 (m, 1H), 3.60 (d, *J* = 3.2 Hz, 1H), 2.92 – 2.85 (m, 2H), 2.23 (s, 3H). **^{13}C-NMR (101 MHz, $CDCl_3$)** δ 208.73, 148.52, 144.93, 131.94, 129.65, 122.73, 120.86, 68.93, 51.64, 30.85. **HRMS** calculated for $C_{13}H_{15}NO_4$ (M-Na): 232.0581, found: 232.0580. The characterization of the compound matches with the data reported in the literature.[55]

2-(hydroxy(4-nitrophenyl)methyl)cyclohexan-1-one (3b) Prepared according to the general procedure using 4-nitrobenzaldehyde **2a** (0.1 mmol, 10 µL) and 2-cyclohexen-1-one **1b** (0.7 mmol, 29 µL). The product **3b** was obtained as yellowish solid (16 mg, 65% yield).

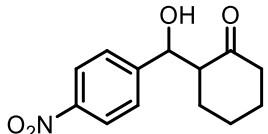

3b

^{1}H-NMR (400 MHz, CD_3OD) δ 8.22 – 8.15 (m, 2H), 7.63 – 7.56 (m, 2H), 5.35-5.10 (m, 1H), 2.76 (tdd, *J* = 11.8, 8.6, 4.9 Hz, 1H), 2.45 – 2.33 (m, 2H), 2.01 (tdd, *J* = 10.6, 6.7, 3.5 Hz, 1H), 1.91 – 1.57 (m, 5H), 1.36 – 1.24 (m, 1H). **^{13}C-NMR (101 MHz, CD_3OD)** δ 212.51, 211.64, 151.69, 150.14, 147.26, 146.69, 127.78, 126.93, 122.79, 122.69, 71.75, 69.48, 57.26, 56.73, 41.61, 41.58, 30.21, 27.68, 26.93, 26.12, 24.03, 23.84. **HRMS** calculated for $C_{13}H_{15}NO_4$ (M-Na): 272.0892, found: 272.0893. The characterization of the compound matches with the data reported in the literature.[56]

3-hydroxy-3-(2-oxopropyl)indolin-2-one (3c) Prepared according to the general procedure using isatin **2d** (0.1 mmol, 15 mg) and acetone **1a** (0.7 mmol, 50 µL). The product **3c** was obtained as brownish solid (18 mg, 90% yield).

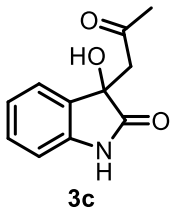

3c

^{1}H-NMR (400 MHz, DMSO) δ 10.21 (s, 1H), 7.23 (dd, *J* = 7.3, 0.5 Hz, 1H), 7.17 (td, *J* = 7.7, 1.3 Hz, 1H), 6.90 (td, *J* = 7.5, 1.0 Hz, 1H), 6.78 (d, *J* = 7.6 Hz, 1H), 6.00 (s, 1H), 3.27 (d, *J* = 16.6 Hz, 1H), 3.00 (d, *J* = 16.6 Hz, 1H), 1.99 (s, *J* = 4.5 Hz, 3H). **^{13}C-NMR (101 MHz, DMSO)** δ 205.38, 178.31, 142.60, 131.58, 129.13, 123.79, 121.42, 109.59, 72.78, 50.35, 30.67. **HRMS** calculated for $C_{11}H_{11}NO_3$ (M-Na): 228.0567, found: 228.0631. The characterization of the compound matches with the data reported in the literature.[57]

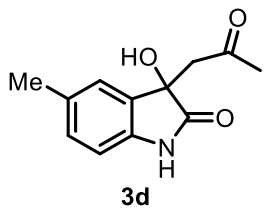

3d

3-hydroxy-5-methyl-3-(2-oxopropyl)indolin-2-one (3d) Prepared according to the general procedure using 5-methylisatin **2e** (0.1 mmol, 17 mg) and acetone **1a** (0.7 mmol, 50 µL). The product **3d** was obtained as brownish solid (17 mg, 78% yield).

^{1}H-NMR (400 MHz, CD_3OD) δ 7.16 – 7.12 (m, 1H), 7.05 (ddd, *J* = 7.9, 1.7, 0.8 Hz, 1H), 6.77 (d, *J* = 7.9 Hz, 1H), 3.39 – 3.28 (m, 1H), 3.14 (d, *J* = 16.6 Hz, 1H), 2.29 (s, 3H), 2.07 (s, 3H). **^{13}C-NMR (101 MHz, CD_3OD)** δ 207.45, 181.16, 141.01, 133.09, 132.29, 130.90, 125.49, 110.99, 74.87, 51.11, 30.69, 21.08. **HRMS** calculated for $C_{12}H_{13}NO_3$ (M-Na): 242.0786, found: 242.0788. The characterization of the compound matches with the data reported in the literature.[57]

5-fluoro-3-hydroxy-3-(2-oxopropyl)indolin-2-one (3e) Prepared according to the general procedure using 5-fluoroisatin **2f** (0.1 mmol, 17 mg) and acetone **1a** (0.7 mmol, 50 µL). The product **3e** was obtained as brownish solid (18 mg, 81% yield).

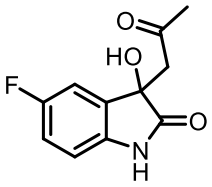

3e

^{1}H-NMR (400 MHz, CD_3OD) δ 7.11 (dd, *J* = 8.0, 2.5 Hz, 1H), 6.97 (ddd, *J* = 9.4, 8.5, 2.7 Hz, 1H), 6.84 (dd, *J* = 8.5, 4.2 Hz, 1H), 3.37 (d, *J* = 18.7 Hz, 1H), 3.18 (d, *J* = 17.2 Hz, 1H), 2.08 (s, 3H). **^{13}C-NMR (101 MHz, CD_3OD)** δ 205.80, 179.67, 160.21, 157.83, 132.75, 132.67, 115.31, 115.08, 111.42, 111.17, 110.51, 110.43, 109.99, 73.50, 49.54, 29.11. **^{19}F-NMR (376 MHz, CD_3OD)** δ -123.21 (ddd, *J* = 9.4, 8.1, 4.3 Hz). **HRMS** calculated for $C_{11}H_{12}FNO_3$ (M-Na): 246.0534, found: 246.0534. The characterization of the compound matches with the data reported in the literature.[57]

5-chloro-3-hydroxy-3-(2-oxopropyl)indolin-2-one (3f) Prepared according to the general procedure using 5-chloroisatin **2g** (0.1 mmol, 18 mg) and acetone **1a** (0.7 mmol, 50 µL). The product **3f** was obtained as white solid (21 mg, 89% yield).

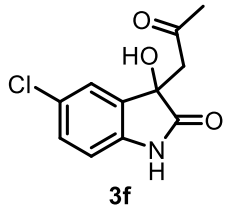

3f

^{1}H-NMR (400 MHz, CD_3OD) δ 7.32 (d, *J* = 2.0 Hz, 1H), 7.23 (dd, *J* = 8.3, 2.2 Hz, 1H), 6.85 (d, *J* = 8.2 Hz, 1H), 3.39 (d, *J* = 17.2 Hz, 1H), 3.19 (d, *J* = 17.2 Hz, 1H), 2.08 (s, 3H). **^{13}C-NMR (101 MHz, CD_3OD)** δ 205.81, 179.36, 141.03, 132.96, 128.98, 127.11, 123.86, 110.92, 73.24, 49.55, 29.04. **HRMS** calculated for $C_{11}H_{10}ClNO_3$ (M-Na): 262.0239, found: 262.0241. The characterization of the compound matches with the data reported in the literature.[58]

5-bromo-3-hydroxy-3-(2-oxopropyl)indolin-2-one (3g) Prepared according to the general procedure using 5-bromoisatin **2h** (0.1 mmol, 18 mg) and acetone **1a** (0.7 mmol, 50 µL). The product **3g** was obtained as as brownish solid (19 mg, 67% yield).

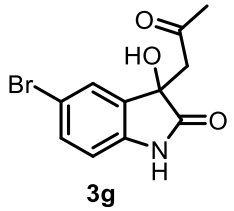

3g

^{1}H-NMR (400 MHz, CD_3OD) δ 7.45 (d, *J* = 1.8 Hz, 1H), 7.37 (dd, *J* = 8.2, 2.0 Hz, 1H), 6.82 – 6.79 (m, 1H), 3.39 (d, *J* = 17.0 Hz, 1H), 3.19 (d, *J* = 17.2 Hz, 1H), 2.08 (s, 3H). **^{13}C-NMR (101 MHz, CD_3OD)** δ 207.53, 180.93, 143.23, 135.07, 133.67, 128.39, 115.93, 113.13, 74.90, 51.28, 49.30, 30.75. **HRMS** calculated for $C_{11}H_{10}BrNO_3$ (M-Na): 305.9737, found: 305.9736. The characterization of the compound matches with the data reported in the literature.[57]

5,7-dibromo-3-hydroxy-3-(2-oxopropyl)indolin-2-one (3h) Prepared according to the general procedure using 5,7-dibromoisatin **2i** (0.1 mmol, 30 mg) and acetone **1a** (0.7 mmol, 50 µL). The product **3h** was obtained as yellowish solid (15 mg, 41% yield).

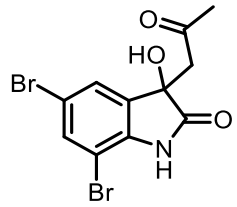

3h

^{1}H-NMR (500 MHz, DMSO) δ 10.70 (s, 1H), 7.68 – 7.56 (m, 1H), 7.46 (d, *J* = 1.8 Hz, 1H), 6.27 (s, 1H), 3.13 (d, *J* = 17.8 Hz, 1H), 2.01 (s, 3H). **^{13}C-NMR (126 MHz, DMSO)** δ 205.67, 177.76, 141.86, 135.53, 133.52, 125.88, 113.56, 102.64, 73.45, 50.08, 30.19. **HRMS** calculated for $C_{11}H_9Br_2NO_3$ (M-Na): 383.8843, found: 383.8841. The characterization of the compound matches with the data reported in the literature.[57]

3-hydroxy-3-(2-oxopropyl)-1-phenylindolin-2-one (3i) Prepared according to the general procedure using 1-phenylisatin **2j** (0.1 mmol, 22 mg) and acetone **1a** (0.7 mmol, 50 µL). The product **3i** was obtained as brownish solid (24 mg, 85% yield).

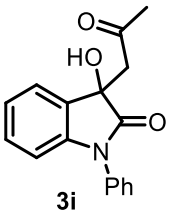

3i

^{1}H-NMR (400 MHz, CD_3OD) δ 7.61 – 7.53 (m, 2H), 7.49 – 7.39 (m, 4H), 7.24 (td, *J* = 7.8, 1.3 Hz, 1H), 7.09 (td, *J* = 7.5, 1.0 Hz, 1H), 6.73 – 6.67 (m, 1H), 3.62 – 3.51 (m, 1H), 3.37 (s, 1H), 2.07 (s, 3H). **^{13}C-NMR (101 MHz, CD_3OD)** δ 205.91, 177.41, 144.47, 134.56, 130.16, 129.31, 129.27, 128.05, 126.65, 123.27, 122.94, 109.14, 72.92, 50.38, 28.97. **HRMS** calculated for $C_{17}H_{15}NO_3$ (M-Na): 304.0943, found: 304.0944. The characterization of the compound matches with the data reported in the literature.[59]

3-hydroxy-1-methyl-3-(2-oxopropyl)indolin-2-one (3j) Prepared according to the general procedure using 1-methylisatin **2k** (0.1 mmol, 17 mg) and acetone **1a** (0.7 mmol, 50 µL). The product **3j** was obtained as brownish solid (8 mg, 37% yield).

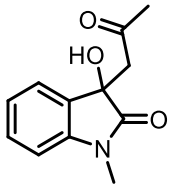

3j

^{1}H-NMR (400 MHz, $CDCl_3$) δ 7.38 – 7.34 (m, 1H), 7.32 (dd, *J* = 7.8, 1.3 Hz, 1H), 7.06 (td, *J* = 7.6, 1.0 Hz, 1H), 6.83 (d, *J* = 7.8 Hz, 1H), 3.18 (m, 4H), 2.94 (d, *J* = 17.0 Hz, 1H), 2.17 (s, 3H). **^{13}C-NMR (101 MHz, $CDCl_3$)** δ 207.68, 176.02, 143.50, 130.03, 129.70, 123.85, 123.13, 108.58, 74.22, 48.62, 29.68, 28.74, 26.28. **HRMS** calculated for $C_{12}H_{13}NO_3$ (M-Na): 242.0788, found: 242.0788. The characterization of the compound matches with the data reported in the literature.[59]

3-hydroxy-3-(2-oxocyclohexyl)indolin-2-one (3k) Prepared according to the general procedure using isatin **2d** (0.1 mmol, 15 mg) and cyclohexanone **1b** (0.7 mmol, 73 µL). The product **3k** was obtained as brownish solid (15 mg, 62% yield, d.r. 13:1).

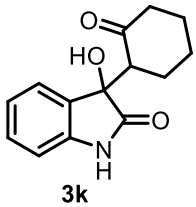

3k

^{1}H-NMR (400 MHz, CD_3CN) δ 7.34 – 7.30 (m, 1H), 7.26 (td, *J* = 7.7, 1.3 Hz, 1H), 6.99 (td, *J* = 7.6, 1.0 Hz, 1H), 6.92 – 6.88 (m, 1H), 4.30 (s, 1H), 3.12 (ddd, *J* = 13.1, 5.3, 1.2 Hz, 1H), 2.46 – 2.29 (m, 2H), 2.26 – 2.20 (m, 1H), 2.08 – 1.99 (m, 1H), 1.88 – 1.47 (m, 4H). **^{13}C-NMR (101 MHz, CD_3CN)** δ 211.63, 179.15, 143.71, 131.00, 130.29, 125.81, 122.71, 118.26, 110.59, 76.35, 57.47, 42.56, 27.92, 27.37, 25.32. **HRMS** calculated for $C_{14}H_{15}NO_3$ (M-Na): 268.0946, found: 268.0944. The characterization of the compound matches with the data reported in the literature.[59]

1-(4-(tert-butyl)benzyl)-3-hydroxy-3-(2-oxocyclohexyl)indolin-2-one (3l). Prepared according to the general procedure using 1-para-tertbutilphenylisatin **2l** (0.1 mmol, 29 mg) and cyclohexanone **1b** (0.7 mmol, 73 µL). The product **3l** was obtained as red solid (19 mg, 67% yield, d.r. >20:1).

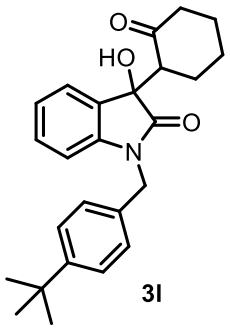

3l

^{1}H-NMR (400 MHz, $CDCl_3$) δ 7.33 (dt, *J* = 8.4, 2.0 Hz, 3H), 7.30 – 7.25 (m, 2H), 7.21 (td, *J* = 7.8, 1.2 Hz, 1H), 7.02 (td, *J* = 7.6, 0.9 Hz, 1H), 6.72 (d, *J* = 7.8 Hz, 1H), 4.96 (dd, *J* = 34.2, 18.5 Hz, 1H), 4.78 (d, *J* = 15.7 Hz, 1H), 3.03 (dd, *J* = 12.1, 5.4 Hz, 1H), 2.48 (dd, *J* = 8.9, 6.2 Hz, 1H), 2.39 – 2.26 (m, 1H), 1.87 (t, *J* = 9.1 Hz, 1H), 1.73 – 1.53 (m, 3H), 1.31 – 1.24 (m, 9H). **^{13}C-NMR (126 MHz, $CDCl_3$)** δ 211.94, 176.90, 150.62, 143.87, 132.70, 129.94, 129.04, 127.18, 125.79, 124.08, 123.00, 109.66, 77.23, 55.46, 43.71, 42.23, 34.63, 31.44, 27.34, 26.14, 24.62. **HRMS** calculated for $C_{25}H_{29}NO_3$ (M-Na): 414.2014, found: 414.2040.

AMINOCATALYTIC MANNICH REACTIONS (5a-5d)

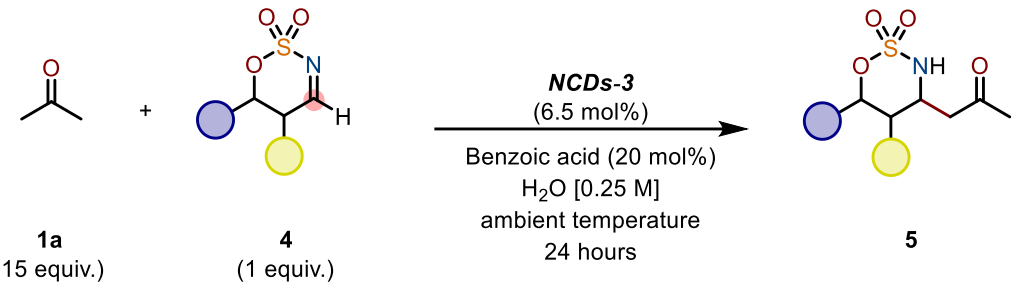

A 4 mL glass vial was charged with the appropriate cyclic imine **4** (0.1 mmol, 1 equiv.), NCDs-**3** (3.3% mol, 2 mg), acetone **1a** (1.5 mmol, 15 equiv.), benzoic acid (0.02 mmol, 0.2 equiv.) and water (final concentration: 0.25 M). The resulting mixture was stirred for the indicated time (24 hours) at ambient temperature. The reaction crude was then extracted with EtOAc and the organic phase was filtered through sodium sulfate. The solvent was removed under reduced pressure and the residue was purified by column chromatography (eluent: dicloromethane) to give the corresponding product **5**.

Characterization Data

1-(2,2-dioxido-3,4-dihydrobenzo[e][1,2,3]oxathiazin-4-yl)propan-2-one (5a)

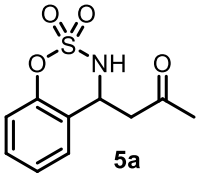

Prepared according to the general procedure using benzo[e][1,2,3]oxathiazine 2,2-dioxide **4a** (0.1 mmol, 19 mg), benzoic acid (0.02 mmol, 2.5 mg) and acetone **1a** (1.5 mmol, 110 µL). The product **5a** was obtained as white solid (22 mg, 91% yield).

^{1}H-NMR (400 MHz, $CDCl_3$) δ 7.32 (dddd, *J* = 8.1, 7.5, 1.7, 0.7 Hz, 1H), 7.18 (td, *J* = 7.6, 1.2 Hz, 1H), 7.13 – 7.08 (m, 1H), 7.04 (dd, *J* = 8.3, 1.2 Hz, 1H), 5.17 (dd, *J* = 7.3, 4.0 Hz, 1H), 3.63 (dd, *J* = 18.2, 7.3 Hz, 1H), 2.97 (dd, *J* = 18.2, 4.0 Hz, 1H), 2.24 (s, 3H). **^{13}C-NMR (101 MHz, $CDCl_3$)** δ 206.80, 151.31, 129.83, 125.88, 125.61, 121.46, 119.33, 53.55, 46.43, 31.20. **HRMS** calculated for $C_{10}H_{11}NO_4S$(M-Na): 264.0307, found: 264.0301.

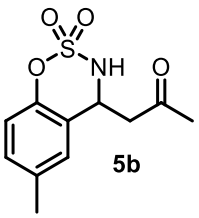

1-(6-methyl-2,2-dioxido-3,4-dihydrobenzo[e][1,2,3]oxathiazin-4-yl)propan-2-one (5b) Prepared according to the general procedure using 6-methylbenzo[e][1,2,3]oxathiazine 2,2-dioxide **4b** (0.1 mmol, 20 mg), benzoic acid (0.02 mmol, 2.5 mg) and acetone **1a** (1.5 mmol, 110 µL). The product **5b** was obtained as white solid (13 mg, 51% yield).

^{1}H-NMR (400 MHz, $CDCl_3$) δ 7.13 – 7.07 (m, 1H), 6.95 – 6.86 (m, 2H), 5.62 (d, *J* = 7.8 Hz, 1H), 5.13 (td, *J* = 7.7, 3.9 Hz, 1H), 3.61 (dd, *J* = 18.1, 7.6 Hz, 1H), 2.95 (dd, *J* = 18.2, 3.9 Hz, 1H), 2.31 (s, 3H), 2.24 (s, 3H). **^{13}C-NMR (101 MHz, $CDCl_3$)** δ 206.80, 149.17, 135.40, 130.40, 126.19, 121.01, 119.01, 53.50, 46.71, 31.17, 20.98. **HRMS** calculated for $C_{11}H_{13}NO_4S$(M-Na): 278.0455, found: 278.0457.

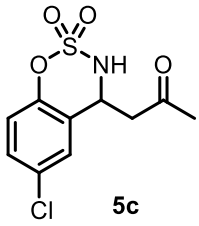

5c

1-(6-chloro-2,2-dioxido-3,4-dihydrobenzo[e][1,2,3]oxathiazin-4-yl)propan-2-one (5c) Prepared according to the general procedure using 6-chlorobenzo[e][1,2,3]oxathiazine 2,2-dioxide **4c** (0.1 mmol, 22 mg), benzoic acid (0.02 mmol, 2.5 mg) and acetone **1a** (1.5 mmol, 110 µL). The product **5c** was obtained as white solid (8 mg, 30% yield).

^{1}H-NMR (400 MHz, $CDCl_3$) δ 7.33 – 7.23 (m, 1H), 7.09 (dd, *J* = 2.4, 0.8 Hz, 1H), 6.99 (d, *J* = 8.8 Hz, 1H), 5.71 (s, 1H), 5.12 (m, 1H), 3.60 (dd, *J* = 18.4, 7.1 Hz, 1H), 2.99 (dd, *J* = 18.4, 4.0 Hz, 1H), 2.26 (s, 3H). **^{13}C-NMR (101 MHz, $CDCl_3$)** δ 206.46, 149.82, 130.85, 129.91, 125.85, 123.07, 120.71, 53.25, 46.23, 31.11. **HRMS** calculated for $C_{10}H_{10}ClNO_4S$(M-Na): 297.9910, found: 297.9911.

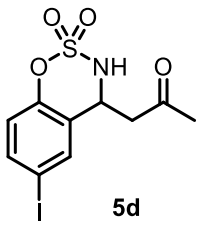

5d

1-(6-iodo-2,2-dioxido-3,4-dihydrobenzo[e][1,2,3]oxathiazin-4-yl)propan-2-one (5d) Prepared according to the general procedure using 6-iodobenzo[e][1,2,3]oxathiazine 2,2-dioxide **4d** (0.1 mmol, 31 mg), benzoic acid (0.02 mmol, 2.5 mg) and acetone **1a** (1.5 mmol, 110 µL). The product **5d** was obtained as white solid (16 mg, 44% yield).

^{1}H-NMR (400 MHz, $CDCl_3$) δ 7.61 (ddd, *J* = 8.7, 2.1, 0.6 Hz, 1H), 7.42 (dd, *J* = 2.0, 0.8 Hz, 1H), 6.79 (d, *J* = 8.7 Hz, 1H), 5.75 (s, 1H), 5.13 (s, 1H), 3.60 (dd, *J* = 18.3, 7.3 Hz, 1H), 2.97 (dd, *J* = 18.3, 3.9 Hz, 1H), 2.26 (s, 3H). **^{13}C-NMR (101 MHz, $CDCl_3$)** δ 206.47, 151.24, 138.73, 134.75, 123.81, 121.25, 88.71, 52.92, 46.34, 31.14. HRMS calculated for $C_{10}H_{10}INO_4S$(M-Na): 389.9268, found: 389.9267.

<u>AMINOCATALYTIC KNOEVENAGEL REACTIONS (7a-7d)</u>

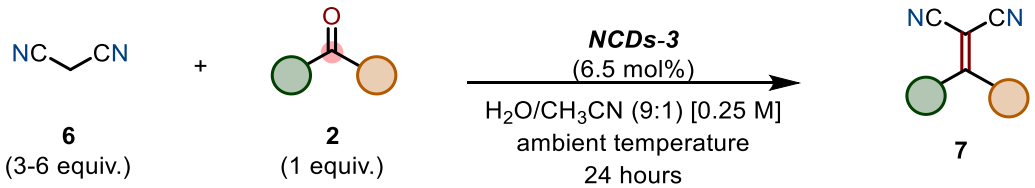

6
(3-6 equiv.)

2
(1 equiv.)

7

A 4 mL glass vial was charged with malononitrile **6** (0.3-0.6 mmol, 3-6 equiv.), NCDs-**3** (6.5% mol, 3.7 mg), the appropriate electrophiles **2** (0.1 mmol, 1 equiv.), and water/acetonitrile (9:1) (final

concentration: 0.25 M). The resulting mixture was stirred for the indicated time (24 hours) at ambient temperature. The reaction crude was then extracted with EtOAc and the organic phase was filtered through sodium sulfate. The solvent was removed under reduced pressure and the residue was purified by column chromatography (eluent: Hex/EtOAc) to give the corresponding product **7**.

Characterization Data

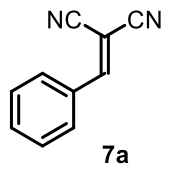

7a

2-benzylidenemalononitrile (7a) Prepared according to the general procedure using malononitrile **6** (0.6 mmol, 6 equiv.), and benzaldehyde **2m** (0.1 mmol, 1 equiv.). The product **7a** was obtained as white solid (9 mg, 58% yield).

^{1}H-NMR (400 MHz, $CDCl_3$) δ 7.96 – 7.85 (m, 2H), 7.78 (s, 1H), 7.70 – 7.61 (m, 1H), 7.58 – 7.47 (m, 2H).**^{13}C-NMR (101 MHz, $CDCl_3$)** δ 160.05, 134.76, 131.07, 130.86, 129.77, 113.83, 112.66, 83.06. It was not possible to measure the HRMS (ESI-MS) of compound **7a** due to its poor tendency to ionize. The characterization of the compound matches with the data reported in the literature.[60]

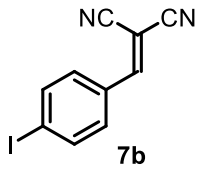

7b

2-(4-iodobenzylidene)malononitrile (7b) Prepared according to the general procedure using malononitrile **6** (0.6 mmol, 6 equiv.), and 4-iodobenzaldehyde **2n** (0.1 mmol, 1 equiv.). The product **7b** was obtained as white solid (13 mg, 46% yield).

^{1}H-NMR (400 MHz, $CDCl_3$) δ 7.94 – 7.88 (m, 2H), 7.69 (s, 1H), 7.63 – 7.57 (m, 2H). **^{13}C-NMR (101 MHz, $CDCl_3$)** δ 158.79, 139.21, 131.65, 130.28, 113.60, 112.47, 102.97, 83.73. It was not possible to measure the HRMS (ESI-MS) of compound **7b** due to its poor tendency to ionize. The characterization of the compound matches with the data reported in the literature.[61]

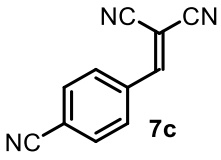

7c

2-(4-cyanobenzylidene)malononitrile (7c) Prepared according to the general procedure using malononitrile **6** (0.6 mmol, 6 equiv.), and 4-cyanobenzaldehyde **2o** (0.1 mmol, 1 equiv.). The product **7c** was obtained as white solid (8 mg, 45% yield).

^{1}H-NMR (400 MHz, $CDCl_3$) δ 7.99 (d, *J* = 8.3 Hz, 2H), 7.86 – 7.75 (m, 2H). **^{13}C-NMR (101 MHz, $CDCl_3$)** δ 158.79, 139.21, 131.65, 130.28, 113.60, 112.47, 102.97, 83.73. It was not possible to measure the HRMS (ESI-MS) of compound **7c** due to its poor tendency to ionize. The characterization of the compound matches with the data reported in the literature.[61]

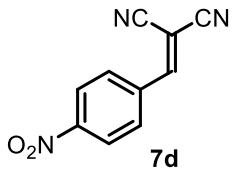

7d

2-(4-nitrobenzylidene)malononitrile (7d) Prepared according to the general procedure using malononitrile **6** (0.3 mmol, 3 equiv.), and 4-nitrobenzaldehyde **2a** (0.1 mmol, 1 equiv.). The product **7d** was obtained as yellow solid (13 mg, 65% yield).

^{1}H-NMR (400 MHz, $CDCl_3$) δ 8.45 – 8.35 (m, 2H), 8.11 – 8.03 (m, 2H), 7.88 (s, 1H). **^{13}C-NMR (101 MHz, $CDCl_3$)** δ 156.97, 135.92, 131.45, 124.79, 112.75, 111.73, 87.71. It was not possible to measure the HRMS (ESI-MS) of compound **7d** due to its poor tendency to ionize. The characterization of the compound matches with the data reported in the literature.[61]

AMINOCATALYTIC MICHAEL ADDITIONS (**10a**-**10l**)

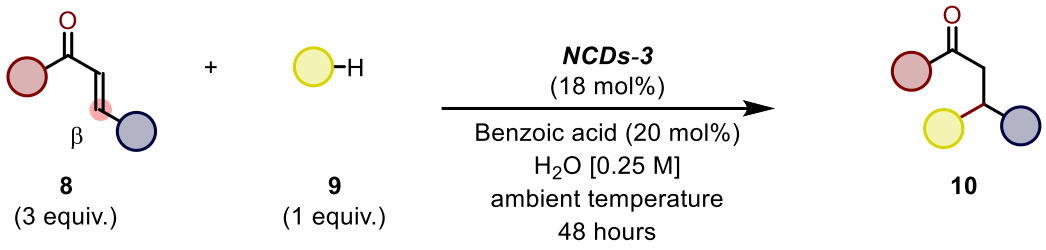

8
(3 equiv.)

9
(1 equiv.)

10

A 4 mL glass vial was charged with the appropriate α,β-unsaturated carbonyl compound **8** (0.3 mmol, 3 equiv.), NCDs-**3** (18 mol%, 11 mg), the appropriate nucleophile **9** (0.1 mmol, 1 equiv.), benzoic acid (0.02 mmol, 0.2 equiv.) and water (final concentration: 0.25 M). The resulting mixture was stirred for the indicated time (48 hours) at ambient temperature. The reaction crude was then extracted with EtOAc and the organic phase was filtered through sodium sulfate. The solvent was removed under reduced pressure and the residue was purified by column chromatography (eluent: Hex/EtOAc) to give the corresponding β-substituted carbonyl compound **10**.

Characterization Data

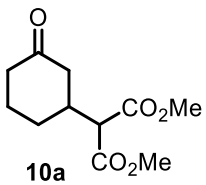

10a

Dimethyl 2-(3-oxocyclohexyl)malonate (10a) Prepared according to the general procedure using dimethyl malonate **9a** (0.1 mmol, 11 µL) and 2-cyclohexen-1-one **8a** (0.3 mmol, 29 µL). The product **10a** was obtained as yellowish oil (9 mg, 40% yield).

^{1}H-NMR (400 MHz, $CDCl_3$) δ 3.75 (d, *J* = 3.5 Hz, 6H), 3.34 (d, *J* = 8.0 Hz, 1H), 2.54 (dddd, *J* = 15.5, 11.4, 7.7, 3.7 Hz, 1H), 2.47 – 2.35 (m, 2H), 2.26 (m, 2H), 2.14 – 2.02 (m, 1H), 2.00 – 1.88 (m, 1H), 1.78 – 1.61 (m, 1H), 1.56 – 1.43 (m, 1H). **^{13}C-NMR (101 MHz, $CDCl_3$)** δ 209.62, 168.40, 168.31, 56.77,

52.74, 45.23, 41.13, 38.26, 28.94, 24.66. HRMS calculated for $C_{11}H_{16}O_3$ (M-Na): 251.0892, found: 251.0890. The characterization of the compound matches with the data reported in the literature.[62]

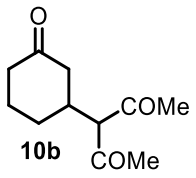

10b

3-(3-oxocyclohexyl)pentane-2,4-dione (10b) Prepared according to the general procedure using acetylacetone **9b** (0.1 mmol, 10 µL) and 2-cyclohexen-1-one **8a** (0.3 mmol, 29 µL). The product **10b** was obtained as yellowish oil (12 mg, 59% yield).

^{1}H-NMR (400 MHz, $CDCl_3$) δ 3.63 (d, *J* = 10.2 Hz, 1H), 2.76 – 2.60 (m, 1H), 2.45 – 2.35 (m, 1H), 2.34 – 2.20 (m, 2H), 2.17 (d, *J* = 9.4 Hz, 6H), 2.10 – 1.98 (m, 2H), 1.89 – 1.63 (m, 2H), 1.44 – 1.30 (m, 1H). **^{13}C-NMR (101 MHz, $CDCl_3$)** δ 209.04, 202.88, 202.70, 74.91, 45.22, 41.06, 38.39, 29.75, 29.58, 28.81, 24.45. **HRMS** calculated for $C_{11}H_{16}O_3$ (M-Na): 219.0993, found: 219.0992. The characterization of the compound matches with the data reported in the literature.[58]

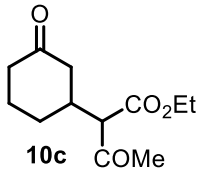

10c

Ethyl 3-oxo-2-(3-oxocyclohexyl)butanoate (10c) Prepared according to the general procedure using ethyl acetoacetate **9c** (0.1 mmol, 13 µL) and 2-cyclohexen-1-one **8a** (0.3 mmol, 29 µL). The product **10c** was obtained as yellowish oil (14 mg, 60% yield, d.r. 1:1).

^{1}H-NMR (400 MHz, $CDCl_3$) δ 4.26 – 4.14 (m, 2H), 3.38 (dd, *J* = 8.7, 7.5 Hz, 1H), 2.66 – 2.50 (m, 1H), 2.46 – 2.32 (m, 2H), 2.30 – 2.19 (m, 3H), 2.19 – 2.12 (m, 1H), 2.11 – 1.99 (m, 1H), 1.96 – 1.81 (m, 1H), 1.77 – 1.62 (m, 1H), 1.61 – 1.49 (m, 1H), 1.32 – 1.23 (m, 4H). **^{13}C-NMR (101 MHz, CDCl3)** δ 209.68, 209.59, 201.77, 201.65, 168.42, 168.22, 65.33, 64.91, 61.83, 61.76, 45.55, 45.17, 41.25, 41.19, 37.90, 29.66, 29.64, 29.18, 28.72, 24.69, 14.28, 14.25. **HRMS** calculated for $C_{12}H_{18}O_6$ (M-Na): 249.1096, found: 249.1097. The characterization of the compound matches with the data reported in the literature.[63]

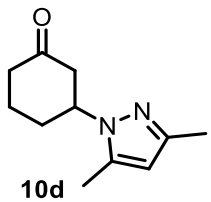

10d

3-(3,5-dimethyl-1H-pyrazol-1-yl)cyclohexan-1-one (10d) Prepared according to the general procedure using 3,5-dimethyl-pyrazol **9d** (0.1 mmol, 10 mg) and 2-cyclohexen-1-one **8a** (0.3 mmol, 28 µL). The product **10d** was obtained as yellowish oil (17 mg, 88% yield).

^{1}H-NMR (400 MHz, $CDCl_3$) δ 5.76 (s, 1H), 4.35 – 4.17 (m, 1H), 3.09 (dd, *J* = 14.3, 11.5 Hz, 1H), 2.74 – 2.52 (m, 1H), 2.48 – 2.38 (m, 2H), 2.37 – 2.23 (m, 1H), 2.22 – 2.18 (m, 6H), 2.17 – 2.09 (m, 1H), 2.09 – 1.99 (m, 1H), 1.87 (s, 1H), 1.74 – 1.58 (m, 1H). **^{13}C-NMR (101 MHz, $CDCl_3$)** δ 208.95, 147.82, 137.92,

105.16, 55.80, 48.12, 40.70, 31.50, 22.32, 13.71, 10.95. **HRMS** calculated for $C_{11}H_{16}N_2O$ (M-Na): 215.1157, found: 215.1155.

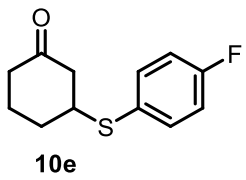

10e

3-((4-fluorophenyl)thio)cyclohexan-1-one (10e) Prepared according to the general procedure using 4-fluorophenylthiol **9e** (0.1 mmol, 11 µL) and 2-cyclohexen-1-one **8a** (0.3 mmol, 28 µL). The product **10e** was obtained with 97% yield (22 mg).

^{1}H-NMR (400 MHz, $CDCl_3$) δ 7.47 – 7.38 (m, 2H), 7.09 – 6.96 (m, 2H), 3.40 – 3.24 (m, 1H), 2.64 (ddt, *J* = 14.3, 4.5, 1.6 Hz, 1H), 2.42 – 2.19 (m, 3H), 2.19 – 2.06 (m, 2H), 1.80 – 1.55 (m, 2H). ^{19}F-NMR (376 MHz, $CDCl_3$) δ -113.07. **^{13}C-NMR (101 MHz, $CDCl_3$)** δ 208.55, δ 162.81 (d, J = 248.7 Hz), 136.16 (d, J = 8.2 Hz), 116.18 (d, J = 21.8 Hz), 47.66, 46.85, 40.82, 31.17, 23.96. **HRMS** calculated for $C_{12}H_{13}FOS$ (M-Na): 247.0564, found: 247.0563. The characterization of the compound matches with the data reported in the literature.[64]

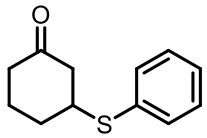

10f

3-((4-fluorophenyl)thio)cyclohexan-1-one (10f) Prepared according to the general procedure using thiophenol **9f** (0.1 mmol, 10 µL) and 2-cyclohexen-1-one **8a** (0.3 mmol, 28 µL). The product **10f** was obtained as yellowish oil (15 mg, 75% yield).

^{1}H-NMR (400 MHz, $CDCl_3$) δ 7.43 (m, 2H), 7.36 – 7.27 (m, 3H), 3.43 (ddd, *J* = 14.1, 10.1, 4.2 Hz, 1H), 2.69 (dd, *J* = 14.3, 4.4 Hz, 1H), 2.43 – 2.23 (m, 3H), 2.22 – 2.06 (m, 2H), 1.88 – 1.63 (m, 2H). **^{13}C-NMR (101 MHz, $CDCl_3$)** δ 208.71, 133.23, 132.98, 129.05, 127.78, 47.77, 46.12, 40.87, 31.26, 24.04. **HRMS** calculated for $C_{12}H_{14}OS$ (M-Na): 229.0657, found: 229.0658. The characterization of the compound matches with the data reported in the literature.[65]

3-((4-fluorophenyl)thio)cyclopentan-1-one (10g) Prepared according to the general procedure using 4-fluorophenylthiol **9e** (0.1 mmol, 11 µL) and 2-cyclopenten-1-one **8b** (0.3 mmol, 25 µL). The product **10g** was obtained as yellowish oil (17 mg, 82% yield).

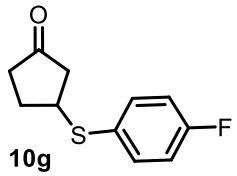

10g

^{1}H-NMR (400 MHz, $CDCl_3$) δ 7.45 – 7.37 (m, 2H), 7.08 – 6.97 (m, 2H), 3.84 – 3.71 (m, 1H), 2.64 – 2.39 (m, 1H), 2.37 – 2.14 (m, 3H), 2.04 – 1.91 (m, 1H). ^{19}F-NMR (376 MHz, $CDCl_3$) δ -108.99 – -120.35 (m). **^{13}C-NMR (101 MHz, $CDCl_3$)** δ 216.29, 162.76 (d, *J* = 248.5 Hz), 135.25 (d, *J* = 8.2 Hz), 129.07 (d, *J* = 3.4 Hz), 116.41 (d, *J* = 22.0 Hz), 45.23, 44.49, 36.87, 29.42. **HRMS** calculated for $C_{11}H_{11}FOS$ (M-Na): 233.0406, found: 233.0407.

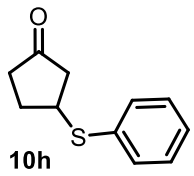

10h

3-(phenylthio)cyclopentan-1-one (10h) Prepared according to the general procedure using thiophenol **9f** (0.1 mmol, 10 µL) and 2-cyclopenten-1-one **8b** (0.3 mmol, 25 µL). The product **10h** was obtained as yellowish oil (10 mg, 55% yield).

^{1}H-NMR (400 MHz, $CDCl_3$) δ 7.44 – 7.38 (m, 1H), 7.36 – 7.24 (m, 2H), 3.95 – 3.82 (m, 1H), 2.61 (dd, *J* = 18.7, 7.2 Hz, 1H), 2.54 – 2.43 (m, 1H), 2.41 – 2.17 (m, 2H), 2.09 – 1.96 (m, 1H). **^{13}C-NMR (101 MHz, $CDCl_3$)** δ 216.54, 134.31, 132.16, 129.25, 127.58, 45.38, 43.55, 36.93, 29.49. **HRMS** calculated for $C_{11}H_{12}OS$ (M-Na): 215.0502, found: 215.0501. The characterization of the compound matches with the data reported in the literature.[65]

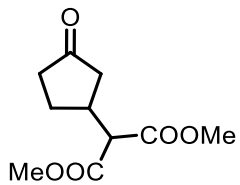

10i

Dimethyl 2-(3-oxocyclopentyl)malonate (10i) Prepared according to the general procedure using dimethyl malonate **9a** (0.1 mmol, 11 µL) and 2-cyclopenten-1-one **8b** (0.3 mmol, 25 µL). The product **10i** was obtained as yellowish oil (14 mg, 65% yield).

^{1}H-NMR (400 MHz, $CDCl_3$) δ 3.76 (s, 3H), 3.74 (s, *J* = 1.6 Hz, 3H), 3.37 (d, *J* = 9.4 Hz, 1H), 2.93 – 2.78 (m, 1H), 2.50 (dd, *J* = 18.4, 7.6 Hz, 1H), 2.41 – 2.29 (m, 1H), 2.29 – 2.13 (m, 2H), 2.00 (ddd, *J* = 18.4, 11.0, 1.4 Hz, 1H), 1.75 – 1.54 (m, 2H). **^{13}C-NMR (101 MHz, $CDCl_3$)** δ 217.04, 168.65, 168.57, 56.24, 52.79, 52.78, 43.01, 38.31, 36.53, 27.62. **HRMS** calculated for $C_{10}H_{14}O_5$ (M-Na): 237.0733, found: 237.0733. The characterization of the compound matches with the data reported in the literature.[62]

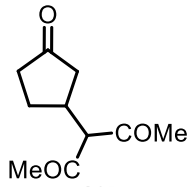

10j

3-(3-oxocyclopentyl)pentane-2,4-dione (10j) Prepared according to the general procedure using acetylacetone **9b** (0.1 mmol, 10 µL) and 2-cyclopenten-1-one **8b** (0.3 mmol, 25 µL). The product **10j** was obtained as yellowish oil (10 mg, 55% yield).

^{1}H-NMR (400 MHz, $CDCl_3$) δ 3.62 (d, *J* = 10.5 Hz, 1H), 2.95 (qdd, *J* = 10.4, 7.1, 5.5 Hz, 1H), 2.47 – 2.27 (m, 2H), 2.24 – 2.21 (m, 3H), 2.21 – 2.09 (m, 5H), 1.78 (ddd, *J* = 18.2, 11.0, 1.3 Hz, 1H), 1.54 – 1.44 (m, 1H). **^{13}C-NMR (101 MHz, $CDCl_3$)** δ 216.55, 202.85, 202.63, 75.10, 42.81, 38.07, 36.36, 29.70, 29.45, 27.67. The characterization of the compound matches with the data reported in the literature.[66]

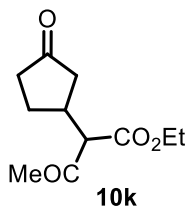

10k

3-(3-oxocyclohexyl)pentane-2,4-dione(10k) Prepared according to the general procedure using ethyl acetoacetate **9c** (0.1 mmol, 13 µL) and 2-cyclopenten-1-one **8b** (0.3 mmol, 25 µL). The product **10k** was obtained as yellowish oil (18 mg, 86% yield).

^{1}H-NMR (400 MHz, $CDCl_3$) δ 4.29 – 4.09 (m, 1H), 3.41 (dd, J = 9.8, 6.3 Hz, 1H), 2.95 – 2.79 (m, 1H), 2.45 (ddd, J = 12.1, 7.1, 3.2 Hz, 1H), 2.36 – 2.10 (m, 6H), 1.88 (dddd, J = 53.0, 18.3, 11.0, 1.4 Hz, 1H), 1.69 – 1.41 (m, 1H), 1.36 – 1.18 (m, 4H). **^{13}C-NMR (101 MHz, $CDCl_3$)** δ 217.03, 216.99, 201.54, 201.38, 168.37, 168.29, 64.81, 64.60, 61.70, 61.68, 42.94, 42.69, 38.15, 38.00, 35.83, 35.74, 29.44, 29.21, 27.61, 27.33, 14.10, 14.07. **HRMS** calculated for $C_{11}H_{16}O_4$ (M-Na): 235.0943, found: 235.0941. The characterization of the compound matches with the data reported in the literature.[63]

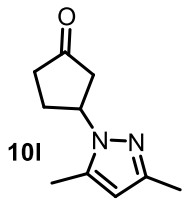

3-(3,5-dimethyl-1H-pyrazol-1-yl)cyclopentan-1-one (10l) Prepared according to the general procedure using 3,5-dimethyl-pyrazol **9d** (0.1 mmol, 10 mg) and 2-cyclopenten-1-one **8b** (0.3 mmol, 25 µL). The product **10l** was obtained as yellowish oil (16 mg, 88% yield).

^{1}H-NMR (499 MHz, $CDCl_3$) δ 5.79 (s, 1H), 4.77 (p, *J* = 7.2 Hz, 1H), 2.94 – 2.82 (m, 1H), 2.64 (dddd, *J* = 30.4, 21.7, 11.8, 4.6 Hz, 2H), 2.48 – 2.32 (m, 2H), 2.31 – 2.21 (m, 4H), 2.19 (s, 3H).**^{13}C-NMR (101 MHz, $CDCl_3$)** δ 215.59, 147.58, 138.27, 105.29, 77.27, 77.01, 76.76, 54.41, 44.35, 37.16, 29.86, 13.58, 10.93. **HRMS** calculated for $C_{10}H_{14}N_2O$ (M-Na): 201.0997, found: 201.0998.

AMINOCATALYTIC TANDEM KNOEVENAGEL-MICHAEL REACTIONS (**12a**-**12h**)

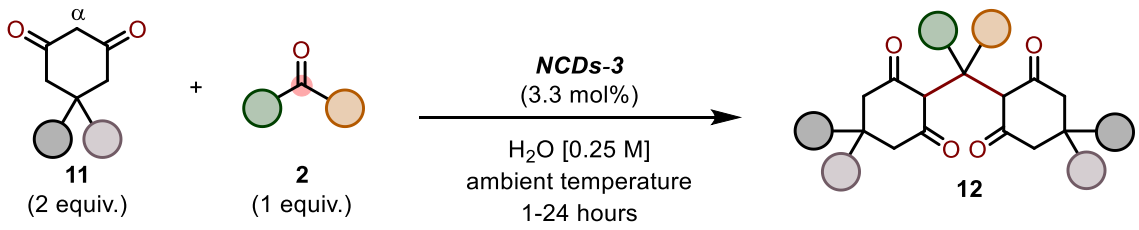

A 4 mL glass vial was charged with the appropriate diketone **11** (0.2 mmol, 2 equiv.), NCDs-**3** (3.3% mol, 2 mg), the appropriate electrophiles **2** (0.1 mmol, 1 equiv.) and water (final concentration: 0.25 M). The resulting mixture was stirred for the indicated time (1-24 hours) at ambient temperature. The reaction crude was then extracted with EtOAc and the organic phase was filtered through sodium sulfate. The solvent was removed under reduced pressure and the residue was purified by column chromatography (eluent: Hex/EtOAc) to give the corresponding β-sostituited carbonyl compound **12**.

Characterization Data

2,2'-(phenylmethylene)bis(5,5-dimethylcyclohexane-1,3-dione) (12a) Prepared according to the general procedure using cyclohexane-1,3-dione (0.2 mmol, 28 mg) and benzaldehyde (0.1 mmol, 10 µL) for 1 hour. The product **12a** was obtained as white solid (35 mg, 94% yield).

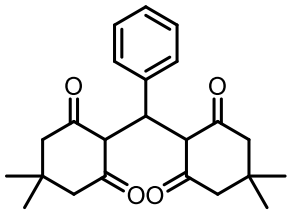

12a

^{1}H-NMR (400 MHz, $CDCl_3$) δ 11.90 (s, 1H), 7.30 – 7.22 (m, 2H), 7.21 – 7.14 (m, 1H), 7.12 – 7.06 (m, 2H), 5.54 (s, 1H), 2.57 – 2.21 (m, 8H), 1.24 (s, *J* = 8.0 Hz, 7H), 1.10 (s, *J* = 20.1 Hz, 6H). **^{13}C-NMR (101 MHz, $CDCl_3$)** δ 190.59, 189.52, 138.20, 128.34, 126.91, 125.97, 115.73, 47.21, 46.60, 32.89, 31.56, 29.80, 27.55. **HRMS** calculated for $C_{23}H_{28}O_4$ (M-Na): 369.2063, found: 369.2060. The characterization of the compound matches with the data reported in the literature.[44]

2,2'-((4-nitrophenyl)methylene)bis(5,5-dimethylcyclohexane-1,3-dione)(12b) Prepared according to the general procedure using 5,5-dimethylcyclohexane-1,3-dione (0.2 mmol, 28 mg) and 4-nitrobenzaldehyde (0.1 mmol, 15 µL) for 2 hours. The product **12b** was obtained as white solid (37 mg, 90% yield).

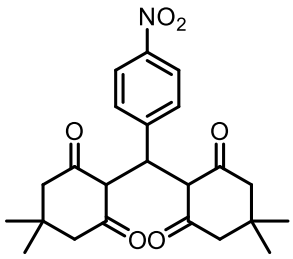

12b

^{1}H-NMR (400 MHz, $CDCl_3$) δ 11.81 (s, 1H), 8.27 – 8.00 (m, 2H), 7.33 – 7.14 (m, 2H), 5.54 (s, 1H), 2.40 (dq, *J* = 27.6, 17.6 Hz, 8H), 1.23 (s, *J* = 7.4 Hz, 6H), 1.11 (s, *J* = 22.8 Hz, 6H). **^{13}C-NMR (101 MHz, $CDCl_3$)** δ 191.09, 189.70, 146.67, 146.24, 127.77, 123.64, 115.04, 47.13, 46.56, 33.38, 31.61, 29.67, 27.59. **HRMS** calculated for $C_{23}H_{27}NO_6$ (M-Na): 414.1917, found: 414.1919. The characterization of the compound matches with the data reported in the literature.[67]

4-(bis(4,4-dimethyl-2,6-dioxocyclohexyl)methyl)benzonitrile (12c) Prepared according to the general procedure using 5,5-dimethylcyclohexane-1,3-dione (0.2 mmol, 28 mg) and 4-formylbenzonitrile (0.1 mmol, 14 µL) for 2 hours. The product **12c** was obtained as white solid (36 mg, 93% yield).

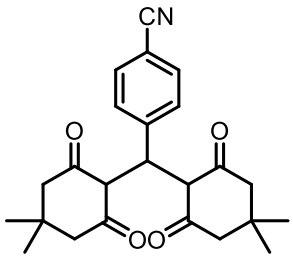

12c

^{1}H-NMR (400 MHz, $CDCl_3$) δ 11.79 (s, 1H), 7.62 – 7.46 (m, 2H), 7.19 (dd, *J* = 8.6, 1.0 Hz, 2H), 5.52 (s, 1H), 2.55 – 2.29 (m, 8H), 1.22 (s, 6H), 1.11 (s, 6H). **^{13}C-NMR (101 MHz, $CDCl_3$)** δ 191.06, 189.65, 144.47, 132.21, 127.74, 119.05, 114.96, 109.89, 47.14, 46.56, 33.38, 31.60, 29.69, 27.60. **HRMS** calculated for $C_{24}H_{27}NO_4$ (M-Na):394.2017, found: 394.2013. The characterization of the compound matches with the data reported in the literature.[68]

2,2'-((4-bromophenyl)methylene)bis(5,5-dimethylcyclohexane-1,3-dione) (12d) Prepared according to the general procedure using 5,5-dimethylcyclohexane-1,3-dione (0.2 mmol, 28 mg) and 4-bromobenzaldehyde (0.1 mmol, 11 µL) for 2 hours. The product **12d** was obtained as white solid (39 mg, 92% yield).

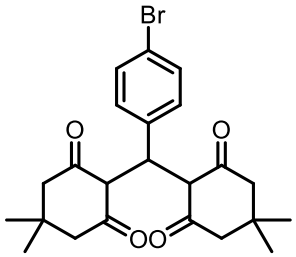

12d

^{1}H-NMR (499 MHz, $CDCl_3$) δ 12.32 (s, 1H), 12.07 (s, 1H), 7.40 – 7.34 (m, 2H), 7.00 – 6.95 (m, 2H), 5.38 (s, 1H), 2.61 (ddt, *J* = 32.7, 17.8, 3.7 Hz, 4H), 2.51 – 2.33 (m, 4H), 2.11 – 1.96 (m, 4H). **^{13}C-NMR (126 MHz, $CDCl_3$)** δ 192.42, 191.03, 137.22, 131.36, 128.50, 119.79, 116.26, 33.63, 33.13, 32.78, 20.21. **HRMS** calculated for $C_{23}H_{27}BrO_6$ (M-Na): 469.0986, found: 469.0985. The characterization of the compound matches with the data reported in the literature.[67]

2,2'-((4-fluorophenyl)methylene)bis(5,5-dimethylcyclohexane-1,3-dione) (12e) Prepared according to the general procedure using 5,5-dimethylcyclohexane-1,3-dione (0.2 mmol, 28 mg) and 4-fluorobenzaldehyde (0.1 mmol, 11 µL) for 2 hours. The product **12e** was obtained as white solid (36 mg, 92% yield).

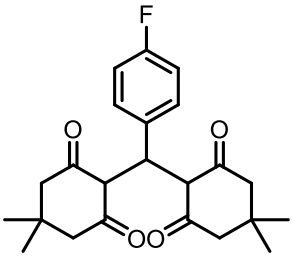

12e

^{1}H-NMR (400 MHz, $CDCl_3$) δ 11.88 (s, 1H), 7.08 – 7.00 (m, 2H), 6.99 – 6.89 (m, 2H), 5.48 (s, 1H), 2.38 (dq, *J* = 26.2, 17.7 Hz, 8H), 1.22 (s, *J* = 22.7 Hz, 6H), 1.10 (s, *J* = 19.4 Hz, 6H). ^{19}F-NMR (376 MHz, $CDCl_3$) δ -117.79. **^{13}C-NMR (101 MHz, $CDCl_3$)** δ 190.67, 189.51, 162.36, 159.93, 133.76, 133.72, 128.42, 128.34, 115.67, 115.24, 115.03, 47.19, 46.56, 32.36, 31.54, 29.74, 27.53. **HRMS** calculated for $C_{23}H_{27}FO_4$ (M-Na): 387.1965, found: 387.1966. The characterization of the compound matches with the data reported in the literature.[67]

2,2'-((3,5-bis(trifluoromethyl)phenyl)methylene)bis(5,5-dimethylcyclohexane-1,3-dione)(12f)

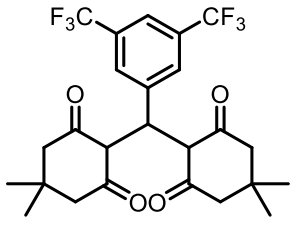

12f

Prepared according to the general procedure using 5,5-dimethylcyclohexane-1,3-dione (0.2 mmol, 28 mg) and 3,5-bis(trifluoromethyl)benzaldehyde (0.1 mmol, 17 µL) for 2 hours. The product **12f** was obtained as white solid (42 mg, 83% yield).

^{1}H-NMR (400 MHz, $CDCl_3$) δ 11.85 (s, 1H), 7.69 (s, 1H), 7.54 (s, 2H), 5.54 (s, 1H), 2.64 – 2.23 (m, 8H), 1.23 (s, 6H), 1.12 (s, 6H).^{19}F-NMR (376 MHz, $CDCl_3$) δ -63.04. **^{13}C-NMR (101 MHz, $CDCl_3$)** δ 191.31, 189.74, 141.37, 132.07, 131.75, 131.42, 131.09, 127.27, 124.89, 122.18, 120.17, 114.60, 47.09, 46.53, 33.11, 31.48, 29.92, 27.01. **HRMS** calculated for $C_{25}H_{26}F_6O_4$ (M-Na): 505.1807, found: 505.1808.

2,2'-(thiophen-2-ylmethylene)bis(5,5-dimethylcyclohexane-1,3-dione) (12 g) Prepared according to the general procedure using 5,5-dimethylcyclohexane-1,3-dione (0.2 mmol, 28 mg) and thiophene-2-carbaldehyde (0.1 mmol, 9 µL) for 24 hours. The product **12g** was obtained as white solid (40 mg, 98% yield).

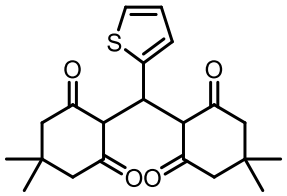

12g

^{1}H-NMR (400 MHz, $CDCl_3$) δ 12.34 (s, 1H), 7.10 (d, *J* = 5.1 Hz, 1H), 6.87 (dd, *J* = 5.1, 3.6 Hz, 1H), 6.66 – 6.59 (m, 1H), 5.63 (s, 1H), 2.44 – 2.21 (m, 9H), 1.21 (s, *J* = 15.8 Hz, 6H), 1.10 (s, *J* = 19.4 Hz, 6H). **^{13}C-NMR (101 MHz, $CDCl_3$)** δ 190.11, 189.63, 143.85, 126.48, 124.66, 123.60, 116.11, 47.15, 46.41, 31.31, 30.51, 30.09, 26.90. **HRMS** calculated for $C_{21}H_{26}O_4S$ (M-Na): 397.1444, found: 397.1444. The characterization of the compound matches with the data reported in the literature.[67]

2,2'-(phenylmethylene)bis(cyclohexane-1,3-dione) (12h) Prepared according to the general procedure using cyclohexane-1,3-dione (0.2 mmol, 23 mg) and benzaldehyde (0.1 mmol, 11 µL) for 2 hours. The product **12h** was obtained as white solid (23 mg, 75% yield).

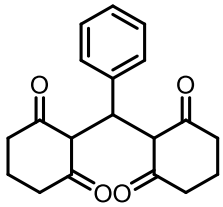

12h

^{1}H-NMR (400 MHz, $CDCl_3$) δ 12.35 (s, 1H), 7.29 – 7.23 (m, 1H), 7.17 (ddd, *J* = 7.9, 3.8, 1.1 Hz, 1H), 7.13 – 7.08 (m, 1H), 2.61 (dd, *J* = 22.2, 18.1 Hz, 4H), 2.42 (m, 4H), 2.10 – 1.97 (m, 4H). **^{13}C-NMR (101 MHz, $CDCl_3$)** δ 192.23, 191.01, 137.99, 128.30, 126.62, 125.99, 116.58, 33.66, 33.15, 33.06, 20.27. **HRMS** calculated for $C_{19}H_{20}O_4$ (M-Na): 335.1299, found: 335.1254.

MANIPULATION OF COMPOUND **12a** (**13a**-**13b**)

3,3,6,6-tetramethyl-9-phenyl-3,4,5,6,7,9-hexahydro-1H-xanthene-1,8(2H)-dione (13a)

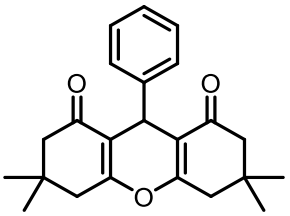

13a

A 4 mL glass vial was charged with the compound **12a** (0.5 mmol, 1 equiv.), acetic acid (2 mL). The resulting mixture was stirred for 18 hours at ambient temperature. The reaction crude was purified by crystallization from ethanol/water (8:2) to give the corresponding product **13a** (121 mg, 71% yield over two steps).

^{1}H-NMR (400 MHz, $CDCl_3$) δ 7.28 (dt, *J* = 3.1, 1.7 Hz, 2H), 7.24 – 7.18 (m, 2H), 7.12 – 7.06 (m, 1H), 4.75 (s, 1H), 2.46 (s, 4H), 2.20 (q, *J* = 16.3 Hz, 4H), 1.10 (s, 6H), 0.99 (s, 6H). **^{13}C-NMR (101 MHz, $CDCl_3$)** δ 196.50, 162.36, 144.22, 128.51, 128.18, 126.50, 115.82, 50.89, 41.03, 32.35, 31.98, 29.42,

27.48. **HRMS** calculated for $C_{23}H_{27}O_3$ (M-Na): 373.1773, found: 373.1774. The characterization of the compound matches with the data reported in the literature.[69]

3,3,6,6-tetramethyl-9-phenyl-3,4,6,7,9,10-hexahydroacridine-1,8(2H,5H)-dione (13b)

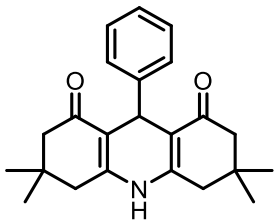

13b

A 4 mL glass vial was charged with the compound **12a** (0.5 mmol, 1 equiv.), ammonium acetate (2.5 mmol, 5 equiv.), and water (2 mL). The resulting mixture was stirred for the indicated time (16 hours) at ambient temperature. The reaction crude was purified by crystallization from ethanol/water (8:2) to give the corresponding product **13b** (98 mg, 57% yield over two steps).

^{1}H-NMR (400 MHz, $CDCl_3$) δ 7.37 – 7.29 (m, 2H), 7.18 (t, *J* = 7.6 Hz, 2H), 7.06 (t, *J* = 7.3 Hz, 1H), 6.37 (s, 1H), 5.08 (s, 1H), 2.44 – 2.11 (m, 8H), 1.08 (s, 6H), 0.96 (s, 6H). **^{13}C-NMR (101 MHz, $CDCl_3$)** δ 196.04, 149.31, 146.75, 128.14, 128.08, 126.10, 113.36, 51.02, 40.80, 33.76, 32.74, 29.69, 27.23. **HRMS** calculated for $C_{23}H_{27}NO_2$ (M-Na): 350.2113, found: 350.2115. The characterization of the compound matches with the data reported in the literature.[69]

2.5.6 ^{19}F-NMR Studies

First, we studied the formation and stability of the imines and enamines derived from different representative amines, namely butylamine, aniline, benzyl amine with 4-fluorobenzaldehyde. Then, the corresponding derivatives obtained from benzyl amine and pyrrolidine with 4-fluorophenylacetaldehyde, in DMSO-d_6. In Figure 2.36-2.39 are depicted the ^{19}F-NMR spectra to characterize the so-formed imine and enamine derivatives from NCDs-**3**.

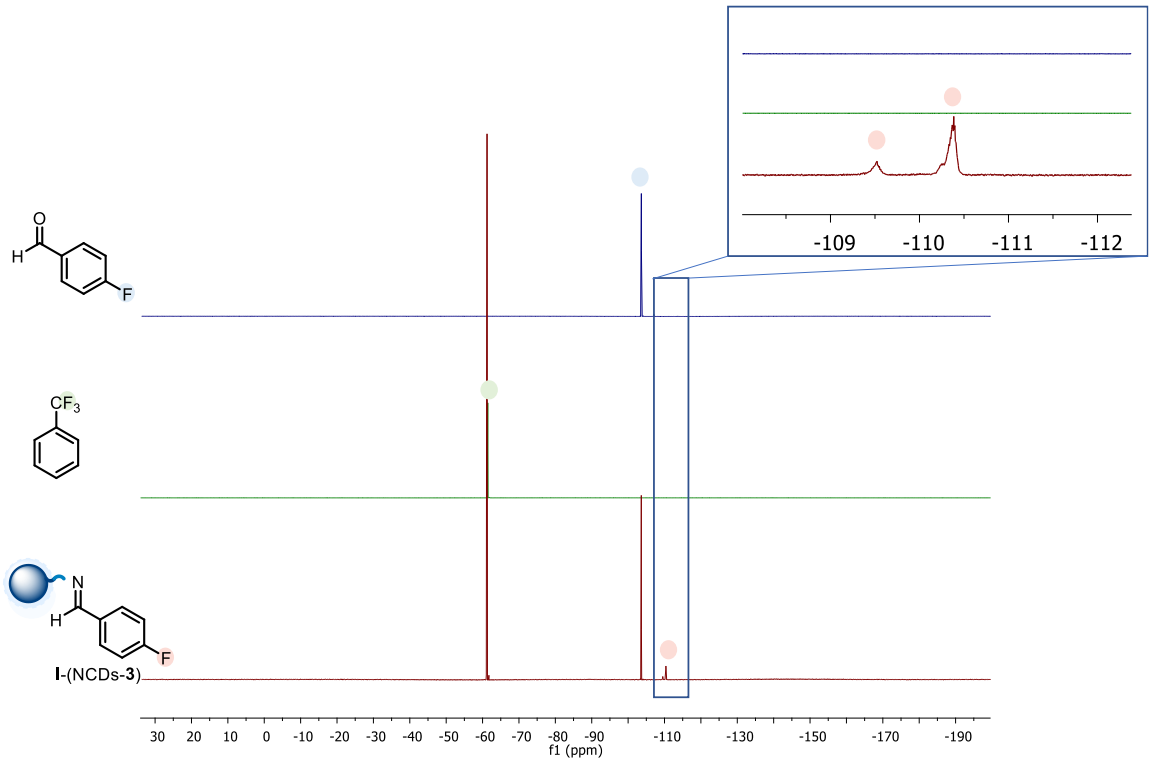

*Figure 2.36 ^{19}F-NMR spectra of the in-situ formation of the imine derived from 4-fluorobenzaldehyde and NCDs-**3** in DMSO-d_6. Comparison between ^{19}F-NMR spectra of 4-fluorobenzaldehyde (blue), trifluorotoluene as internal standard (green) and **I**-(NCDs-**3**) (red). The ^{19}F-NMR expansion between -109 and -112 ppm shows the broad fluorine signal of **I**-(NCDs-**3**) that experience different chemical environments.*

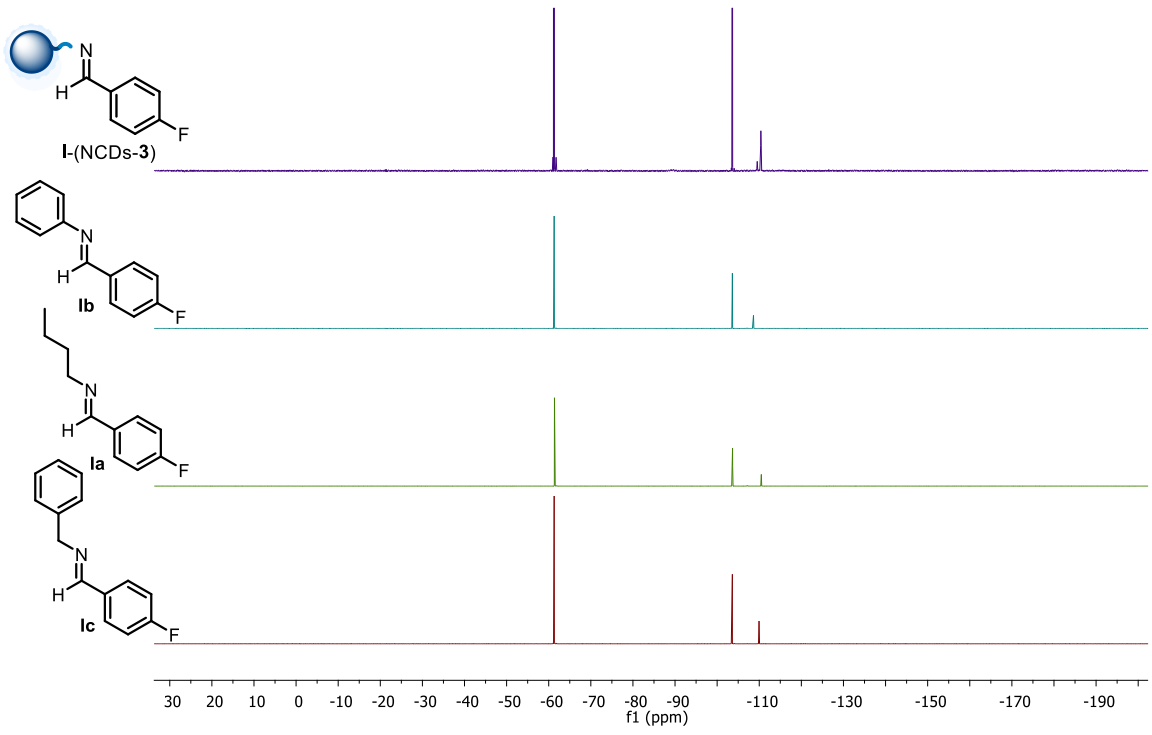

*Figure 2.37 Comparison between ^{19}F-NMR spectra of imine **I**-(NCDs-**3**) (blue), **Ib** (light blue), **Ia** (green) and **Ic** (red).*

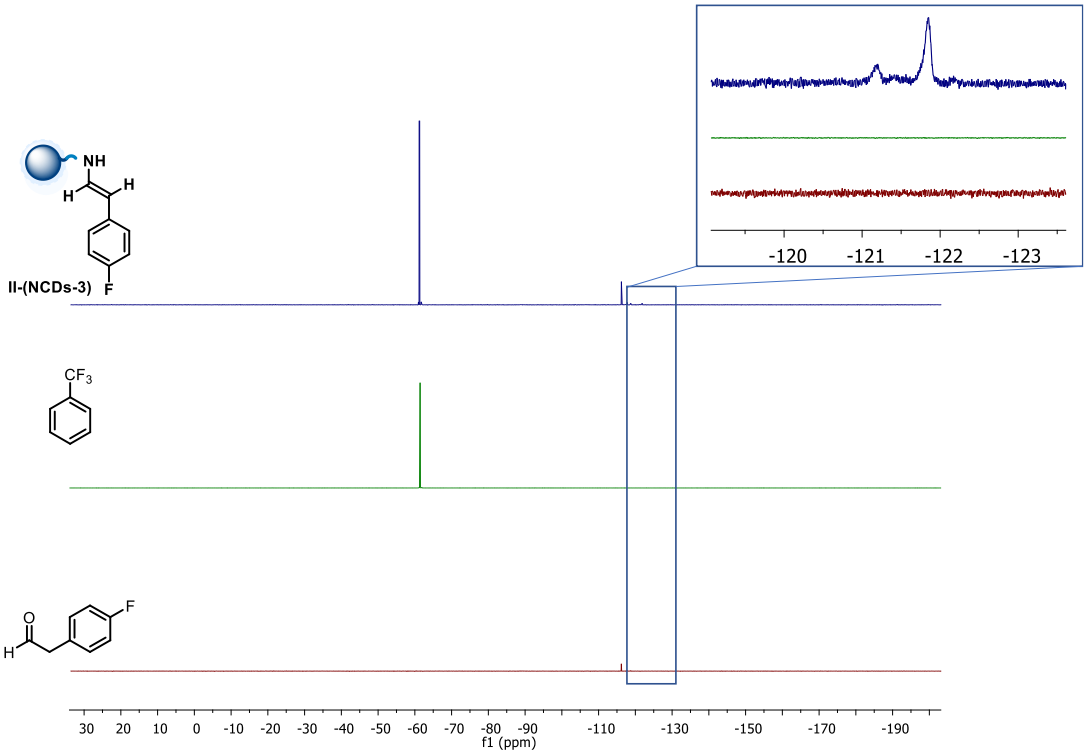

*Figure 2.38 ^{19}F-NMR spectra of the in-situ formation of the enamine derived from 4-fluorophenylacetaldehyde and NCDs-**3** in DMSO-d_6. Comparison between ^{19}F-NMR spectra of 4-fluorophenylacetaldehyde (blue), trifluorotoluene as internal standard (green) and **II**-(NCDs-**3**) (red). The ^{19}F-NMR expansion between -120 and -123 ppm shows the broad fluorine signal of **II**-(NCDs-**3**) that experience different chemical environments.*

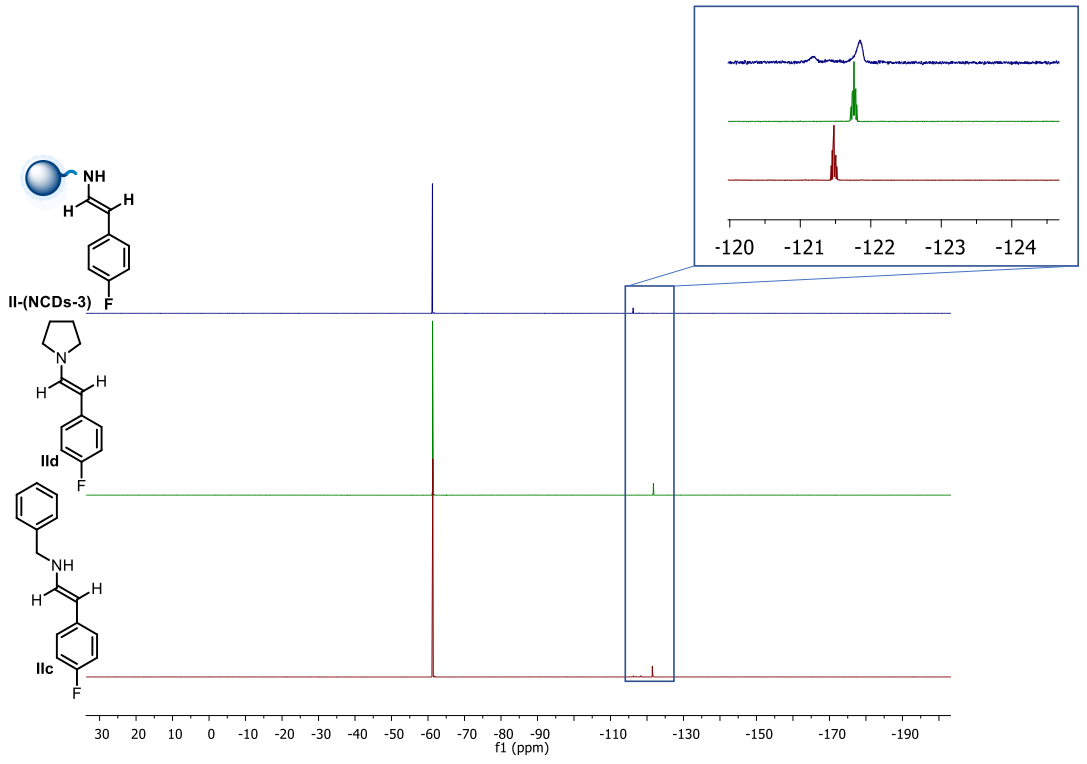

*Figure 2.39 Comparison between ^{19}F-NMR spectra of enamine **II**-(NCDs-**3**) (blue), **IId** (green) and **IIc** (red).*

2.6 References Chapter 2

(1) Gentile, G.; Mamone, M.; Rosso, C.; Amato, F.; Lanfrit, C.; Filippini, G.; Prato, M. Tailoring the Chemical Structure of Nitrogen-Doped Carbon Dots for Nano-Aminocatalysis in Aqueous Media. *ChemSusChem* **2023**, *16* (7), e202202399. https://doi.org/10.1002/cssc.202202399.

(2) Corti, V.; Bartolomei, B.; Mamone, M.; Gentile, G.; Prato, M.; Filippini, G. Amine-Rich Carbon Dots as Novel Nano-Aminocatalytic Platforms in Organic Synthesis. *European Journal of Organic Chemistry* **2022**, *2022* (41), e202200879. https://doi.org/10.1002/ejoc.202200879.

(3) Arcudi, F.; Đorđević, L.; Prato, M. Synthesis, Separation, and Characterization of Small and Highly Fluorescent Nitrogen-Doped Carbon NanoDots. *Angew. Chem. Int. Ed.* **2016**, *55* (6), 2107–2112. https://doi.org/10.1002/anie.201510158.

(4) Xu, X.; Ray, R.; Gu, Y.; Ploehn, H. J.; Gearheart, L.; Raker, K.; Scrivens, W. A. Electrophoretic Analysis and Purification of Fluorescent Single-Walled Carbon Nanotube Fragments. *J. Am. Chem. Soc.* **2004**, *126* (40), 12736–12737. https://doi.org/10.1021/ja040082h.

(5) Baker, S. N.; Baker, G. A. Luminescent Carbon Nanodots: Emergent Nanolights. *Angew. Chem. Int. Ed.* **2010**, *49* (38), 6726–6744. https://doi.org/10.1002/anie.200906623.

(6) Arcudi, F.; Đorđević, L.; Prato, M. Design, Synthesis, and Functionalization Strategies of Tailored Carbon Nanodots. *Acc. Chem. Res.* **2019**, *52* (8), 2070–2079. https://doi.org/10.1021/acs.accounts.9b00249.

(7) Cui, L.; Ren, X.; Sun, M.; Liu, H.; Xia, L. Carbon Dots: Synthesis, Properties and Applications. *Nanomaterials* **2021**, *11* (12), 3419. https://doi.org/10.3390/nano11123419.

(8) Yan, F.; Jiang, Y.; Sun, X.; Bai, Z.; Zhang, Y.; Zhou, X. Surface Modification and Chemical Functionalization of Carbon Dots: A Review. *Microchim Acta* **2018**, *185* (9), 424. https://doi.org/10.1007/s00604-018-2953-9.

(9) Lim, S. Y.; Shen, W.; Gao, Z. Carbon Quantum Dots and Their Applications. *Chem. Soc. Rev.* **2014**, *44* (1), 362–381. https://doi.org/10.1039/C4CS00269E.

(10) de Boëver, R.; Town, J. R.; Li, X.; Claverie, J. P. Carbon Dots for Carbon Dummies: The Quantum and The Molecular Questions Among Some Others. *Chemistry – A European Journal* **2022**, *28* (47), e202200748. https://doi.org/10.1002/chem.202200748.

(11) Manjupriya, R.; Roopan, S. M. Carbon Dots-Based Catalyst for Various Organic Transformations. *J Mater Sci* **2021**, *56* (31), 17369–17410. https://doi.org/10.1007/s10853-021-06354-7.

(12) Rosso, C.; Filippini, G.; Prato, M. Carbon Dots as Nano-Organocatalysts for Synthetic Applications. *ACS Catal.* **2020**, *10* (15), 8090–8105. https://doi.org/10.1021/acscatal.0c01989.

(13) Semeniuk, M.; Yi, Z.; Poursorkhabi, V.; Tjong, J.; Jaffer, S.; Lu, Z.-H.; Sain, M. Future Perspectives and Review on Organic Carbon Dots in Electronic Applications. *ACS Nano* **2019**, *13* (6), 6224–6255. https://doi.org/10.1021/acsnano.9b00688.

(14) Li, H.; Yan, X.; Kong, D.; Jin, R.; Sun, C.; Du, D.; Lin, Y.; Lu, G. Recent Advances in Carbon Dots for Bioimaging Applications. *Nanoscale Horiz.* **2020**, *5* (2), 218–234. https://doi.org/10.1039/C9NH00476A.

(15) Wang, J.; Koo, K. M.; Wang, Y.; Trau, M. Engineering State-of-the-Art Plasmonic Nanomaterials for SERS-Based Clinical Liquid Biopsy Applications. *Advanced Science* **2019**, *6* (23), 1900730. https://doi.org/10.1002/advs.201900730.

(16) Alafeef, M.; Srivastava, I.; Aditya, T.; Pan, D. Carbon Dots: From Synthesis to Unraveling the Fluorescence Mechanism. *Small* **2024**, *20* (4), 2303937. https://doi.org/10.1002/smll.202303937.

(17) Rocco, D.; Moldoveanu, V. G.; Feroci, M.; Bortolami, M.; Vetica, F. Electrochemical Synthesis of Carbon Quantum Dots. *ChemElectroChem* **2023**, *10* (3), e202201104. https://doi.org/10.1002/celc.202201104.

(18) Xia, C.; Zhu, S.; Feng, T.; Yang, M.; Yang, B. Evolution and Synthesis of Carbon Dots: From Carbon Dots to Carbonized Polymer Dots. *Advanced Science* **2019**, *6* (23), 1901316. https://doi.org/10.1002/advs.201901316.

(19) Filippini, G.; Amato, F.; Rosso, C.; Ragazzon, G.; Vega-Peñaloza, A.; Companyó, X.; Dell'Amico, L.; Bonchio, M.; Prato, M. Mapping the Surface Groups of Amine-Rich Carbon Dots Enables Covalent Catalysis in Aqueous Media. *Chem* **2020**, *6* (11), 3022–3037. https://doi.org/10.1016/j.chempr.2020.08.009.

(20) Zhao, Z.; Pieber, B.; Delbianco, M. Modulating the Surface and Photophysical Properties of Carbon Dots to Access Colloidal Photocatalysts for Cross-Couplings. *ACS Catal.* **2022**, *12* (22), 13831–13837. https://doi.org/10.1021/acscatal.2c04025.

(21) Bartolomei, B.; Prato, M. The Importance of the Purification Step and the Characterization of the Products in the Synthesis of Carbon Nanodots. *Small* **2023**, *19* (31), 2206714. https://doi.org/10.1002/smll.202206714.

(22) Đorđević, L.; Arcudi, F.; Cacioppo, M.; Prato, M. A Multifunctional Chemical Toolbox to Engineer Carbon Dots for Biomedical and Energy Applications. *Nat. Nanotechnol.* **2022**, *17* (2), 112–130. https://doi.org/10.1038/s41565-021-01051-7.

(23) Baragau, I.-A.; P. Power, N.; J. Morgan, D.; Heil, T.; Alvarez Lobo, R.; Simon Roberts, C.; Titirici, M.-M.; Dunn, S.; Kellici, S. Continuous Hydrothermal Flow Synthesis of Blue-Luminescent, Excitation-Independent Nitrogen-Doped Carbon Quantum Dots as Nanosensors. *Journal of Materials Chemistry A* **2020**, *8* (6), 3270–3279. https://doi.org/10.1039/C9TA11781D.

(24) Bartolomei, B.; Sbacchi, M.; Rosso, C.; Günay-Gürer, A.; Zdražil, L.; Cadranel, A.; Kralj, S.; Guldi, D. M.; Prato, M. Synthetic Strategies for the Selective Functionalization of Carbon Nanodots Allow Optically Communicating Suprastructures. *Angewandte Chemie* **2024**, *136* (5), e202316915. https://doi.org/10.1002/ange.202316915.

(25) Li, H.; Sun, C.; Ali, M.; Zhou, F.; Zhang, X.; MacFarlane, D. R. Sulfated Carbon Quantum Dots as Efficient Visible-Light Switchable Acid Catalysts for Room-Temperature Ring-Opening Reactions. *Angewandte Chemie* **2015**, *127* (29), 8540–8544. https://doi.org/10.1002/ange.201501698.

(26) Tejwan, N.; Saha, S. K.; Das, J. Multifaceted Applications of Green Carbon Dots Synthesized from Renewable Sources. *Advances in Colloid and Interface Science* **2020**, *275*, 102046. https://doi.org/10.1016/j.cis.2019.102046.

(27) Majumdar, B.; Mandani, S.; Bhattacharya, T.; Sarma, D.; Sarma, T. K. Probing Carbocatalytic Activity of Carbon Nanodots for the Synthesis of Biologically Active Dihydro/Spiro/Glyco Quinazolinones and Aza-Michael Adducts. *J. Org. Chem.* **2017**, *82* (4), 2097–2106. https://doi.org/10.1021/acs.joc.6b02914.

(28) Mayank; Singh, A.; Kaur, N.; Singh, N.; Jang, D. O. A Carbon Quantum Dot-Encapsulated Micellar Reactor for the Synthesis of Chromene Derivatives in Water. *Molecular Catalysis* **2017**, *439*, 100–107. https://doi.org/10.1016/j.mcat.2017.06.032.

(29) Pei, X.; Xiong, D.; Wang, H.; Gao, S.; Zhang, X.; Zhang, S.; Wang, J. Reversible Phase Transfer of Carbon Dots between an Organic Phase and Aqueous Solution Triggered by CO2. *Angewandte Chemie* **2018**, *130* (14), 3749–3753. https://doi.org/10.1002/ange.201800037.

(30) List, B.; Lerner, R. A.; Barbas, C. F. Proline-Catalyzed Direct Asymmetric Aldol Reactions. *J. Am. Chem. Soc.* **2000**, *122* (10), 2395–2396. https://doi.org/10.1021/ja994280y.

(31) Ahrendt, K. A.; Borths, C. J.; MacMillan, D. W. C. New Strategies for Organic Catalysis: The First Highly Enantioselective Organocatalytic Diels−Alder Reaction. *J. Am. Chem. Soc.* **2000**, *122* (17), 4243–4244. https://doi.org/10.1021/ja000092s.

(32) MacMillan, D. W. C. The Advent and Development of Organocatalysis. *Nature* **2008**, *455* (7211), 304–308. https://doi.org/10.1038/nature07367.

(33) Mukherjee, S.; Yang, J. W.; Hoffmann, S.; List, B. Asymmetric Enamine Catalysis. *Chem. Rev.* **2007**, *107* (12), 5471–5569. https://doi.org/10.1021/cr0684016.

(34) Erkkilä, A.; Majander, I.; Pihko, P. M. Iminium Catalysis. *Chem. Rev.* **2007**, *107* (12), 5416–5470. https://doi.org/10.1021/cr068388p.

(35) Hasani, M.; Kalhor, H. R. Enzyme-Inspired Lysine-Modified Carbon Quantum Dots Performing Carbonylation Using Urea and a Cascade Reaction for Synthesizing 2-Benzoxazolinone. *ACS Catal.* **2021**, *11* (17), 10778–10788. https://doi.org/10.1021/acscatal.1c01276.

(36) Bartolomei, B.; Corti, V.; Prato, M. Chiral Carbon Nanodots Can Act as Molecular Catalysts in Chemical and Photochemical Reactions. *Angewandte Chemie* **2023**, *135* (32), e202305460. https://doi.org/10.1002/ange.202305460.

(37) Đorđević, L.; Arcudi, F.; Prato, M. Preparation, Functionalization and Characterization of Engineered Carbon Nanodots. *Nat Protoc* **2019**, *14* (10), 2931–2953. https://doi.org/10.1038/s41596-019-0207-x.

(38) Rigodanza, F.; Burian, M.; Arcudi, F.; Đorđević, L.; Amenitsch, H.; Prato, M. Snapshots into Carbon Dots Formation through a Combined Spectroscopic Approach. *Nat Commun* **2021**, *12* (1), 2640. https://doi.org/10.1038/s41467-021-22902-w.

(39) Gawande, M. B.; Shelke, S. N.; Zboril, R.; Varma, R. S. Microwave-Assisted Chemistry: Synthetic Applications for Rapid Assembly of Nanomaterials and Organics. *Acc. Chem. Res.* **2014**, *47* (4), 1338–1348. https://doi.org/10.1021/ar400309b.

(40) Bian, Z.; Wallum, A.; Mehmood, A.; Gomez, E.; Wang, Z.; Pandit, S.; Nie, S.; Link, S.; Levine, B. G.; Gruebele, M. Properties of Carbon Dots versus Small Molecules from “Bottom-up” Synthesis. *ACS Nano* **2023**, *17* (22), 22788–22799. https://doi.org/10.1021/acsnano.3c07486.

(41) Bartolomei, B.; Bogo, A.; Amato, F.; Ragazzon, G.; Prato, M. Nuclear Magnetic Resonance Reveals Molecular Species in Carbon Nanodot Samples Disclosing Flaws. *Angew Chem Int Ed* **2022**, *61* (20), e202200038. https://doi.org/10.1002/anie.202200038.

(42) Hill, H. D.; Straka, J. G. Protein Determination Using Bicinchoninic Acid in the Presence of Sulfhydryl Reagents. *Analytical Biochemistry* **1988**, *170* (1), 203–208. https://doi.org/10.1016/0003-2697(88)90109-1.

(43) Smith, P. K.; Krohn, R. I.; Hermanson, G. T.; Mallia, A. K.; Gartner, F. H.; Provenzano, M. D.; Fujimoto, E. K.; Goeke, N. M.; Olson, B. J.; Klenk, D. C. Measurement of Protein Using Bicinchoninic Acid. *Analytical Biochemistry* **1985**, *150* (1), 76–85. https://doi.org/10.1016/0003-2697(85)90442-7.

(44) Yu, J.-J.; Wang, L.-M.; Liu, J.-Q.; Guo, F.-L.; Liu, Y.; Jiao, N. Synthesis of Tetraketones in Water and under Catalyst -Free Conditions. *Green Chemistry* **2010**, *12* (2), 216–219. https://doi.org/10.1039/B913816A.

(45) Timpe, H. J.; Ulrich, S.; Decker, C.; Fouassier, J. P. Photoinitiated Polymerization of Acrylates and Methacrylates with Decahydroacridine-1,8-Dione/Onium Salt Initiator Systems. *Macromolecules* **1993**, *26* (17), 4560–4566. https://doi.org/10.1021/ma00069a022.

(46) Singla, R.; Gupta, K. B.; Upadhyay, S.; Dhiman, M.; Jaitak, V. Design, Synthesis and Biological Evaluation of Novel Indole-Xanthendione Hybrids as Selective Estrogen Receptor Modulators. *Bioorganic & Medicinal Chemistry* **2018**, *26* (1), 266–277. https://doi.org/10.1016/j.bmc.2017.11.040.

(47) Shi, F.; Tao, Z.-L.; Luo, S.-W.; Tu, S.-J.; Gong, L.-Z. Scaffold-Inspired Enantioselective Synthesis of Biologically Important Spiro[Pyrrolidin-3,2′-Oxindoles] with Structural Diversity through Catalytic Isatin-Derived 1,3-Dipolar Cycloadditions. *Chemistry – A European Journal* **2012**, *18* (22), 6885–6894. https://doi.org/10.1002/chem.201200358.

(48) Laina-Martín, V.; Humbrías-Martín, J.; A. Fernández-Salas, J.; Alemán, J. Asymmetric Vinylogous Mukaiyama Aldol Reaction of Isatins under Bifunctional Organocatalysis: Enantioselective Synthesis of Substituted 3-Hydroxy-2-Oxindoles. *Chemical Communications* **2018**, *54* (22), 2781–2784. https://doi.org/10.1039/C8CC00759D.

(49) Park, J.-U.; Ahn, H.-I.; Cho, H.-J.; Xuan, Z.; Kim, J. H. Asymmetric Synthesis of N-Fused 1,3-Oxazolidines via Pd-Catalyzed Decarboxylative (3+2) Cycloaddition. *Advanced Synthesis & Catalysis* **2020**, *362* (9), 1836–1840. https://doi.org/10.1002/adsc.201901497.

(50) Jethava, K. P.; Fine, J.; Chen, Y.; Hossain, A.; Chopra, G. Accelerated Reactivity Mechanism and Interpretable Machine Learning Model of N-Sulfonylimines toward Fast Multicomponent Reactions. *Org. Lett.* **2020**, *22* (21), 8480–8486. https://doi.org/10.1021/acs.orglett.0c03083.

(51) Banuprakash Goud, S.; Guin, S.; Prakash, M.; Samanta, S. Cu(OAc) 2 /DABCO-Mediated Domino Reaction of Vinyl Malononitriles with Cyclic Sulfamidate Imines: Access to 6-Hydroxyaryl-2-Aminonicotinonitriles. *Organic & Biomolecular Chemistry* **2022**, *20* (2), 352–357. https://doi.org/10.1039/D1OB02095A.

(52) Kolonko, K. J.; Reich, H. J. Stabilization of Ketone and Aldehyde Enols by Formation of Hydrogen Bonds to Phosphazene Enolates and Their Aldol Products. *J. Am. Chem. Soc.* **2008**, *130* (30), 9668–9669. https://doi.org/10.1021/ja804221x.

(53) Chen, X.; Lin, C.; Du, H.; Xu, J. Efficient Direct Synthesis of Aziridine-Containing Chiral Tridentate Ligands by the Iminium-Mediated Self-Ring Opening Reaction of Enantiopure Aziridines and Salicylaldehydes. *Advanced Synthesis & Catalysis* **2019**, *361* (7), 1647–1661. https://doi.org/10.1002/adsc.201801545.

(54) Fernandez-Lopez, R.; Kofoed, J.; Machuqueiro, M.; Darbre, T. A Selective Direct Aldol Reaction in Aqueous Media Catalyzed byZinc–Proline. *European Journal of Organic Chemistry* **2005**, *2005* (24), 5268–5276. https://doi.org/10.1002/ejoc.200500352.

(55) A. Fernandes, R.; V. Ramakrishna, G.; Bethi, V. MnO 2 as a Terminal Oxidant in Wacker Oxidation of Homoallyl Alcohols and Terminal Olefins. *Organic & Biomolecular Chemistry* **2020**, *18* (31), 6115–6125. https://doi.org/10.1039/D0OB01344G.

(56) Chen, Z.; Zhou, P.; Guo, Y.; Anna; Bai, J.; Qiao, R.; Li, C. Guanosine Borate Hydrogel and Self-Assembled Nanostructures Capable of Enantioselective Aldol Reaction in Water. *J. Org. Chem.* **2022**, *87* (5), 2624–2631. https://doi.org/10.1021/acs.joc.1c02573.

(57) Gupta, N.; Roy, T.; Ghosh, D.; R. Abdi, S. H.; I. Kureshy, R.; H. Khan, N.; C. Bajaj, H. Ordered Short Channel Mesoporous Silica Modified with 1,3,5-Triazine–Piperazine as a Versatile Recyclable Basic Catalyst for Cross-Aldol, Knoevenagel and Conjugate Addition Reactions with Isatins. *RSC Advances* **2015**, *5* (23), 17843–17850. https://doi.org/10.1039/C5RA00406C.

(58) Sundar, M. S.; Bedekar, A. V. Synthesis of Biphenyl-Based Ligand: Application in Copper-Mediated Chemoselective Michael Reaction. *Synthetic Communications* **2014**, *44* (24), 3582–3593. https://doi.org/10.1080/00397911.2014.946996.

(59) Gasonoo, M.; Klumpp, D. A. Synthesis of Functionalized 2-Oxindoles by Friedel–Crafts Reactions. *Tetrahedron Letters* **2015**, *56* (33), 4737–4739. https://doi.org/10.1016/j.tetlet.2015.06.028.

(60) Karam, A.; Villandier, N.; Delample, M.; Koerkamp, C. K.; Douliez, J.-P.; Granet, R.; Krausz, P.; Barrault, J.; Jérôme, F. Rational Design of Sugar-Based-Surfactant Combined Catalysts for

Promoting Glycerol as a Solvent. *Chemistry – A European Journal* **2008**, *14* (33), 10196–10200. https://doi.org/10.1002/chem.200801495.

(61) Gentile, G.; Rosso, C.; Criado, A.; Gombac, V.; Filippini, G.; Melchionna, M.; Fornasiero, P.; Prato, M. New Insights into the Exploitation of Oxidized Carbon Nitrides as Heterogeneous Base Catalysts. *Inorganica Chimica Acta* **2022**, *531*, 120732. https://doi.org/10.1016/j.ica.2021.120732.

(62) Dub, P. A.; Wang, H.; Watanabe, M.; Gridnev, I. D.; Ikariya, T. A Practical Asymmetric Conjugate Addition to Cyclic Enones with Chiral Bifunctional Ru Amido Catalysts. *Tetrahedron Letters* **2012**, *53* (27), 3452–3455. https://doi.org/10.1016/j.tetlet.2012.04.100.

(63) Majima, K.; Takita, R.; Okada, A.; Ohshima, T.; Shibasaki, M. Catalytic Asymmetric Michael Reaction of β-Keto Esters: Effects of the Linker Heteroatom in Linked-BINOL. *J. Am. Chem. Soc.* **2003**, *125* (51), 15837–15845. https://doi.org/10.1021/ja037635t.

(64) Guo, W.; Lv, G.; Chen, J.; Gao, W.; Ding, J.; Wu, H. Rongalite® and Base-Promoted Cleavage of Disulfides and Subsequent Michael Addition to α,β-Unsaturated Ketones/Esters: An Odorless Synthesis of β-Sulfido Carbonyl Compounds. *Tetrahedron* **2010**, *66* (13), 2297–2300. https://doi.org/10.1016/j.tet.2010.02.001.

(65) Civit, M. G.; Sanz, X.; Vogels, C. M.; Webb, J. D.; Geier, S. J.; Decken, A.; Bo, C.; Westcott, S. A.; Fernández, E. Thioboration of α,β-Unsaturated Ketones and Aldehydes toward the Synthesis of β-Sulfido Carbonyl Compounds. *J. Org. Chem.* **2015**, *80* (4), 2148–2154. https://doi.org/10.1021/jo5026354.

(66) Gunduz, H.; Ece, H.; Atsay, A.; Kumbaraci, V.; Talinli, N. Amberlyst-15 Catalyzed Michael Addition of β-Dicarbonyl Compounds to the Enones and Unexpected Ring Closure Products. *Tetrahedron* **2017**, *73* (30), 4335–4340. https://doi.org/10.1016/j.tet.2017.05.092.

(67) Yokote, S.; Nishikawa, S.; Shibuya, K.; Hisano, K.; Nishino, H. Selective Synthesis of Spiro and Dispiro Compounds Using Mn(III)-Based Oxidation of Tetracarbonyl Compounds. *Tetrahedron* **2020**, *76* (20), 131165. https://doi.org/10.1016/j.tet.2020.131165.

(68) Teli, P.; Sethiya, A.; Agarwal, S. Black yet Green: A Heterogenous Carbon-Based Acid Catalyst for the Synthesis of Biscyclic Derivatives under Eco-Friendly Conditions. *Res Chem Intermed* **2022**, *48* (2), 731–750. https://doi.org/10.1007/s11164-021-04622-4.

(69) Ilangovan, A.; Muralidharan, S.; Sakthivel, P.; Malayappasamy, S.; Karuppusamy, S.; Kaushik, M. P. Simple and Cost Effective Acid Catalysts for Efficient Synthesis of 9-Aryl-1,8-

Dioxooctahydroxanthene. *Tetrahedron Letters* **2013**, *54* (6), 491–494. https://doi.org/10.1016/j.tetlet.2012.11.058.

Chapter 3.

Phenol-Rich Carbon Dots: Metal-free and Recyclable Photocatalyst for Different Reactivities

Abstract

In the following chapter, a deeper look into new photo-active green and recyclable CDs is taken to drive challenging photocatalytic reactivities. Thanks to the proper selection of precursors and synthetic conditions, it was envisaged to transfer the appealing photoredox properties of phenolate anions, that can be obtained upon deprotonation of phenols, from a molecular level to the nanoscale. Consequently, L-tyrosine was selected along with L-arginine for the *bottom-up* preparation of the phenol-rich carbon dots (*p*-CDs). The nanoparticles proved to be effective in promoting both the Homolytic Aromatic Substitution (HAS) of different arenes and the [3+2] cycloaddition of cyclopropanes and unsaturated hydrocarbons. In particular, a detailed study of the [3+2] cycloaddition was carried out. In this case, *p*-CDs were used, in combination with a suitable base and an organocatalyst, namely the Schreiner thiourea (**A**), as nano-photocatalysts to access the densely functionalized five membered rings (*17 examples, up to 99% yield*). Interestingly, *p*-CDs could be easily recovered and reused up to three times without any significant drop in yield.

This work was conducted in the carbon nanotechnology group at the University of Trieste. The project was supervised and conceived by *Prof. Maurizio Prato* and *Dr Giacomo Filippini*. *Dr Giuseppe Gentile* helped to perform the synthesis and characterization of the *p*-CDs. The manuscript of this project is currently under preparation. A minireview article titled "*Shining Light on Carbon Dots: New Opportunities in Photocatalysis*" published in 2021 served as a base for this chapter introduction.[1]

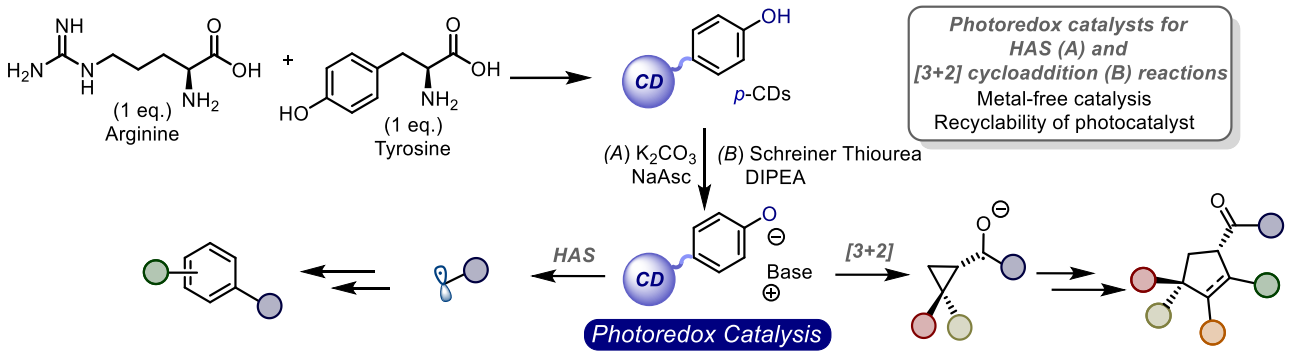

3.1 Introduction

3.1.1 Photoredox Properties of Phenols and Their Application as Photocatalysts

The advent of photocatalysis has led to the development of light-absorbing catalysts that enable unique bond formation not accessible through classical protocols. In the past years, the literature has primarily focused on metal complexes as visible light photoredox catalysts to promote a plethora of fascinating reactivities.[2–5] In particular, photoredox catalysis, involving the light-induced movement of one electron from or to a substrate, paved the way for the direct functionalization of organic molecules under mild operative conditions. The well-known polypyridyl complexes of both ruthenium and iridium have played a crucial role in defining modern photoredox catalysis. Some notable examples include the reductive dehalogenation of unactivated alkyl, alkenyl, and aryl iodides[6] and the crossed intermolecular [2+2] cycloaddition of aryl enones with vinyl ketones, reported by Tehshik P. Yoon.[7]

Despite the widespread application of these photocatalysts, they have significant drawbacks, including high cost and potential toxicity.[8] Moreover, the Earth's crust contains a meager amount of ruthenium and iridium, at a concentration of around 0.001 ppm, which makes them two of the rarest metals.

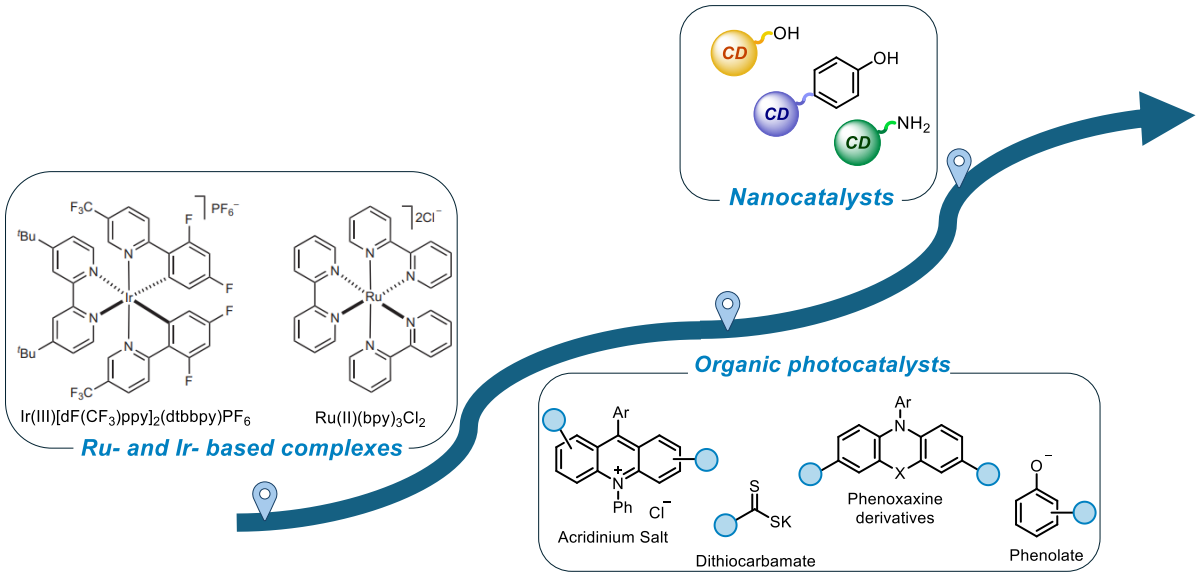

Figure 3.1 Schematic overview of different classes of photocatalysts

Consequently, recent years have seen a shift towards more sustainable and metal-free photochemistry. It follows that numerous organic dyes have been recently investigated in photoredox catalysis. As a result, significant efforts have been dedicated in designing new organic photocatalysts; however, these initiatives are often hampered by the high costs and time-consuming multi-step synthetic processes.[9]

Interestingly, many photoredox catalysts feature densely functionalized aromatic cores such as acridinium compounds, phenoxazine, dithiocarbamate or phenolates (Figure 3.1).[9] Importantly, the acid dissociation constant (pKa) of phenols depends on the electronic nature of the substituents attached to the aromatic ring.[10] Specifically, the presence of electron-withdrawing groups (EWGs) on the aromatic ring enhances the acidity of the systems, while electron-donating groups (EDGs) decrease it.[11] Among these aromatic compounds, the conjugate bases of phenols, namely phenolate anions, are both electron rich organic intermediates and active chromophores. The hydroxyl groups directly attached to an aromatic ring make phenols more acidic than aliphatic alcohols. Both phenols and their corresponding phenolate anions can absorb light, sometimes even extending into the visible range. However, the formation of phenolate anions is associated with a bathochromic shift in the absorption spectrum compared to the phenol precursor. This shift arises from increased conjugation between the negatively charged oxygen atom and the aromatic ring.[12] Additionally, the overall shift in absorption bands can be influenced by the properties of the substituents on the aromatic ring; EWGs lead to a red shift, while EDGs have the opposite effect. Upon light excitation, both phenols and phenolates exhibit properties markedly different from those of their ground-state counterparts. Light excitation causes charge redistribution, altering both the acidity and redox properties of these species.[13] The n->π* transition promotes the species to the excited singlet state, decreasing the electron density on the oxygen atom and increasing the acidity of the excited-state. Moreover, excited-state phenols exhibit enhanced reductant and oxidant properties compared to their ground states, as reflected by a decrease in ionization potential (IP) and an increase in electron affinity (EA), as shown in Figure 3.2.

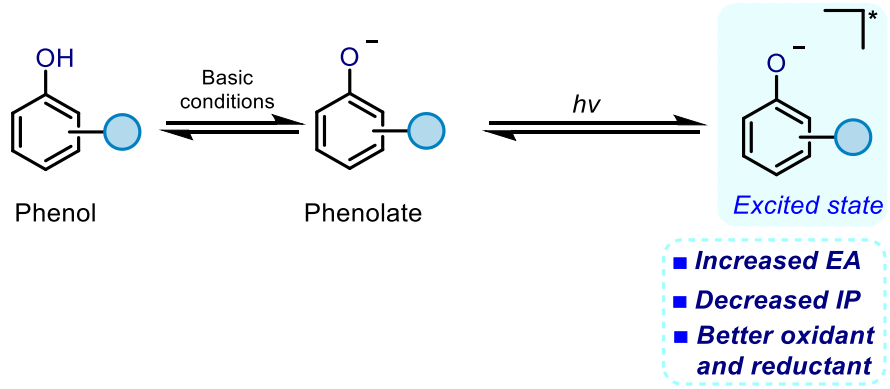

Figure 3.2 Trends of acidity, redox properties, electron affinity and ionization energy for phenol and its corresponding phenolate in the ground and excited-states.

Thanks to the peculiar photochemistry of phenolate anions, they can effectively generate reactive open shell species from suitable electron-poor radical substrates. This can occur either through reaching an electronically excited-state upon light absorption or by forming photoactive electron donor-acceptor (EDA) complexes. In their excited-state, phenolates possess reductive properties that can initiate single electron transfer (SET) reactions with electron-deficient acceptors (such as R−X, X=halogen), triggering the formation of open shell reactive intermediates. As depicted in Figure 3.3, the corresponding oxygen-centered radicals, namely phenoxyl radicals, are generated. Consequently, these oxygen-centered radicals can remain stable in solution for quite long periods and can be reduced to the original ground state through mild reductants. However, phenoxyl radicals may also participate in side reactions, such as polymerization, which typically leads to the formation of phenolic polymers.[14]

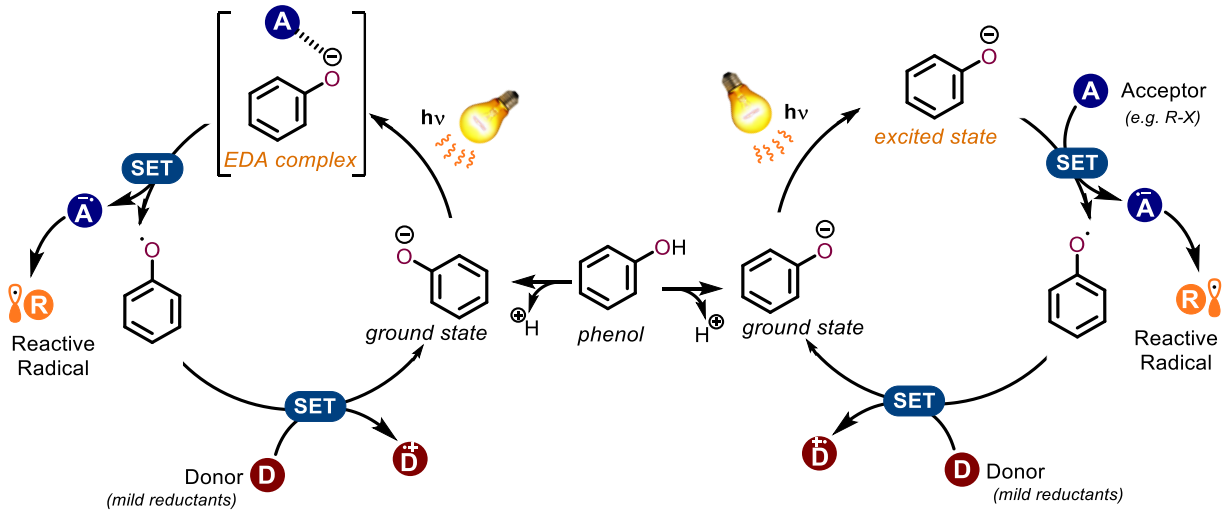

Figure 3.3 Generic photocatalytic pathways of a phenolate.

The Stern-Volmer experiment is crucial in determining quenching mechanisms in catalytic processes, likely SET mechanism. Furthermore, the rate constant of this process can be derived from the Stern-Volmer equation.[15]

So far, we discussed the photoredox properties of phenols. Below, we will present several case studies illustrating their applications.

In 2019 König and co-workers reported the use of 10-bromo-9-anthrolate (PC-A) to promote the C-H arylation reactions between electron-abundant arenes and aryl chlorides under blue LEDs light (Figure 3.4a).[16] The coupling products were obtained in excellent yields (up to 99%) in the presence of Cs_2CO_3 as base and 18-crown-16 as solubilizing additive in dimethyl sulfoxide (DMSO). An excess of base is fundamental to generate the photocatalytic active phenolates from the PC-A and to neutralize the HCl formed during the reaction. From a mechanistic point of view, the excited anthrolate PC-A* (*E*p*= - 3.0 V vs. SCE) reduces different aryl chlorides to give the corresponding open-shell phenyl species.

The same research group demonstrated that tetramethoxyanthrolate (PC-B) could activate various styrenes and arenes *via* SET under blue light irradiation (Figure 3.4b).[17] They investigated the C-H carboxylation of styrenes and arenes using CO_2 in the presence of Cs_2CO_3 as base. The corresponding carboxylic acids were achieved from moderate to excellent yields. In this case study, the reactivity is initiated by the light-excited tetramethoxyanthrolate PC-B* (*E*p*=-2.9 V vs. SCE) which reduces arenes or styrenes to the resonance-stabilized radical anions that subsequently undergo nucleophilic attack by CO_2 affording the open-shell carboxylates.

Another representative application was reported by Xia and collaborators, who demonstrated the photoreduction of aryl halides by PC-C, leading to oxyarylation reactions with olefins (Figure 3.4c).[18] The phenolate anions were generated by Cs_2CO_3, while 2,2,6,6-tetramethylpiperidin-1ol (TEMPOH) acted as a radical scavenger and donor of H-atoms. Through optimization studies, the authors found out that PC-C, which had bulky *tert*-butyl groups in ortho position, presented the highest catalytic effectiveness for this oxyarylation reactivity. Stern-Volmer quenching studies on the PC-C revealed a progressive and linear decrease in emission intensity with increasing concentrations of the aryl halide (*i.e.,* iodobenzene), confirming a single quenching mechanism, likely through SET.

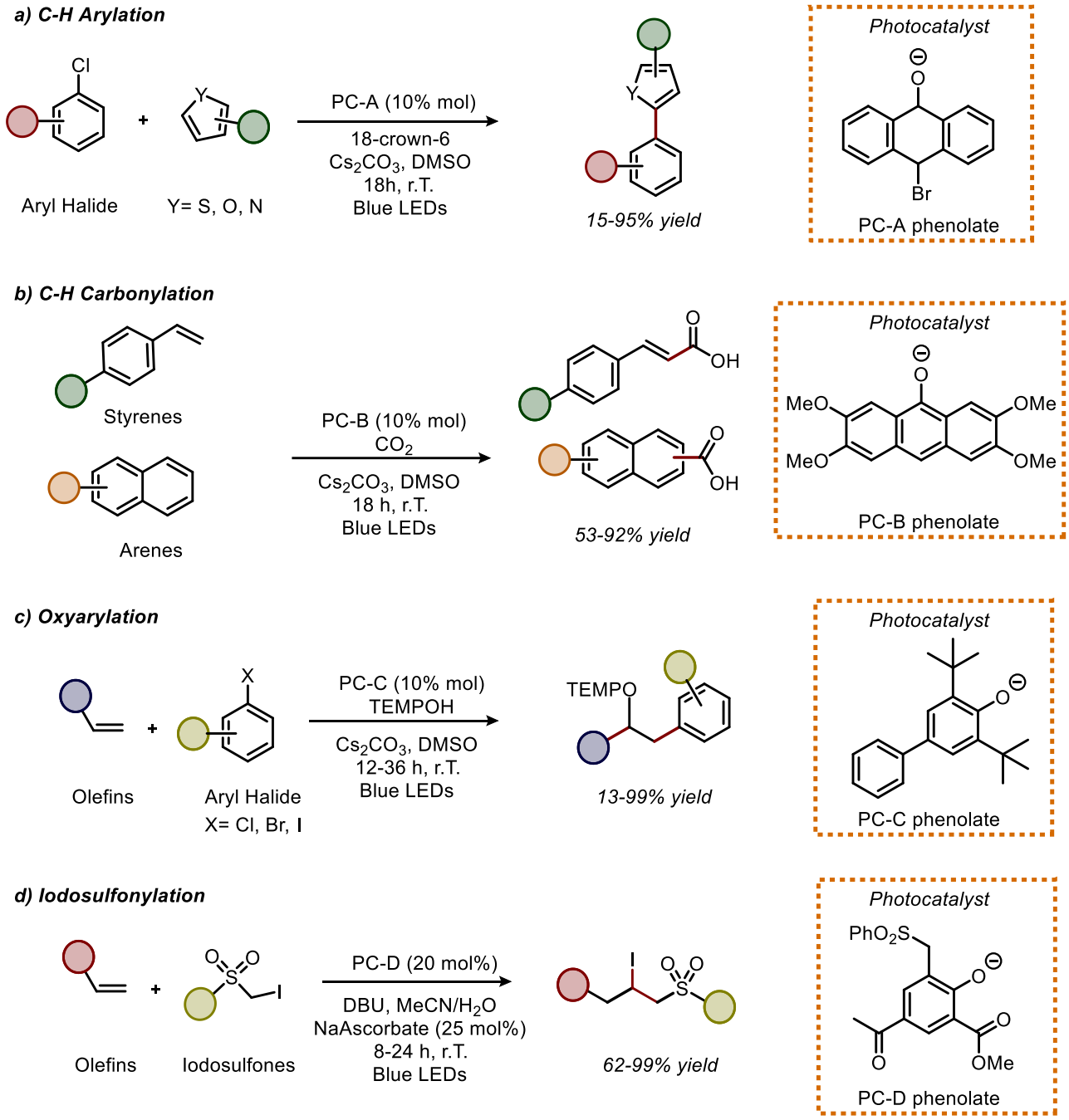

Figure 3.4 Examples of the utilization of molecular phenols as photocatalyst: a) hetero arylation of aryl halides; b) C-H carboxylation of styrenes and heteroaromatic compounds; c) direct oxyarylation of olefins; d) Iodosulfonylation of olefins.

Recently, a photocatalytic procedure was developed for the direct iodosulfonylation of terminal olefins with α-iodo phenylsulfones.[19] The process used the trisubstituted phenol (PC-D) in Figure 3.4d to drive the formation of functionalized alkyl iodides (up to 99% yield) under visible-light irradiation (450 nm). In particular, the deprotonation of the PC-D thanks to the 1,5-diazabiciclo(5.4.0)undec-7-ene (DBU) led to the formation of the excited anionic PC-D* which

initiated the formation of sulfonyl radicals, starting the catalytic cycle. In addition to the DBU, sodium ascorbate was included in the reaction mixture, thus allowing a more efficient in situ regeneration of the photocatalyst.

3.1.2 Carbon Dots in Photocatalysis

As discussed in the chapter I, carbon dots (CDs) are an emerging class of photoactive inexpensive, low toxic and potentially reusable nanoparticles that possess multiple appealing optical properties.[20,21] Specifically, these nanomaterials consist of a carbon core which can be surrounded by a shell that contains several functional groups (*e.g.,* amines and alcohols). The preferred method for synthesizing CDs is the versatile *bottom-up* approach, which uses mild experimental conditions to yield nanoparticles with controlled characteristics.[22] In fact, some of the properties of the CDs can be tuned by choosing the proper starting materials or synthetic conditions. For example, by carefully choosing precursors, it is possible to produce nanoparticles enriched with specific functional groups derived from the starting molecules.[23] As mentioned in the previous chapter, the surface groups of CDs can promote efficiently different organocatalytic transformations proving to be a critical and significant feature for catalysis. Furthermore, the heteroatom or metal doping of the CDs' core or shell can be desirable to customize their photochemical and optical properties. During synthesis, atoms such as nitrogen, sulfur, or boron from the starting materials can be incorporated into the core or shell of the CDs.[24] This can improve charge carrier separation and so photocatalytic performances, and further slow the kinetics of the redox reactions by trapping the photogenerated electrons at surface sites.[1] Nitrogen-doped CDs, for instance, exhibit improved catalytic performances in photoreduction reactions, as this atom has a similar size to the carbon atom and integrates into the π orbitals system, raising the highest occupied molecular orbital (HOMO) level and narrowing the bandgap.[25,26] Metal-doped CDs, typically derived from organometallic complexes or metallic salts, have also been reported but not discussed in this thesis.[27,28]

Customized synthetic conditions can also lead to CDs with either a graphitic or amorphous core. In detail, when the temperature is above 300°C, the formation of CDs with a graphitic core will be favoured, while those produced below 300°C are more likely to be amorphous.[29] Accordingly, high graphitization degree results in a longer excitation lifetime which can lead to non-radiative relaxation mechanisms, reducing photoluminescence quantum yield but improving photostability.[30] The excited-state lifetime is an important parameter for a photocatalyst since it is correlated to the efficiency of the quenching process of the PC's excited-state, often carried out by energy or electron

transfer phenomena.[15] As mentioned earlier, Stern-Volmer experiments can evaluate the interaction between the photocatalyst, such as CDs, and a quencher, often the reactive substrate.[31]

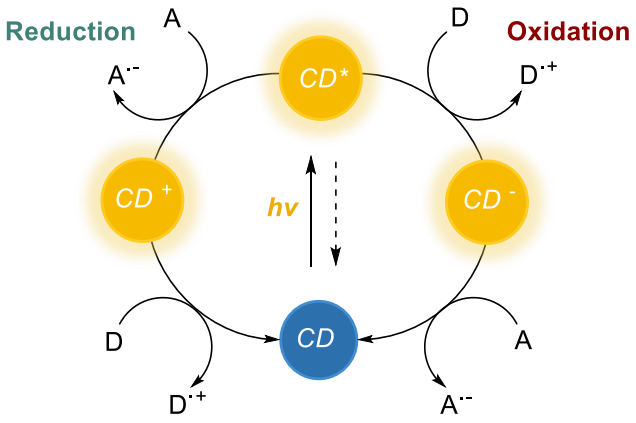

Figure 3.5 CDs undergoing a general photocatalytic cycle. D: Electron Donor; $D^{\cdot+}$: Radical Cation Donor; A: Electron Acceptor; $A^{\cdot-}$: Radical Anion Acceptor.

Under suitable light source, CDs may reach an excited-state (CDs*) which can then start the photocatalytic cycles acting as either: (*i*) photooxidants by gaining an electron from donor (D) and restoring to their ground state with a suitable electron acceptor, or (*ii*) photoreductants by giving an electron to an acceptor (A) and regaining an electron from a donor compound. The resulting donor or acceptor radical ions may rapidly undergo further transformations to yield the final reaction products.[32] Single electron transfer (SET) is the most common mechanism employed by CDs, although they can also act as photosensitizers, promoting organic reactions through energy transfer.[33,34]

The aim of the next section is to discuss the most recent and cited examples of metal-free CDs as photo-organocatalysts.

One of the first application of CDs using light irradiation to promote a catalytic transformation was reported by Kang and colleagues (Figure 3.6a).[35] In particular, they investigated the aldol condensation between acetone and aromatic aldehydes to achieve α,β-unsaturated compounds from good to excellent yields (63-99%). This methodology relies on the photoenhanced hydrogen-bond catalytic activity of CDs-A towards aldehydes, under a Xenon lamp with $\lambda \geq 420$ nm. Specifically, the authors synthesized the water-soluble CDs-A through the electrochemical ablation of graphite rods. After the purification, CDs-A about 5 nm were obtained with a graphitic core (lattice spacing 0.212 nm) and hydroxyl groups on their surface (0.75 mmol/L). Thanks to these alcohol moieties,

CDs-A were capable of catalyse the aldol addition forming hydrogen bonds with the aldehydes. Remarkably, upon light irradiation, CDs-A enhanced the electrophilicity of aldehydes thus accelerating the aldol condensation.

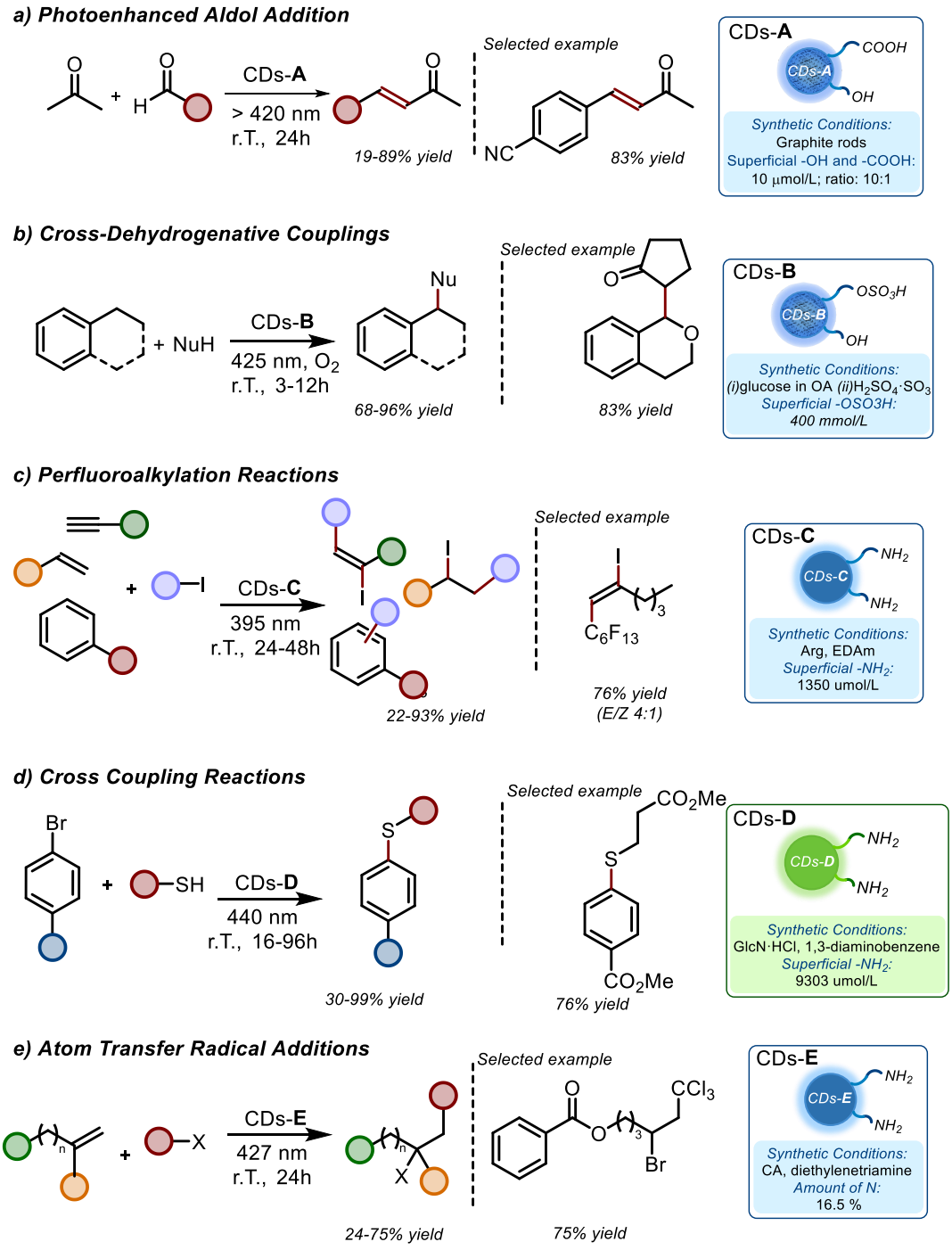

Figure 3.6 Examples of applications of CDs as photoredox catalyst: a) light-promoted aldol condensation; b) aerobic carbon–carbon bond formation; c) perfluoroalkylations of organic compounds; d)carbon-heteroatom cross-coupling; e)Atom transfer radical additions on olefins.

In 2019, Sarma and co-workers developed the synthesis of sulfur-doped CDs-B demonstrating the dual-catalytic properties of the nanomaterials for dehydrogenative cross-coupling reactions (Figure 3.6b).[36] Specifically, they synthetised CDs-B through a microwave-assisted thermal method using glucose in oleic acid followed by a post-synthetic treatment with fuming sulfuric acid to introduce sulfur-based functionalities. The resulting graphitic nanoparticles possessed carboxylic and sulfuric acid monoesters groups (0.5 mmol/L and 0.4 mmol/L, respectively) on their surfaces. Then, CDs-B were used in the reaction between benzyl hydrocarbons and different nucleophiles to deliver coupling products with remarkable results (yields 68-98%). Specifically, CDs-B, owing to their reductive properties, promoted the formation of the hydroperoxyl intermediate of benzyl hydrocarbons. Then, the sulfur-based moieties on the catalysts facilitated the reaction with the nucleophiles.

In the same year, our group reported the use of amorphous amine-rich CDs for photocatalytic perfluoroalkylation reaction of unsaturated compounds (Figure 3.6c).[31] The synthesis of CDs-C consisted in the hydrothermal treatment of arginine and ethylenediamine (EDAm) to gain nanoparticles about 2.5±0.8 nm. Because of their photo-reductive nature, the excited-state potential of CDs-C, estimated by using the Rehm-Weller equation, was found to be - 2.2 V (vs. saturated calomel electrode, SCE). Therefore, CDs-C acted as photo reductive catalysts towards perfluoroalkylated halides upon irradiation at 395 nm. This process generated the radical intermediates, which then reacted with a variety of organic substrates to afford a library of products in very good yields (up to 90%).

Recently, the group of Pieber studied the photo-reductive properties of green emitted nitrogen-doped carbon dots for a photocatalytic cross coupling reaction.[37] In particular, they use CDs in combination with Ni(II) complex exploiting the dual-catalysis to drive different carbon-heteroatom cross-coupling reactions (C–O, C–S, C–N). By utilizing a hydrothermal method, glucosamine hydrochloride (GlcN·HCl) and 1,3-diaminobenzene reacted to create CDs-D. The amorphous nanoparticles obtained presented a high number of primary amines on the surface (9303 µmol/g by Kaiser test). Under 440 nm light, the nucleophilic amino groups promoted the interaction between the CDs-D and the Ni complexes, overcoming the short lifetime of the excited-state of the nanoparticles. Then, the photoreduction of Ni complex initiated the cross-coupling transformations. Figure 3.6d illustrates an example of this reactivity, showing the reaction between aryl halides and thiols, mediated by Ni(dtbbpy)Br_2 (dtbbpy = 4,4'-di-*tert*-butyl-2,2'-dipyridyl) as the metal complex.

Under optimized conditions, the coupling products were obtained in nearly quantitative yields. This work underscores how the careful selection of starting materials can lead to the development of a CDs-based photocatalysts with excellent photo-redox properties.

Last year, the use of nitrogen-doped carbon dots was extended to the visible light-driven 1,2 functionalization of olefins. The authors synthetized amorphous CDs-E from citric acid and diethylentriamine (DETA) under hydrothermal conditions (Figure 3.6e).[38] These nanomaterials exhibited a significant absorption in the visible light region and have been successfully employed as photoredox catalysts. Specifically, the photoexcited CDs-E induced the reductive cleavage of the halogen carbon bond of the alkyl halides by SET, generating an electrophilic radical that reacts with the olefins. Through an atom transfer radical addition (ATRA) process, the authors smoothly produced various functionalised products (up to 75% yields) under metal-free conditions in an aqueous medium.

3.2 Aim of the Project

In recent times, increasing attention has been devoted to the design and synthesis of new efficient, inexpensive, low toxic and potentially recyclable photocatalysts. Interestingly, carbon dots fulfil all these requirements due to their unique physicochemical properties combined with their carbon-based nanoparticle structure. By carefully selecting the precursors and controlling the synthetic conditions, also some of the chemical qualities and attributes of the starting materials are conveyed into the resultant CDs. Within this project, we aimed to develop and optimize a novel synthetic methodology for the preparation of phenol-rich carbon dots (*p*-CDs) with enhanced photocatalytic features by exploiting the appealing photoredox properties of phenolate anions. This work specifically investigates these tailored nanomaterials in different photocatalytic transformations, namely homolytic aromatic substitution (HAS) and [3+2] cycloaddition reactions.

Ultimately, this research aspires to contribute to the broader field of nano-photocatalysis by demonstrating how molecular-like behaviour can be integrated into nanomaterials, by implementing a novel photo-active, metal-free and recyclable nano-photocatalytic material, namely *p*-CDs.

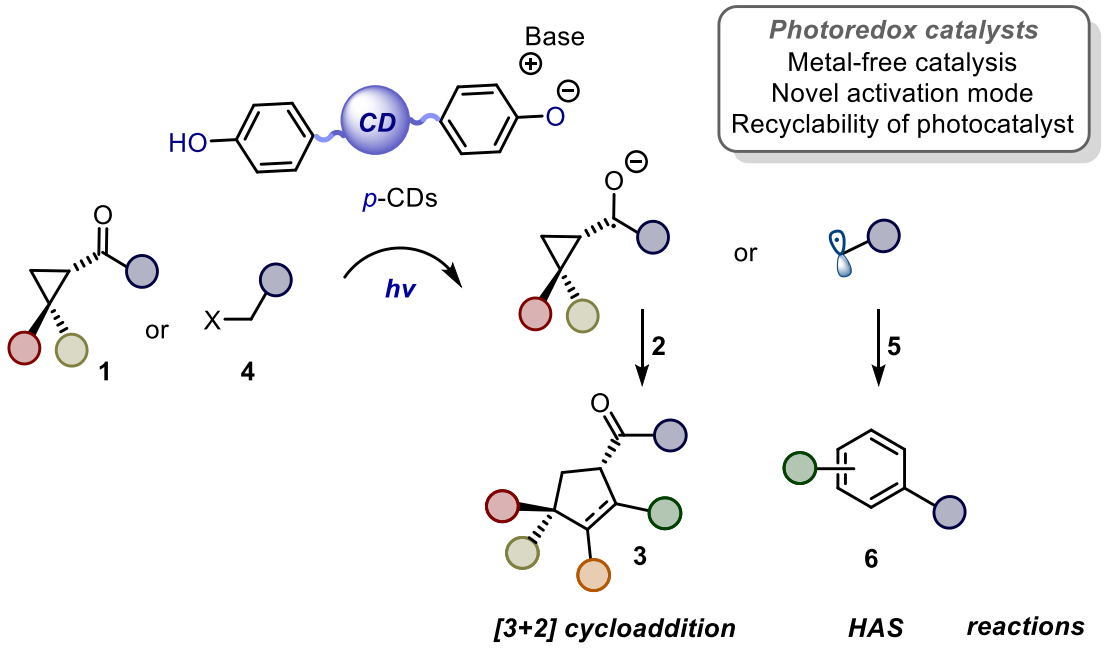

Figure 3.7 p-CDs as photoredox catalyst for alkyl halides and cyclopropyl ketones.

3.3 Results and Discussion

3.3.1 Synthesis of *p*-CDs

The synthesis of phenol-rich carbon dots (*p*-CDs) follows a fast and simple microwave (MW)-assisted method using inexpensive amino acids as precursors. L-tyrosine (Tyr) was selected as a precursor to introduce phenol moieties in the synthesis, while L-arginine (Arg) was used as a bulk carbon resource. Indeed, previous works regarding the synthesis of carbon dots using Arg demonstrated that the formation of the aromatic core comes from this amino acid.[39] In the previous chapter, we discussed about the synthesis of amine-rich carbon dots starting from arginine and dialkylamines to introduce accessible amines on the surface of the nanoparticles.[40] Consequently, for this study, Arg was maintained in the synthesis while incorporating a suitable phenol shell precursor (Tyr). During preliminary tests, milliQ water was used as the reaction medium. Unfortunately, the strategy proved to be ineffective probably due to the restricted solvent heat transfer which left unreacted precursors in the reaction crude. Consequently, ethylene glycol (EG) was chosen as the optimal solvent thanks to its convenient dielectric constant that allows higher conversion of electromagnetic energy into heat.[41] Moreover, EG has a high loss factor (tanδ) which means it can be superheated to above its boiling point (197.3°C). Thus, the same equivalents of Arg (0.5 mmol) and Tyr were combined into a MW reaction vessel with EG (0.25 M) and thermally treated for 15 minutes at 250°C. The crude oil obtained was diluted with *N,N*-dimethylformamide (DMF) and the precipitation of *p*-CDs was induced under sonication by drop-wise addition of milliQ water. The precipitate was collected by

filtration over polytetrafluoroethylene membrane. The so obtained solid was then solubilized again in DMF and reprecipitated from water up to 5 times. Finally, the purified *p*-CDs were rinsed in diethyl ether to speed up the drying process and remove DMF traces. Figure 3.8 summarizes the synthetic procedure. The pure *p*-CDs were obtained as a brownish powder with a remarkably good yield (20% yield based on weight, 350 mg). These nanoparticles have good solubility in DMSO, DMF, basic water solutions and quite solubility in methanol and acetonitrile. Based on several reports in the literature, we assumed that *p*-CDs possess different polar chemical functionalities on their surfaces, including phenols, that were left over from the polymerization of the molecular precursors.[42]

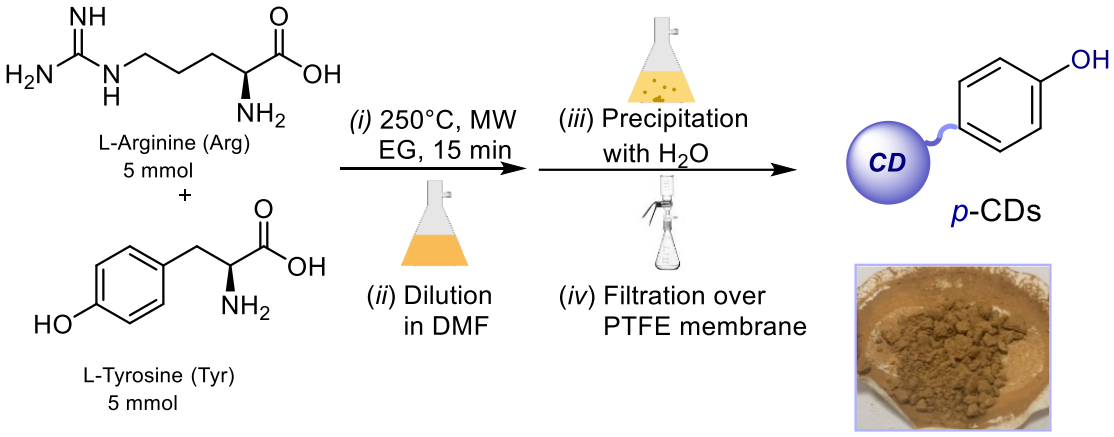

Figure 3.8 Schematic representation of the synthetic workflow for p-CDs production.

The purification of CDs is a critical step during synthesis and involves removing the starting materials and by-products. However, this aspect is often overlooked in the pursuit of new CDs, leading to misinterpretations of the materials' properties.[42] Consequently, the effective purification of the nanoparticles from molecular species was verified by nuclear magnetic resonance (NMR) analysis. The ^{1}H-NMR spectrum of *p*-CDs indicates the successful purification of the nanoparticles showing only broad signals typical of nanostructured materials (Figure 3.9a).[40,43] However, the absence of sharp signals can exclude the presence of molecular species. Additionally, the broad band in the aromatic region of the spectrum was a clear indication of the presence of aromatic moieties within the *p*-CDs, such as phenols.

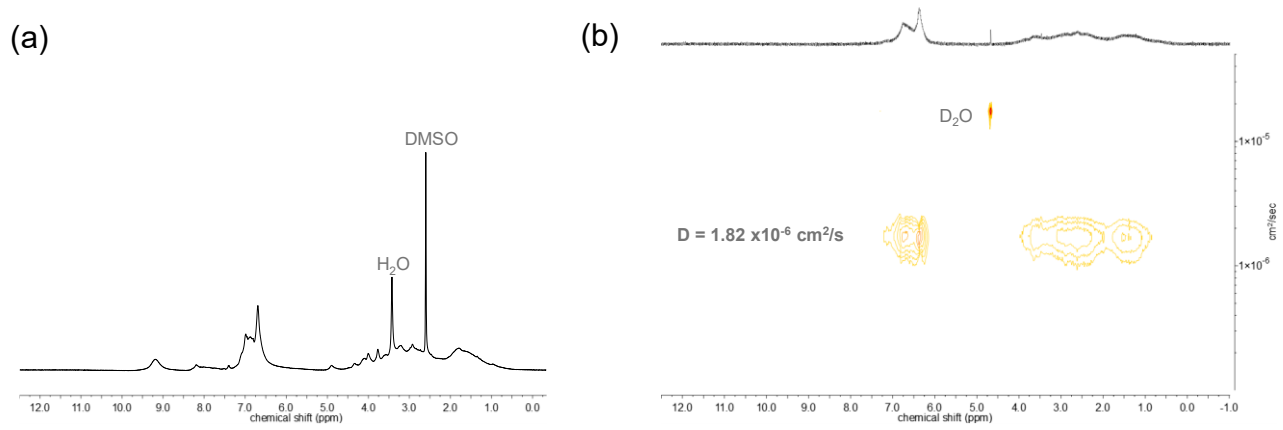

Figure 3.9 NMR characterization of p-CDs: a) ^{1}H-NMR recorded in DMSO-d_6 of p-CDs; b) DOSY spectrum of p-CDs recorded in basic deuterated water [NaOD 0.2M].

As further proof of the purity of our nanoparticles, the diffusion-ordered spectroscopy (DOSY) analysis revealed that the carbon nanoparticles have a distinctive diffusion coefficient (D = 1.82x10^{-6} cm^2/s), comparable to literature values of similar nanomaterials (Figure 3.9b).[28] This demonstrated that *p*-CDs are a monodispersed nanomaterial with no side products of lower molecular mass present within it.

Structural and morphological information on the nanoparticles was gathered by thermogravimetric analysis (TGA), attenuated total reflectance-Fourier-transform infrared spectroscopy (ATR-FTIR), elemental analysis (XPS) and atomic force microscopy (AFM).

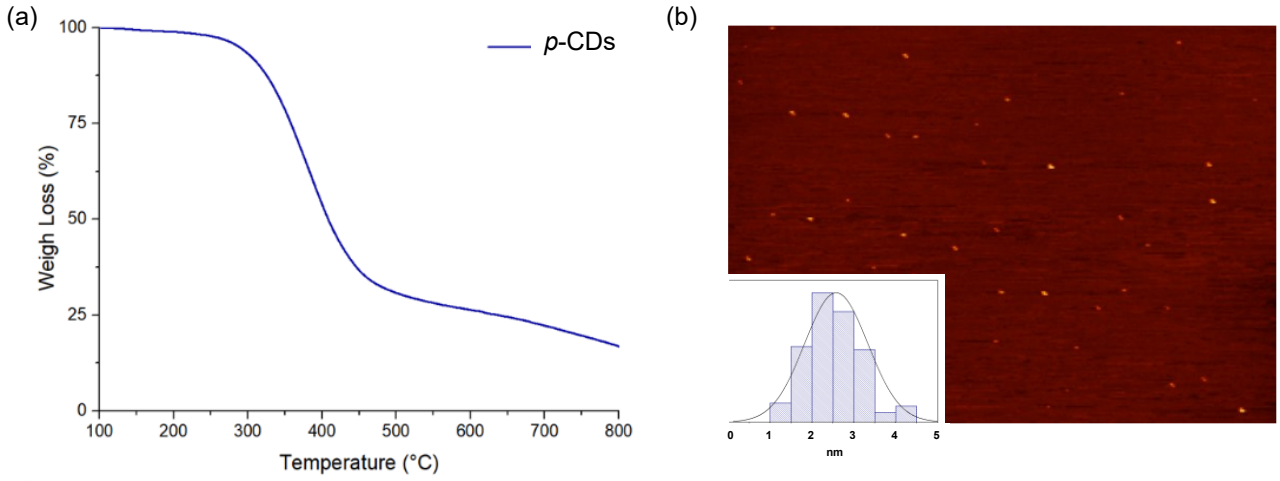

Figure 3.10 Morphological information on p-CDs: a) Thermogravimetric analysis under nitrogen of p-CDs; b) Tapping mode AFM of p-CDs deposited on a mica substrate. inset is the height profile.

As shown in Figure 3.10a, TGA established the predominantly amorphous structure of the *p*-CDs through a relative thermal stability up to 300°C and a subsequent loss of mass between 300°C and 500°C. The IR spectrum of the nanoparticles revealed an intense broad band from 3650 cm^{-1} to 3000 cm^{-1} that corresponds to -OH and -NH and -CH aromatics stretching, while C=C stretching of aromatics occurs in the region of 1600-1500 cm^{-1} (Figure 3.18, see section 3.5.3). Elemental analysis of *p*-CDs specified the listed atomic percentages, C: 63,52%, H: 6,19%, N: 10,27%, O: 20.02%. Comparable atom counts are reported for Tyr, especially for the O%, suggesting the pivotal role of this amino acid in the *p*-CDs synthetic process. Figure 3.10b displays the AFM image supporting the nano-scale dimensions of *p*-CDs with an average size of 2.5±0.7nm

The interest in the photochemical properties of *p*-CDs pave the way for a deep study of the photophysical properties. UV-Vis absorption band of *p*-CDs extended up to 450 nm was recorded (Figure 3.11a). The typical excitation wavelength-dependent behaviour of these nanomaterials was recorded with *p*-CDs. Moreover, the emission spectra show an excitation wavelength-dependent profile and the fluorescence peak shifts 380 to 570 nm when the excitation wavelength changes from 300 to 500 nm. The quantum yield (QY) of *p*-CDs is independent of the excitation wavelength, assuming the value of 10.0±0.5%.

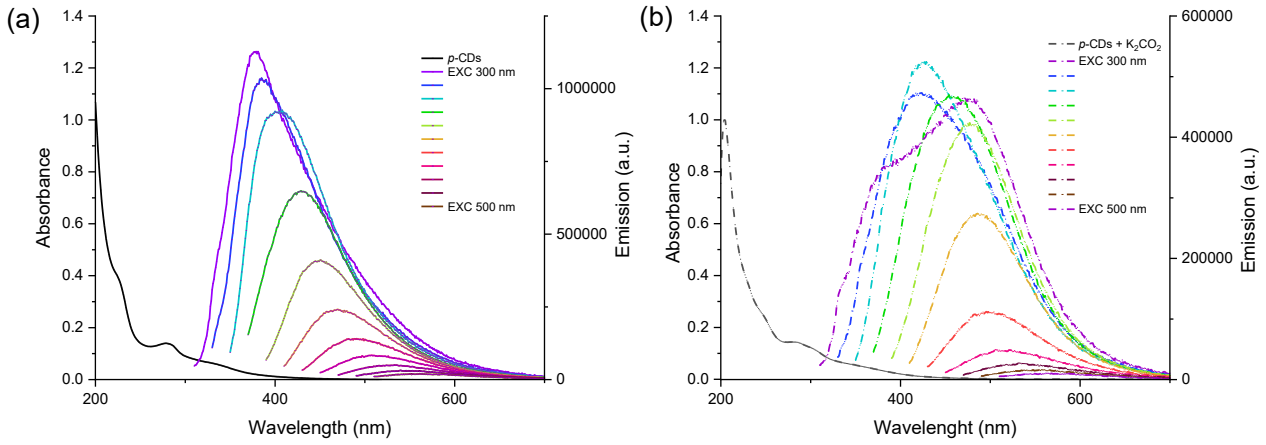

Figure 3.11 Photophysical characterization of p-CDs: (a) Absorption and emission spectra recorded at different excitation wavelengths of p-CDs. (b) Absorption and emission spectra recorded at different excitation wavelengths of deprotonated p-CDs with K_2CO_3 (2 equiv.). All UV-Vis and fluorescence spectra were measured in MeCN/H_2O (3:1) at 0.1 mg/mL concentration.

Interestingly, the addition of 2 equiv. of base K_2CO_3 shifted, towards the red wavelength, the absorption band and the emission profile of *p*-CDs (Figure 3.11b). Phenolate compounds are recognized for having red-shifted absorption and emission compared to their protonated

counterparts, due to the enhanced conjugation within these aromatic anions.[13] Consequently, these observations provided further proof of the presence of phenol groups on the *p*-CDs' surfaces. Besides, the fluorescence lifetimes of *p*-CDs were measured resulting in a double-exponential fit with a short τ_1=2.8 ns and a longer τ_2=6.8 ns component.

To provide further evidence of the presence of phenol moieties on *p*-CD surfaces, we employed the ^{19}F-NMR analysis. In the previous chapter, we have already explored this technique as a valuable tool not only for studying the nature of surface functionalities on CDs, but also for quantifying them, thanks to the high sensitivity of the fluorine nucleus.[40,44] Here, this technique was employed to detect and quantify the phenol hydroxyl moieties present on the surfaces of *p*-CDs through a post-synthetic strategy to covalently bond a suitable fluorinated probe to the surface moieties of *p*-CDs. Considering the various groups present on the surfaces of *p*-CDs, the targeting functionalization of the surface polar groups would form different fluorinated species. Therefore, a series of molecular alcohols and amines were reacted with the 4-fluorobenzoyl chloride in the presence of 4-(dimethylamino)pyridine (DMAP) and triethylamine (NEt_3). The acylated products, namely esters and amides, were then analysed using ^{19}F-NMR in DMSO-d_6. Figure 3.12 shows the stacked spectra of the model products **7a**-**c**, **8a**-**c**. Interestingly, the chemical shifts of the amides **8a**-**c** (from -108.9 to -110.1 ppm) can be differentiated from those of the esters **7a**-**c** (from -104.9 to 106.2 ppm). In addition, aliphatic amides and esters also could be distinguished by their chemical shifts from the aromatic derivatives.[44]

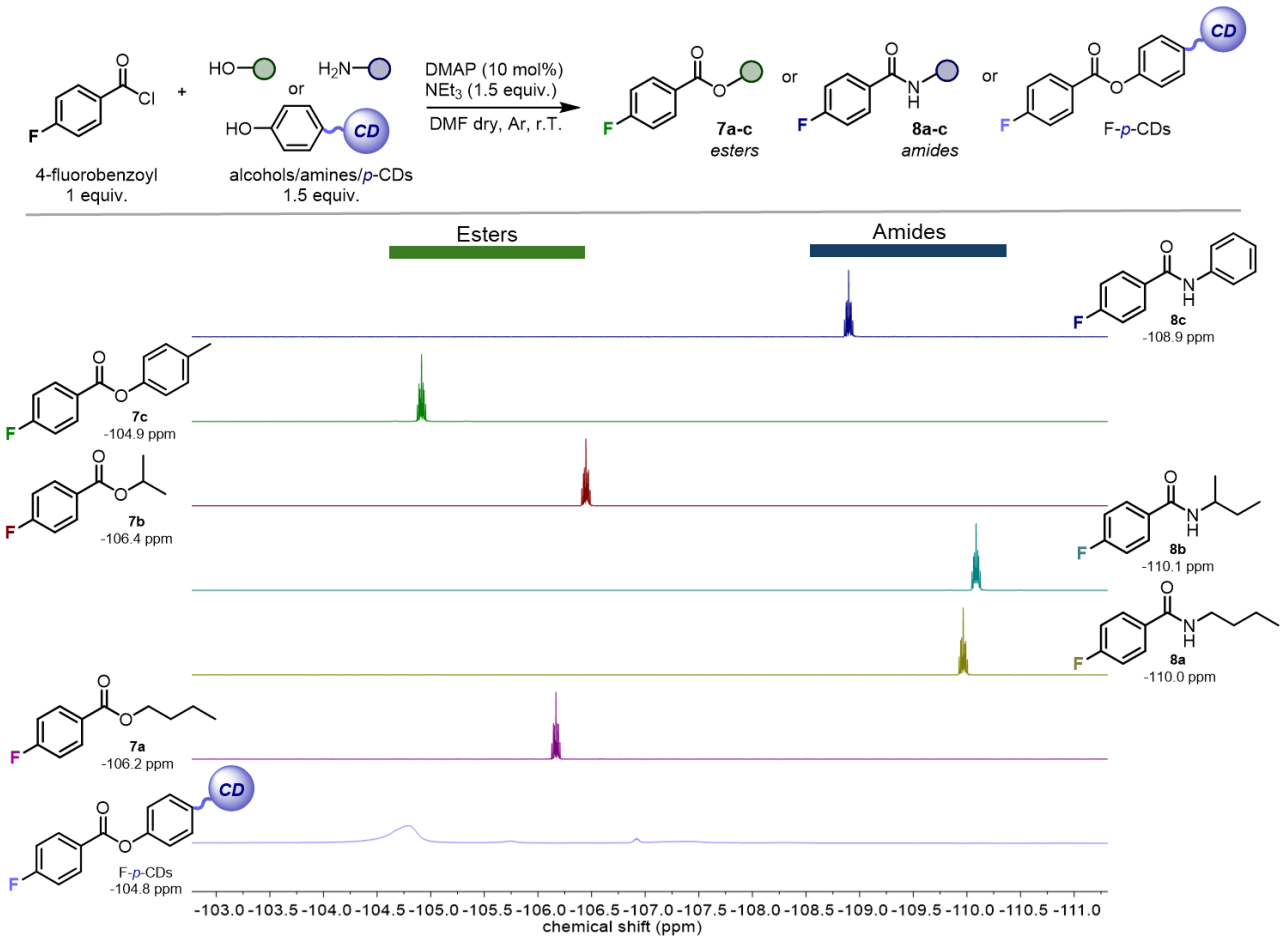

*Figure 3.12 Acylations of alcohols/amines/p-CDs with 4-fluorobenzoyl chloride (1 equiv., 0.5 mmol) were performed in DMF (0.05 M). Stacked ^{19}F-NMR spectra of their corresponding esters 7**a**-**c**, amides **8a**-**c** and p-CDs were recorded in DMSO-d_6. DMAP = 4-(dimethylamino)pyridine.*

Consequently, we performed the acylation reaction of *p*-CDs to yield the fluorinated nanoparticles (F-*p*-CDs). In particular, the ^{19}F-NMR spectrum of the purified material showed a broad signal in the ^{19}F-NMR spectrum centred around -104.8 ppm matching the model product obtained from *p*-cresol (**7c**). This easy and precise qualitative examination established available phenol groups on the *p*-CDs surfaces. Specifically, the number of superficial phenol moieties was measured at 2.30±0.2 mmol/g using α,α,α-trifluorotoluene as internal standard. No signal attributable to amides is observed. This finding can be justified considering that amines were not detected through Kaiser test on our dots. Consequently, within this examination, we established available phenol groups on the *p*-CDs surfaces.

3.3.2 Application of *p*-CDs

With these pieces of evidence at hand, we went on to test the feasibility of the photochemical properties of *p*-CDs as photoredox catalysts. We selected the homolytic aromatic substitution (HAS) reaction between arenes **5** and different electron acceptors **4** (Figure 3.13).

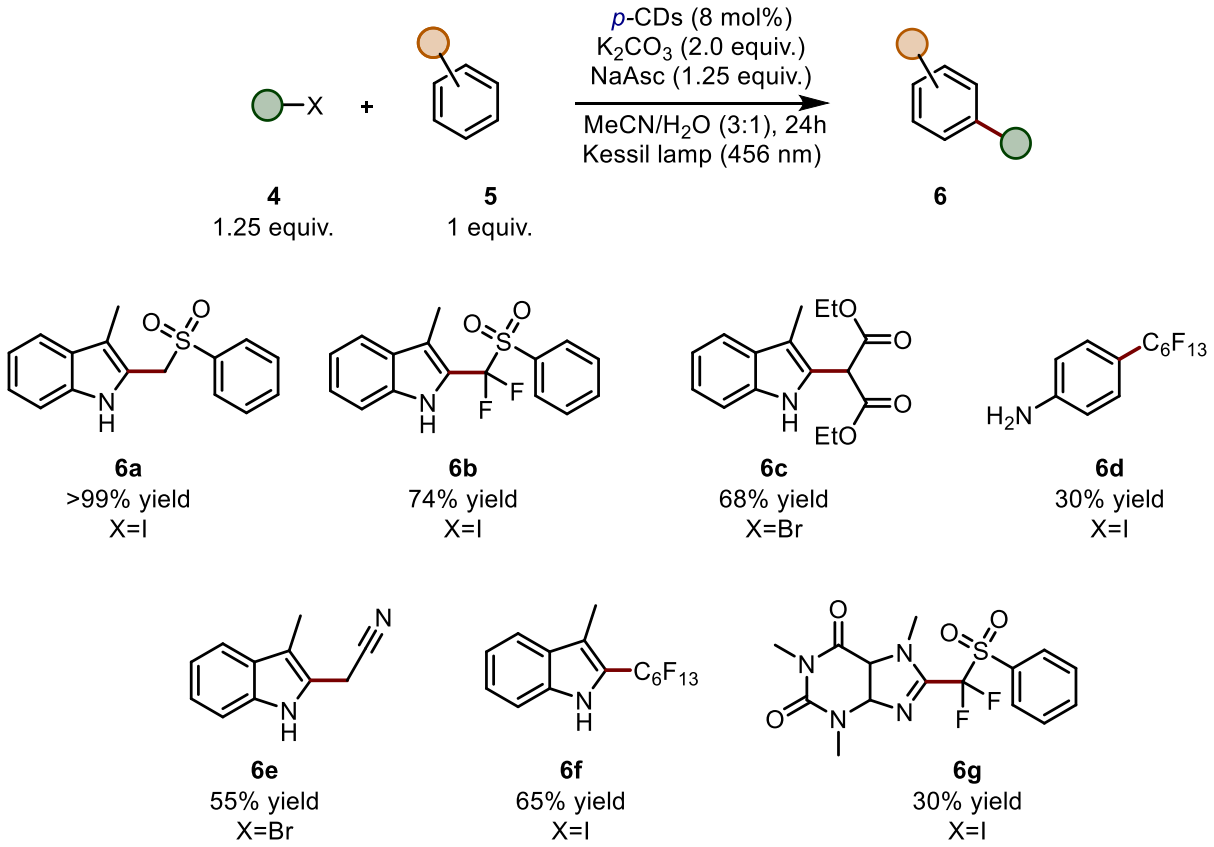

*Figure 3.13 Scope of arenes **5** and acceptors **4** for the homolytic aromatic substitution reaction. NaAsc: sodium ascorbate.*

Specifically, the products **6** were obtained using K_2CO_3 as the base, to deprotonate the phenol moieties on *p*-CDs and to neutralize the acid produced from the halide during the process, and the reductive quencher sodium ascorbate (NaAscorbate), to donate an electron to the catalyst and restore the catalytic cycle. The reaction was performed using a blue light irradiation (Kessil lamp at 456 nm) in a 3:1 MeCN/H_2O solvent solution to facilitate the solubilization of the inorganic base and the saline electron donor. Control experiments showed that no formation of product **6a** was observed in the absence of light, indicating the photochemical nature of the process.

To investigate the generality of this reactivity, we achieved different products **6a**-**g** from moderate to excellent yields. The reaction with 3-methylindole could react with different α-iodosulfones to

afford the products **6a**-**b**, diethyl bromomalonate to obtain product **6c** and bromoacetonitrile to deliver product **6e**. All these products were obtained from moderate to excellent yields (up to >99%). Pleasantly, perfluorohexyl iodide could be used to produce the alkylation product **6d** with aniline. Lastly, caffeine was employed with fluorinated iodosulfone giving product **6g** with satisfactory results. During the optimization experiments on HAS reaction, we noticed the formation of product **6a** without the use of *p*-CDs. Indeed, we found out that in the presence of only the base 1,5-diazabiciclo(5.4.0)undec-7-ene (DBU) instead of K_2CO_3, the reaction between 3-methylindole and iodosulfone provided 56% yield of **6a**. Even though the yield of **6a** using *p*-CDs as photocatalysts was much higher, this observation has prompted us to reflect on why we obtained that result. Based on this observation, we developed a new light-driven catalytic-free protocol for the synthesis of sulfone-containing indoles. This work will be discussed in the next chapter of this thesis (Chapter 4).

Meanwhile, we continued our research looking forward to other interesting reactivities using *p*-CDs as photocatalysts. In particular, our attention was focused on the [3+2] photocycloaddition reaction between cyclopropyl ketones **1** and olefins/alkynes **2**. Building on the work of Yoon about this reactivity using $Ru(bpy)_3(PF_6)_2$ as the PC in combination with a chiral gadolinium-based Lewis acid, we envisioned a novel metal-free strategy.[45] We aimed to exploit the unique photoredox characteristics of phenolates in their excited-state. To do this, the phenol moieties on *p*-CDs should be deprotonated effectively. Therefore, it is evident that a proper base had to be added to the reaction mixture. A reductive quencher to restore the photocatalyst and a Lewis acid to activate the cyclopropyl ketone also appeared necessary. For these reasons, cyclopropane **1a** was selected to react with styrene **2a** in the presence of *p*-CDs (13 mol% of phenol), $Gd(OTf)_2$ (20 mol%) and DIPEA (*i*-Pr_2NEt, 2 equiv.). This preliminary experiment was conducted at room temperature in acetonitrile and under irradiation by a Kessil lamp at 456 nm. Under these conditions, the corresponding cyclopentane **3a** was isolated in 94% yield as diastereomeric mixture (Table 3.1, Entry 1). This promising result prompted us to pursue a metal-free reactivity, avoiding the use of expensive and toxic lanthanide Lewis acid.

Table 3.1 Control and optimization experiments of the [3+2] cycloaddition

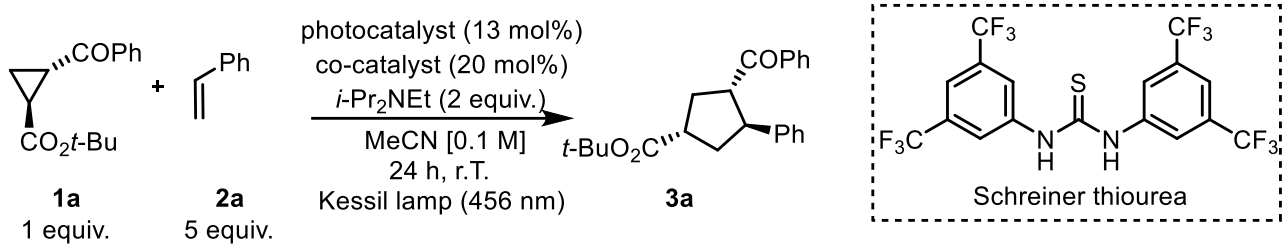

1a 1 equiv. **2a** 5 equiv. **3a**

Entry	Deviation of conditions	Photocatalyst	Co-catalyst	Yield % (d.r.) [a]
1	-	*p*-CDs	$Gd(OTf)_3$	94 (4:1)
2	-	*p*-CDs	$B(C_6F_5)_3$	0
3	-	*p*-CDs	$SiMe_3Cl$	90 (3:1)
4	-	*p*-CDs	**A**	98 (3:1)
5	In the dark or 50°C	*p*-CDs	**A**	0
6	In air	*p*-CDs	**A**	0
7[b]	-	*p*-CDs	**A**	0
8	-	-	**A**	0
9	-	*p*-CDs	-	12
10	-	Tyrosine[c]	**A**	46 (3:1)
11	-	Phenol[c]	**A**	25 (3:1)

Reactions were performed on a 0.1 mmol scale. **A**: Schreiner thiourea, *p*-CDs: *phenol*-Carbon Dots. [a]Yield determined by ^{1}H-NMR using 1,3,5-trimethoxybenzene as an internal standard; d.r. was determined from crude ^{1}H-NMR. [b]Without DIPEA or adding TEMPO (5 equiv.). [c] 20 mol%

Consequently, we screened various metal-free co-catalysts for the activation of cyclopropyl ketone **1**. When the reaction was carried out with $B(C_6F_6)_3$, the final product was not observed (Table 3.1, Entry 2). From entry 3, a 90% yield of **3a** was achieved using $SiMe_3Cl$ as the co-catalyst. Notably, the use of Schreiner thiourea (**A**) as the co-catalyst led to the formation of **3a** in 98% yield with a good diastereomeric ratio, making it the optimal choice for a metal-free variant of the studied reactivity (Table 3.1, Entry 4).

Control experiments demonstrated that no product formation occurred in the absence of light, both at room temperature and at 50°C, indicating the photochemical nature of the process (Table 3.1, Entry 5). Furthermore, the reaction was inhibited under aerobic conditions, supporting a radical

mechanism (Table 3.1, Entry 6). This was further corroborated by an experiment in the presence of 2,2,6,6-tetramethylpiperidine 1-oxyl (TEMPO, 5 equivalents), where **3a** was not detected (Table 3.1, Entry 9). The exclusion of any of the reaction components, namely *p*-CDs, A and DIPEA, completely suppressed the process (Table 3.1, Entries 7-9). Conducting the reaction with 20 mol% of molecular photocatalysts, such as Tyr (Table 3.1, Entry 10) and phenol (Table 3.1, Entry 11) provided the desired product in low yields (up to 46%). These results suggest that the photochemical properties of the nanometric catalysts (*p*-CDs) are essential to achieve high productivity in the studied transformation. We assumed that DIPEA might play a dual role as this tertiary amine can act (*i*) as a base to deprotonate the phenol moieties on *p*-CDs and/or (*ii*) as an electron donor to close the photocatalytic cycle.

Specifically, UV-Vis spectroscopy studies were utilized to evaluate the level of deprotonation of the surface groups on *p*-CDs upon the addition of DIPEA. In particular, we observed that the addition of DIPEA to a solution of *p*-CDs did not show any appreciable change in the absorption spectrum, thus excluding an effective deprotonation of the nanoparticles under such conditions.

Given the pKa values of molecular phenols and DIPEA in acetonitrile, the deprotonation of surface aromatic groups should be minimal. During additional UV analysis, we noticed a pale yellow colour in the solution containing *p*-CDs, **A**, and DIPEA after 2 hours (Figure 3.14a). In fact, the optical absorption spectrum of this mixture showed a bathochromic shift towards the visible spectral region (pink dashed line, Figure 3.14b). The yellow color became even more prominent overtime (light blue dashed line, Figure 3.14b), suggesting the formation of species that absorb visible light. The absorption spectrum of a freshly prepared solution of *p*-CDs, **A** and DIPEA displayed a limited bathochromic shift, possibly implying that in this case the new chromophore was not completely formed. Therefore, we envisioned that the combination of these three components (*p*-CDs, **A** and DIPEA) could result in the formation of coloured complexes, capable of photochemically initiating the cycloaddition reaction. Concerning this, thioureas have been reported as effective chelating agents for spherical anions through hydrogen bonding.[46] The presence of electron-withdrawing CF_3 groups within **A** makes the protons of the thioamide moiety highly acidic, thus improving their anion binding affinity and enhancing the thiourea's ability to disperse the negative charge of the bound anion.[47] Consequently, we hypothesized that **A** could shift the deprotonation equilibrium of phenol groups on *p*-CDs by coordinating and stabilizing their conjugate bases, namely phenolate anions. These surface anionic aggregates, which are held together by non-covalent interaction, may effectively absorb light at 456 nm (Figure 3.14b). Some reports in the literature have demonstrated

the red-shifted absorption of photocatalytic complexes due to the formation of electron-rich phenol anions and conjugate acids.[48]

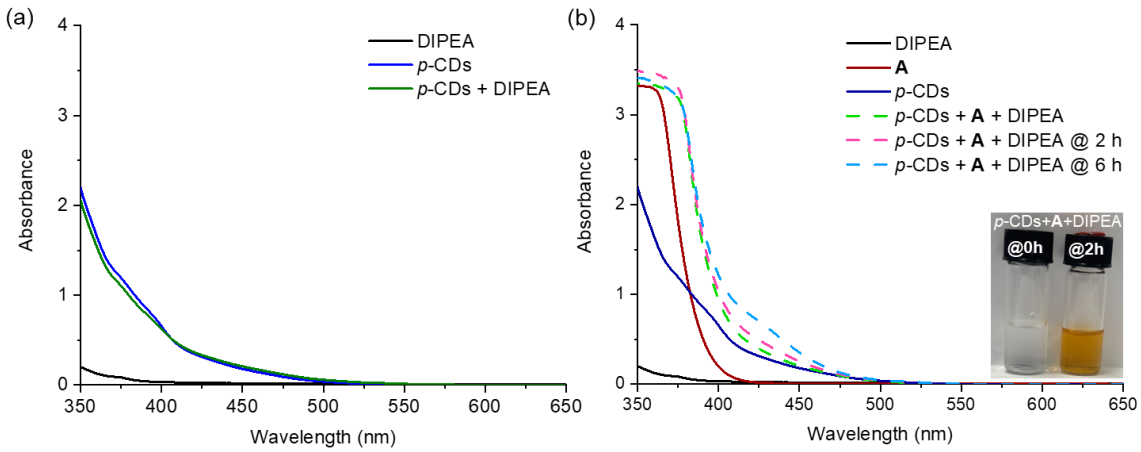

*Figure 3.14 Optical absorption spectra recorded in MeCN: [DIPEA] = 100 mM; [**A**] = 10 mM; [p-CDs] = 50 mM. (a) green line corresponds to the mixture of p-CDs + DIPEA; (b) dashed lines correspond to the mixture of p-CDs + **A** + DIPEA (green line after 0 h, pink line after 2 h, light blue line after 6 h). Imagine shows the yellow colour of the solution with p-CDs + **A** + DIPEA after 2h compared with the same mixture at 0h.*

Other phenomena were excluded through additional absorption studies (see section 3.5.9). To further confirm the presence of phenolic moieties on *p*-CDs, which can form a visible-light-absorbing system with **A** and DIPEA, we recorded absorption spectra using a molecular phenol under the same conditions. Thus, the solution containing 4-*tert*-butylphenol, **A** and DIPEA was prepared and analysed by UV-Vis spectroscopy. Even in this case, a red-shifted absorption was observed after 2 hours (more details in section 3.5.9). This test confirmed the photochemical behaviour of phenol groups when in the presence of **A** and DIPEA, while also supporting the presence of phenol groups on *p*-CDs. The model reaction was also performed in the absence of **A** and using strong bases instead of DIPEA to completely deprotonate the acidic sites on *p*-CDs. Specifically, the use of 2 equiv. of either NaO*t*-Bu or Cs_2CO_3 resulted in the formation of only traces of product **3a**. These experiments further highlighted the unique activation mode of phenols which can be obtained by employing **A** and DIPEA. We then examined the reaction kinetics under the optimized conditions (Table 3.1, Entry 4) at different reaction times, spanning from 1 h to 24 h. In particular, we observed that, within the first 2 h, the starting materials were not consumed. After this induction period, the yield of **3a** began to grow, becoming quantitative after 8 h (Figure 3.15a). Based on these results and the UV-Vis spectroscopic studies, we supposed that the formation of a certain number of anionic surface aggregates, that are capable of photochemically initiating the cycloaddition reaction, required at

least 2 h. To further validate this claim, we monitored the progress of the model reaction between **1a** and **2a** as follows. First, *p*-CDs, **A**, and DIPEA were mixed in acetonitrile to assess the formation of the photocatalytic system, then the reactants (**1a** and **2a**) were added to this solution which was stirred for an additional 6 h under light irradiation. This experiment almost provided a quantitative yield of product **3a**, therefore corroborating our hypothesis (more details in section 3.5.7).

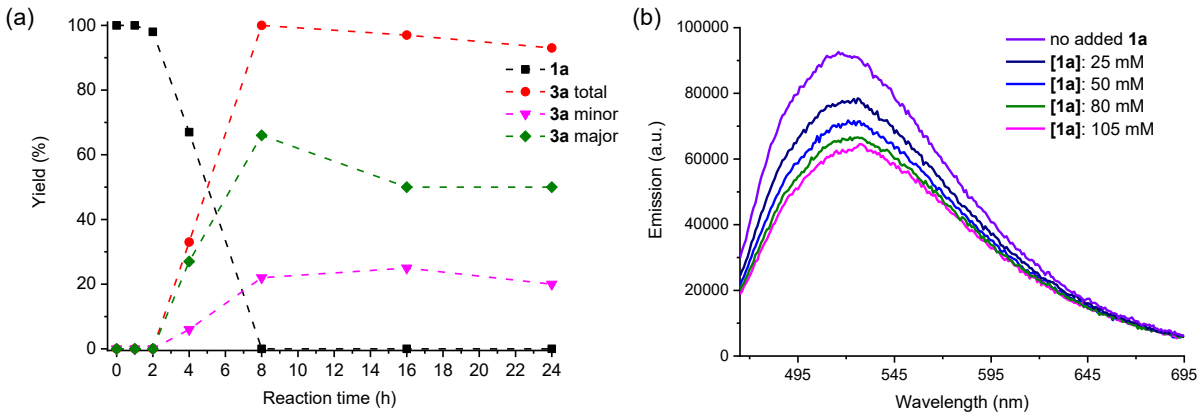

*Figure 3.15 (a) Kinetic study of the reaction time versus yield of the **3a**, major diastereoisomer **3a** and minor diastereoisomer **3a**. (b) Quenching of the catalytic system (p-CDs + **A** + DIPEA) emission ([p-CDs + **A** + DIPEA] = 0.015 M in MeCN, excitation at 456nm) in the presence of increasing amounts of **1a**.*

Additionally, Stern-Volmer quenching experiments were conducted to better understand the photocatalytic reaction mechanism. Thus, the emission spectrum of the coloured adduct, formed by mixing *p*-CDs, **A** and DIPEA, was recorded after excitation at 456 nm. A progressive quenching of its emission intensity was observed upon increasing the concentration of cyclopropane **1a**. In particular, the quenching of emission can occur through a variety of processes.[15] However, the data incorporated in the Stern-Volmer equation revealed a linear correlation in the range 25-105 mM of the quencher (K_{sv} = 4.66 M^{-1}, see Figure 3.20). This is indicative of the occurrence of a single type of quenching mechanism, likely *via* a single electron transfer (SET) process. With this data in mind, we proposed a reaction mechanism (Figure 3.16) that starts from the crucial deprotonating equilibrium of phenols on *p*-CDs.

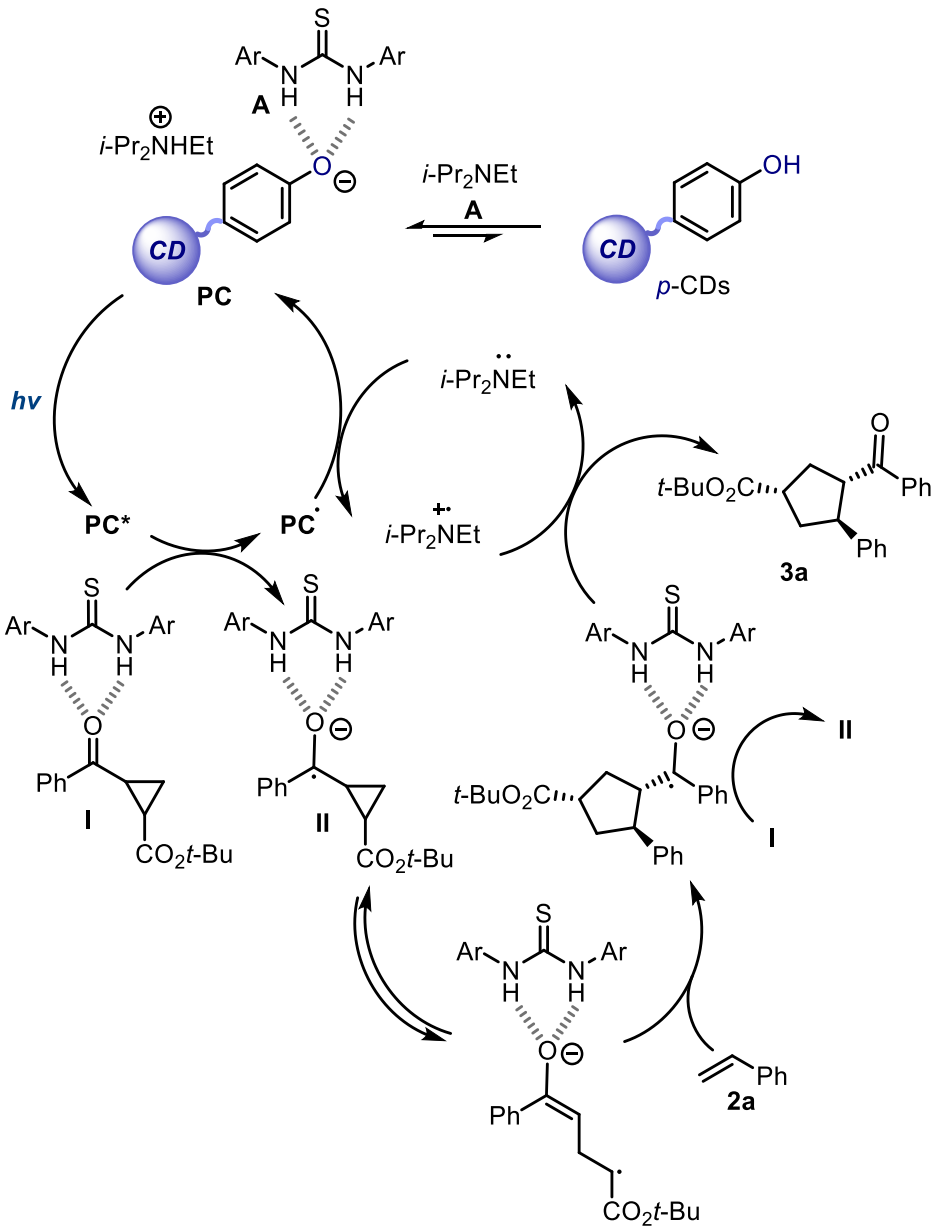

Figure 3.16 Mechanism of the photocatalytic [3+2] cycloaddition process.

In fact, in the presence of DIPEA, this equilibrium is completely shifted towards its neutral form. On the other hand, thanks to the coordination between **A** and surface phenolate anions, the equilibrium may shift towards the anionic form of *p*-CDs. In this way, the actual photocatalytic system (PC) can be produced in solution. When subjected to 456 nm light irradiation, this PC reaches its electronically excited-state (PC*) and becomes a strong reducing agent. Then, a single electron transfer occurs from the PC* to the cyclopropane **1a**, which is presumably activated by **A**. The reduced intermediate **II** then fragments giving its corresponding ring-opening form. Subsequently, this intermediate reacts with **2a** to afford a ketyl radical. Lastly, the oxidation of this radical anion leads to the formation of

product **3a**. Specifically, either **I** or the radical cation of DIPEA could serve as oxidants in this redox step.

To demonstrate the broader applicability of our approach, we evaluated the effect of different dipolarophiles and cyclopropanes on the yields and diastereoselectivity of **3**.

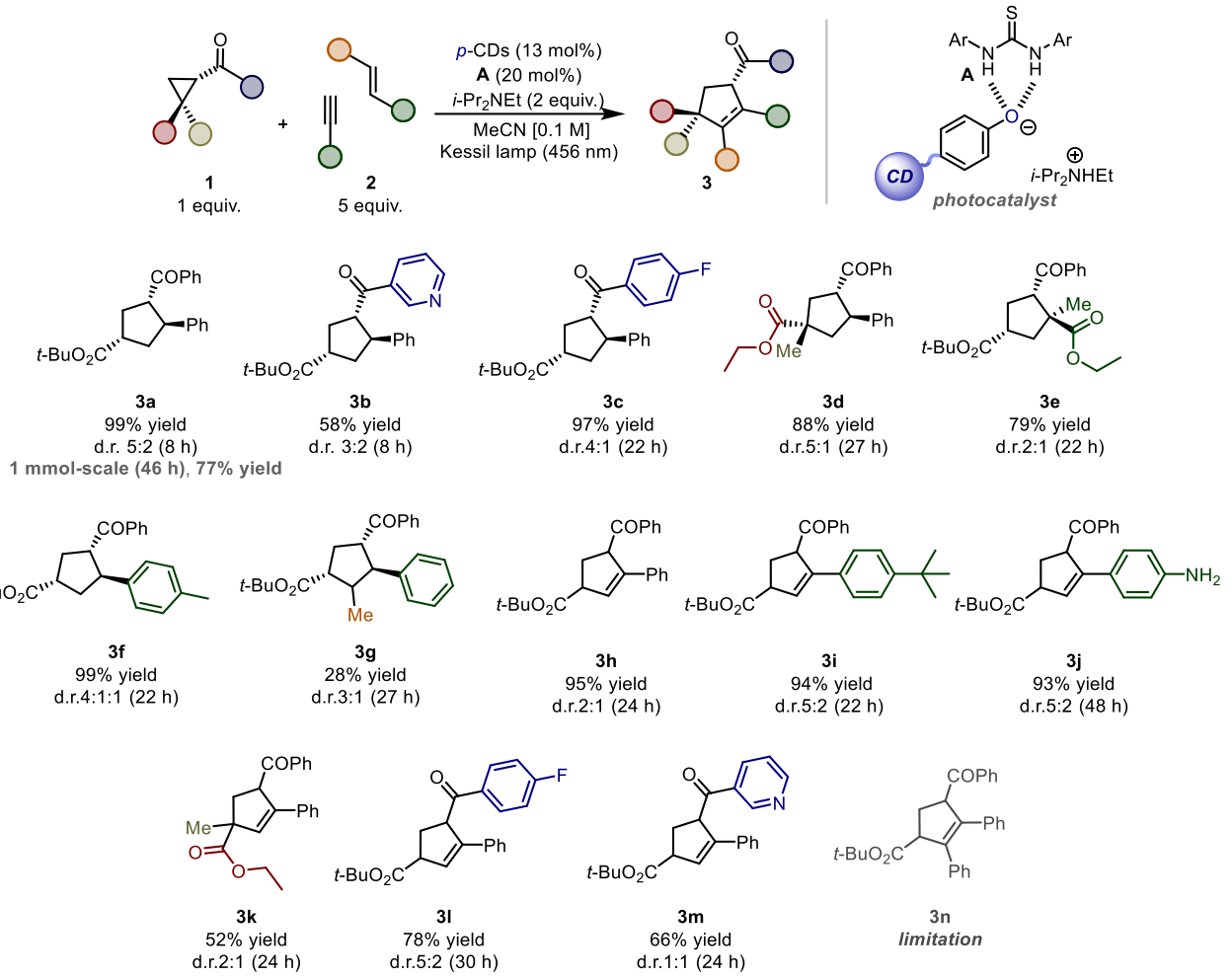

*Scheme 3.1 Evaluation of the scope of cyclopropanes **1** and alkenes or alkynes **2** for the [3+2] cycloaddition reaction. Yields reported are the combined isolated yields of all diastereomers; d.r. was determined from crude NMR. Major diastereomers are shown for **3a-g**. Yields of **3a** in the graph were determined by ^{1}H-NMR analyses, using 1,3,5-trimethoxybenzene as internal standard. See the experimental section 3.5 for details.*

The model cycloaddition at 8 hours was demonstrated to provide nearly quantitative yield of **3a**, and 77% yield in a 1 mmol scale-up. As shown in Scheme 3.1, the presence of a heteroaryl ketone on cyclopropanes was well tolerated (**3b**, 58% yield and 3:2 d.r.). Moreover, the use of **1c**, which contains an electron-withdrawing group on the aryl fragment, resulted in a high yield of the desired product **3c** (97%) with good diastereoselectivity (4:1 d.r.). Interestingly, both cyclopropane and olefin containing 1,1-disubstituents were also suitable substrates for this transformation. As a matter of fact, these substrates afforded the corresponding cyclic products **3d-e** in high overall yields as

a mixture of two diastereoisomers (d.r. up to 5:1). An alkyl group decorating the aromatic ring of styrene led to the formation of derivative **3f** in excellent yield and good d.r. Surprisingly, our methodology allowed the use of internal olefins, resulting in product **3g** with moderate yield and d.r. To test the feasibility of producing cyclopentenes, different alkynes (**2h**-**n**) were tested as substrates. In this regard, phenylacetylene gave good results both in terms of diastereoselectivity and yield (product **3h**: 95% yield, d.r. 2:1). Remarkably, alkynes with free primary amines and sterically hindered substituents also reacted to produce cyclopentenes **3i** and **3j** in high yields. In addition, the use of a cyclopropane containing a quaternary carbon provided a moderate yield of the adduct **3k** with poor diastereoselectivity. Lastly, electron-deficient cyclopropyl ketones effectively reacted with the ethynylbenzene leading to very good overall yields of the desired unsaturated rings **3l**-**3m**. Unfortunately, non-terminal alkynes did not participate in the reaction process (**3n**).

In addition, we focused on asymmetric catalysis, to induce enantioselectivity in the products of cycloaddition by using a chiral reagent. To achieve this, we investigated the behaviour of two different enantiopure thioureas, namely (*S*)-2-[[3,5-Bis(trifluoromethyl)phenyl]thioureido]-N-benzyl-N,3,3-trimethylbutanamide and 1-[3,5-bis(trifluoromethyl)phenyl]-3-[(1*R*,2*R*)-(-)-2-(dimethylamino)cyclohexyl]thiourea. These thioureas were tested in the cycloaddition of **1a** and **2a** under optimised reaction conditions. The reactions afforded the product **3a** in moderate yields (up to 68%) after 48 h; however, no enantioselectivity was observed in the formation of **3a** (see section 3.5.6).

Lastly, we also demonstrated that *p*-CDs could be recycled up to 3 times (Figure 3.17). The *p*-CDs were recycled up to three times, as shown in Figure 3.17. To perform the recycling tests, we selected cyclopropane **1a** and styrene **2a** as substrates. The procedure for recyclability consists of the dilution of the crude reaction mixture with diethyl ether to induce the precipitation of the *p*-CDs while the molecular species were collected by liquid extraction. Subsequently, the recovered *p*-CDs were dried and reused in subsequent cycloadditions up to three cycles, maintaining the catalyst in the same reaction vessel. Remarkably, the recyclability tests provided comparable performances in terms of reaction yield and diastereoselectivity. The reuse of *p*-CDs highlights their potential as sustainable nano-photocatalysts.

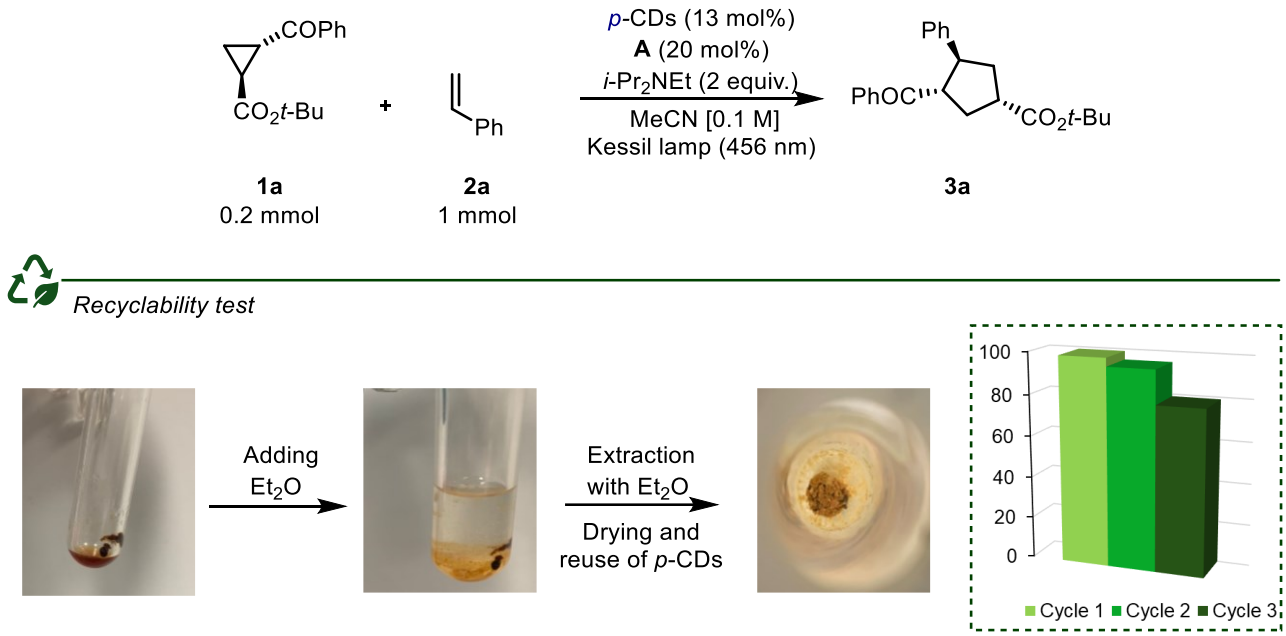

*Figure 3.17 Representation of recyclability workflow of p-CDs. Histogram of yield for product **3a** at each of the three catalytic cycles.*

3.4 Conclusion

The intriguing photocatalytic properties of CDs inspired us to explore the synthesis of new phenol-rich nanoparticles with unique molecular-like behaviour. The wide set of characterization techniques provided evidence about the formation of *p*-CDs with excellent photochemical features. The phenol moieties on the surface of *p*-CDs, quantified by a post-synthetic strategy using ^{19}F-NMR, demonstrated their efficiency as photocatalysts in driving the reduction of suitable acceptors to generate reactive radicals that can proceed towards following transformations. Specifically, halogen compounds were activated for the study of homolytic aromatic substitution. Additionally, the [3+2] photocycloaddition reaction between cyclopropane **1** and unsaturated compounds **2** was performed, yielding a diverse array of relevant products **3** from a moderate to an excellent yield along with good levels of diastereoselectivity. Notably, we demonstrated that the phenol moieties present on the nanoparticles' surfaces can generate, when mixed with **A** and DIPEA, coloured anionic non-covalent aggregates able to drive [3+2] photocycloaddition reactions. The *p*-CDs structure has successfully implemented the photocatalytic activity of phenolate compounds enabling their use as sustainable, metal-free and recyclable photocatalysts.

3.5 Experimental Section

3.5.1 General Information

The microwave synthesis was performed on a CEM Discover-SP instrument. UV-Vis measurements were carried out on Cary 5000 UV-Vis-NIR. All the spectra were recorded at room temperature using 10 mm path-length quartz cuvettes. Absorption spectra of compounds were recorded with an Agilent Cary 5000 UV-Vis spectrophotometer. Emission measurements were performed on an Edinburgh instruments FS5 spectrofluorometer using a 150 W CW Ozone-free xenon arc lamp as source and a Photomultiplier R928P (spectral coverage 200 nm – 900 nm, cooled and stabilised) as detector. Quantum yields were performed using the integrating sphere setup SC-30. Luminescence lifetimes were measured with an Edinburgh Instruments FS5 time-correlated single-photon counting spectrofluorimeter, exciting the sample at 375 nm with a picosecond pulsed diode laser (EPL-375 Edimburgh Instruments). All spectra were recorded using water using a standard quartz cuvette with an optical path length of 1 cm. 30 Integrating Sphere. AFM images were obtained with a Nanoscope IIIa, VEECO Instruments. As a general procedure to perform AFM analyses, tapping mode with a HQ:NSC19/ALBS probe (80kHz; 0.6 N/m) (MikroMasch) from drop cast of samples in an aqueous or MeOH solutions (concentration in the order of μg/mL) on a mica substrate was performed. The AFM raw data were analyzed using S3 Gwyddion 2.35. TGA was performed with a TGA Q500 (TA instruments), under a flow of N_2 (25 mL/min), following a temperature program consisting of the equilibration of the sample at 100°C for 10 minutes followed by a ramp at 5°C/min up to 800°C. The sample aliquot ranged from 1 to 2 mg, exactly weighed. ATR-IR measurements were performed using a Spectrum 2000 FT-IR Instrument (Perkin Elmer). The NMR spectra were recorded on Varian 400 spectrometer (^{1}H: 400 MHz; ^{19}F-NMR: 376.0 MHz ^{13}C: 101.0 MHz). Enantiomeric excess (ee) values were determined by HPLC Agilent Infinity II, employing a Phenomenex chiral stationary phase column (specified in the individual description compound) and a detector operating at 220 and 254 nm. Chromatographic purification of products was accomplished using flash chromatography on silica gel (35-70 mesh). For thin layer chromatography (TLC) analysis throughout this work, Merck pre-coated TLC plates (silica gel 60 GF254, 0.25 mm) were employed, using UV light as the visualizing agent (254 nm), basic aqueous potassium permanganate ($KMnO_4$) stain solution or iodine, and heat as developing agents. Organic solutions were concentrated under reduced pressure on a Büchi rotatory evaporator. The power supply for electrophoresis was bought from Consort (Model E844). Ultrapure fresh water obtained from a Millipore water purification system (>18 MΩ Milli-Q,

Millipore) was used in all experiments. Commercial reagents and solvents were purchased from Sigma-Aldrich, Fluka, Alfa Aesar, Fluorochem and VWR. They were used as received, without further purification unless otherwise stated. Synthesis grade and anhydrous solvents were used as purchased.

3.5.2 Synthesis of *p*-CDs

L-arginine (874.5 mg, 0.5 mmol) and L-tyrosine (905.9 mg, 5 mmol) were introduced in a sealable microwave vessel followed by 2 mL of ethylene glycol. The vessel was closed and then heated at 250°C, and 300 W for 15 minutes. In the process of microwave heating, the solution changes colour from a white suspension to a brown oil because of the formation of P-CDs. The solution was diluted with dimethyl formamide (DMF) ca. 3 mL, put under sonication and precipitation was induced by a dropwise addition of water up to 450 mL. The precipitate was collected though filtration over a polytetrafluoroethylene (PTFE) membrane with a 0.1 mm pore size. The precipitate was collected and dissolved in the minimal quantity of DMF, precipitation was re-induced under sonication using water. The precipitation process was repeated 4 times. The final powder was rinsed with diethyl ether and left to dry under the fume hood. After drying, the final material is obtained as a brownish powder. The mass yield of the process was approximately 20% (350mg).

3.5.3 *p*-CDs Characterizations

Kaiser test procedure. Kaiser tests (KT) were carried out according to a modified procedure using a commercially available Merck kit.[49] About 1 mg of *p*-CDs was placed in a test tube. Then, 75 µL of a phenolic solution in ethanol (Sol A), 100 µL of a KCN solution in pyridine/water (Sol B), and 75 µL of a ninhydrin solution in ethanol (Sol C) were added. The tube was capped, and the obtained solution was heated at 120°C for 10 minutes. The resulting solution should colour violet for the presence of Ruhemann's purple compound as the appeared brown that resulted in a null result.

ATR-FTIR analysis. Arginine, tyrosine and *p*-CDs were analyzed by infrared spectroscopy.

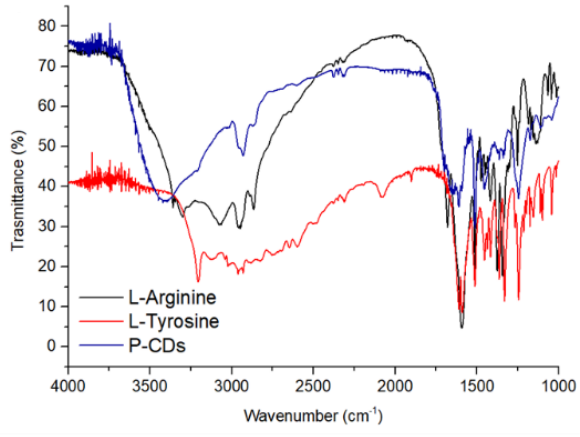

Figure 3.18 Stacked ATR-FTIR spectra of p-CDs, Arginine and Tyrosine

Detection of phenol moieties on *p*-CDs

To synthesize the model compounds for ^{19}F-NMR experiments (0.75 mmol, 1.5 equiv.) of the nucleophile amines or alcohols were introduced in a flame-dried Schlenk tube followed by 10 mL dry DMF, 4-(Dimethylamino)pyridine DMAP (10 mol%) and triethylamine (0.75 mmol, 76.42 mg, 105 mL). The reaction was placed under argon atmosphere and heated at 40°C. The acylating reagent 4-fluorobenzoyl chloride (0.5 mmol, 79 mg, 60 mL, 1.5 equiv.) was solubilized in 2 mL of dry DMF and added dropwise. The solution turned almost immediately to a deep yellow color. The mixture was left to react overnight. The day after, it was quenched by the addition of 0.1 M HCl and extracted three times with ethyl acetate. The combined organic phases were reunited and dried over Na_2SO_4. The organic phase was concentrated under reduced pressure to give the crude product. The residue was purified by flash column chromatography (ethyl acetate/cyclohexane) to afford the desired products.

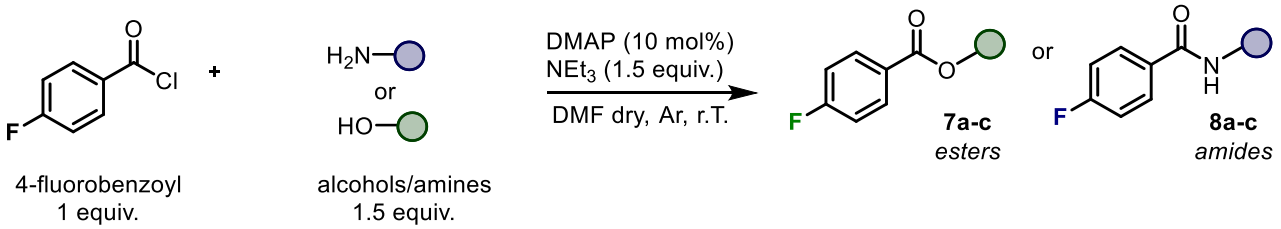

<u>Characterization Data</u>

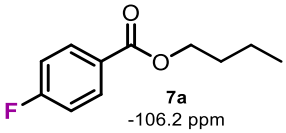

Butyl 4-fluorobenzoate (7a)

Prepared according to the above-described procedure using (0.75 mmol, 52.5mg, 65 mL) of 1-butanol.

^{1}H-NMR (400 MHz, DMSO-d_6) δ 8.20 – 7.78 (m, 2H), 7.50 – 7.19 (m, 2H), 4.25 (t, *J* = 6.5 Hz, 2H), 1.79 – 1.56 (m, 2H), 1.54 – 1.32 (m, 2H), 0.91 (t, *J* = 7.4 Hz, 3H). **^{19}F-NMR (376 MHz, DMSO-d_6)** δ -106.2(m).

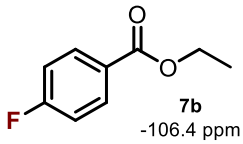

Isopropyl 4-fluorobenzoate (7b)

Prepared according to the foregoing described procedure using (0.75 mmol, 45.0 mg, 58 mL) of 2-propanol.

^{1}H-NMR (400 MHz, DMSO-d_6) δ 8.19 – 7.78 (m, 2H), 7.28 (m, 2H), 5.09 (p, *J* = 6.2 Hz, 1H), 1.27 (d, *J* = 6.3, 6H). **^{19}F-NMR (376 MHz, DMSO-d_6)** δ -106.4 (m).

p-tolyl 4-fluorobenzoate (7c)

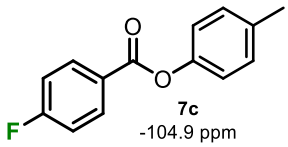

Prepared according to the previously described procedure using (0.75 mmol, 81.0 mg) of p-cresol.

^{1}H-NMR (400 MHz, DMSO-d_6) δ 8.25 – 8.12 (m, 2H), 7.46 – 7.35 (m, 2H), 7.28 – 7.21 (m, 2H), 7.13 (m, 2H), 2.31 (s, 3H). **^{19}F-NMR (376 MHz, DMSO-d_6)** δ -104.9 (m).

N-butyl-4-fluorobenzamide (8a)

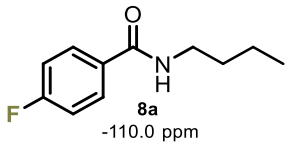

Prepared according to the previously described procedure using (0.75 mmol, 54.85 mg, 74 mL) of butylamine.

^{1}H-NMR (400 MHz, DMSO-d_6) δ 8.43 (t, *J* = 5.7 Hz, 1H), 8.03 – 7.70 (m, 2H), 7.25 (m, 2H), 3.23 (td, *J* = 7.1, 5.6 Hz, 2H), 1.57 – 1.43 (m, 2H), 1.40 – 1.22 (m, 2H), 0.87 (t, *J* = 7.3 Hz, 3H).**^{19}F-NMR (376 MHz, DMSO-d_6)** δ -110.0 (m).

N-(sec-butyl)-4-fluorobenzamide (8b)

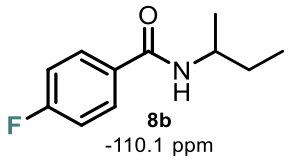

Prepared according to the previously described procedure using (0.75 mmol, 54.85 mg, 76 mL) of sec-butylamine.

^{1}H-NMR (400 MHz, DMSO-d_6) δ 8.14 (d, *J* = 8.2 Hz, 1H), 8.02 – 7.81 (m, 2H), 7.38 – 7.15 (m, 2H), 3.89 (tt, *J* = 7.8, 6.4 Hz, 1H), 1.58 – 1.39 (m, 2H), 1.11 (d, *J* = 6.6 Hz, 3H), 0.84 (t, *J* = 7.4 Hz, 3H).**^{19}F-NMR (376 MHz, DMSO-d_6)** δ -110.1 (m).

4-fluoro-N-phenylbenzamide (8c)

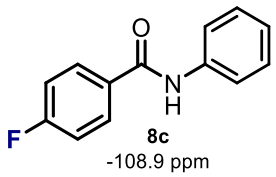

Prepared according to the previously described procedure using (0.75 mmol, 69.84 mg, 64 mL) of aniline.

^{1}H-NMR (400 MHz, DMSO-d_6) δ 10.23 (s, 1H), 8.14 – 7.97 (m, 2H), 7.74 (dt, *J* = 7.9, 1.1 Hz, 2H), 7.46 – 7.28 (m, 4H), 7.22 – 7.01 (m, 1H).**^{19}F-NMR (376 MHz, DMSO-d_6)** δ -108.9 (m).

Then, the acylation reaction was performed on the *p*-CDs.

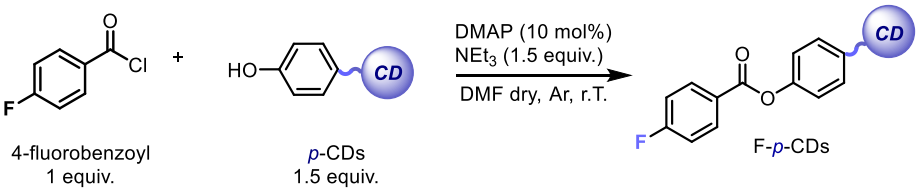

50 mg of *p*-CDs were introduced in a flame-dried Schlenk tube followed by 10 mL dry DMF, 4-(Dimethylamino)pyridine DMAP (0.4 mmol, 48 mg) and triethylamine (6 mmol, 607 mg, 830 mL). The reaction was placed under argon atmosphere and heated at 40°C. The acylating reagent 4-fluorobenzoyl chloride (4 mmol, 634 mg, 478 mL) was solubilized in 5 mL of dry DMF and added dropwise. The mixture was left to react for 48 hours. Then, it was quenched by the addition of 0.1M HCl. This caused the precipitation of fine brown powder. The reaction was extracted with ethyl acetate, in which the functionalized *p*-CDs are soluble, contrarily to the pristine material. The acylated *p*-CDs were purified via flash chromatography. First, the powder is solubilized in 1 mL of DMF and absorbed over silica. A short silica plug was loaded with the powder and eluted with (cyclohexane/ethyl acetate 8:2) to remove the side products. Subsequently, the acylated *p*-CDs were desorbed with DMF. The DMF solution was diluted with a solution of 5% w/w of LiCl and extracted with ethyl acetate. The combined organic phases were reunited, dried over Na_2SO_4 and concentrated under reduced pressure. The procedure afforded the purified F-*p*-CDs.

3.5.4 Procedure for the Preparation of Starting Materials of HAS and [3+2] Cycloaddition

PREPARATION OF α-IODOSULFONES **4a**

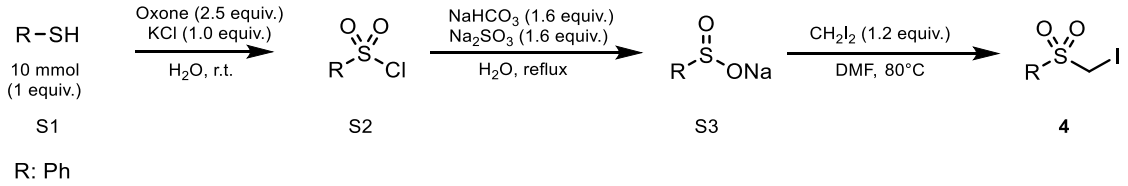

STEP 1, has been carried out following a modified literature procedure.[50] A mixture of thiol S1 (10 mmol, 1 equiv.), Potassium peroxymonosulfate (25 mmol, 2.5 equiv.), KCl (10 mmol, 1 equiv.) and H_2O (30 mL) were introduced in a single neck round bottom flask and stirred at room temperature

for 2 h. The aqueous phase was extracted with ethyl acetate (3 x 50 mL). The combined organic layer was dried over anhydrous Na_2SO_4 and concentrated under reduced pressure. The crude product was purified by flash column chromatography (cyclohexane) affording the desired products S2. The characterization data matched with the reported one.[19]

STEP 2, according to a literature procedure.[51] The selected sulfonyl chloride S2 (7 mmol, 1 equiv.) was dissolved in H_2O (25 mL). Sodium sulfite (11.2 mmol, 1.6 equiv.) and sodium bicarbonate (11.2 mmol, 1.6 equiv.) were added, and the reaction mixture was refluxed for 3 h. Water was removed by evaporation. Ethanol was added to the solid and the so obtained suspension was heated for 10 min., cooled and filtered. This procedure was repeated twice using the residue of the filtration. The ethanol fractions were combined, and the solvent was evaporated under reduced pressure. Sodium sulfinate S3 was used without any further purification. The characterization data matched the reported one.[19]

STEP 3, according to a reported procedure.[52] A solution of sodium sulfinate S3 (5 mmol, 1 equiv.) in DMF (20 mL) was stirred at room temperature for 15 min. Diiodomethane (6 mmol, 1.2 equiv.) was added dropwise, and the solution was heated up to 80°C for 17h. The reaction was quenched by the addition of 5% LiCl water solution (100 mL). Subsequently, the aqueous solution was extracted with ethyl acetate (3 x 30 mL). The organic phases were combined and washed with brine (50 mL), saturated solution of sodium thiosulfate (50 mL) and then dried over Na_2SO_4 before being concentred in vacuo. The product was purified by flash column chromatography (eluent: cyclohexane/ethyl acetate) to afford the desired α-iodo sulfone **4a**. (R= -phenyl 88% Yield)

Characterization data

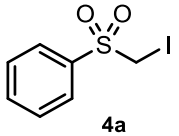

4a

(Iodomethyl)sulfonyl)benzene (4a)

^{1}H-NMR (400 MHz, $CDCl_3$) δ 7.98 (dt, J= 8.5, 1.6 Hz, 2H), 7.74-7.68 (m, 1H), 7.60 (dt, J= 8.0, 1.2 Hz, 2H), 4.46 (s, 2H); The characterization data matched with the reported one.

PREPARATION OF α-IODOSULFONE **4b**

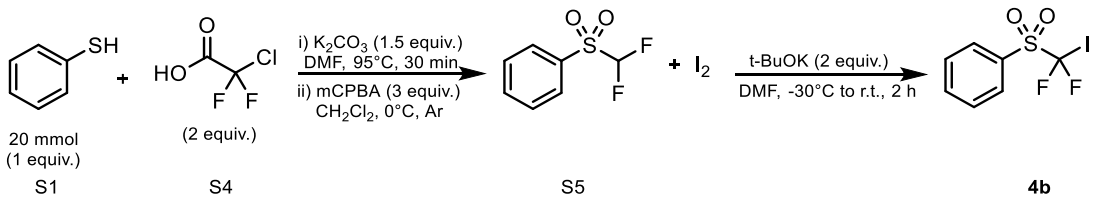

20 mmol (1 equiv.) S1 | (2 equiv.) S4 | S5 | 4b

STEP 1, was performed following a modified reported procedure.[53] Into an oven-dried schlenk tube equipped with a stirring bar, thiophenol (20 mmol, 1 equiv., 2.2g) and K_2CO_3 (1.5 equiv., 30mmol) were introduced and dissolved in dry DMF (25 mL). Chlorodifluoroacetic acid S4 (2.0 equiv., 40 mmol) was solubilized in dry DMF and added dropwise into the reaction mixture. The reaction was kept under argon atmosphere. The reaction was then heated at 95°C for 30 min. Subsequently, it was quenched through the addition of 5% LiCl water solution and extracted with cyclohexane (3 x 20 mL). The organic layers were reunited, dried with Na_2SO_4 and concentrated under reduced pressure. The crude intermediate from the first step was used as obtained after extraction. It was dissolved in 20 mL of CH_2Cl_2 under argon and cooled to 0°C. Meta-chloroperoxybenzoic acid (60 mmol, 3 equiv.) was slowly added. The reaction was stirred overnight (approximately 16 h). The day after, 0.1 M NH_4Cl water was added and the product S5 was extracted with ethyl acetate (3 x 20mL). The ethyl acetate fractions were combined and dried over Na_2SO_4 and the solvent was evaporated under reduced pressure. Product S5 was obtained with a yield of 40%.

^{1}H-NMR ($CDCl_3$, 400 MHz) δ 6.20 (t, J = 53.1 Hz, 1H), 7.62-7.68 (m, 2H), 7.79-7.85 (m, 1H), 7.97-8.02 (m, 2H). **^{19}F-NMR ($CDCl_3$, 376 MHz)** δ -121.9 (d, J = 53.5 Hz, 2F). The characterization of the compound matches with the data reported in the literature.[54]

STEP 2, The last reaction step was carried out according to the literature.[55] S5 (8.5 mmol, 1.470 g) was introduced in an oven-dried double neck round bottom flask with stirring bar along with dry DMF (20 mL). The reaction was cooled to -30°C and placed under argon. I_2 (2.5 equiv., 21.25 mmol) was added in small aliquots followed by a dropwise addition of *t*-BuOK (2.0 equiv., 17 mmol). The reaction was stirred at -30°C for 1h. Subsequently, the reaction was allowed to reach room temperature in approximately 1h. A saturated NaCl aqueous solution (15 mL) was added, and the mixture was extracted with Et_2O (3 x 15 mL). The combined organic phase was dried over Na_2SO_4, and the solvent was removed in a rotary evaporator. The crude was purified by silica gel column chromatography (eluent: cyclohexane/ethyl acetate 9/1) to afford the product (**4b**) (2.22 g, 35% overall yield) as a white crystalline solid. The product has been kept in the dark at 4°C.

^{1}H-NMR (400 MHz, $CDCl_3$) δ 7.65 (t, J = 7.3 Hz, 2H); 7.82 (t, J = 7.4 Hz, 1H); 7.99 (d, J = 7.5 Hz, 2H). **^{19}F-NMR (376 MHz, $CDCl_3$)** δ – 51.9 (s, 2F). The characterization of the compound matches with the data reported in the literature.[54]

PREPARATION OF CYCLOPROPANES **1a-d**

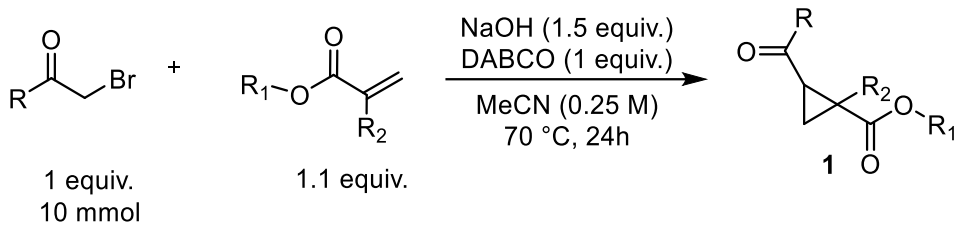

Dry MeCN (17 mL) was added to a round flask with DABCO (10.0 mmol, 1.12 g), and α-halo ketone (10.0 mmol, 1 equiv.). A thick white precipitate formed immediately, and the mixture was allowed to stir at room temperature under a nitrogen atmosphere for 30 min. After this time, NaOH (0.600 g, 15.0 mmol, 1.5 equiv.) and the alkene (11 mmol, 1.1 equiv.) were added. The reaction flask was equipped with a reflux condenser and the reaction mixture brought to 80 °C until completion as indicated by TLC. The reaction was then quenched with saturated aqueous ammonium chloride and extracted three times with Et_2O. The combined organic layers were washed once with brine, then dried over anhydrous sodium sulfate, and concentrated under reduced pressure to give the crude product as a dark oil. The residue was purified by flash chromatography (CyHex/EtOAc) to afford the corresponding cyclopropanes **1a**-**d**.

Characterization Data

tert-Butyl 2-benzoylcyclopropanecarboxylate (1a)

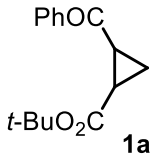

1a

1a was synthesized according to the general procedure from 2-bromo-1-phenylethanone (1.99 g, 10 mmol) and tert-butyl acrylate (1.34 mL, 11 mmol). The cyclopropane **1a** was obtained as solid (1.50 g, 60% yield).

^{1}H-NMR (400 MHz, $CDCl_3$) 8.02 (2H, d, *J*=7.0 Hz), 7.62 – 7.55 (1H, m), 7.49 (2H, t, *J*=7.7 Hz), 3.12 (1H, ddd, *J*=9.1, 5.7, 3.8 Hz), 2.30 (1H, ddd, *J*=8.6, 5.9, 3.8 Hz), 1.55 (2H, dddd, *J*=14.8, 9.1, 5.8, 3.3 Hz), 1.47 (9H, s). **^{13}C-NMR (101 MHz, $CDCl_3$)** δ 197.51, 171.56, 137.31, 133.42, 128.79, 128.41, 81.42, 28.23, 25.94, 25.92, 17.95. The characterization of the compound matches with the data reported in the literature.[45]

trans tert-Butyl 2-nicotinoylcyclopropanecarboxylate (1b)

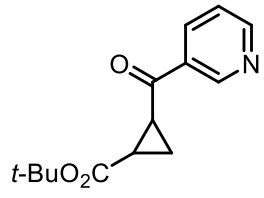

1b

1b was synthesized according to the general procedure from 3-(2-bromoacetyl)pyridin-1-ium bromide (2.8 g, 10 mmol) and tert-butyl acrylate (1.34 mL, 11 mmol). The cyclopropane **1b** was obtained as solid (1.6 g, 65% yield).

^{1}H-NMR (499 MHz, $CDCl_3$) δ 9.25 (d, *J* = 1.6 Hz, 1H), 8.81 (dd, *J* = 4.8, 1.7 Hz, 1H), 8.26 (dt, *J* = 8.0, 1.9 Hz, 1H), 7.44 (ddd, *J* = 8.0, 4.9, 0.9 Hz, 1H), 3.09 (ddd, *J* = 8.6, 5.7, 3.8 Hz, 1H), 2.34 (ddd, *J* = 8.8, 6.0, 3.8 Hz, 1H), 1.68 – 1.54 (m, 2H), 1.47 (s, 9H).**^{13}C-NMR (126 MHz, $CDCl_3$)** δ 196.32, 170.95, 153.67, 149.73, 135.48, 132.38, 123.60, 81.58, 28.06, 26.14, 25.90, 18.03. The characterization of the compound matches with the data reported in the literature.[45]

tert-Butyl 2-(4-fluoro)benzoylcyclopropanecarboxylate (1c)

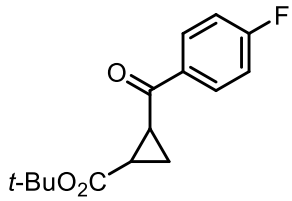

1c

1c was synthesized according to the general procedure from 2-Chloro-4'-fluoroacetophenone (1.7 g, 10 mmol) and tert-butyl acrylate (1.34 mL, 11 mmol). The cyclopropane **1c** was obtained as solid (1.8 g, 69% yield).

^{1}H-NMR (400 MHz, $CDCl_3$) δ 8.05 (dd, *J* = 9.0, 5.4 Hz, 2H), 7.16 (dd, *J* = 9.0, 8.4 Hz, 2H), 3.06 (ddd, *J* = 8.6, 5.7, 3.8 Hz, 1H), 2.30 (ddd, *J* = 8.6, 6.0, 3.8 Hz, 1H), 1.60 – 1.50 (m, 2H), 1.47 (s, 9H). **^{13}C-NMR (101 MHz, $CDCl_3$)** δ 195.91, 171.47, 166.06 (d, *J* = 255.3 Hz), 133.74 (d, *J* = 3.0 Hz), 131.06 (d, *J* = 9.2 Hz), 115.92 (d, *J* = 22.0 Hz), 81.52, 28.23, 25.92, 25.77, 18.00. **^{19}F-NMR (376 MHz, $CDCl_3$)** δ -104.92. **HRMS** calculated for $C_{15}H_{17}FO_3$ (M-Na): 287.1054 found: 287.1053.

ethyl 2-benzoyl-1-methylcyclopropane-1-carboxylate (1d) was synthesized according to the general procedure from 2-bromo-1-phenylethanone (1.99 g, 10 mmol) and ethyl methacrylate (1.37 mL, 11 mmol). The cyclopropane **1d** was obtained as solid (430 mg, 38% yield).

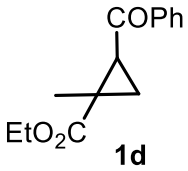

1d

^{1}H-NMR (499 MHz, $CDCl_3$) δ 7.94 – 7.89 (m, 2H), 7.56 – 7.47 (m, 1H), 7.44 – 7.37 (m, 2H), 4.18 (q, *J* = 7.1 Hz, 2H), 3.25 (dd, *J* = 8.3, 6.5 Hz, 1H), 1.62 (dd, *J* = 6.6, 3.9 Hz, 1H), 1.58 (dd, *J* = 8.2, 4.0 Hz, 1H), 1.26 (t, *J* = 7.1 Hz, 3H), 1.23 (s, 3H). **^{13}C-NMR (126 MHz, $CDCl_3$)** δ 195.88, 173.64, 137.98, 133.11, 128.61, 128.18, 61.31, 31.84, 29.57, 20.49, 14.20, 12.71. **HRMS** calculated for $C_{14}H_{16}O_3$ (M-Na): 255.1002 found: 255.1003.

3.5.5 General Procedure for the Photocatalytic Reactions

PHOTOCATALYTIC HOMOLITIC AROMATIC SUBSTITUTION (HAS)

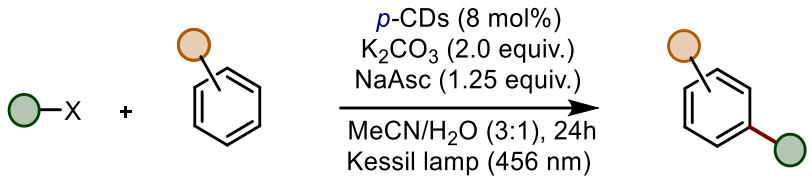

4 1.25 equiv. **5** 1 equiv. **6**

A 10 mL Schlenk tube was charged with the arene **5** (0.2 mmol) and the acceptor **4** (0.25 mmol, 1.25 equiv). The potassium carbonate was added along with sodium ascorbate (K_2CO_3 55.2, NaAscorbate: 79.24 mg). Finally, 400 mL of MeCN/H_2O 3:1 solution was added as solvent. The reaction mixture was thoroughly degassed via 3 cycles of freeze-pump-thaw, and the vessel was refilled with argon and placed under light irradiation for 24 h (λ = 456 nm). The temperature was kept at around 30 °C by using a fan. The reaction was then quenched with an aqueous solution of 0.1 M HCl. The mixture was extracted with ethyl acetate (3 × 10 mL). The volatiles were removed in vacuo and the residue was purified by column chromatography (eluent: cyclohexane/ethyl acetate) to give the afford the products **6a-g**.

Characterization Data

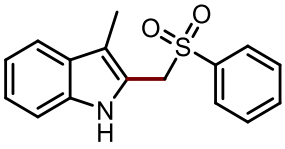

6a

3-Methyl-2-((phenylsulfonyl)methyl)-1H-indole (6a)

Prepared according to the general procedure using 3-methylindole (0.2 mmol, 26.2 mg) and **4a** (0.25 mmol, 70 mg). The final product **6a** was obtained as a white solid (NMR yield:>99%).

^{1}H-NMR (499 MHz, $CDCl_3$) δ 8.50 (s, 1H), 7.63 – 7.56 (m, 3H), 7.45 – 7.38 (m, 3H), 7.36 (d, J = 8.2 Hz, 1H), 7.25 – 7.18 (m, 1H), 7.14 – 7.06 (m, 1H), 4.50 (s, 2H), 1.70 (s, 3H). The characterization data matched the reported one.[56]

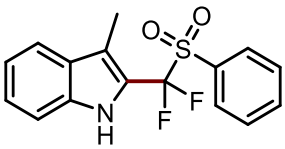

6b

2-(Difluoro(phenylsulfonyl)methyl)-3-methyl-1H-indole (6b)

Prepared according to the general procedure using 3-methylindole (0.2 mmol, 26.2 mg) and **4b** (0.25 mmol, 80 mg). The final product **6b** was obtained as white solid (NMR yield: 74%).

^{1}H-NMR (499 MHz, $CDCl_3$) δ 8.46 (s, 1H), 7.96 (d, J = 7.7 Hz, 2H), 7.77 (ddd, J = 8.7, 2.4, 1.2 Hz, 1H), 7.65 – 7.58 (m, 3H), 7.39 (d, J = 8.3 Hz, 1H), 7.36 – 7.30 (m, 1H), 7.18 (ddd, J = 7.0, 5.4, 0.9 Hz, 1H), 2.31 (t, J = 2.5 Hz, 3H). **^{19}F-NMR (376 MHz, $CDCl_3$)** δ -99.73, -99.73. The characterization data matched the reported one.[56]

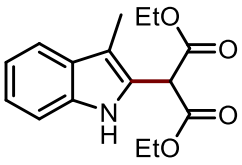

6c

3-Methyl-2-diethylmalonate-1H-indole (6c)

Prepared according to the general procedure using 3-methylindole (0.2 mmol, 26.2 mg) and bromo diethylacetate (0.25 mmol, 52.7 mg, 33 mL). The final product **6c** was obtained as a white solid (NMR yield: 68%).

^{1}H-NMR (400 MHz, $CDCl_3$) δ 7.57 – 7.51 (m, 1H), 7.35 (dt, J = 8.1, 0.9 Hz, 1H), 7.19 (ddd, J = 8.2, 7.1, 1.2 Hz, 1H), 7.10 (ddd, J = 8.0, 7.1, 1.0 Hz, 1H), 4.97 (s, 1H), 4.34 – 4.13 (m, 4H), 2.31 (s, 3H), 1.29 (t, J = 7.1 Hz, 6H). The characterization data matched the reported one.[57]

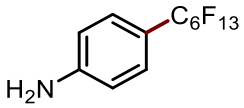

6d

4-(perfluorohexyl)aniline (6d)

Prepared according to the general procedure using aniline (0.2 mmol, 18.6 mg, 18 mL) and perfluorohexyl iodide (0.25 mmol, 111.2 mg, 54 mL). The final product **6d** was obtained as deliquescent white solid (NMR yield: 30%).

^{1}H-NMR (400 MHz, $CDCl_3$) δ 7.34 (d, J = 8.6 Hz, 1H), 6.71 (d, J = 8.7 Hz, 1H). **^{19}F-NMR (376 MHz, $CDCl_3$)** δ -80.83, -109.52, -121.58, -122.09, -122.87, -126.16. The characterization data matched the reported one.[58]

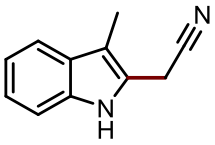

6e

3-methyl-2-(prop-2-yn-1-yl)-1H-indole (6e)

Prepared according to the general procedure using 3-methylindole (0.2 mmol, 26.2 mg) and bromoacetonitrile (0.25 mmol, 30 mg, 18 mL).

^{1}H-NMR (400 MHz, $CDCl_3$) δ 7.53 (d, J = 7.8 Hz, 1H), 7.33 (d, J = 8.1 Hz, 1H), 7.25 – 7.19 (m, 1H), 7.18 – 7.09 (m, 1H), 3.87 (s, 2H), 2.27 (s, 3H). The characterization data matched the reported one.[58]

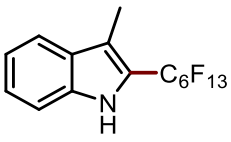

6f

3-methyl-2-(perfluorohexyl)-1H-indole (6f)

Prepared according to the general procedure using 3-methylindole (0.2 mmol, 26.2 mg) and perfluorohexyl iodide

(0.25 mmol, 111.2 mg, 54 mL). The final product **6f** was obtained as white solid (NMR yield: 65%).

^{1}H-NMR (400 MHz, $CDCl_3$) δ 8.18 (s, 1H), 7.66 (d, *J* = 8.1 Hz, 1H), 7.40 (d, *J* = 8.3 Hz, 1H), 7.34 (t, *J* = 7.6 Hz, 1H), 7.20 (ddd, *J* = 8.0, 6.9, 1.0 Hz, 1H), 2.44 (t, *J* = 2.2 Hz, 3H). **^{19}F-NMR (376 MHz, $CDCl_3$)** δ -80.78 (tt, *J* = 10.0, 2.5 Hz), -108.64 (t, *J* = 14.0 Hz), -121.90 (s), -122.17 (s), -122.78 (s), -125.66 – -126.28 (m). The characterization data matched the reported one.[59]

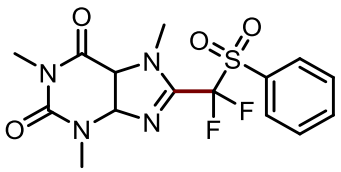

6g

1,3,7-trimethyl-8-(perfluorohexyl)-3,7-dihydro-1H-purine-2,6-dione (6g)

Prepared according to the general procedure using caffeine (0.2 mmol, 26.2 mg) and **4b** (0.25 mmol, 111.2 mg, 54 mL). The final product **6g** was obtained as white solid (NMR yield: 65%).

^{1}H-NMR (400 MHz, $CDCl_3$) δ 8.03 (d, J = 7.7 Hz, 2H), 7.88 – 7.78 (m, 1H), 7.67 (t, J = 7.9 Hz, 2H), 4.30 (t, J = 1.8 Hz, 3H), 3.55 (s, 3H), 3.43 (s, 3H). **^{19}F-NMR (376 MHz, $CDCl_3$)** δ -100.79. The characterization data matched the reported one.[60]

PHOTOCATALYTIC [3+2] CYCLOADDITION REACTION

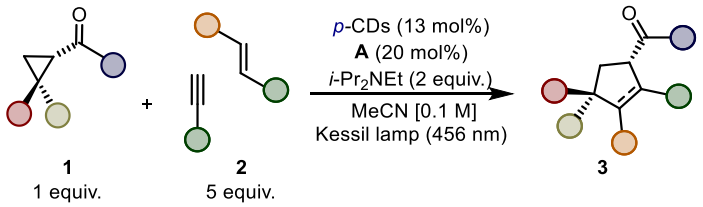

A 10 mL Schlenk tube was charged with cyclopropane **1** (0.1 mmol), unsaturated compounds **2** (0.5 mmol, 5.0 equiv.), *p*-CDs (6 mg, 14 mol%), Schreiner thiourea **A** (0.02 mmol, 20 mol%) and *i*-Pr_2NEt (0.2 mmol, 2 equiv.). Acetonitrile was then added to the Schlenk tube (1 mL, 0.1 M). The reaction mixture was thoroughly degassed via 3 cycles of freeze-pump-thaw, and the vessel was refilled with argon, placed under light irradiation for 8-30h (λ = 456 nm). The temperature was kept at around 30°C by using a fan. The reaction mixture was filtered on cotton with Et_2O. The volatiles were removed in vacuo and the residue was purified by column chromatography to give the corresponding products **3**.

tert-butyl 3-benzoyl-4-phenylcyclopentane-1-carboxylate (3a)

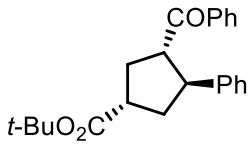

3a

3a was synthesized according to the general procedure from **1a** (24.6 mg, 0.1 mmol) and styrene (58 µL, 0.5 mmol). The reaction was complete after 8 h. The crude product was purified by column chromatography (7:3, Hexane/Et_2O) to give 34 mg (99% yield) of cycloadduct as two separable diastereomers (5:2 d.r.).

Major: **^{1}H-NMR (499 MHz, $CDCl_3$)** δ 7.86 – 7.75 (m, 2H), 7.49 (t, *J* = 7.4 Hz, 1H), 7.37 (t, *J* = 7.8 Hz, 2H), 7.30 – 7.22 (m, 4H), 7.18 – 7.09 (m, 1H), 3.83 (dq, *J* = 34.4, 8.9 Hz, 2H), 3.09 (ddd, *J* = 17.2, 8.4, 6.0 Hz, 1H), 2.57 – 2.45 (m, 2H), 2.28 – 2.18 (m, 1H), 2.13 (dt, *J* = 13.3, 9.0 Hz, 1H), 1.46 (s, *J* = 4.1 Hz, 9H). **^{13}C-NMR (126 MHz, $CDCl_3$)** δ 200.70, 174.35, 143.89, 137.02, 133.05, 128.67, 128.61, 128.53, 127.45, 126.56, 80.66, 54.89, 47.30, 44.62, 37.45, 35.50, 28.22. **HRMS** calculated for $C_{23}H_{26}O_3$ (M-Na): 373.1773 found: 373.1774. The characterization of the compound matches with the data reported in the literature.[45]

Minor: **^{1}H-NMR (499 MHz, $CDCl_3$)** δ 7.59 (dd, *J* = 8.3, 1.2 Hz, 2H), 7.43 – 7.36 (m, 1H), 7.30 – 7.24 (m, 2H), 7.05 – 6.95 (m, 5H), 4.18 (td, *J* = 9.1, 7.3 Hz, 1H), 3.65 (dd, *J* = 17.3, 9.6 Hz, 1H), 2.94 (tt, *J* = 10.5, 8.0 Hz, 1H), 2.65 (ddd, *J* = 13.2, 10.6, 8.7 Hz, 1H), 2.50 – 2.33 (m, 2H), 2.30 – 2.19 (m, 1H), 1.51 (s, 9H). **^{13}C-NMR (101 MHz, $CDCl_3$)** δ 201.07, 174.26, 141.35, 137.95, 132.46, 128.45, 128.24, 128.14, 128.00, 126.49, 80.56, 51.20, 48.99, 44.67, 36.74, 32.52, 28.30. **HRMS** calculated for $C_{23}H_{26}O_3$ (M-Na): 373.1775 found: 373.1774. The characterization of the compound matches with the data reported in the literature.[61]

tert-butyl 3-nicotinoyl-4-phenylcyclopentane-1-carboxylate (3b)

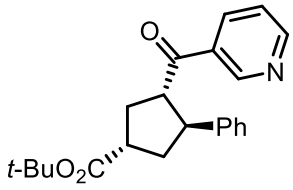

3b

3b was synthesized according to the general procedure from **1b** (24.7 mg, 0.1 mmol) and styrene (58 µL, 0.5 mmol). The reaction was complete after 8 h. The crude product was purified by column chromatography (8:2, Hexane/Et_2O) to give 20 mg (58% yield) of cycloadduct as two separable diastereomers (3:2 d.r.).

Major: **^{1}H-NMR (400 MHz, $CDCl_3$)** δ 8.96 (d, *J* = 1.7 Hz, 1H), 8.69 (dd, *J* = 4.8, 1.7 Hz, 1H), 8.08 – 8.02 (m, 1H), 7.36 – 7.28 (m, 1H), 7.25 – 7.19 (m, 4H), 7.19 – 7.10 (m, 1H), 3.78 (dq, *J* = 26.2, 9.0 Hz, 2H), 3.11 (ddd, *J* = 17.2, 8.1, 5.6 Hz, 1H), 2.57 – 2.44 (m, 2H), 2.33 – 2.23 (m, 1H), 2.16 (dt, *J*

= 13.2, 9.1 Hz, 1H), 1.46 (s, *J* = 4.9 Hz, 9H). The characterization of the compound matches with the data reported in the literature.[45]

Minor: **^{1}H-NMR (400 MHz, $CDCl_3$)** δ 8.81 (d, *J* = 1.3 Hz, 1H), 8.57 (d, *J* = 3.5 Hz, 1H), 7.74 (dt, *J* = 7.9, 1.9 Hz, 1H), 7.15 (dd, *J* = 7.9, 4.8 Hz, 1H), 7.05 – 6.92 (m, 5H), 4.15 (dd, *J* = 17.5, 7.8 Hz, 1H), 3.67 (td, *J* = 10.1, 7.4 Hz, 1H), 2.95 (ddd, *J* = 15.7, 10.5, 7.9 Hz, 1H), 2.68 (ddd, *J* = 13.3, 10.4, 8.1 Hz, 1H), 2.51 – 2.33 (m, 2H), 2.27 (dt, *J* = 13.8, 7.7 Hz, 1H), 1.51 (s, 9H). **^{13}C-NMR (101 MHz, $CDCl_3$)** δ 200.25, 174.01, 152.74, 149.52, 140.70, 135.29, 133.19, 128.37, 128.23, 126.82, 123.28, 80.67, 51.47, 49.11, 44.61, 36.60, 32.11, 28.30. **HRMS** calculated for $C_{22}H_{25}NO_3$ (M-H): 352.1906 found: 352.1907.

tert-butyl 3-(4-fluorobenzoyl)-4-phenylcyclopentane-1-carboxylate (3c)

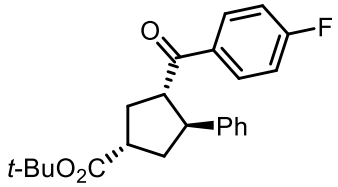

3c

3c was synthesized according to the general procedure from **1c** (26.4 mg, 0.1 mmol) and styrene (58 µL, 0.5 mmol). The reaction was complete after 22 h. The crude product was purified by column chromatography (7:3, Cyhex/DCM) to give 29 mg (97% yield) of cycloadduct as two separable diastereomers (4:1 d.r.)

Major: **^{1}H-NMR (499 MHz, $CDCl_3$)** 7.60 (2H, dd, *J*=8.8, 5.4 Hz), 7.05 – 6.96 (5H, m), 6.92 (2H, t, *J*=8.6 Hz), 4.12 (1H, dd, *J*=16.9, 8.3 Hz), 3.63 (1H, td, *J*=9.8, 7.5 Hz), 2.93 (1H, tt, *J*=10.5, 8.0 Hz), 2.64 (1H, ddd, *J*=13.3, 10.4, 8.4 Hz), 2.40 (2H, qt, *J*=13.1, 9.0 Hz), 2.23 (1H, dt, *J*=13.7, 7.6 Hz), 1.51 (9H, s). **^{19}F-NMR (376 MHz, $CDCl_3$)** δ -106.40.**^{13}C-NMR (126 MHz, $CDCl_3$)** δ 199.59, 174.19, 165.32 (d, *J*=253.7 Hz), 141.10, 134.37 (d, *J*=3.2 Hz), 130.69 (d, *J*=9.3 Hz), 128.41, 128.07, 126.63, 115.28 (d, *J*=21.9 Hz), 51.05, 49.14, 44.62, 36.64, 32.45, 28.30. **HRMS** calculated for $C_{23}H_{25}FO_3$ (M-Na): 391.1680 found: 391.1680.

Minor: **^{1}H-NMR(499 MHz, $CDCl_3$)** 7.80 (2H, ddd, *J*=8.4, 5.3, 2.6 Hz), 7.25 – 7.19 (4H, m), 7.18 – 7.12 (1H, m), 7.04 – 6.98 (2H, m), 3.84 – 3.69 (2H, m), 3.13 – 3.05 (1H, m), 2.56 – 2.42 (2H, m), 2.25 (1H, ddd, *J*=13.3, 9.4, 8.2 Hz), 2.13 (1H, dt, *J*=13.2, 9.0 Hz), 1.46 (9H, s). **^{19}F-NMR (376 MHz, $CDCl_3$)** δ -105.53. **^{13}C-NMR (126 MHz, $CDCl_3$)** δ 199.18, 174.30, 165.75 (d, *J*=254.7 Hz), 143.73, 133.42 (d, *J*=2.9 Hz), 131.14 (d, *J*=9.3 Hz), 128.71, 127.41, 126.66, 115.66 (d, *J*=21.9 Hz), 80.69, 54.88, 47.58, 44.56, 37.48, 35.27, 28.20. **HRMS** calculated for $C_{23}H_{25}FO_3$ (M-Na): 369.1860 found: 369.1861.

ethyl 3-benzoyl-1-methyl-4-phenylcyclopentane-1-carboxylate (3d)

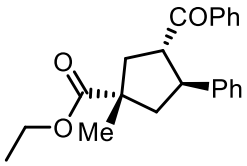

3d

3d was synthesized according to the general procedure from **1d** (22.2 mg, 0.1 mmol) and styrene (58 µL, 0.5 mmol). The reaction was completed after 27 h. The crude product was purified by column chromatography (7:3, Hexane/Et_2O) to give 27 mg (88% yield) of cycloadduct as diastereomers (5:1 d.r.).

Major: **^{1}H-NMR (400 MHz, $CDCl_3$)** δ 7.82 (d, *J* = 7.7 Hz, 2H), 7.56 – 7.44 (m, 1H), 7.39 (t, *J* = 7.8 Hz, 2H), 7.26 (q, 4H), 7.16 (td, *J* = 5.8, 2.8 Hz, 1H), 4.18 (q, *J* = 7.1 Hz, 2H), 4.02 – 3.81 (m, 2H), 2.83 (dd, *J* = 13.0, 7.2 Hz, 1H), 2.58 (dd, *J* = 13.3, 7.9 Hz, 1H), 2.17 (dd, *J* = 13.4, 9.0 Hz, 1H), 1.85 (dd, *J* = 13.1, 11.2 Hz, 1H), 1.47 (s, 3H), 1.28 (t, *J* = 7.1 Hz, 3H).**^{13}C-NMR (126 MHz, $CDCl_3$)** δ 200.61, 177.34, 143.21, 137.00, 132.99, 128.60, 128.59, 128.52, 127.47, 126.55, 61.02, 54.09, 49.30, 47.31, 45.96, 42.85, 26.34, 14.30. **HRMS** calculated for $C_{22}H_{24}O_3$ (M-H): 337.1798 found: 337.1798.

Major+minor: **^{1}H-NMR (400 MHz, $CDCl_3$)** δ 7.83 – 7.76 (2H major, m), 7.56 – 7.46 (1H major + 2H minor, m), 7.42 – 7.34 (2H major + 1H minor, m), 7.25 – 7.20 (4H major + 2H minor, m), 7.19 – 7.11 (1H major, m), 7.01 – 6.89 (5H minor, m), 4.35 (1H minor, dt, *J*=10.2, 8.0 Hz), 4.22 (2H minor, q, *J*=7.1 Hz), 4.18 (2H major, q, *J* = 7.1 Hz), 3.95 (1H major, td, *J*=9.6, 7.6 Hz), 3.85 (1H major, ddd, *J*=11.8, 9.5, 7.4 Hz), 3.80 – 3.72 (1H minor, m), 2.80 (1H major, ddd, *J*=13.1, 7.4, 1.1 Hz), 2.67 (1H minor, ddd, *J*=13.1, 7.2, 1.8 Hz), 2.59 (1H major, ddd, *J*=13.4, 7.7, 1.1 Hz), 2.31 (1H minor, dd, *J*=13.5, 8.4 Hz), 2.17 (1H major, dd, *J*=13.4, 9.6 Hz), 2.06 (1H minor, dd, *J*=13.1, 11.2 Hz), 1.86 (1H major, dd, *J*=13.1, 11.7 Hz), 1.53 (3H minor, s), 1.47 (3H major, s), 1.32 (3H minor, t, *J*=7.1 Hz), 1.28 (3H major, t, *J* = 7.1 Hz). **^{13}C NMR (126 MHz, $CDCl_3$)** δ 201.16, 200.61 (major), 178.14, 177.34 (major), 143.21 (major), 142.83, 138.16, 137.00 (major), 133.17, 132.99 (major), 128.79, 128.60 (major), 128.59 (major), 128.63, 128.52 (major), 128.43, 128.38, 128.15, 127.95, 127.47 (major), 126.55 (major), 126.39, 61.54, 61.02 (major), 54.80, 54.09 (major), 50.72, 49.65, 49.30 (major), 48.83, 47.31 (major), 47.20, 45.96 (major), 45.73, 45.01, 43.40, 42.85 (major), 26.34 (major), 25.64, 14.30 (major), 14.39.

3-(tert-butyl) 1-ethyl 5-benzoyl-1-methylcyclopentane-1,3-dicarboxylate (3e)

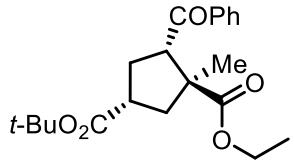

3e

3e was synthesized according to the general procedure from **1a** (24.6 mg, 0.1 mmol) and ethyl methacrylate (55 µL, 0.5 mmol). The reaction was complete after 22 h. The crude product was purified by column chromatography (8:2, Hexane/Et_2O) to give 28 mg (79% yield) of cycloadduct as two separable diastereomers (2:1 d.r.).

Major: **^{1}H-NMR (400 MHz, $CDCl_3$)** δ 7.96 – 7.87 (m, 2H), 7.55 (t, *J* = 7.3 Hz, 1H), 7.45 (q, *J* = 7.7 Hz, 2H), 4.41 (dd, *J* = 10.0, 7.1 Hz, 1H), 4.08 (dd, *J* = 14.1, 7.0 Hz, 2H), 2.97 – 2.84 (m, 1H), 2.57 – 2.42 (m, 2H), 2.24 – 2.11 (m, 1H), 1.94 (dt, *J* = 16.0, 8.0 Hz, 1H), 1.47 (s, 9H), 1.17 (t, *J* = 7.1 Hz, 3H), 1.08 (s, 3H).**^{13}C-NMR (101 MHz, $CDCl_3$)** δ 200.63, 177.13, 173.88, 138.01, 133.23, 128.72, 128.54, 80.63, 61.36, 52.29, 51.55, 43.38, 42.43, 32.55, 28.24, 20.94, 14.15. **HRMS** calculated for $C_{21}H_{28}O_5$ (M-Na): 383.1829 found: 383.1829.

Minor: **^{1}H-NMR (400 MHz, $CDCl_3$)** δ 7.96 – 7.84 (m, 2H), 7.55 (t, *J* = 7.4 Hz, 1H), 7.45 (t, *J* = 7.8 Hz, 2H), 4.03 (q, *J* = 7.2 Hz, 2H), 3.77 (dd, *J* = 9.1, 5.3 Hz, 1H), 2.98 (dd, *J* = 17.0, 9.0 Hz, 1H), 2.71 (dd, *J* = 13.1, 10.3 Hz, 1H), 2.54 – 2.37 (m, 1H), 2.36 – 2.24 (m, 1H), 2.05 (dd, *J* = 13.1, 8.5 Hz, 1H), 1.40 (s, 9H), 1.37 (s, 3H), 1.09 (t, *J* = 7.1 Hz, 3H). **^{13}C-NMR (101 MHz, $CDCl_3$)** δ 200.81, 176.23, 173.89, 136.69, 132.98, 128.64, 128.61, 80.62, 60.59, 54.89, 52.84, 42.87, 39.24, 32.00, 28.15, 25.65, 14.10. **HRMS** calculated for $C_{21}H_{28}O_5$ (M-Na): 383.1829 found: 383.1828.

tert-butyl 3-benzoyl-4-(p-tolyl)cyclopentane-1-carboxylate (3f)

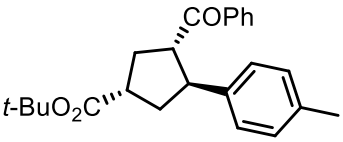

3f

3f was synthesized according to the general procedure from **1a** (24.6 mg, 0.1 mmol) and 4-methylstyrene (59 µL, 0.5 mmol). The reaction was complete after 22 h. The crude product was purified by column chromatography (7:3, Hexane/Et_2O) to give 36 mg (99% yield) of cycloadduct as three separable diastereomers (4:1:1 d.r.).

Major: **^{1}H-NMR (499 MHz, $CDCl_3$)** δ 7.86 – 7.77 (m, 2H), 7.49 (t, *J* = 7.4 Hz, 1H), 7.37 (t, *J* = 7.7 Hz, 2H), 7.12 (d, *J* = 8.0 Hz, 2H), 7.05 (d, *J* = 8.0 Hz, 2H), 3.85 (dd, *J* = 17.7, 8.9 Hz, 1H), 3.76 (q, *J* = 8.7 Hz, 1H), 3.13 – 3.02 (m, 1H), 2.49 (m, 2H), 2.27 (s, 3H), 2.19 (m, 1H), 2.14 – 2.05 (m, 1H), 1.45 (s, 9H). **^{13}C-NMR (126 MHz, $CDCl_3$)** δ 200.84, 174.44, 140.82, 137.03, 136.06, 133.03, 129.33, 128.60, 128.54, 127.29, 80.64, 54.84, 46.90, 44.57, 37.53, 35.45, 28.21, 21.10. **HRMS** calculated for $C_{24}H_{28}O_3$ (M-Na): 387.1932 found: 387.1931. The characterization of the compound matches with the data reported in the literature.[45]

Minor a: **^{1}H-NMR (499 MHz, $CDCl_3$)** δ 7.82 (dd, *J* = 8.3, 1.2 Hz, 2H), 7.52 – 7.46 (m, 1H), 7.40 – 7.34 (m, 2H), 7.15 (d, *J* = 8.1 Hz, 2H), 7.05 (d, *J* = 7.9 Hz, 2H), 3.96 (dd, *J* = 17.2, 9.5 Hz, 1H), 3.70 – 3.58 (m, 1H), 3.04 – 2.93 (m, 1H), 2.55 – 2.43 (m, 2H), 2.27 (s, 3H), 2.15 – 2.03 (m, 2H), 1.48 (s, *J* = 3.9 Hz, 9H). **^{13}C-NMR (126 MHz, $CDCl_3$)** δ 201.68, 175.11, 140.02, 136.81, 136.21, 133.17, 129.33, 128.65, 128.64, 127.41, 80.62, 53.85, 48.10, 44.34, 39.07, 34.97, 28.27, 21.11. **HRMS** calculated for $C_{24}H_{28}O_3$ (M-Na): 387.1931 found: 387.1931.

Minor b: **^{1}H-NMR (499 MHz, $CDCl_3$)** δ 7.59 (t, *J* = 12.6 Hz, 2H), 7.41 (t, *J* = 7.4 Hz, 1H), 7.31 – 7.24 (m, 2H), 6.84 (dd, *J* = 19.5, 8.1 Hz, 4H), 4.14 (td, *J* = 9.1, 7.3 Hz, 1H), 3.63 (dd, *J* = 17.2, 9.4 Hz, 1H), 2.92 (tt, *J* = 10.5, 8.0 Hz, 1H), 2.63 (ddd, *J* = 13.2, 10.6, 9.0 Hz, 1H), 2.49 – 2.32 (m, 2H), 2.21 (dt, *J* = 21.3, 7.4 Hz, 1H), 2.15 (s, 3H), 1.50 (s, 9H). **^{13}C-NMR (126 MHz, $CDCl_3$)** δ 201.10, 174.33, 138.30, 137.98, 135.93, 132.42, 128.68, 128.29, 128.22, 128.19, 80.52, 51.31,48.59, 44.63, 36.79, 32.48, 28.30, 21.01. **HRMS** calculated for $C_{24}H_{28}O_3$ (M-Na): 387.1930 found: 387.1931. The characterization of the compound matches with the data reported in the literature.[61]

tert-butyl 4-benzoyl-2-methyl-3-phenylcyclopentane-1-carboxylate (3g)

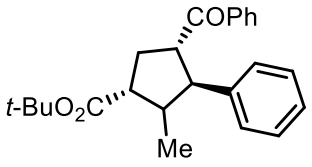

3g

3g was synthesized according to the general procedure from **1a** (24.6 mg, 0.1 mmol) and trans-β-Methylstyrene (59 µL, 0.5 mmol). The reaction was complete after 27 h. The crude product was purified by column chromatography (8:2, Hexane/Et_2O) to give 15 mg (28% yield) of cycloadduct as two diastereomers (3:1 d.r.).

Major: **^{1}H-NMR (499 MHz, $CDCl_3$)** δ 7.79 (d, *J* = 7.5 Hz, 2H), 7.46 (t, *J* = 7.4 Hz, 1H), 7.35 (t, *J* = 7.8 Hz, 2H), 7.27 – 7.22 (m, 4H), 7.15 (dt, *J* = 8.5, 2.3 Hz, 1H), 3.84 (q, *J* = 9.5 Hz, 1H), 3.46 (t, *J*=10.1 Hz, 1H), 3.09 (dd, *J* = 15.5, 8.1 Hz, 1H), 2.61 – 2.50 (m, 1H), 2.47 – 2.37 (m, 1H), 2.29 (ddd, *J* = 13.5, 9.5, 6.5 Hz, 1H), 1.47 (s, 9H), 0.99 (d, *J* = 6.9 Hz, 3H). **^{13}C-NMR (126 MHz, $CDCl_3$)** δ 200.28, 173.63, 142.71, 137.15, 132.83, 128.64, 128.51, 128.50, 127.95, 126.64, 80.85, 54.58, 54.28, 48.85, 44.63, 33.36, 28.36, 15.09. **HRMS** calculated for $C_{24}H_{28}O_3$ (M-Na): 387.1932 found: 387.1931.

Major + minor: **^{1}H-NMR (499 MHz, $CDCl_3$)** δ 7.81 – 7.77 (2H major, m), 7.54 – 7.51 (2H minor, m), 7.46 (1H major, ddt, *J*=7.8, 7.0, 1.3 Hz), 7.37 – 7.31 (2H major + 1H minor, m), 7.29 – 7.19 (4H major + 2H minor, m), 7.15 (1H major, ddt, *J*=6.8, 5.8, 2.2 Hz), 7.03 – 6.97 (2H minor, m), 6.97 – 6.92 (3H minor, m), 4.21 (1H minor, ddd, *J*=10.6, 8.8, 7.3 Hz), 3.85 (1H major, q, *J*=9.5 Hz), 3.46 (1H major, t, *J*=10.1 Hz), 3.16 – 3.02 (1H major + 1H minor, m), 2.73 (1H minor, ddd, *J*=13.0, 11.1, 8.8 Hz), 2.66 – 2.38 (2H major + 2H minor, m), 2.29 (1H major, ddd, *J* = 13.5, 9.5,

6.5 Hz), 2.21 (1H minor, dt, *J*=13.0, 7.4 Hz), 1.52 (9H minor, s), 1.48 (9H major, s), 1.04 (3H minor, d, *J*=6.5 Hz), 1.00 (3H major, d, *J*=6.9 Hz). **^{13}C-NMR (126 MHz, $CDCl_3$)** δ 201.40, 200.29 (major), 173.96, 173.63 (major), 142.70 (major), 140.37, 137.96, 137.14 (major), 132.83 (major), 132.28, 129.02, 128.63 (major), 128.50 (major), 128.49 (major), 128.12, 128.06, 128.00, 127.95 (major), 126.64 (major), 126.52, 80.84 (major), 80.50, 57.26, 54.56 (major), 54.26 (major), 52.45, 50.25, 48.83 (major), 45.28, 44.61 (major), 33.34 (major), 32.42, 28.34 (major), 28.27, 17.81, 15.07 (major).

tert-butyl 4-benzoyl-3-phenylcyclopent-2-ene-1-carboxylate (3h)

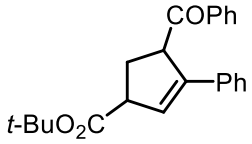

3h

3h was synthesized according to the general procedure from **1a** (24.6 mg, 0.1 mmol) and phenylacetylene (59 µL, 0.5 mmol). The reaction was complete after 20 h. The crude product was purified by column chromatography (8:2, Hexane/Et_2O) to give 33 mg (95% yield) of cycloadduct as two separable diastereomers (2:1 d.r.)

Major: **^{1}H-NMR (499 MHz, $CDCl_3$)** 8.05 (2H, dd, *J*=8.3, 1.4 Hz), 7.65 – 7.58 (1H, m), 7.51 (2H, t, *J*=7.7 Hz), 7.32 – 7.29 (2H, m), 7.25 – 7.16 (3H, m), 6.40 (1H, dd, *J*=2.5, 1.4 Hz), 5.12 (1H, ddt, *J*=10.1, 3.9, 1.8 Hz), 3.79 (1H, ddt, *J*=8.8, 6.5, 2.4 Hz), 2.82 (1H, ddd, *J*=13.3, 10.1, 6.5 Hz), 2.29 (1H, ddd, *J*=13.2, 8.6, 4.2 Hz), 1.48 (9H, s). **^{13}C-NMR (126 MHz, $CDCl_3$)** δ 200.77, 173.05, 143.92, 136.41, 135.00, 133.48, 128.94, 128.81, 128.57, 128.24, 127.83, 126.20, 81.14, 53.06, 51.56, 32.87, 28.28. The characterization of the compound matches with the data reported in the literature.[62]

Minor: **^{1}H-NMR (499 MHz, $CDCl_3$)** 8.04 (2H, dd, *J*=8.3, 1.3 Hz), 7.61 – 7.54 (1H, m), 7.48 (2H, t, *J*=7.7 Hz), 7.32 (2H, dd, *J*=7.2, 1.6 Hz), 7.25 – 7.15 (3H, m), 6.40 (1H, dd, *J*=2.9, 1.6 Hz), 4.90 (1H, ddt, *J*=9.8, 5.9, 1.7 Hz), 3.73 (1H, ddd, *J*=8.4, 4.8, 2.0 Hz), 2.75 (1H, ddd, *J*=13.4, 10.0, 9.0 Hz), 2.49 (1H, dt, *J*=13.4, 5.6 Hz), 1.45 (9H, s).**^{13}C-NMR (126 MHz, $CDCl_3$)** δ 199.94, 172.03, 143.68, 136.41, 135.18, 133.20, 128.86, 128.80, 128.55, 127.81, 127.75, 126.22, 81.16, 53.48, 51.59, 32.38, 28.20. The characterization of the compound matches with the data reported in the literature.[62]

tert-butyl 4-benzoyl-3-(4-(tert-butyl)phenyl)cyclopent-2-ene-1-carboxylate (3i)

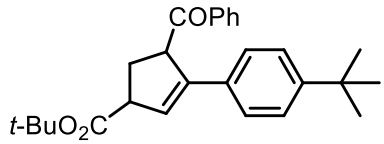

3i

3i was synthesized according to the general procedure from **1a** (24.6 mg, 0.1 mmol) and 4-tert-Butylphenylacetylene (90 µL, 0.5 mmol). The reaction was complete after 22 h. The crude product was purified by column chromatography (8:2, Hexane/Et_2O) to give 40 mg (94% yield) of cycloadduct as two separable diastereomers (5:2 d.r.).

Major: **^{1}H-NMR (101 MHz, $CDCl_3$)** δ 8.09 – 8.01 (2H, m), 7.58 (1H, t, *J*=7.3 Hz), 7.48 (2H, t, *J*=7.6 Hz), 7.25 (4H, m), 6.37 (1H, dd, *J*=2.9, 1.6 Hz), 4.88 (1H, dd, *J*=10.1, 5.6 Hz), 3.71 (1H, t, *J*=4.5 Hz), 2.72 (1H, dt, *J*=13.4, 9.6 Hz), 2.47 (1H, dt, *J*=13.4, 5.4 Hz), 1.55 (9H, s), 1.44 (9H, s). **^{13}C-NMR (101 MHz, $CDCl_3$)** δ 200.06, 172.16, 150.74, 143.38, 136.48, 133.17, 132.24, 128.90, 128.80, 126.96, 125.93, 125.51, 81.10, 53.43, 51.60, 32.35, 31.36, 31.08, 28.19. **HRMS** calculated for $C_{27}H_{32}O_3$ (M-H): 427.2244 found: 427.2244.

Minor **^{1}H-NMR (499 MHz, $CDCl_3$)** δ 8.10 – 8.02 (2H, m), 7.65 – 7.58 (1H, m), 7.51 (2H, t, *J*=7.7 Hz), 7.24 (4H, m), 6.36 (1H, dd, *J*=2.5, 1.4 Hz), 5.18 – 5.05 (1H, m), 3.78 (1H, ddt, *J*=8.7, 6.4, 2.3 Hz), 2.81 (1H, ddd, *J*=13.3, 10.1, 6.4 Hz), 2.26 (1H, ddd, *J*=13.1, 8.6, 4.3 Hz), 1.47 (9H, s), 1.26 (9H, s). **^{13}C-NMR (126 MHz, $CDCl_3$)** δ 200.96, 173.12, 150.82, 143.67, 136.47, 133.44, 132.10, 128.93, 128.82, 127.41, 125.88, 125.51, 81.06, 53.01, 51.57, 34.66, 32.85, 31.36, 28.28. **HRMS** calculated for $C_{27}H_{32}O_3$ (M-H): 427.2244 found: 427.2243.

tert-butyl 3-(4-aminophenyl)-4-benzoylcyclopent-2-ene-1-carboxylate (3j)

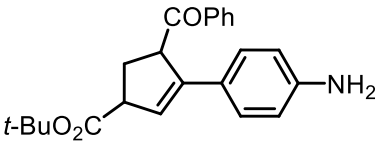

3j

3j was synthesized according to the general procedure from **1a** (24.6 mg, 0.1 mmol) and 4-ethynylaniline (58 mg, 0.5 mmol). The reaction was complete after 48 h. The crude product was purified by column chromatography (8:2, Cyhex/EtOAc) to give 33 mg (93% yield) as two cycloadducts (5:2 d.r.).

Major: **^{1}H-NMR (400 MHz, $CDCl_3$)** δ 8.05 – 7.98 (m, 2H), 7.63 – 7.52 (m, 1H), 7.52 – 7.40 (m, 2H), 7.12 (d, *J* = 8.6 Hz, 2H), 6.56 (d, *J* = 8.6 Hz, 2H), 6.21 (dd, *J* = 2.9, 1.6 Hz, 1H), 4.81 (ddt, *J* = 10.0, 5.9, 1.8 Hz, 1H), 3.70 (dddd, *J* = 8.6, 5.0, 2.9, 1.8 Hz, 1H), 2.71 (ddd, *J* = 13.5, 10.0, 9.1 Hz, 1H), 2.46 (dt, *J* = 13.4, 5.6 Hz, 1H), 1.43 (s, 9H).**^{13}C-NMR (126 MHz, $CDCl_3$)** δ 200.30, 172.41, 146.09, 143.40, 136.50, 133.06, 128.90, 128.73, 127.41, 124.31, 115.08, 113.86, 80.96, 53.84, 51.52, 32.35, 28.20. **HRMS** calculated for $C_{23}H_{25}NO_3$ (M-Na): 386.1727 found: 386.1729.

Minor + major: **^{1}H-NMR (400 MHz, $CDCl_3$)** δ 8.04 (m, 4H (2Hmajor + 2Hminor)), 7.62 – 7.53 (m, 2H(1Hmajor + 1Hminor)), 7.53 – 7.41 (m, 4H (2Hmajor + 2Hminor)), 7.11 (dd, *J* = 8.5, 6.2 Hz, 4H (2Hmajor + 2Hminor)), 6.58 – 6.50 (m, 4H (2Hmajor + 2Hminor)), 6.21 (dt, *J* = 3.0, 1.4 Hz, 2H (1Hmajor + 1Hminor)), 5.04 (ddt, *J* = 10.3, 3.9, 1.7 Hz, 1H minor), 3.75 (ddt, *J* = 8.8, 6.5, 2.3 Hz, 1H minor), 3.07 (broad, 2H), 2.85 – 2.64 (m, 2H (1Hmajor + 1Hminor)), 2.46 (m, 2H (1Hmajor + 1Hminor)), 2.25 (ddd, *J* = 13.3, 8.5, 4.1 Hz, 1H), 1.47 (s, 9H).**^{13}C-NMR (101 MHz, $CDCl_3$)** δ 200.35, 200.30 (major) 172.43, 172.41 (major), 146.09 (major), 145.70, 143.56, 143.40 (major), 136.53, 136.50 (major), 133.37, 133.06 (major), 128.90 (major), 128.80, 128.73 (major), 127.41 (major), 127.39, 126.08, 124.31(major), 124.84, 115.31, 115.08 (major), 113.86 (major), 110.15, 80.96 (major), 80.95, 53.84 (major), 53.12, 51.52 (major), 51.45, 32.84, 32.35 (major), 28.27, 28.20 (major).

ethyl 4-benzoyl-1-methyl-3-phenylcyclopent-2-ene-1-carboxylate (3k)

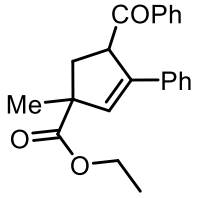

3k

3k was synthesized according to the general procedure from **1d** (22.2 mg, 0.1 mmol) and phenylacetylene (59 mg, 0.5 mmol). The reaction was complete after 24 h. The crude product was purified by column chromatography (9:1, Hexane/Et_2O) to give 23 mg (52% yield) of cycloadduct as two separable diastereomers (2:1 d.r.).

Major: **^{1}H-NMR (400 MHz, $CDCl_3$)** δ 8.03 (dt, *J* = 8.5, 1.7 Hz, 2H), 7.61 – 7.55 (m, 1H), 7.51 – 7.45 (m, 2H), 7.35 – 7.29 (m, 2H), 7.25 – 7.16 (m, 3H), 6.39 (d, *J* = 1.5 Hz, 1H), 4.97 (ddd, *J* = 9.8, 5.0, 1.4 Hz, 1H), 4.13 (dtt, *J* = 10.8, 7.3, 3.7 Hz, 2H), 2.81 (dd, *J* = 13.4, 5.1 Hz, 1H), 2.38 (dd, *J* = 13.4, 9.9 Hz, 1H), 1.47 (s, 3H), 1.24 (t, *J* = 7.1 Hz, 3H). **^{13}C-NMR (101 MHz, $CDCl_3$)** δ 199.87, 175.55, 141.86, 136.41, 135.02, 133.40, 133.23, 128.82, 128.58, 127.84, 126.22, 110.15, 61.11, 55.54, 53.13, 40.45, 25.95, 14.27. **HRMS** calculated for $C_{22}H_{22}O_3$ (M-Na): 357.1461 found: 357.1461.

Minor: **^{1}H-NMR (400 MHz, $CDCl_3$)** δ 8.09 – 8.01 (m, 2H), 7.64 – 7.59 (m, 1H), 7.56 – 7.43 (m, 3H), 7.32 – 7.27 (m, 2H), 7.26 – 7.17 (m, 2H), 6.36 (d, *J* = 1.6 Hz, 1H), 5.12 (ddd, *J* = 10.2, 5.3, 1.6 Hz, 1H), 4.26 – 4.07 (m, 2H), 3.20 (dd, *J* = 13.4, 10.2 Hz, 1H), 1.94 (dd, *J* = 13.4, 5.4 Hz, 1H), 1.45 (s, 3H), 1.28 (t, *J* = 7.1 Hz, 3H). **^{13}C-NMR (101 MHz, $CDCl_3$)** δ 201.13, 176.23, 142.36, 136.42, 135.00, 133.49, 133.26, 128.83, 128.57, 127.83, 126.22, 110.15, 61.15, 56.18, 53.01, 40.40, 25.49, 14.38. **HRMS** calculated for $C_{22}H_{22}O_3$ (M-Na): 357.1461 found: 357.1462.

tert-butyl 4-(4-fluorobenzoyl)-3-phenylcyclopent-2-ene-1-carboxylate (3l)

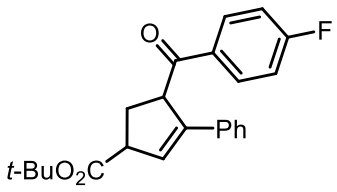

3l

3l was synthesized according to the general procedure from **1c** (26.4 mg, 0.1 mmol) and phenylacetylene (90 µL, 0.5 mmol). The reaction was complete after 30 h. The crude product was purified by column chromatography (9:1, Hexane/Et_2O) to give 28 mg (78% yield) of cycloadduct as two separable diastereomers (5:2 d.r.).

Major: **^{1}H-NMR (499 MHz, $CDCl_3$)** δ 8.09 – 8.03 (2H, m), 7.32 – 7.28 (2H, m), 7.25 – 7.22 (2H, m), 7.21 – 7.17 (1H, m), 7.17 – 7.10 (2H, m), 6.39 (1H, dd, *J*=2.9, 1.7 Hz), 4.83 (1H, ddt, *J*=9.6, 5.8, 1.8 Hz), 3.73 (1H, dddd, *J*=8.8, 5.1, 2.8, 1.8 Hz), 2.74 (1H, ddd, *J*=13.4, 10.0, 9.0 Hz), 2.48 (1H, dt, *J*=13.4, 5.6 Hz), 1.45 (9H, s). **^{19}F NMR (376 MHz, $CDCl_3$)** δ -105.31. **^{13}C-NMR (126 MHz, $CDCl_3$)** δ 198.43, 172.00, 165.86 (d, *J* = 254.9 Hz), 143.63, 135.09, 132.74 (d, *J* = 3.0 Hz), 131.52 (d, *J* = 9.3 Hz), 128.60, 128.01, 127.86, 126.19, 115.90 (d, *J* = 21.8 Hz), 81.24, 53.73, 51.57, 32.28, 28.21. **HRMS** calculated for $C_{23}H_{23}FO_3$ (M-Na): 389.1523 found: 389.1522.

Minor: **^{1}H-NMR (499 MHz, $CDCl_3$)** δ 8.10 – 8.04 (2H, m), 7.31 – 7.22 (5H, m), 7.22 – 7.14 (2H, m), 6.39 (1H, dd, *J*=2.5, 1.4 Hz), 5.10 – 5.05 (1H, m), 3.79 (1H, ddt, *J*=8.7, 6.4, 2.4 Hz), 2.82 (1H, ddd, *J*=13.4, 10.1, 6.4 Hz), 2.27 (1H, ddd, *J*=13.2, 8.6, 4.3 Hz), 1.48 (9H, s). **^{19}F NMR (376 MHz, $CDCl_3$)** δ -104.77. **^{13}C-NMR (126 MHz, $CDCl_3$)** δ 199.22, 172.95, 166.06 (d, *J* = 255.6 Hz), 143.80, 134.94, 132.81 (d, *J* = 3.0 Hz), 131.46 (d, *J* = 9.3 Hz), 128.60, 128.33, 127.91, 126.16, 116.07 (d, *J* = 21.9 Hz), 81.22, 53.05, 51.56, 32.80, 28.28. **HRMS** calculated for $C_{23}H_{23}FO_3$ (M-Na): 389.1523 found: 389.1524.

tert-butyl-4-nicotinoyl-3-phenylcyclopent-2-ene-1-carboxylate (3m)

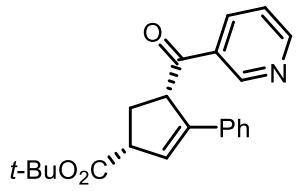

3m

3m was synthesized according to the general procedure from **1b** (24.7 mg, 0.1 mmol) and phenylacetylene (59 mg, 0.5 mmol). The reaction was complete after 24 h. The crude product was purified by column chromatography (2:1, Cyclohex/EtOAc) to give 25 mg (66% yield) of cycloadduct as two separable diastereomers (1:1 d.r.).

Major: **^{1}H-NMR (400 MHz, $CDCl_3$)** δ 9.28 (s, 1H), 8.84 (s, 1H), 8.38 (d, *J* = 7.8 Hz, 1H), 7.58 – 7.52 (m, 1H), 7.31 – 7.18 (m, 5H), 6.41 (dd, *J* = 2.5, 1.4 Hz, 1H), 5.07 (d, *J* = 9.9 Hz, 1H), 3.81 (dd, *J* = 8.7, 6.4 Hz, 1H), 2.86 (ddd, *J* = 13.5, 10.1, 6.5 Hz, 1H), 2.31 (ddd, *J* = 13.2, 8.6, 4.3 Hz, 1H), 1.48 (s, 9H).**^{13}C-NMR (126 MHz, $CDCl_3$)** δ 199.64, 172.73, 153.50, 149.84, 143.36, 136.48, 134.75, 131.83, 128.72, 128.68, 128.06, 126.20, 124.17, 81.36, 53.70, 51.58, 32.44, 28.25. **HRMS** calculated for $C_{22}H_{23}NO_3$ (M-H): 350.1751 found: 350.1752.

Minor: **^{1}H-NMR (400 MHz, $CDCl_3$)** δ 9.26 (1H, s), 8.79 (1H, m), 8.34 (1H, dt, *J*=8.0, 1.9 Hz), 7.47 (1H, m), 7.33 – 7.20 (5H, m), 6.40 (1H, dd, *J*=2.9, 1.6 Hz), 4.84 (1H, ddt, *J*=9.9, 5.4, 1.6 Hz), 3.82 – 3.72 (1H, m), 2.77 (1H, ddd, *J*=13.5, 10.2, 9.1 Hz), 2.52 (1H, dt, *J*=13.5, 5.3 Hz), 1.45 (9H, s). **^{13}C NMR (126 MHz, $CDCl_3$)** δ 198.90, 171.86, 153.57, 150.21, 143.16, 136.32, 134.91, 131.66, 128.69, 128.21, 128.01, 126.21, 123.87, 81.38, 54.22, 51.59, 31.93, 28.20. **HRMS** calculated for $C_{22}H_{23}NO_3$ (M-Na): 372.1570 found: 372.1572.

3.5.6 Screening of the Conditions of the [3+2] Cycloaddition

We compared different bases for the [3+2] cycloaddition between **1a** and **2a**. DIPEA significantly outperformed all the bases tested.

*Table 3.2 Comparative study on different bases in the [3+2] cycloaddition reaction between **2a** and **1a**. The general procedure of this reaction is described in Section 3.5.5*

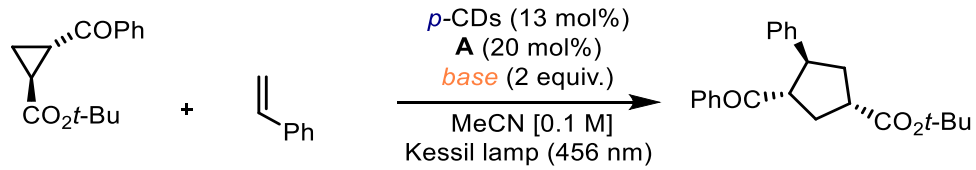

1a 0.1 mmol | **2a** 0.5 mmol | **3a**

Entry	Base	Yield [%][a]
1	DIPEA	98
2	DABCO	0
3	TMG	<5
4[b]	NaO*t*-Bu	9
5[b]	Cs_2CO_3	0

[a] ^{1}H-NMR based yields using 1,3,5-trimethoxybenzene as the internal standard. [b] Reactions performed without **A** because NaO*t*-Bu and Cs_2CO_3 are strong bases.

We performed the [3+2] cycloaddition between **1a** and **2a** using chiral thioureas $\mathbf{A_1}$ and $\mathbf{A_2}$. Unfortunately, no satisfying results in terms of enantiomeric excess (ee) were obtained.

*Table 3.3 Study of enantioselective version of [3+2] cycloaddition reaction between **2a** and **1a** using enantiopure thioureas. The general procedure of this reaction is described in Section 3.5.5*

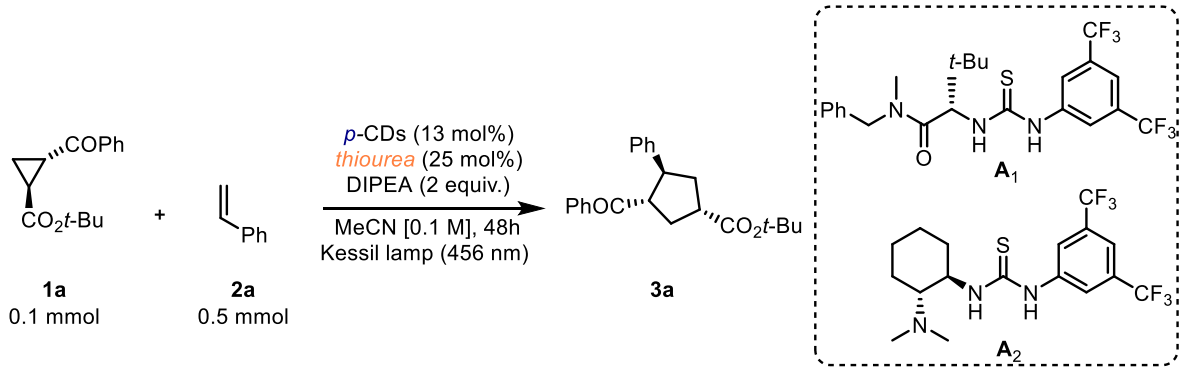

Entry	Enantiopure thiourea	Yield [%][a]	ee [%][b]
1	(*S*)-2-[[3,5-Bis(trifluoromethyl)phenyl]thioureido]-*N*-benzyl-*N*-3,3-trimethylbutanamide (**A**$_1$)	68	7
2	1-[3,5-bis(trifluoromethyl)phenyl]-3-[(1*R*,2*R*)-(-)-2-(dimethylamino)cyclohexyl]thiourea (**A**$_2$)	55	0

[a] The yield was determined by ^{1}H-NMR analysis on the crude mixture using 1,3,5-trimethoxybenzene as internal standard. [b] The enantiomeric excess was evaluated on the crude mixture. HPLC: Phenomenex AD-H; n-hexane/iPrOH, 10 to 20% iPrOH, flow-rate 0.75 mL/min; t_1 = 11.6 min; t_2 = 14.4 min.

3.5.7 Experiment for the Monitoring of the Catalytic Adduct

To confirm the formation of the complex between *p*-CDs + **A** + DIPEA in the initial 2h of the [3+2] cycloaddition, we performed the reaction between **1a** and **2a** as follows. First (*i*) *p*-CDs, **A** and DIPEA were mixed in acetonitrile for 2 h to assess the formation of the photocatalytic system under 456 nm irradiation, then (*ii*) the reactants (**1a** and **2a**) were added to this solution which was stirred for additional 6 h under light irradiation. This experiment almost provided a quantitative yield of product **3a.**

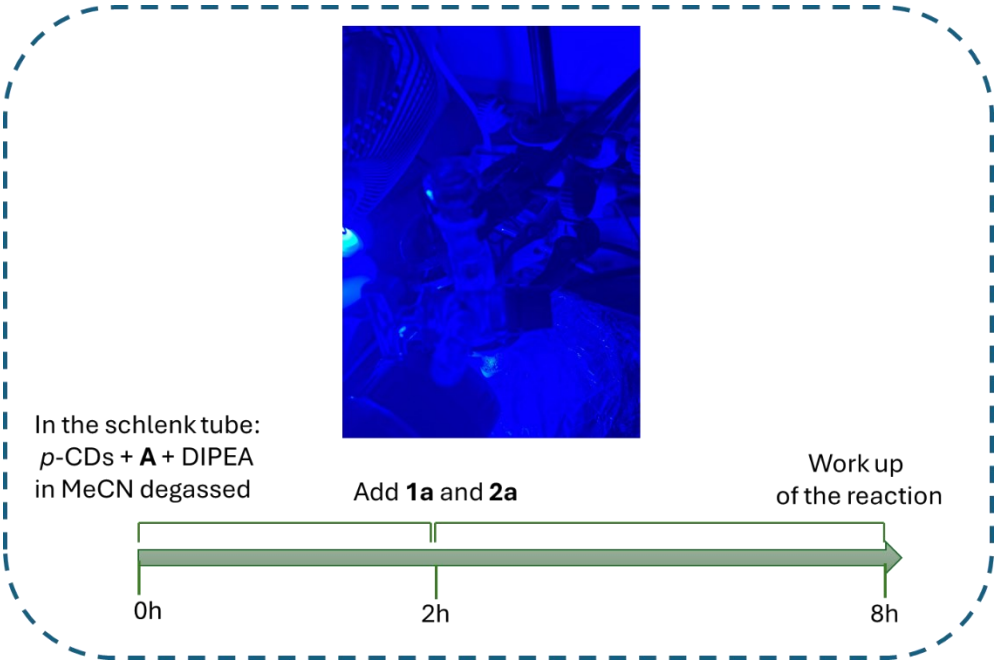

*Figure 3.19 Illustration of the experiment about the formation of the catalytic adduct (p-CDs + **A** + DIPEA)*

3.5.8 Stern-Volmer Study

To further demonstrate the feasibility of a SET between the catalytic system (composed by *p*-CDs, **A** and DIPEA) and cyclopropane **1a**, a series of Stern-Volmer quenching studies were performed in acetonitrile. The emission spectrum, depicted in Figure 3.15b, was obtained upon excitation at 456 nm, and showed a decreased intensity when **1a** was added. The fluorescence quenching turned out to be linear in the range 25 - 80 mM. The Stern-Volmer constant was derived by the slope of equation below, which is 4.66 M^{-1}.

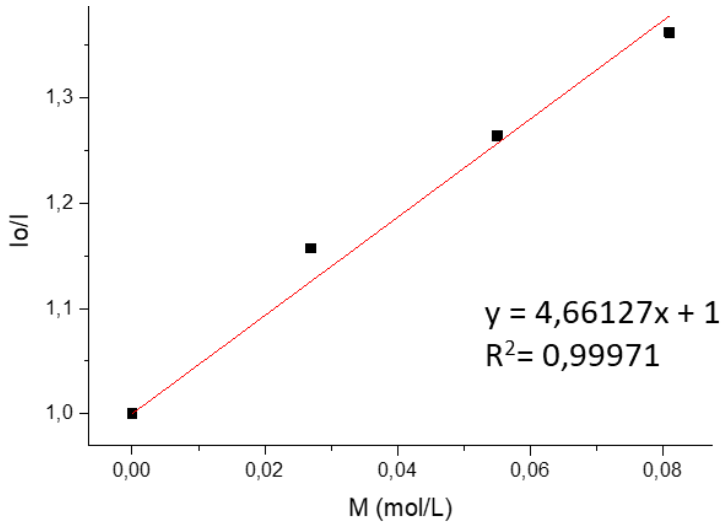

Figure 3.20 Stern-Volmer study

3.5.9 Uv-Vis Experiments

Absorption spectra for [3+2] cycloaddition

We carried out UV-Vis experiments of each component (**1a**, **2a**, *p*-CDs, DIPEA, **A**) of the [3+2] cycloaddition and their relative mixtures in acetonitrile. Within these experiments, the possible formation of an EDA complex between the components of the reaction in acetonitrile was excluded. A red-shifted absorption was observed only for the solution containing *p*-CDs + **A** + DIPEA overtime.

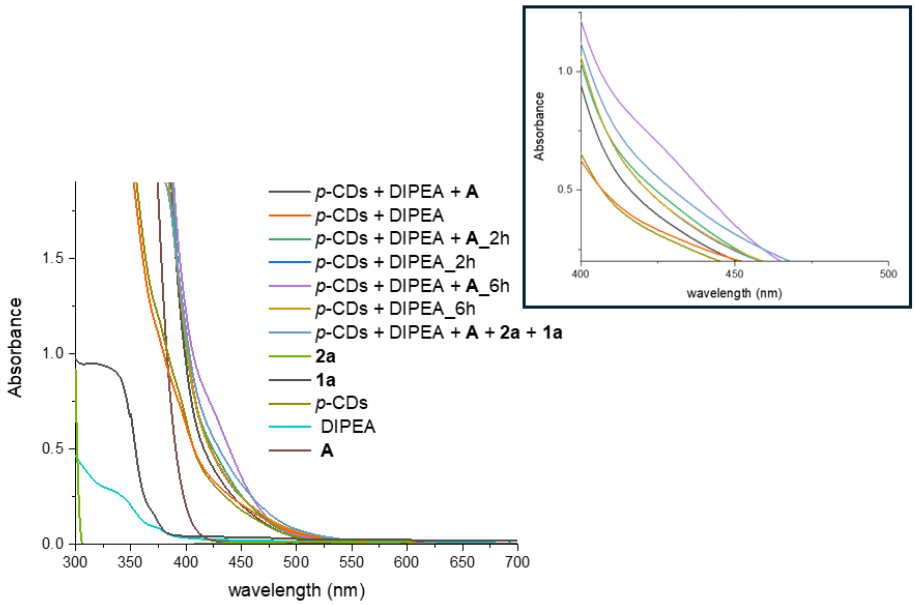

*Figure 3.21 Optical absorption spectra recorded in MeCN: [DIPEA] = 100 mM; [**A**] = 10 mM; [p-CDs] = 50 mM; [**1a**] = 50 mM; [**2a**] = 250 mM.*

Absorption spectra with molecular phenol

To test the behaviour of molecular phenols in the presence of DIPEA and **A** in acetonitrile, we carried out UV-Vis experiments using the 4-*tert*-butylphenol as molecular phenol. We recorded absorption spectra of the components (4-*tert*-butylphenol red line, **A** black line, DIPEA blue line) and the mixture containing 4-*tert*-butylphenol + **A** + DIPEA. A red-shifted absorption was observed after 2 h (violet line) and after 5 h (yellow line) for the solution containing 4-*tert*-butylphenol + **A** + DIPEA.

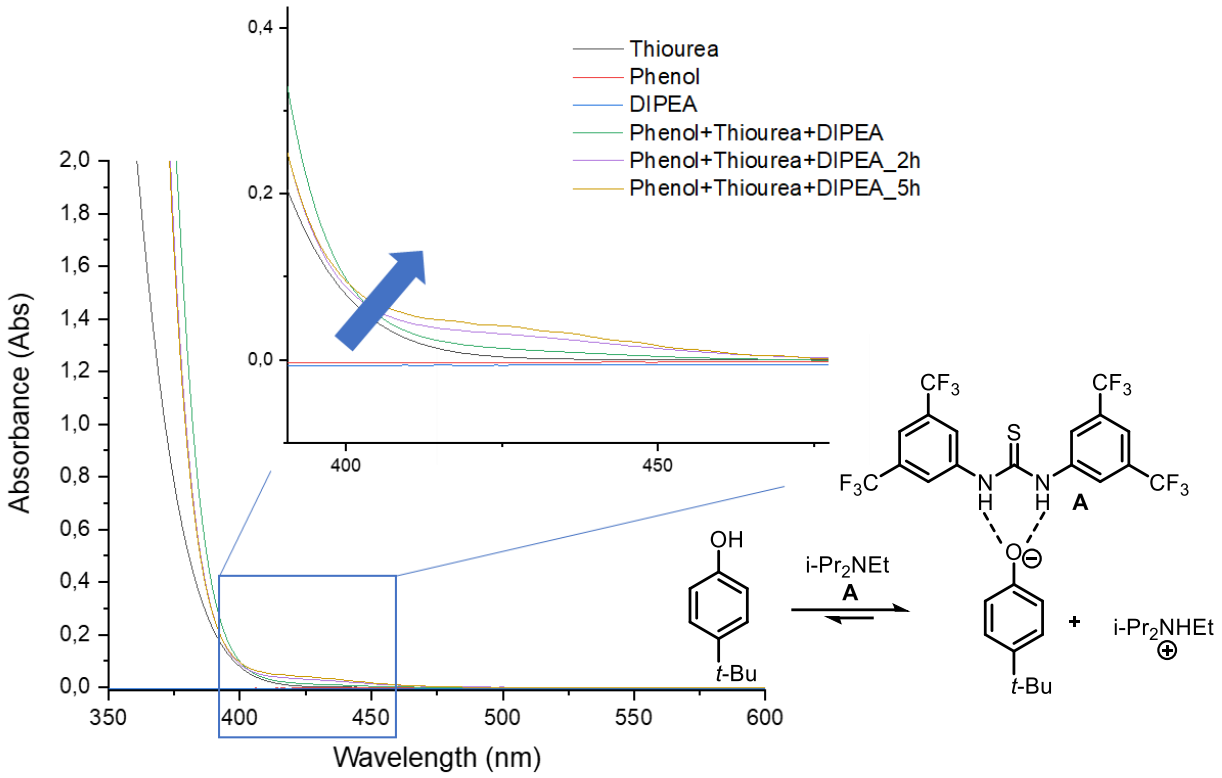

*Figure 3.22 Optical absorption spectra recorded in MeCN: [DIPEA] = 100 mM; [**A**] = 10 mM; [phenol] = 50 mM;*

3.5.10 Recycling Experiments

To perform the recycling tests of the [3+2] cycloaddition, we selected the substrates cyclopropane **1a** and styrene **2a** under the optimised reaction conditions for 16h. In Figure 3.23 is illustrated the procedure for the recyclability. The reaction was set into a Schlenk tube with the standard ground socket to allow direct attachment to rotavapor equipment. After the reaction, the reaction vessel was exposed to reduce pressure to remove the solvent mixture. Then, the crude was diluted with diethyl ether (2 mL) and sonicated to induce the precipitation of the *p*-CDs. The solids were allowed to decant and then the supernatant, containing the molecular species, were removed always maintaining the catalyst in the same reaction vessel. The extraction and *p*-CDs washing step were repeated for three times. Subsequently, the recovered *p*-CDs were dried and reused in subsequent cycloaddition up to three cycles in the same reaction vessel. Meanwhile, the combined organic phases were reunited and dried over Na_2SO_4. The crude was diluted with deuterated solvent and spiked with the internal standard to allow for NMR analysis. At the end of each cycle, the vessel was again exposed to reduce pressure to eliminate diethyl ether and then it was re-charged with the precursors and 50% of the quantity of base and **A**. The catalyst was recycled 3 times. At the end of

the recycling process, the catalyst was collected by filtration over a PTFE membrane and washed with 0.1M HCl. After this, 21% of the mass of *p*-CDs could be collected. Remarkably, the recyclability tests were performed two times to have a deviation. The performances in terms of reaction yield and diastereoselectivity are depicted in the histogram below (Figure 3.24). In addition, the UV-Vis and fluorescence analysis of the *p*-CDs, after 3 recycling cycles, were carried out (Figure 3.25).

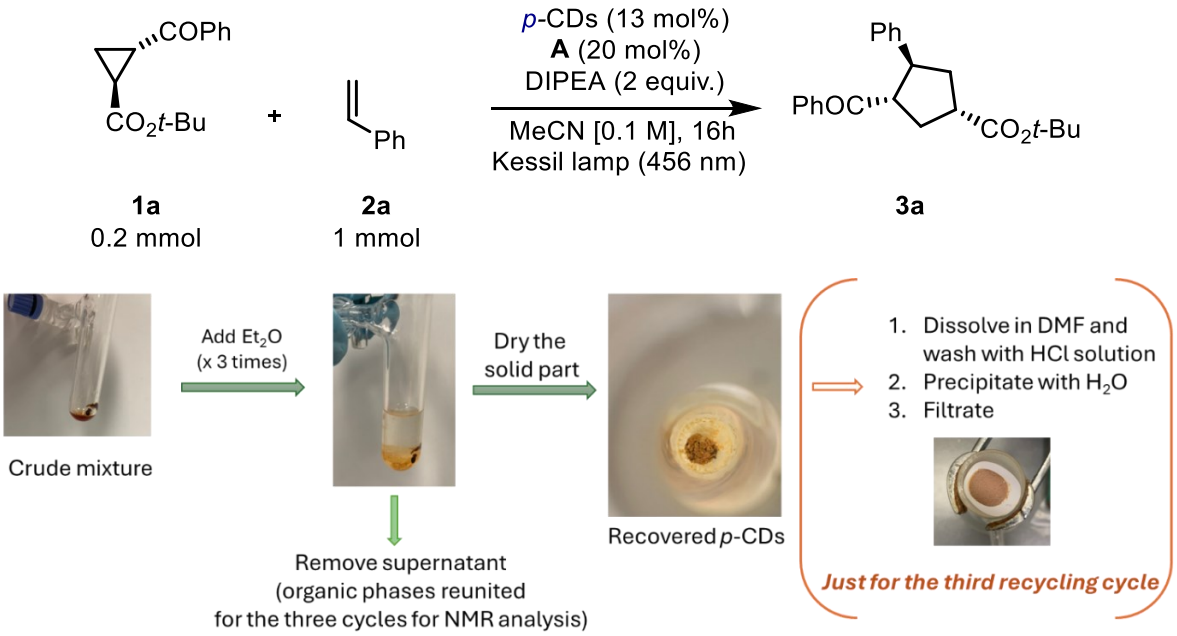

Figure 3.23 Illustration of the recycling test procedure.

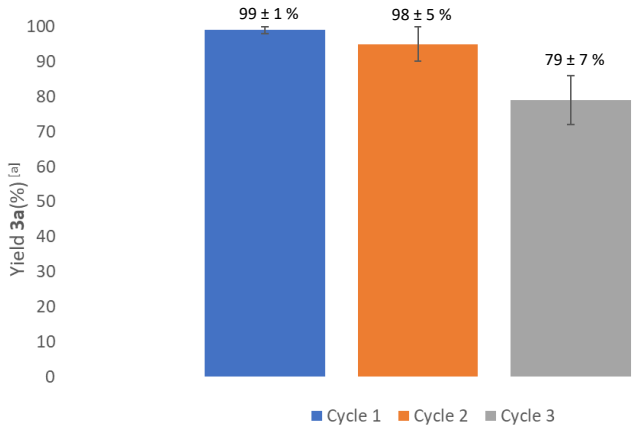

*Figure 3.24 Histogram of the reaction yields of **3a** after each recycling cycle.*

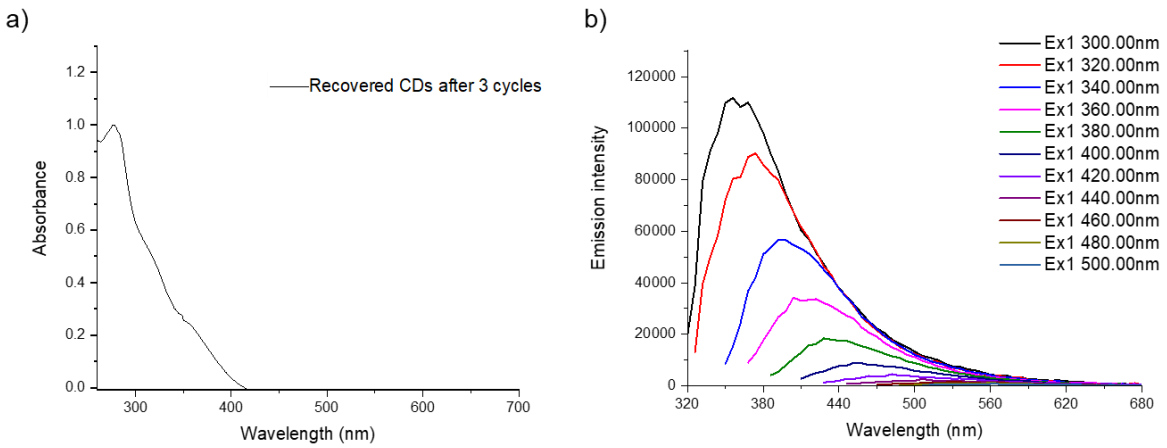

Figure 3.25 Optical absorption and fluorescence of recovered p-CDs after 3 recycling cycles

3.6 References Chapter 3

(1) Sbacchi, M.; Mamone, M.; Morbiato, L.; Gobbo, P.; Filippini, G.; Prato, M. Shining Light on Carbon Dots: New Opportunities in Photocatalysis. *ChemCatChem* **2023**, *15* (16), e202300667. https://doi.org/10.1002/cctc.202300667.

(2) Constantin, T.; Zanini, M.; Regni, A.; Sheikh, N. S.; Juliá, F.; Leonori, D. Aminoalkyl Radicals as Halogen-Atom Transfer Agents for Activation of Alkyl and Aryl Halides. *Science* **2020**, *367* (6481), 1021–1026. https://doi.org/10.1126/science.aba2419.

(3) Nagib, D. A.; MacMillan, D. W. C. Trifluoromethylation of Arenes and Heteroarenes by Means of Photoredox Catalysis. *Nature* **2011**, *480* (7376), 224–228. https://doi.org/10.1038/nature10647.

(4) Gandolfo, E.; Tang, X.; Raha Roy, S.; Melchiorre, P. Photochemical Asymmetric Nickel-Catalyzed Acyl Cross-Coupling. *Angewandte Chemie* **2019**, *131* (47), 17010–17014. https://doi.org/10.1002/ange.201910168.

(5) Prier, C. K.; Rankic, D. A.; MacMillan, D. W. C. Visible Light Photoredox Catalysis with Transition Metal Complexes: Applications in Organic Synthesis. *Chem. Rev.* **2013**, *113* (7), 5322–5363. https://doi.org/10.1021/cr300503r.

(6) Nguyen, J. D.; D'Amato, E. M.; Narayanam, J. M. R.; Stephenson, C. R. J. Engaging Unactivated Alkyl, Alkenyl and Aryl Iodides in Visible-Light-Mediated Free Radical Reactions. *Nature Chem* **2012**, *4* (10), 854–859. https://doi.org/10.1038/nchem.1452.

(7) Du, J.; Yoon, T. P. Crossed Intermolecular [2+2] Cycloadditions of Acyclic Enones via Visible Light Photocatalysis. *J. Am. Chem. Soc.* **2009**, *131* (41), 14604–14605. https://doi.org/10.1021/ja903732v.

(8) Quintavalla, A.; Carboni, D.; Lombardo, M. Green Metrics and Sustainability in Photocatalysis. *ChemCatChem* **2024**, *16* (14), e202301225. https://doi.org/10.1002/cctc.202301225.

(9) Vega-Peñaloza, A.; Mateos, J.; Companyó, X.; Escudero-Casao, M.; Dell'Amico, L. A Rational Approach to Organo-Photocatalysis: Novel Designs and Structure-Property Relationships. *Angew. Chem. Int. Ed.* **2021**, *60* (3), 1082–1097. https://doi.org/10.1002/anie.202006416.

(10) Siano, G.; Crespi, S.; Bonesi, S. M. Direct Irradiation of Phenol and Para-Substituted Phenols with a Laser Pulse (266 Nm) in Homogeneous and Micro-Heterogeneous Media. A Time-Resolved Spectroscopy Study. *J. Org. Chem.* **2020**, *85* (21), 14012–14025. https://doi.org/10.1021/acs.joc.0c02031.

(11) Klikar, M.; Solanke, P.; Tydlitát, J.; Bureš, F. Alphabet-Inspired Design of (Hetero)Aromatic Push–Pull Chromophores. *The Chemical Record* **2016**, *16* (4), 1886–1905. https://doi.org/10.1002/tcr.201600032.

(12) Ichino, T.; Fessenden, R. W. Energy Requirements for Inverted CIDEP in Reactions between Eaq- or Radical Anions and Phenoxyl Radicals. *J. Phys. Chem. A* **2003**, *107* (44), 9257–9268. https://doi.org/10.1021/jp030153j.

(13) Bartolomei, B.; Gentile, G.; Rosso, C.; Filippini, G.; Prato, M. Turning the Light on Phenols: New Opportunities in Organic Synthesis. *Chemistry – A European Journal* **2021**, *27* (65), 16062–16070. https://doi.org/10.1002/chem.202102276.

(14) Kobayashi, S.; Higashimura, H. Oxidative Polymerization of Phenols Revisited. *Progress in Polymer Science* **2003**, *28* (6), 1015–1048. https://doi.org/10.1016/S0079-6700(03)00014-5.

(15) Buzzetti, L.; Crisenza, G. E. M.; Melchiorre, P. Mechanistic Studies in Photocatalysis. *Angew Chem Int Ed* **2019**, *58* (12), 3730–3747. https://doi.org/10.1002/anie.201809984.

(16) Schmalzbauer, M.; Ghosh, I.; König, B. Utilising Excited State Organic Anions for Photoredox Catalysis: Activation of (Hetero)Aryl Chlorides by Visible Light-Absorbing 9-Anthrolate Anions. *Faraday Discuss.* **2019**, *215* (0), 364–378. https://doi.org/10.1039/C8FD00176F.

(17) Schmalzbauer, M.; Svejstrup, T. D.; Fricke, F.; Brandt, P.; Johansson, M. J.; Bergonzini, G.; König, B. Redox-Neutral Photocatalytic C−H Carboxylation of Arenes and Styrenes with CO2. *Chem* **2020**, *6* (10), 2658–2672. https://doi.org/10.1016/j.chempr.2020.08.022.

(18) Liang, K.; Liu, Q.; Shen, L.; Li, X.; Wei, D.; Zheng, L.; Xia, C. Intermolecular Oxyarylation of Olefins with Aryl Halides and TEMPOH Catalyzed by the Phenolate Anion under Visible Light. *Chem. Sci.* **2020**, *11* (27), 6996–7002. https://doi.org/10.1039/D0SC02160A.

(19) Rosso, C.; Cuadros, S.; Barison, G.; Costa, P.; Kurbasic, M.; Bonchio, M.; Prato, M.; Dell'Amico, L.; Filippini, G. Unveiling the Synthetic Potential of Substituted Phenols as Fully Recyclable Organophotoredox Catalysts for the Iodosulfonylation of Olefins. *ACS Catal.* **2022**, *12* (8), 4290–4295. https://doi.org/10.1021/acscatal.2c00565.

(20) Kang, Z.; Lee, S.-T. Carbon Dots: Advances in Nanocarbon Applications. *Nanoscale* **2019**, *11* (41), 19214–19224. https://doi.org/10.1039/C9NR05647E.

(21) Zdražil, L.; Cadranel, A.; Medved', M.; Otyepka, M.; Zbořil, R.; Guldi, D. M. Designing Carbon Dots for Enhanced Photo-Catalysis: Challenges and Opportunities. *Chem* **2024**, *10* (9), 2700–2723. https://doi.org/10.1016/j.chempr.2024.07.018.

(22) Gao, J.; Zhu, M.; Huang, H.; Liu, Y.; Kang, Z. Advances, Challenges and Promises of Carbon Dots. *Inorganic Chemistry Frontiers* **2017**, *4* (12), 1963–1986. https://doi.org/10.1039/C7QI00614D.

(23) Đorđević, L.; Arcudi, F.; Cacioppo, M.; Prato, M. A Multifunctional Chemical Toolbox to Engineer Carbon Dots for Biomedical and Energy Applications. *Nat. Nanotechnol.* **2022**, *17* (2), 112–130. https://doi.org/10.1038/s41565-021-01051-7.

(24) Bartolomei, B.; Dosso, J.; Prato, M. New Trends in Nonconventional Carbon Dot Synthesis. *Trends in Chemistry* **2021**, *3* (11), 943–953. https://doi.org/10.1016/j.trechm.2021.09.003.

(25) Jeon, I.-Y.; Noh, H.-J.; Baek, J.-B. Nitrogen-Doped Carbon Nanomaterials: Synthesis, Characteristics and Applications. *Chemistry – An Asian Journal* **2020**, *15* (15), 2282–2293. https://doi.org/10.1002/asia.201901318.

(26) Hu, C.; Li, M.; Qiu, J.; Sun, Y.-P. Design and Fabrication of Carbon Dots for Energy Conversion and Storage. *Chemical Society Reviews* **2019**, *48* (8), 2315–2337. https://doi.org/10.1039/C8CS00750K.

(27) Yu, Y.; Zeng, Q.; Tao, S.; Xia, C.; Liu, C.; Liu, P.; Yang, B. Carbon Dots Based Photoinduced Reactions: Advances and Perspective. *Advanced Science* **2023**, *10* (12), 2207621. https://doi.org/10.1002/advs.202207621.

(28) Cardo, L.; Martínez-Parra, L.; Cesco, M.; Echeverría-Beistegui, B. M.; Martínez-Moro, M.; Herrero-Álvarez, N.; Cabrerizo, M.-B.; Carregal-Romero, S.; Ramos-Cabrer, P.; Ruiz-Cabello, J.; Prato, M. Luminescent Carbon Nanodots Doped with Gadolinium (III): Purification Criteria, Chemical and Biological Characterization of a New Dual Fluorescence/MR Imaging Agent. *Small* **2023**, *19* (31), 2206442. https://doi.org/10.1002/smll.202206442.

(29) Hutton, G. A. M.; Martindale, B. C. M.; Reisner, E. Carbon Dots as Photosensitisers for Solar-Driven Catalysis. *Chem. Soc. Rev.* **2017**, *46* (20), 6111–6123. https://doi.org/10.1039/C7CS00235A.

(30) Javed, N.; O'Carroll, D. M. Carbon Dots and Stability of Their Optical Properties. *Particle & Particle Systems Characterization* **2021**, *38* (4), 2000271. https://doi.org/10.1002/ppsc.202000271.

(31) Rosso, C.; Filippini, G.; Prato, M. Use of Nitrogen-Doped Carbon Nanodots for the Photocatalytic Fluoroalkylation of Organic Compounds. *Chemistry A European J* **2019**, *25* (70), 16032–16036. https://doi.org/10.1002/chem.201903433.

(32) Kavarnos, G. J. Fundamental Concepts of Photoinduced Electron Transfer. In *Photoinduced Electron Transfer I*; Mattay, J., Ed.; Dewar, M. J. S., Dunitz, J. D., Hafner, K., Itô, S., Lehn, J.-M.,

Niedenzu, K., Raymond, K. N., Rees, C. W., Vögtle, F., Series Eds.; Topics in Current Chemistry; Springer Berlin Heidelberg: Berlin, Heidelberg, 1990; Vol. 156, pp 21–58. https://doi.org/10.1007/3-540-52379-0_2.

(33) Kütahya, C.; Wang, P.; Li, S.; Liu, S.; Li, J.; Chen, Z.; Strehmel, B. Carbon Dots as a Promising Green Photocatalyst for Free Radical and ATRP-Based Radical Photopolymerization with Blue LEDs. *Angew. Chem. Int. Ed.* **2020**, *59* (8), 3166–3171. https://doi.org/10.1002/anie.201912343.

(34) Zhao, Z.; Reischauer, S.; Pieber, B.; Delbianco, M. Carbon Dot/TiO 2 Nanocomposites as Photocatalysts for Metallaphotocatalytic Carbon–Heteroatom Cross-Couplings. *Green Chemistry* **2021**, *23* (12), 4524–4530. https://doi.org/10.1039/D1GC01284C.

(35) Han, Y.; Huang, H.; Zhang, H.; Liu, Y.; Han, X.; Liu, R.; Li, H.; Kang, Z. Carbon Quantum Dots with Photoenhanced Hydrogen-Bond Catalytic Activity in Aldol Condensations. *ACS Catal.* **2014**, *4* (3), 781–787. https://doi.org/10.1021/cs401118x.

(36) Sarma, D.; Majumdar, B.; Sarma, T. K. Visible-Light Induced Enhancement in the Multi-Catalytic Activity of Sulfated Carbon Dots for Aerobic Carbon–Carbon Bond Formation. *Green Chem.* **2019**, *21* (24), 6717–6726. https://doi.org/10.1039/C9GC02658D.

(37) Zhao, Z.; Pieber, B.; Delbianco, M. Modulating the Surface and Photophysical Properties of Carbon Dots to Access Colloidal Photocatalysts for Cross-Couplings. *ACS Catal.* **2022**, *12* (22), 13831–13837. https://doi.org/10.1021/acscatal.2c04025.

(38) Hamadamin, A.; Benazzi, V.; Campalani, C.; Quattri, L.; Ravelli, D.; Hussain, F.; Perosa, A.; Selva, M.; Protti, S. Nitrogen-Doped Carbon Dots as Biobased Catalysts for Visible Light Driven 1,2-Functionalization of Olefins through an Atom Transfer Radical Addition Process. *ChemCatChem* **2023**, *15* (17), e202300708. https://doi.org/10.1002/cctc.202300708.

(39) Rigodanza, F.; Burian, M.; Arcudi, F.; Đorđević, L.; Amenitsch, H.; Prato, M. Snapshots into Carbon Dots Formation through a Combined Spectroscopic Approach. *Nat Commun* **2021**, *12* (1), 2640. https://doi.org/10.1038/s41467-021-22902-w.

(40) Gentile, G.; Mamone, M.; Rosso, C.; Amato, F.; Lanfrit, C.; Filippini, G.; Prato, M. Tailoring the Chemical Structure of Nitrogen-Doped Carbon Dots for Nano-Aminocatalysis in Aqueous Media. *ChemSusChem* **2023**, *16* (7), e202202399. https://doi.org/10.1002/cssc.202202399.

(41) Asakuma, Y.; Matsumura, S.; Asada, M.; Phan, C. In Situ Investigation of Microwave Impacts on Ethylene Glycol Aqueous Solutions. *Int J Thermophys* **2017**, *39* (2), 21. https://doi.org/10.1007/s10765-017-2343-2.

(42) Bartolomei, B.; Prato, M. The Importance of the Purification Step and the Characterization of the Products in the Synthesis of Carbon Nanodots. *Small* **2023**, *19* (31), 2206714. https://doi.org/10.1002/smll.202206714.

(43) Bartolomei, B.; Bogo, A.; Amato, F.; Ragazzon, G.; Prato, M. Nuclear Magnetic Resonance Reveals Molecular Species in Carbon Nanodot Samples Disclosing Flaws. *Angew Chem Int Ed* **2022**, *61* (20), e202200038. https://doi.org/10.1002/anie.202200038.

(44) Rosenau, C. P.; Jelier, B. J.; Gossert, A. D.; Togni, A. Exposing the Origins of Irreproducibility in Fluorine NMR Spectroscopy. *Angew. Chem. Int. Ed.* **2018**, *57* (30), 9528–9533. https://doi.org/10.1002/anie.201802620.

(45) Amador, A. G.; Sherbrook, E. M.; Yoon, T. P. Enantioselective Photocatalytic [3 + 2] Cycloadditions of Aryl Cyclopropyl Ketones. *J. Am. Chem. Soc.* **2016**, *138* (14), 4722–4725. https://doi.org/10.1021/jacs.6b01728.

(46) Li, A.-F.; Wang, J.-H.; Wang, F.; Jiang, Y.-B. Anion Complexation and Sensing Using Modified Urea and Thiourea-Based Receptors. *Chem. Soc. Rev.* **2010**, *39* (10), 3729–3745. https://doi.org/10.1039/B926160P.

(47) Yang, Y.; Wu, X.; Busschaert, N.; Furuta, H.; Gale, P. A. Dissecting the Chloride–Nitrate Anion Transport Assay. *Chem. Commun.* **2017**, *53* (66), 9230–9233. https://doi.org/10.1039/C7CC04912A.

(48) Filippini, G.; Dosso, J.; Prato, M. Phenols as Novel Photocatalytic Platforms for Organic Synthesis. *Helvetica Chimica Acta* **2023**, *106* (7), e202300059. https://doi.org/10.1002/hlca.202300059.

(49) Iannazzo, D.; Piperno, A.; Ferlazzo, A.; Pistone, A.; Milone, C.; Lanza, M.; Cimino, F.; Speciale, A.; Trombetta, D.; Saija, A.; Galvagno, S. Functionalization of Multi-Walled Carbon Nanotubes with Coumarin Derivatives and Their Biological Evaluation. *Org. Biomol. Chem.* **2012**, *10* (5), 1025–1031. https://doi.org/10.1039/C1OB06598J.

(50) Madabhushi, S.; Jillella, R.; Sriramoju, V.; Singh, R. Oxyhalogenation of Thiols and Disulfides into Sulfonyl Chlorides/Bromides Using Oxone-KX (X = Cl or Br) in Water. *Green Chem.* **2014**, *16* (6), 3125–3131. https://doi.org/10.1039/C4GC00246F.

(51) Cuadros, S.; Rosso, C.; Barison, G.; Costa, P.; Kurbasic, M.; Bonchio, M.; Prato, M.; Filippini, G.; Dell'Amico, L. The Photochemical Activity of a Halogen-Bonded Complex Enables the Microfluidic Light-Driven Alkylation of Phenols. *Org. Lett.* **2022**, *24* (16), 2961–2966. https://doi.org/10.1021/acs.orglett.2c00604.

(52) Filippini, G.; Silvi, M.; Melchiorre, P. Enantioselective Formal α-Methylation and α-Benzylation of Aldehydes by Means of Photo-organocatalysis. *Angew Chem Int Ed* **2017**, *56* (16), 4447–4451. https://doi.org/10.1002/anie.201612045.

(53) Nobile, E.; Castanheiro, T.; Besset, T. C–H Electrophilic (Phenylsulfonyl)Difluoromethylation of (Hetero)Arenes with a Newly Designed Reagent. *Chem. Commun.* **2021**, *57* (92), 12337–12340. https://doi.org/10.1039/D1CC04737J.

(54) Gu, Y.; Leng, X.; Shen, Q. Cooperative Dual Palladium/Silver Catalyst for Direct Difluoromethylation of Aryl Bromides and Iodides. *Nat Commun* **2014**, *5* (1), 5405. https://doi.org/10.1038/ncomms6405.

(55) Prakash, G. K. S.; Hu, J.; Wang, Y.; Olah, G. A. Nucleophilic Difluoromethylation of Primary Alkyl Halides Using Difluoromethyl Phenyl Sulfone as a Difluoromethyl Anion Equivalent. *Org. Lett.* **2004**, *6* (23), 4315–4317. https://doi.org/10.1021/ol048166i.

(56) Mamone, M.; Gentile, G.; Dosso, J.; Prato, M.; Filippini, G. Direct C2–H Alkylation of Indoles Driven by the Photochemical Activity of Halogen-Bonded Complexes. *Beilstein J. Org. Chem.* **2023**, *19*, 575–581. https://doi.org/10.3762/bjoc.19.42.

(57) Bottecchia, C.; Martín, R.; Abdiaj, I.; Crovini, E.; Alcazar, J.; Orduna, J.; Blesa, M. J.; Carrillo, J. R.; Prieto, P.; Noël, T. De Novo Design of Organic Photocatalysts: Bithiophene Derivatives for the Visible-Light Induced C–H Functionalization of Heteroarenes. *Advanced Synthesis & Catalysis* **2019**, *361* (5), 945–950. https://doi.org/10.1002/adsc.201801571.

(58) Adam, C.; Yang, L.; Cockroft, S. L. Partitioning Solvophobic and Dispersion Forces in Alkyl and Perfluoroalkyl Cohesion. *Angew. Chem. Int. Ed.* **2015**, *54* (4), 1164–1167. https://doi.org/10.1002/anie.201408982.

(59) He, R.-Y.; Zeng, H.-T.; Huang, J.-M. Direct Fluoroalkylation of Indoles with Fluoroalkyl Halides Mediated by Copper. *European Journal of Organic Chemistry* **2014**, *2014* (20), 4258–4263. https://doi.org/10.1002/ejoc.201402526.

(60) Gui, J.; Zhou, Q.; Pan, C.-M.; Yabe, Y.; Burns, A. C.; Collins, M. R.; Ornelas, M. A.; Ishihara, Y.; Baran, P. S. C–H Methylation of Heteroarenes Inspired by Radical SAM Methyl Transferase. *J. Am. Chem. Soc.* **2014**, *136* (13), 4853–4856. https://doi.org/10.1021/ja5007838.

(61) Sun, W.; Zhao, M.; Meng, Y.; Zheng, C.; Yang, K.; Wang, S.; Ke, C.; Zhang, Z. Photoinduced [3 + 2] Cycloadditions of Aryl Cyclopropyl Ketones with Alkynes and Alkenes. *Org. Lett.* **2024**, *26* (18), 3762–3766. https://doi.org/10.1021/acs.orglett.4c00843.

(62) Nguyen, T. V. T.; Bossonnet, A.; Wodrich, M. D.; Waser, J. Photocatalyzed [2σ + 2σ] and [2σ + 2π] Cycloadditions for the Synthesis of Bicyclo[3.1.1]Heptanes and 5- or 6-Membered Carbocycles. *J. Am. Chem. Soc.* **2023**, *145* (46), 25411–25421. https://doi.org/10.1021/jacs.3c09789.

Chapter 4.

Direct C2–H Alkylation of Indoles Driven by the Photochemical Activity of Halogen-bonded Complexes

Abstract

In this Chapter is discussed the development of a new protocol for the metal-free homolytic aromatic substitution of indoles under visible light absorption.

Specifically, different substituted indoles reacted with α-iodosulfones **2** leading to the alkylated heteroaromatic compounds **3** in high yields (up to 96%). The process is driven by the photochemical activity of halogen-bonded complexes formed upon the complexation of a sacrificial donor, namely 1,4-diazabicyclo[2.2.2]octane (DABCO), with α-iodosulfones. This new aggregate may be defined as electron-donor acceptor complex (EDA). This system is capable of absorbing visible light and turning into the excited-state undergoing an intramolecular single-electron-transfer (SET) process. Moreover, we investigated deeply the reaction mechanism using both UV-Vis and nuclear magnetic resonance (NMR) spectroscopies which confirmed the formation of the halogen-bonded EDA complex between the α-iodosulfones **3** and DABCO.

This project was conducted in the carbon nanotechnology group, together with *Prof. Maurizio Prato*, who supervised the project, and with *Dr Giacomo Filippini*, who conceived the idea. *Dr Giuseppe Gentile* collaborated in the scope study. *Dr Jacopo Dosso* helped to perform the NMR experiments. A significant part of this work has been published in 2023 under the title: "Direct C2–H alkylation of indoles driven by the photochemical activity of halogen-bonded complexes".[1]

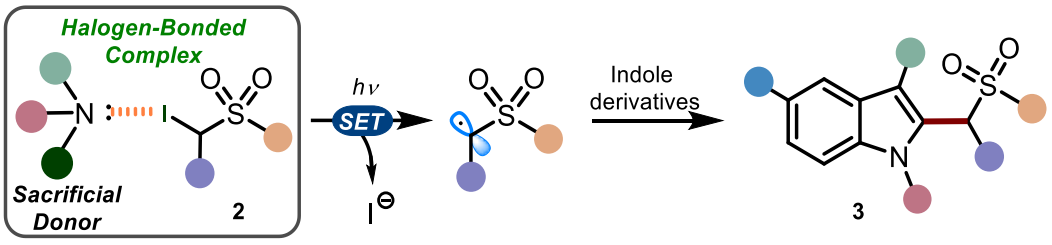

4.1 Introduction

4.1.1 Aromatic C-H Functionalization Strategy

Organic chemistry relies on the transformations of natural or available structures to achieve different molecules through customized synthetic strategies. Generally, the installment of a new bond requires the presence of either a heteroatom, such as oxygen or a halogen, or unsaturation in the carbon backbone.[2] Over the past two decades there has been an explosive growth in the development of methods for the transformation of aromatic carbon-hydrogen (C-H) bonds unlocking opportunities for significantly different synthetic methodologies.[3,4] First of all, the direct C-H bond functionalization of simple arenes avoids the need for the pre-installation of a leaving group on the aromatics.[2] Notably, these reactions enable the formation of new carbon-carbon (C-C) or carbon-heteroatom (C-X) bonds.[5,6] These methodologies have been widely applied in the synthesis of complex targets, including natural products and pharmaceutical agents.[7,8] Historically, organic chemists have extensively relied on the use of noble metal-based catalysts (*e.g.*, Pd, Rh, Ir, among others) to achieve such type of functionalization.[9–11] There is a multitude of examples where expensive metals were employed as catalysts, such as the use of iridium complexes to catalyse regioselective borylation on different arenes.[12] Another representative case reported the directed metalation by a platinum complex enabling selective aromatic C-H functionalization in a synthetic step of the total synthesis of the Antimitotic Rhazinilam.[13]

However, metal complexes have become a declining trend in recent years due to their toxicity, high cost and lack of availability.[14] As a result, modern principles of sustainable chemical production schemes have discouraged their use. For this reason, organic photochemistry has emerged as a powerful tool to guide the development of environmentally friendly and more convenient synthetic protocols for aromatic C-H functionalization.[15,16] By harnessing the energy of light, photochemical methods offer milder reaction conditions, reduced use of toxic reagents, and often increased selectivity in synthetic transformations.[17,18]
Photoredox catalysis has mostly been responsible for the advancement of novel photochemical methods. This strategy relies on the use of coloured photocatalysts which absorb visible light to activate available bench-stable substrates generating reactive radicals under very mild reaction conditions.[19,20] However, the limitations of this approach may include the utilization of expensive photocatalysts that require multi-step synthesis and are usually not recyclable.

Paving the way for atom-economical functionalization reactions, in recent years the synthetic community has recognized the potential of a novel photochemical approach. This method exploits the association of an electron acceptor substrate and a donor molecule leading to the formation of a new molecular aggregation in the ground state, called an electron donor–acceptor (EDA).[21,22]

In the next paragraph, we will discuss the characteristics of these photochemically activated complexes.

4.1.2 EDA Complex

EDA complexes are non-covalent aggregates that involve the interaction between an electron acceptor substrate "A" and a donor molecule "D" (Figure 4.1).[21,23] While the two compounds may not directly absorb visible light, the resulting formed complex typically exhibits a charge transfer state which causes a bathochromic shift of the absorption towards the visible range.[24,25]

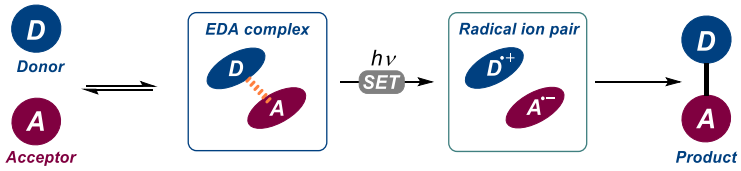

Figure 4.1 Exploitation of EDA complexes in organic synthesis.

Upon light irradiation, the EDA complex may undergo an intramolecular single-electron-transfer (SET) process, from the highest occupied molecular orbital (HOMO) of the electron donor to the lowest occupied molecular orbital (LUMO) of the acceptor, to produce radical ions ($D^{\bullet+}$, $A^{\bullet-}$).[26] The radical ion pair, formed after the first photo-induced electron transfer, may either return to the initial state through a rapid back-electron-transfer (BET) process or undergo subsequent transformations (Figure 4.2). The BETs typically occur faster than other processes that could happen after the SET ($k_{BET} > k_P$). To prevent BET, a suitable leaving group (LG) may be included in one of the precursors. In this manner, reactive intermediates (*e.g.*, radical species) may be generated in solution through the irreversible fragmentation of the substrates.[27,28] These intermediates eventually can initiate synthetically useful transformations to yield the final products "A-D".

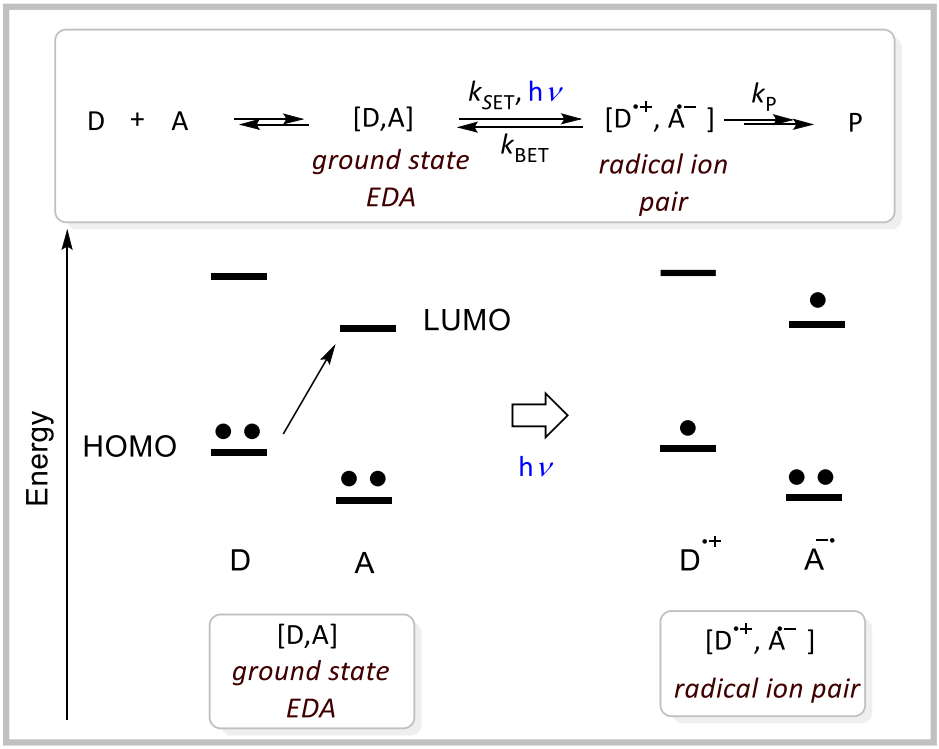

Figure 4.2 Photochemical activity of electron donor-acceptor (EDA) complexes.

In 2013, the Melchiorre group discovered the formation of an EDA complex upon aggregation of an electron-rich enamine and a suitable alkyl halide capable of generating reactive radical species under mild reaction conditions.[29] The authors investigated the direct α-alkylation of aldehydes with electron-deficient alkyl bromides, catalysed by a chiral amine, to obtain the corresponding enantioenriched products (Figure 4.3a). Firstly, the condensation of aldehydes with the chiral aminocatalyst led to the formation of chiral enamines. Subsequently, the electron-rich enamine intermediates, in the presence of the electron-deficient benzyl bromide, underwent the formation of a yellow-colored EDA complex and confirmed by the optical absorption spectroscopic studies. Noteworthy, the colored solution is characteristic of the formation of an EDA complex. Then, the irradiation with visible light (23W CFL bulb) of the EDA complex promoted the SET from the enamine to the bromo compound providing the two reactive open-shell species that triggered the stereoselective catalytic α-alkylation of the aldehydes. The reaction efficiently afforded enantioenriched aldehyde products in good yields and excellent enantiomeric excess (e.e.).

Another representative example was reported by Melchiorre and co-workers which used 23W CFL light to promote carbon–carbon bond-forming processes.[27] Specifically, electron-rich 3-substituted indoles have served as donor, while electron-poor benzyl bromide compounds have been used as

acceptors for the direct alkylation of indoles at the C2-H position (Figure 4.3b). In this case, the halides acted as suitable leaving groups. Significantly, the X-ray single-crystal spectroscopic analysis of the visible-light-absorbing EDA complex confirmed the intermolecular binding between the indole scaffold and the aromatic ring of the bromide compound.

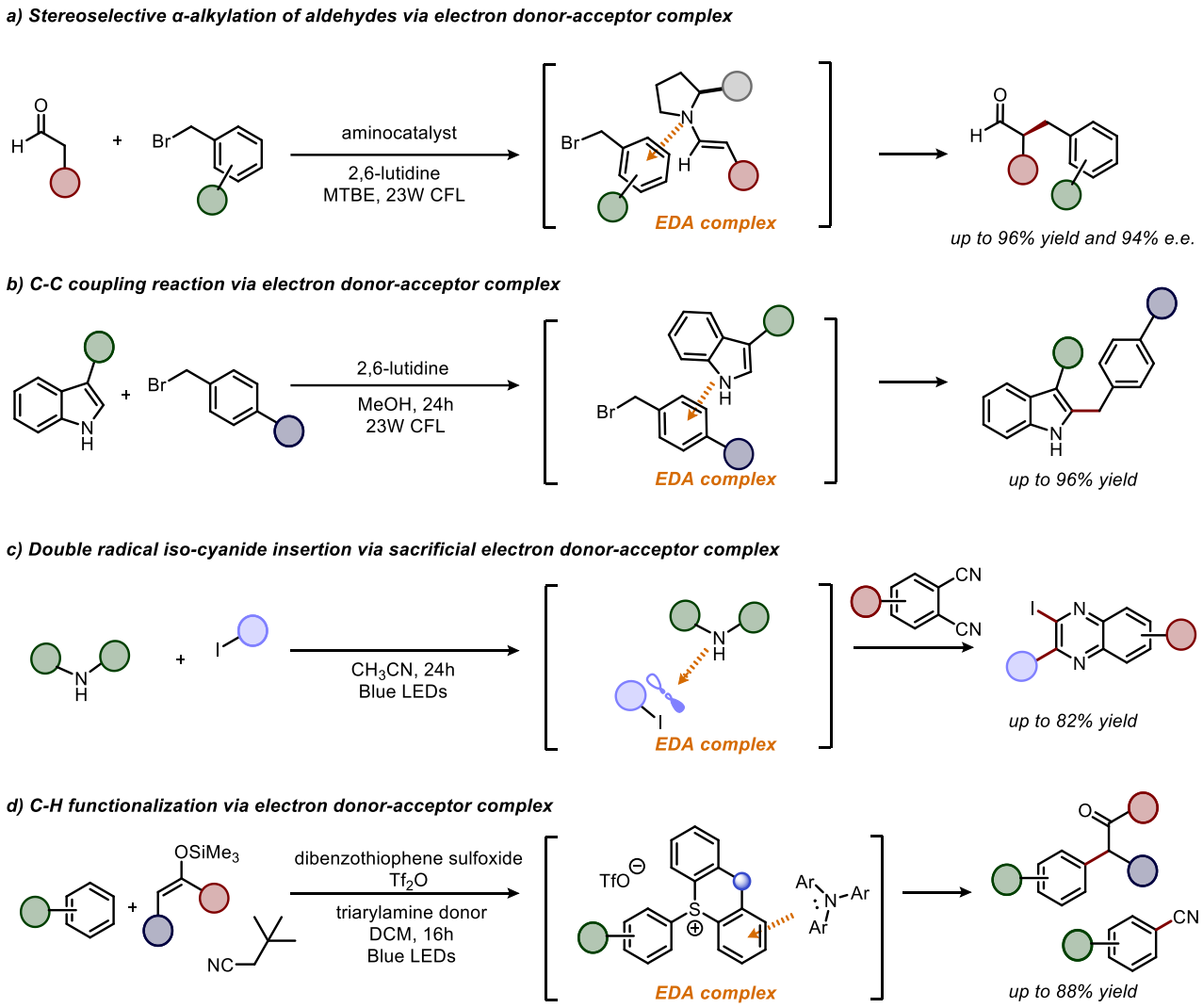

Figure 4.3 a) Photochemical C2-alkylation of indoles via EDA complex, formed upon association of indole and benzyl bromide; b) C-H alkylation and cyanation of arenes upon formation of EDA complex between the acceptor sulfonium salt and the sacrificial donor triarylamine.

Importantly, this method is not limited to reagents with appropriate donor-acceptor characteristics.[21] One strategy to bypass this limitation is to use sacrificial electron donor compounds that promote the EDA formation with electron-deficient radical precursors.[28,30–32] Upon photoinduced formation of corresponding radicals, electrophilic open-shell species can subsequently react with electron-rich substrates, which serve as radical trap.[33]

For instance, Yu and colleagues reported the use of stoichiometric amounts of a secondary amine as a sacrificial donor to activate perfluoroalkyl iodides via EDA complex formation (Figure 4.3c).[33] In particular, the halogen-bonded EDA complex generated perfluoroalkyl radicals by visible-light-induced SET process between the donor and acceptor. Then, the perfluoroalkyl open-shell species were trapped by diisocyanoarenes to give quinoxaline derivatives while propagating a radical chain via regeneration of perfluoroalkyl radicals carried on the reactivity. This strategy allowed the construction of 2-fluoroalkylated 3-iodoquinoxalines in high yields under mild conditions.

Recently, Procter and colleagues reported an elegant example of an EDA complex for the C-H functionalization of arenes (Figure 4.3d).[34] In detail, heterocyclic sulfonium molecules, used as redox-active label, formed with arenes the corresponding in situ triarylsulfonium salts, capable of generating visible light-absorbing EDA complexes in combination with triarylamines, present in catalytic amounts. The photoactivation of these complexes led to the formation of aryl radicals, offering a mild and metal-free strategy for the C-H functionalization of the aryl open-shell intermediates. Specifically, these radicals reacted with silyl enol ethers to give the corresponding C-H alkylated arenes. Moreover, the authors explored the cyanation of the aryl radicals using the *tert*-butyl isocyanide to yield aryl nitriles. Thus, a broad scope study provided α-arylated carbonyl compounds and C–H-cyanation products in excellent yields.

Overall, the design and application of EDA complexes demonstrate the potential for greener, more sustainable methodologies in organic synthesis. Therefore, novel sophisticated EDA strategies are nowadays investigated.

4.2 Aim of the Project

In this project, we investigated the process of the direct C2-H alkylation of indoles **1** with α-iodosulfones **2** to achieve alkylated heteroaromatic compounds **3** under blue light irradiation (Figure 4.4). Interestingly, this strategy exploited the EDA complex formation between 1,4-diazabicyclo[2.2.2]octane (DABCO) with substrates **2**.

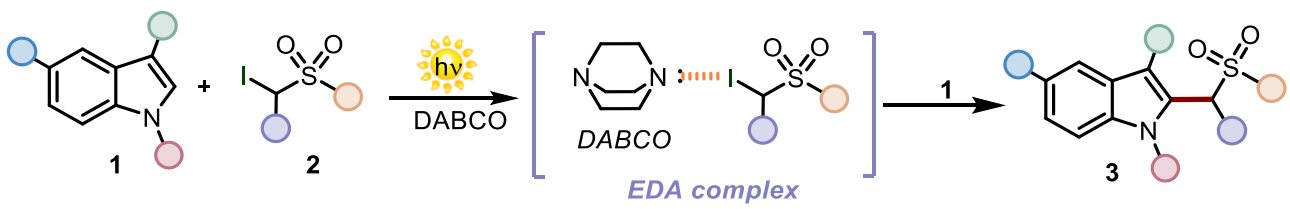

*Figure 4.4 C-H alkylation of indoles **1** with α-iodosulfones **2** using halogen-bonded EDA complexes*

4.3 Results and Discussion

Originally, as described in the previous chapter, the HAS reaction between 3-methylindole **1a** and α-iodosulfone **2a** was explored utilizing the photoredox catalysts phenol rich carbon dots (*p*-CDs). During control experiments, we noticed the formation of the corresponding product **3a** in moderate yield without the use of *p*-CDs. The experiment was performed at ambient temperature and under visible-light irradiation in the presence of 1,8-diazabiciclo[5.4.0]undec-7-ene (DBU) in acetonitrile. This result prompted us to investigate deeply the formation of the product **3a** in a catalytic-free environment.

Table 4.1 Optimization of the reaction conditions and control experiments.

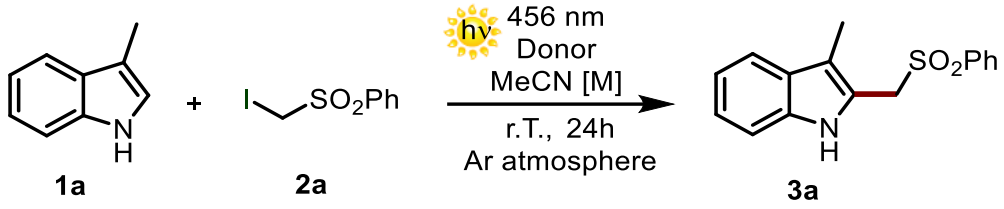

Entry	Donor	[M]	**2a**:**1a**:Donor (equiv.)	Light Source (nm)	Yield (%)[a]
1[b]	DBU	0.5	1:2:1	456	56
2	DBU	0.5	1:2:1	Light off	0
3	-	0.5	1:2:1	456	0
4[c]	DBU	0.5	1:2:1	456	0
5[d]	DBU	0.5	1:2:1	456	0
6	2,6-lutidine	0.5	1:2:1	456	0
7	TMG	0.5	1:2:1	456	64
8	NEt_3	0.5	1:2:1	456	64
9	DABCO	0.5	1:2:1	456	77
10	DABCO	0.25	1:2:1	456	64
11	DABCO	1.0	1:2:1	456	69

12	DABCO	0.5	1:1:1	456	65
13	DABCO	0.5	2:1:1	456	73
14	DABCO	0.5	2:1:1.5	456	95

[a] Yield determined by ^{1}H-NMR spectroscopy using 1,3,5-trimethoxybenzene as the internal standard. [b] Conditions: indole **1a** (0.1 mmol), α-iodosolfone **2a** (0.2 mmol), acetonitrile MeCN (200 µL), DABCO (0.1 mmol), ambient temperature. [c] Reaction in air. [d] Reaction performed in the presence of 2 equiv. of TEMPO.

The first result showed 56% yield of **3a** in the presence of DBU in acetonitrile under 456 nm light irradiation (Table 4.1, Entry 1). Meanwhile, a set of control experiments were conducted to obtain more mechanistic clues (Table 4.1, Entries 2-5). The photochemical nature of the reaction was established by the experiment in the dark which proved the complete inhibition of the process (Table 4.1, Entry 2). In addition, we verified the requirement of the donor for the transformation, since no reaction occurred in its absence (Table 4.1, Entry 3). The reactivity was also suppressed under an aerobic atmosphere and in the presence of 2,2,6,6-tetramethylpiperidinyloxyl (TEMPO). These experiments supported the postulated radical mechanism (Table 4.1, Entries 4-5).[35] Subsequently, we started a thorough optimization of the reaction conditions. The impact of the different sacrificial donors on the reaction was evaluated (Table 4.1, Entries 6-9). Specifically, we tested 2,6-lutidine, 1,1,3,3-tetramethylguanidine (TMG), triethylamine (NEt_3) and DABCO. Surprisingly, DABCO was found to be the best candidate in terms of reactivity, delivering compound **3a** in 77% yield. Either increasing or decreasing the concentration of the reaction mixture did not provide any beneficial effects in terms of yield (Table 4.1, Entries 10-11). Then we moved to set the best **2a**/**1a**/DABCO ratio to optimize the alkylation reaction. Using 1:1:1 ratio of **2a**/**1a**/DABCO slightly dropped the yield of **3a** (Table 4.1, Entry 12), while increasing the equivalent of **2a** resulted in 73% yield of **3a** (Table 4.1, Entries 13). Due to an easier purification of **3a** from the reaction crude by flash column chromatography, we decided to keep optimizing the transformation using the stoichiometric ratio indicated in Entry 13. Remarkably, a 2:1:1.5 ratio between **2a**/**1a**/DABCO reached the best yield observed so far (Table 4.1, Entry 14).

Moving to the investigation of the reaction mechanism, the interaction between the α-iodosulfone **2a** and DABCO was examined using both UV-Vis and nuclear magnetic resonance (NMR) spectroscopy.[23]

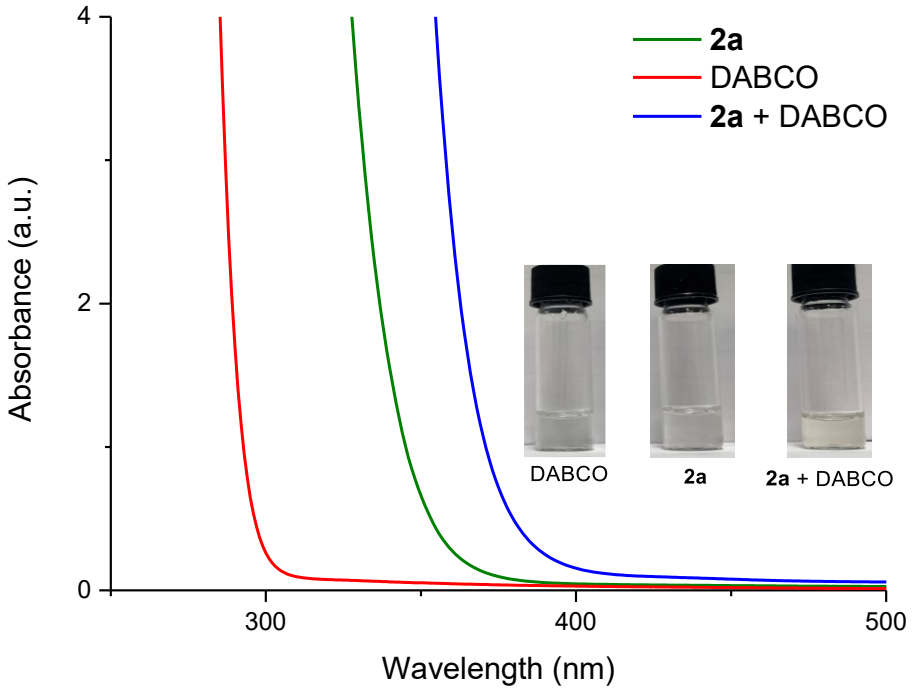

*Figure 4.5 Optical absorption spectra recorded in acetonitrile in 1 mm path quartz cuvettes. [DABCO]: 0.5 M; [**2a**]: 0.5 M.*

Firstly, the optical absorption spectra of **2a**, DABCO and the solution containing both **2a** and DABCO (blue line) were recorded in acetonitrile. Notably, the addition of DABCO to the solution of **2a** induced a bathochromic shift of the absorption bands towards visible region. Moreover, the yellowish color observed for the solution containing **2a** and DABCO suggested the visible-light shift (Figure 4.5). This effect indicates the formation of an EDA complex between these chemical species. In fact, a red-shifted absorption is typical of the formation of these aggregates. Importantly, additional UV-Vis spectroscopic analysis was performed to exclude other chemical interactions between the components of the reaction.

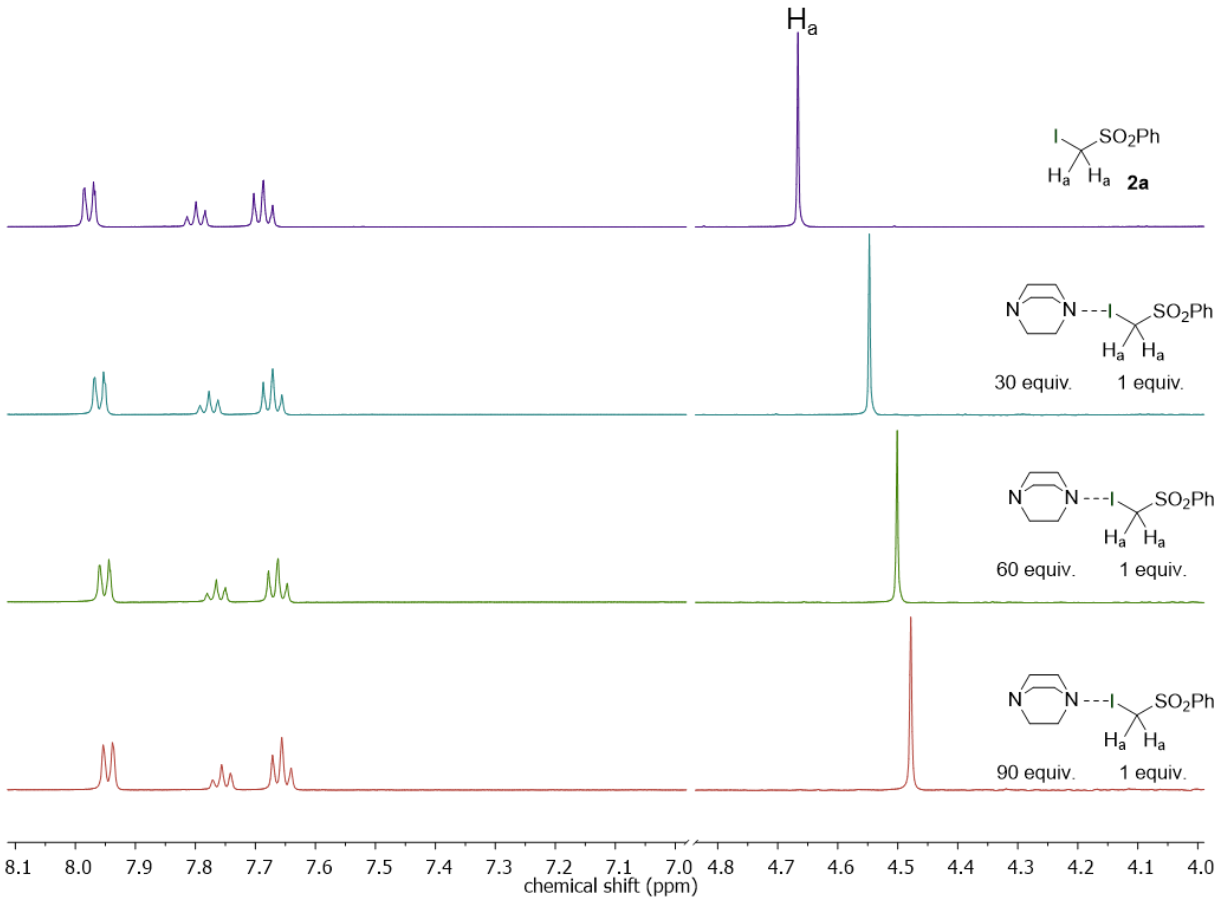

*Figure 4.6 ^{1}H-NMR titration of DABCO in a solution of **2a** in ACN-d_3 to detect their halogen-bonding association through the shift of the signal of Hα.*

To further support the hypothesis that an EDA complex underlies the observed reactivity, NMR studies were conducted. An NMR sample containing iodosulfone **2a** and additional concentrations of DABCO in deuterated acetonitrile was analyzed. Notably, a shift in the chemical signal of the diagnostic α-protons of **2a** was observed with increasing amounts of DABCO, indicating the presence of a halogen-bond interaction. Specifically, the ^{1}H-NMR signal corresponding to the α-hydrogens (Hα) in **2a** shifted to lower ppm values, suggesting that the Hα nuclei experienced increased electron density due to the formation of a halogen-bonded complex between **2a** and DABCO (Figure 4.6). To further verify that this shift in Hα was indeed caused by halogen-bonding, ^{19}F-NMR analysis was performed on compound **2d**, which contains a difluoromethylene group (-CF2-) adjacent to the iodine (Figure 4.10, section 4.5.5). A significant shift in the fluorine signal was also detected in this case.

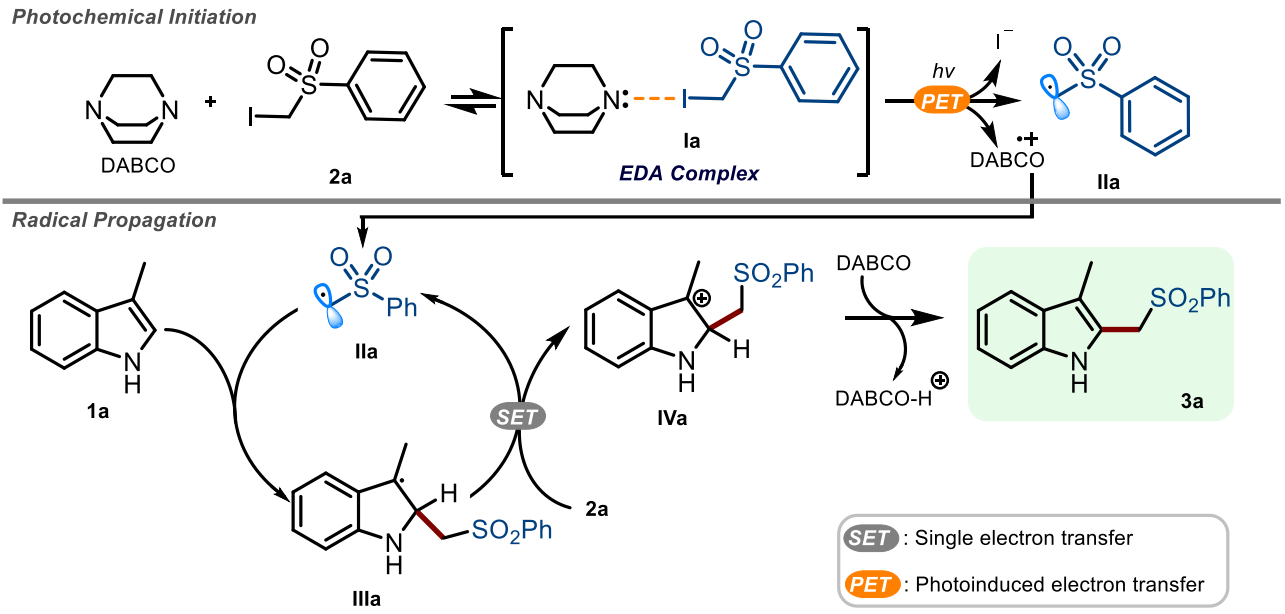

*Figure 4.7 Proposed reaction mechanism for the photochemical alkylation of **1a** with the α-iodosulfone **2a** in the presence of DABCO.*

Mechanistically, this experiment corroborated that the reaction is driven by the formation of a halogen-bonded EDA complex (**Ia**) between **2a** and DABCO. Hence, the proposed mechanism for this C-H alkylation was based on the photoinduced electron transfer step from DABCO to the iodosulfone. As shown in Figure 4.7, the irradiation at 456 nm of this aggregate would generate reactive alkyl radicals (**IIa**), which may react with indole **1a** forming the open-shell intermediate **IIIa**. This species can undergo SET with another molecule of **2a** yielding **3a** through a classical HAS pathway.[36–38]

After the mechanistic studies, we evaluated the reaction scope (Scheme 4.1). The formation of the EDA intermediate occurred with a diverse set of α-iodosulfones **2** affording the corresponding products **3a**-**d** from moderate to excellent yields (up to 73% yield). Different indoles actively participated in the photochemical alkylation, leading to the products **3e**-**h** (up to 96% yield). In particular, alkyl substituents at the N position of indoles were well tolerated providing products **3g**-**h** up to 96% yield. Remarkably, derivatives **3e**-**f** were isolated in moderate yields as single regioisomer since the alkylation step took place exclusively in position two of the starting indoles. In contrast, the presence of an aldehyde in position 3 of indole, instead of the methyl group, unveiled the limitation of this methodology.

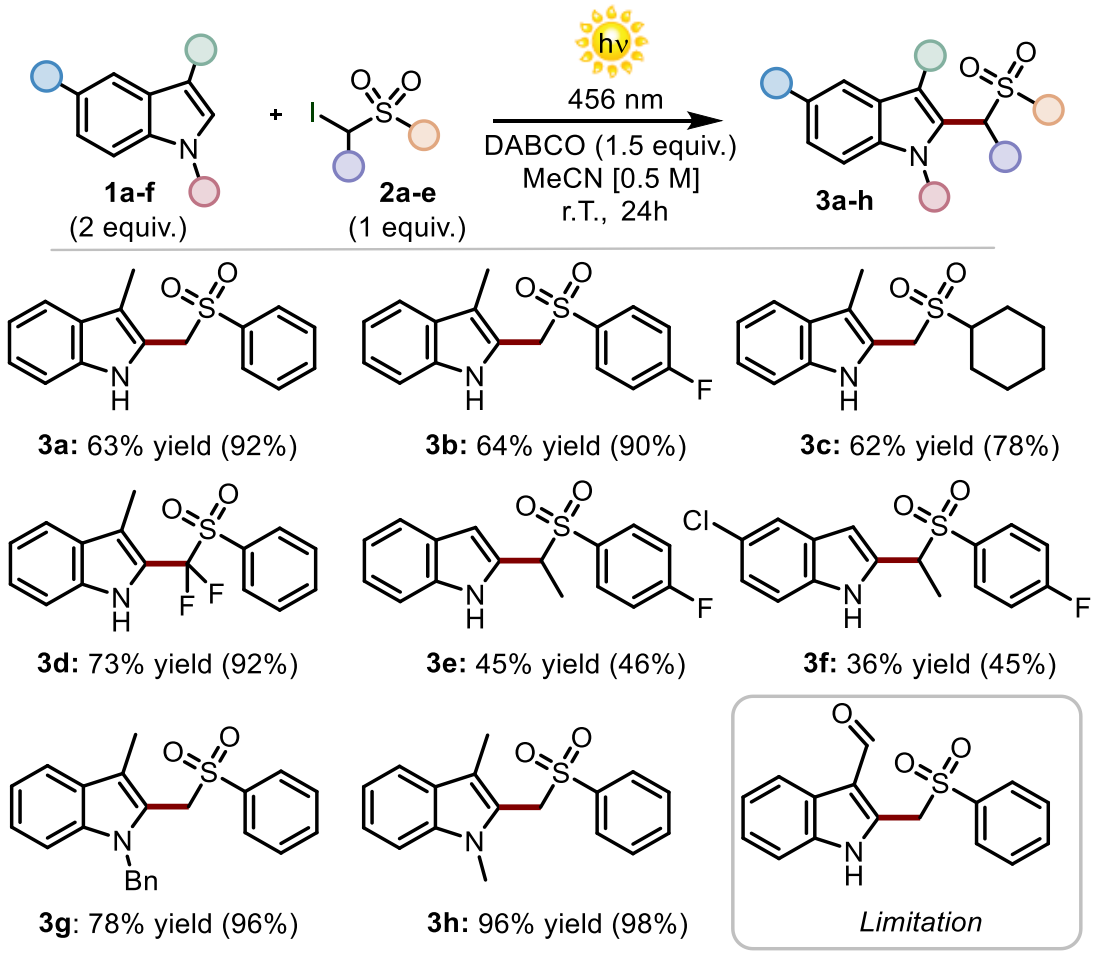

*Scheme 4.1 Study scope of the HAS reaction between indoles **1** and α-iodosulfones **2**. Yields in parentheses were determined by ^{1}H-NMR analyses, using 1,3,5-trimethoxybenzene as an internal standard.*

4.4 Conclusion

In this study, we presented a catalytic-free, light-driven alkylation reaction of indoles with α-iodosulfones under mild conditions. The C-C bond-forming process has been successfully optimized. In detail, through a series of mechanistic experiments, we established the formation of the halogen-bonded EDA complex between the sacrificial donor DABCO and α-iodosulfones. This EDA complex played a pivotal role in generating reactive alkyl radicals under visible light, leading to the alkylation of the indoles.

4.5 Experimental Section

4.5.1 General Information

UV-Vis measurements were carried out on Cary 5000 UV-Vis-NIR. All the spectra were recorded at room temperature using 10 mm path-length quartz cuvettes. The NMR spectra were recorded on Varian 400 spectrometer (^{1}H: 400 MHz; ^{19}F NMR: 376.0 MHz ^{13}C: 101.0 MHz) or Varian Inova

spectrometer (500 MHz ^{1}H and 126 MHz ^{13}C). The chemical shifts (δ) for ^{1}H and ^{13}C are given in ppm relative to residual signals of the solvents ($CHCl_3$ @ 7.26 ppm for ^{1}H-NMR, and @ 77.16 ppm for ^{13}C NMR).

General procedures. Chromatographic purification of products was accomplished using flash chromatography on silica gel (SiO_2, 0.04-0.063 mm, 60 Å) or using a Biotage Isolera automated flash chromatography system with cartridges packed with silica (SiO_2, 0.04-0.063 mm, 60 Å). For thin layer chromatography (TLC) analysis throughout this work, Merck pre-coated TLC plates (silica gel 60 GF254, 0.25 mm) were employed, using UV light as the visualizing agent (254 nm), basic aqueous potassium permanganate ($KMnO_4$) or vanillin stain solutions, and heat as developing agents. Organic solutions were concentrated under reduced pressure on a Büchi rotatory evaporator.

The homolytic-aromatic-substitution (HAS) reactions were set up under an argon atmosphere in Schlenk tubes unless otherwise stated. The light sources used in this work were purchased from Kessil. Detail Kessil lamp 456nm PR160L-456 (50W).

ESI-High resolution mass spectrometry (ESI-HRMS). ESI-HRMS was performed at University of Trieste Chemistry department, High resolution mass spectra (HRMS) were obtained on Bruker micrOTOF-Q (ESI-TOF). ***Photophysical analysis***: Absorption spectra of compounds were recorded on air equilibrated solutions at room temperature with an Agilent Cary 5000 UV-Vis spectrophotometer, using quartz cells with path length of 1.0 cm.

Materials. Commercial reagents and solvents were purchased from Sigma-Aldrich, Fluka, Alfa Aesar, Fluorochem and VWR. They were used as received, without further purification, unless otherwise stated. Synthesis grade and anhydrous solvents were used as purchased. The preparation of starting materials **1d-e**, **2a-e** is detailed in Section 4.5.2.

4.5.2 General Procedures for the Synthesis of Starting Materials

PREPARATION OF INDOLE **1d**

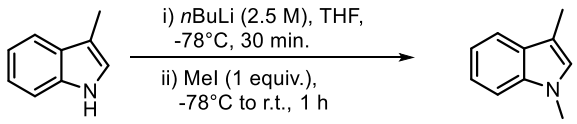

1a

3.8 mmol
(1 equiv.)

1d

3-Methylindole (3.8 mmol, 500 mg) was added in a flame dried Schlenk tube under argon and dissolved in anhydrous THF (10 mL). The solution was then cooled to -78°C (acetone liq. N_2) and *n*BuLi (2.5 M hexanes) was then added dropwise. After 30 min. the reaction was quenched by addition of MeI (237 mL, 3.8 mmol), allowed to reach room temperature and stirred for 1h at the same temperature. The resulting solution was then added H_2O (30 mL) and extracted with CH_2Cl_2 (3 x 20 mL). The organic layers were then washed with H_2O (2 x 20 mL) and brine (30 mL), dried over Na_2SO_4, filtered and evaporated. The residue was purified on a silica gel plug (eluent: PE to PE/ CH_2Cl_2 4/1) to give **1d** as a white solid (350 mg, 63% yield).

Characterization Data

^{1}H-NMR ($CDCl_3$, 400 MHz) δ 7.57 (dt, J = 7.9 Hz, 1.0 Hz, 1H), 7.28 (dt, J = 8.2 Hz, 0.9 Hz, 1H), 7.22 (ddd, J = 8.2 Hz, 6.9 Hz, 1.2 Hz, 1H), 7.11 (ddd, J = 7.9 Hz, 6.9 Hz, 1.1 Hz, 1H), 6.83 (d, J = 1.0 Hz, 1H), 3.74 (s, 3H), 2.33 (d, J = 1.1 Hz, 3H). The characterization of the compound matches with the data reported in the literature.[39]

PREPARATION OF INDOLE **1e**

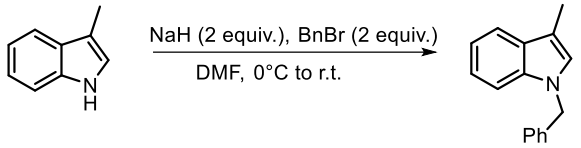

1a
2 mmol
(1 equiv.)

1e

Procedure for the synthesis of **1e** has been carried out following a modified literature procedure.[40] To a stirred solution of NaH (160 mg, 4 mmol, 60% suspension in mineral oil) in dry DMF (1.6 mL), 3-methylindole (263 mg, 2 mmol, 1.0 equiv.) in DMF (1.0 mL) was added dropwise at 0°C. The mixture was then stirred at room temperature for 30 min. After cooling down to 0°C, a solution of benzyl bromide (475 µL, 4 mmol) in DMF (2.0 mL) was added dropwise. The reaction mixture was stirred at room temperature for another 5 h. and then it was quenched by the addition of water and was extracted with ethyl acetate (3 x 10 mL). The combined organic layer was washed with brine, dried over anhydrous Na_2SO_4, and concentrated under reduced pressure. The residue was purified by column chromatography on silica gel (eluent: Cyclohexane/ CH_2Cl_2 7/3) to give the corresponding product as white solid (345 mg, 78% yield).

Characterization Data

^{1}H-NMR (400 MHz, $CDCl_3$) δ 7.89 – 7.76 (m, 1H), 7.52 – 7.30 (m, 6H), 7.27 (m, 2H), 7.03 (d, *J* = 0.8 Hz, 1H), 5.36 (s, 2H), 2.55 (d, *J* = 1.0 Hz, 3H). The characterization of the compound matches with the data reported in the literature.[40]

PREPARATION OF α-IODOSULFONES **2a-c**

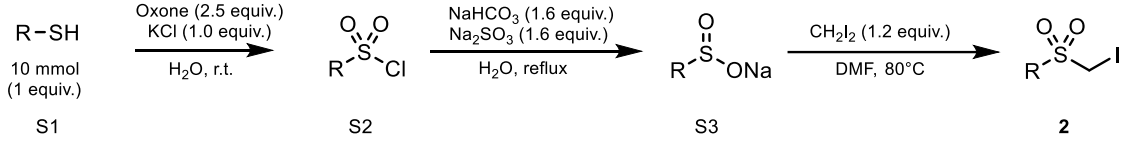

STEP 1, has been carried out following a modified literature procedure.[41] A mixture of thiol S1 (10 mmol, 1 equiv.), Potassium peroxymonosulfate (25 mmol, 2.5 equiv.), KCl (10 mmol, 1 equiv.) and H_2O (30 mL) were introduced in a single neck round bottom flask and stirred at room temperature for 2 h. The aqueous phase was extracted with ethyl acetate (3 x 50 mL). The combined organic layer was dried over anhydrous Na_2SO_4 and concentrated under reduced pressure. The crude product was purified by flash column chromatography (cyclohexane) affording the desired products S2. The characterization data matched with the reported one.[42]

STEP 2, according to a literature procedure.[43] The selected sulfonyl chloride S2 (7 mmol, 1 equiv.) was dissolved in H_2O (25 mL). Sodium sulfite (11.2 mmol, 1.6 equiv.) and sodium bicarbonate (11.2 mmol, 1.6 equiv.) were added, and the reaction mixture was refluxed for 3 h. Water was removed by evaporation. Ethanol was added to the solid and the so obtained suspension was heated for 10 min., cooled and filtered. This procedure was repeated twice using the residue of the filtration. The ethanol fractions were combined, and the solvent was evaporated under reduced pressure. Sodium sulfinate S3 was used without any further purification. The characterization data matched the reported one.[42]

STEP 3, according to a reported procedure.[44] A solution of sodium sulfinate S3 (5 mmol, 1 equiv.) in DMF (20 mL) was stirred at room temperature for 15 min. Diiodomethane (6 mmol, 1.2 equiv.) was added dropwise, and the solution was heated up to 80°C for 17h. The reaction was quenched by the addition of 5% LiCl water solution (100 mL). Subsequently, the aqueous solution was extracted with ethyl acetate (3 x 30 mL). The organic phases were combined and washed with brine (50 mL), saturated solution of sodium thiosulfate (50 mL) and then dried over Na_2SO_4 before being concentred in vacuo. The product was purified by flash column chromatography (eluent:

cyclohexane/ethyl acetate) to afford the desired α-iodo sulfone **2a-c**. (R= -phenyl 88% Yield; R= 4-fluorophenyl 75% Yield; R= cyclohexyl- 35% Yield)

PREPARATION OF α-IODOSULFONE **2d**

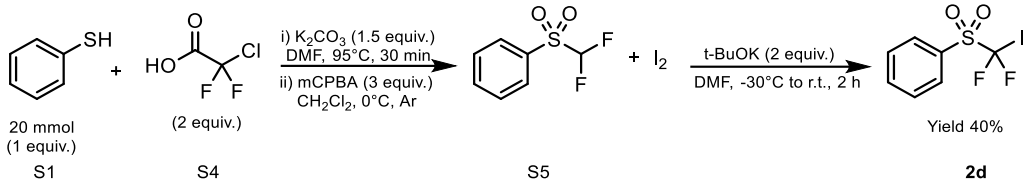

STEP 1, was performed following a modified reported procedure.[45] Into an oven-dried schlenk tube equipped with a stirring bar, thiophenol (20 mmol, 1 equiv., 2.2g) and K_2CO_3 (1.5 equiv., 30mmol) were introduced and dissolved in dry DMF (25 mL). Chlorodifluoroacetic acid S4 (2.0 equiv., 40 mmol) was solubilized in dry DMF and added dropwise into the reaction mixture. The reaction was kept under argon atmosphere. The reaction was then heated at 95°C for 30 min. Subsequently, it was quenched through the addition of 5% LiCl water solution and extracted with cyclohexane (3 x 20 mL). The organic layers were reunited, dried with Na_2SO_4 and concentrated under reduced pressure. The crude intermediate from the first step was used as obtained after extraction. It was dissolved in 20 mL of CH_2Cl_2 under argon and cooled to 0°C. Meta-Chloroperoxybenzoic acid (60 mmol, 3 equiv.) was slowly added. The reaction was stirred overnight (approximately 16 h). The day after, 0.1 M NH_4Cl water was added and the product S5 was extracted with ethyl acetate (3 x 20mL). The ethyl acetate fractions were combined and dried over Na_2SO_4 and the solvent was evaporated under reduced pressure. Product S5 was obtained with a yield of 40%.

^{1}H-NMR ($CDCl_3$, 400 MHz) δ 6.20 (t, J = 53.1 Hz, 1H), 7.62-7.68 (m, 2H), 7.79-7.85 (m, 1H), 7.97-8.02 (m, 2H). **^{19}F NMR ($CDCl_3$, 376 MHz)** δ -121.9 (d, J = 53.5 Hz, 2F). The characterization of the compound matches with the data reported in the literature.[46]

STEP 2, The last reaction step was carried out according to the literature.[47] S5 (8.5 mmol, 1.470 g) was introduced in an oven-dried double neck round bottom flask with stirring bar along with dry DMF (20 mL). The reaction was cooled to -30°C and placed under argon. I_2 (2.5 equiv., 21.25 mmol) was added in small aliquots followed by a dropwise addition of *t*-BuOK (2.0 equiv., 17 mmol). The reaction was stirred at -30°C for 1h. Subsequently, the reaction was allowed to reach room temperature in approximately 1h. A saturated NaCl aqueous solution (15 mL) was added, and the mixture was extracted with Et_2O (3 x 15 mL). The combined organic phase was dried over Na_2SO_4, and the solvent was removed in a rotary evaporator. The crude was purified by silica gel column

chromatography (eluent: cyclohexane/ethyl acetate 9/1) to afford the product (**2d**) (2.22 g, 35% overall yield) as a white crystalline solid. The product has been kept in the dark at 4°C.

^{1}H-NMR (400 MHz, $CDCl_3$) δ 7.65 (t, J = 7.3 Hz, 2H); 7.82 (t, J = 7.4 Hz, 1H); 7.99 (d, J = 7.5 Hz, 2H). **^{19}F NMR (376 MHz, $CDCl_3$)** δ – 51.9 (s, 2F). The characterization of the compound matches with the data reported in the literature.[46]

PREPARATION OF α-IODOSULFONE **2e**

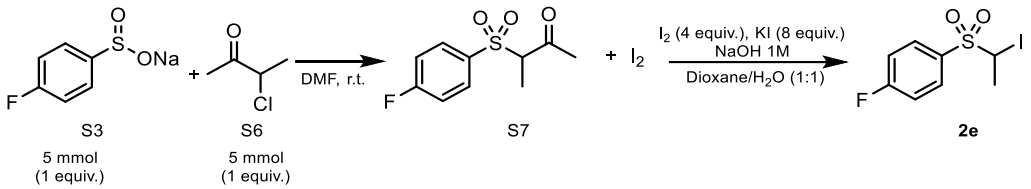

STEP 1, according to a modified literature procedure.[44] S3 (5 mmol, 1 equiv.) and 3-chloro butanone S6 (5 mmol, 1 equiv.) were mixed in DMF (10 mL, 0.5 M). The reaction mixture was stirred at room temperature for 24 h. The reaction was quenched by the addition of water (50 mL) and extracted with ethyl acetate (3 x 35 mL), dried over Na_2SO_4 and the solvent was removed under reduced pressure. The corresponding adduct S7 was used without any further purification.

STEP 2, iodine (10 mmol, 4 equiv.) has been added to a dioxane-water (1:1, 0.5 M) solution of the starting material S7 (2.5 mmol, 1 equiv.) in the presence of potassium iodide (20 mmol, 8 equiv.). Then a 1 M solution of NaOH was added dropwise until the discolouration of the excess of iodine. After 20 min. of stirring, the reaction mixture was diluted with water and extracted with CH_2Cl_2 (3 x 20 mL). The final α-iodo sulfones **2e** was used without any further purification.

4.5.3 General Procedure for the C-H Alkylation of Indoles

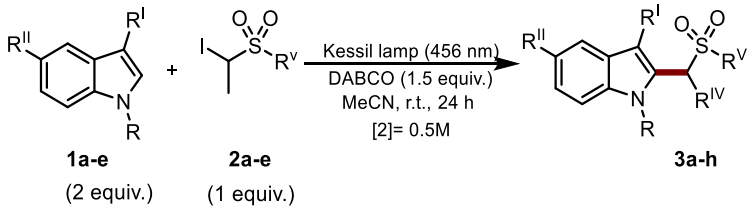

A 10 mL Schlenk tube was charged with indole 1 (0.2 mmol), α-iodosulfone 2 (0.1 mmol, 1.0 equiv.) and DABCO (0.15 mmol, 1.5 equiv.). Acetonitrile was then added to this mixture (200 µL). The reaction mixture was thoroughly degassed via 3 cycles of freeze-pump-thaw, and the vessel was refilled with argon, placed under light irradiation for 24h (λ = 456 nm). The temperature was kept at around 30°C by using a fan. The reaction mixture was then quenched with an aqueous solution of

HCl (5 mL, 0.5 M). The reaction was extracted with ethyl acetate (3 x 10 mL). The volatiles were removed in vacuo and the residue was purified by column chromatography (eluent: Cyclohexane/ CH_2Cl_2) to give the C-H functionalization products **3**.

Characterization Data

3-methyl-2-((phenylsulfonyl)methyl)-1H-indole (3a)

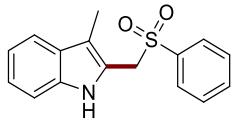

3a

Prepared according to the general procedure **3.** using indole **1a** (0.2 mmol, 26 mg), and α-iodosolfone **2a** (0.1 mmol, 28 mg). The product **3a** was obtained as white solid (20 mg, 71% yield).

^{1}H-NMR (499 MHz, $CDCl_3$) δ 8.50 (s, 1H), 7.63 – 7.56 (m, 3H), 7.45 – 7.38 (m, 3H), 7.36 (d, *J* = 8.2 Hz, 1H), 7.25 – 7.18 (m, 1H), 7.14 – 7.06 (m, 1H), 4.50 (s, 2H), 1.70 (s, 3H). **^{13}C NMR (126 MHz, $CDCl_3$)** δ 137.50, 136.56, 134.10, 129.21, 128.43, 128.13, 123.18, 121.08, 119.60, 119.12, 113.45, 111.23, 54.48, 7.80. The characterization of the compound matches with the data reported in the literature.[48]

2-(((4-fluorophenyl)sulfonyl)methyl)-3-methyl-1H-indole (3b)

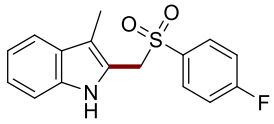

3b

Prepared according to the general procedure **3.** using indole **1a** (0.2 mmol, 26 mg), and α-iodosulfone **2b** (0.1 mmol, 30 mg). The product **3b** was obtained as white solid (20 mg, 64% yield).

^{1}H-NMR (400 MHz, $CDCl_3$) δ 8.50 (s, 1H), 7.63 – 7.53 (m, 2H), 7.43 (d, *J* = 8.1 Hz, 1H), 7.39 – 7.33 (m, 1H), 7.23 (m, 1H), 7.15 – 7.03 (m, 3H), 4.49 (s, 2H), 1.72 (s, 3H). **^{19}F NMR (376 MHz, $CDCl_3$)** δ -102.73 (tt, *J* = 8.3, 5.1 Hz). **^{13}C NMR (101 MHz, $CDCl_3$)** δ 166.16 (d, *J* = 257.1 Hz), 136.55, 133.44 (d, *J* = 3.2 Hz), 131.36 (d, *J* = 9.7 Hz), 128.06, 123.35, 120.88, 119.74, 119.20, 116.51 (d, *J* = 22.6 Hz), 113.47, 111.24, 54.58, 7.89. **HRMS** calculated for $C_{13}H_{14}FNO_2S$ (M-Na): 326.0623, found: 326.0621.

2-((cyclohexylsulfonyl)methyl)-3-methyl-1H-indole (3c)

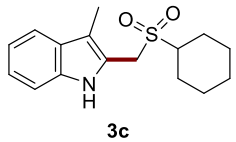

3c

Prepared according to the general procedure **3.** using indole **1a** (0.2 mmol, 26 mg), and α-iodosulfone **2c** (0.1 mmol, 29 mg). The product **3c** was obtained as white solid (20 mg, 62% yield).

^{1}H-NMR (499 MHz, $CDCl_3$) δ 8.65 (s, 1H), 7.56 (d, *J* = 7.9 Hz, 1H), 7.36 (d, *J* = 8.1 Hz, 1H), 7.27 – 7.21 (m, 1H), 7.18 – 7.10 (m, 1H), 4.40 (s, 2H), 2.72 (tt, *J* = 12.2, 3.5 Hz, 1H), 2.31 (s, 3H), 2.14 – 1.98 (m,

2H), 1.87 (dd, *J* = 7.4, 2.6 Hz, 2H), 1.67 (d, *J* = 5.6 Hz, 1H), 1.60 – 1.45 (m, 2H), 1.25 – 1.05 (m, 3H). **^{13}C NMR (101 MHz, $CDCl_3$)** δ 136.58, 128.35, 123.23, 121.30, 119.75, 119.10, 112.07, 111.37, 59.06, 48.02, 25.11, 25.02, 24.98, 8.82. **HRMS** calculated for $C_{16}H_{21}NO_2S$ (M-Na): 314.1184, found: 314.1185.

2-(difluoro(phenylsulfonyl)methyl)-3-methyl-1H-indole (3d)

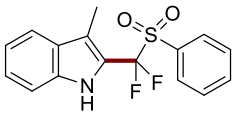

3d

Prepared according to the general procedure **3.** using indole **1a** (0.2 mmol, 44 mg), and α-iodosulfone **2d** (0.1 mmol, 28 mg). The product **3d** was obtained as white solid (24 mg, 73% yield).

^{1}H-NMR (499 MHz, $CDCl_3$) δ 8.46 (s, 1H), 7.96 (d, *J* = 7.7 Hz, 2H), 7.77 (ddd, *J* = 8.7, 2.4, 1.2 Hz, 1H), 7.65 – 7.58 (m, 3H), 7.39 (d, *J* = 8.3 Hz, 1H), 7.36 – 7.30 (m, 1H), 7.18 (ddd, *J* = 7.0, 5.4, 0.9 Hz, 1H), 2.31 (t, *J* = 2.5 Hz, 3H). **^{19}F NMR (376 MHz, $CDCl_3$)** δ -99.73, -99.73. **^{13}C NMR (126 MHz, $CDCl_3$)** δ 136.69, 135.57, 132.77, 130.92, 129.50, 128.24, 125.32, 120.44, 120.42 (t, J = 285.4 Hz), 120.21, 118.87 (t, J = 2.8 Hz), 117.97 (t, J = 27.2 Hz), 111.82, 8.72 (t, *J* = 2.0 Hz). The characterization of the compound matches with the data reported in the literature.[45]

(S)-2-(1-((4-fluorophenyl)sulfonyl)ethyl)-1H-indole (3e)

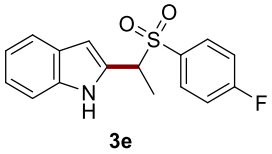

3e

Prepared according to the general procedure **3.** using indole **1b** (0.2 mmol, 23 mg), and α-iodosulfone **2e** (0.1 mmol, 31 mg). The product **3e** was obtained as white solid (14 mg, 45% yield).

^{1}H-NMR (400 MHz, $CDCl_3$) δ 8.83 (s, 1H), 7.49 (ddd, *J* = 8.0, 5.0, 2.6 Hz, 3H), 7.42 (d, *J* = 8.2 Hz, 1H), 7.23 (dd, *J* = 8.2, 1.1 Hz, 1H), 7.13 – 7.08 (m, 1H), 7.07 – 7.00 (m, 2H), 6.16 – 6.10 (m, 1H), 4.48 (q, *J* = 7.1 Hz, 1H), 1.75 (d, *J* = 7.1 Hz, 3H). **^{19}F NMR (376 MHz, $CDCl_3$)** δ -102.81 (dd, *J* = 9.2, 4.2 Hz). **^{13}C NMR (101 MHz, $CDCl_3$)** δ 166.14 (d, *J* = 257.0 Hz), 136.94, 132.08 (d, *J* = 9.6 Hz), 130.41, 127.40, 123.23, 120.88, 120.35, 116.29 (d, *J* = 22.7 Hz), 111.37, 110.16, 104.24, 60.48, 13.63. **HRMS** calculated for $C_{16}H_{14}FNO_2S$ (M-Na): 326.0621, found: 326.0624.

5-chloro-2-(1-((4-fluorophenyl)sulfonyl)ethyl)-1H-indole (3f)

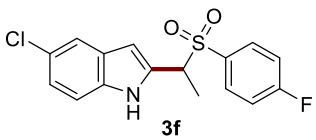

3f

Prepared according to the general procedure **3.** using indole **1c** (0.2 mmol, 30 mg), and α-iodosulfone **2e** (0.1 mmol, 31 mg). The product **3f** was obtained as white solid (12 mg, 36% yield).

^{1}H-NMR (499 MHz, $CDCl_3$) δ 8.88 (s, 1H), 7.51 – 7.46 (m, 2H), 7.45 (d, *J* = 1.9 Hz, 1H), 7.34 (d, *J* = 8.7 Hz, 1H), 7.19 (dd, *J* = 8.7, 2.0 Hz, 1H), 7.11 – 7.00 (m, 2H), 6.11 – 6.02 (m, 1H), 6.14 – 6.00 (m, 1H), 1.74 (d, *J* = 7.1 Hz, 3H). **^{19}F NMR (376 MHz, $CDCl_3$)** δ -102.43 – -102.53 (m). **^{13}C NMR (126 MHz, $CDCl_3$)** δ 166.05 (d, *J* = 257.4 Hz), 135.23, 132.04 (d, *J* = 9.8 Hz), 131.94, 131.14 – 130.98 (m), 128.40, 125.40, 123.64, 120.25, 116.23 (d, *J* = 22.6 Hz), 112.41, 103.79, 60.36, 13.57. **HRMS** calculated for $C_{16}H_{13}ClFNO_2S$ (M-Na): 360.0235, found: 360.0232.

1-benzyl-3-methyl-2-((phenylsulfonyl)methyl)-1H-indole (3g)

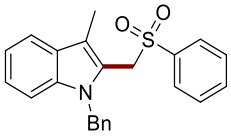

3g

Prepared according to the general procedure **3.** using indole **1d** (0.2 mmol, 44 mg), and α-iodosulfone **2a** (0.1 mmol, 28 mg). The product **3g** was obtained as white solid (29 mg, 78% yield).

^{1}H-NMR (499 MHz, $CDCl_3$) δ 7.65 (m, 3H), 7.48 (m, 3H), 7.36 – 7.17 (m, 5H), 7.13 (t, *J* = 7.4 Hz, 1H), 6.87 (d, *J* = 6.8 Hz, 2H), 5.56 (s, 2H), 4.41 (s, 2H), 1.66 (s, 3H). **^{13}C NMR (126 MHz, $CDCl_3$)** δ 137.84, 137.65, 137.57, 134.01, 129.14, 128.87, 128.73, 127.52, 127.43, 125.88, 123.04, 122.64, 119.37, 119.16, 114.26, 109.67, 53.38, 46.65, 8.12. **HRMS** calculated for $C_{23}H_{21}NO_2S$ (M-Na): 376.1364, found: 376.1366.

1,3-dimethyl-2-((phenylsulfonyl)methyl)-1H-indole (3h)

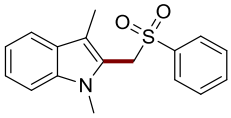

3h

Prepared according to the general procedure **3.** using indole **1e** (0.2 mmol, 23 mg), and α-iodosulfone **2a** (0.1 mmol, 31 mg). The product **3h** was obtained as white solid (29 mg, 45% yield).**^{1}H-NMR (499 MHz, $CDCl_3$)** δ 7.70 – 7.57 (m, 3H), 7.51 – 7.39 (m, 3H), 7.35 – 7.21 (m, 2H), 7.10 (t, *J* = 7.3 Hz, 1H), 4.56 (s, 2H), 3.72 (s, 3H), 1.66 (s, 3H). **^{13}C NMR (126 MHz, $CDCl_3$)** δ 137.94, 137.68, 134.11, 129.23, 128.88, 127.43, 122.98, 122.83, 119.24, 119.16, 113.24, 109.46, 53.38, 30.38, 8.21. **HRMS** calculated for $C_{17}H_{17}NO_2S$ (M-Na): 322.0877, found: 322.0872.

4.5.4 UV-Vis Experiments

Herein, we reported the absorption spectrum of all components of the C-H alkylation of indole **1a**. The absorption bands of the mixtures containing indole **1a** (line violet and green and brown) do not absorb at 456 nm confirming that **1a** and **2a** do not form a photo-active EDA complex. Only the absorption band of the mixture of **2a** and DABCO (line blue) is bathochromic shifted towards the visible region thus indicating the formation of the EDA complex between these chemical specie.

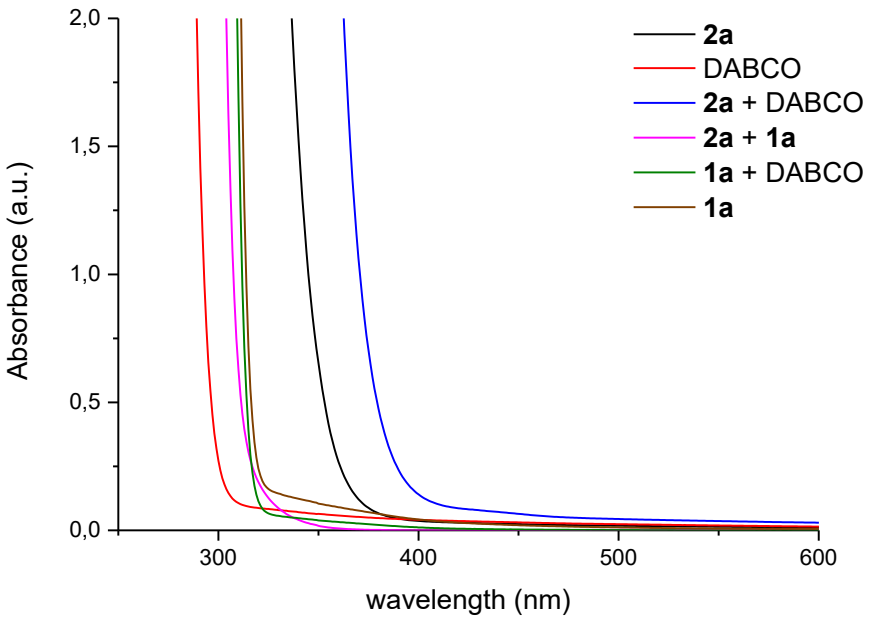

*Figure 4.8 Optical absorption spectra of α-iodosulfone **2a** (black line), DABCO (red line), the mixture between α-iodosulfone **2a** and DABCO (blue line), the mixture between α-iodosulfone **2a** and 3-methylindole **1a** (violet line), the mixture between α-iodosulfone **2a** and 3-methylindole **1a** (green line) and 3-methylindole **1a** (brown line). Recorded in CH_3CN in quartz cuvettes (1 mm path). [**1a**] = [DABCO] = [**2a**] = 0.05 M.*

4.5.5 NMR Titration

GENERAL PROCEDURE

A solution of host iodosulfone **2a** (17 mM) in ACN-d_3 was prepared. To this solution, 10 equiv. of guest DABCO was added as solid until saturation of the change in chemical shift ($\Delta\delta$) at the host's observed nuclei was reached (100 equiv. of DABCO). 1,3,5-trimethoxybenzene (δ = 6.1 ppm) was used as an internal standard for the determination of DABCO in solution. The constant component during the titration is called "host" and the varied component is called "guest" throughout. ^{1}H and ^{19}F NMR spectra were recorded on a 500 and 400 MHz Varian Mercury spectrometer.

^{1}H-NMR studies

Regarding the ^{1}H-NMR studies, a change to lower chemical shift of the diagnostic α-protons of **2a** was displayed upon addition of increasing amounts of DABCO, suggesting the presence of the halogen-bonding interaction. After adding 100 equiv. of DABCO, the saturation of the formation of the complex was achieved.

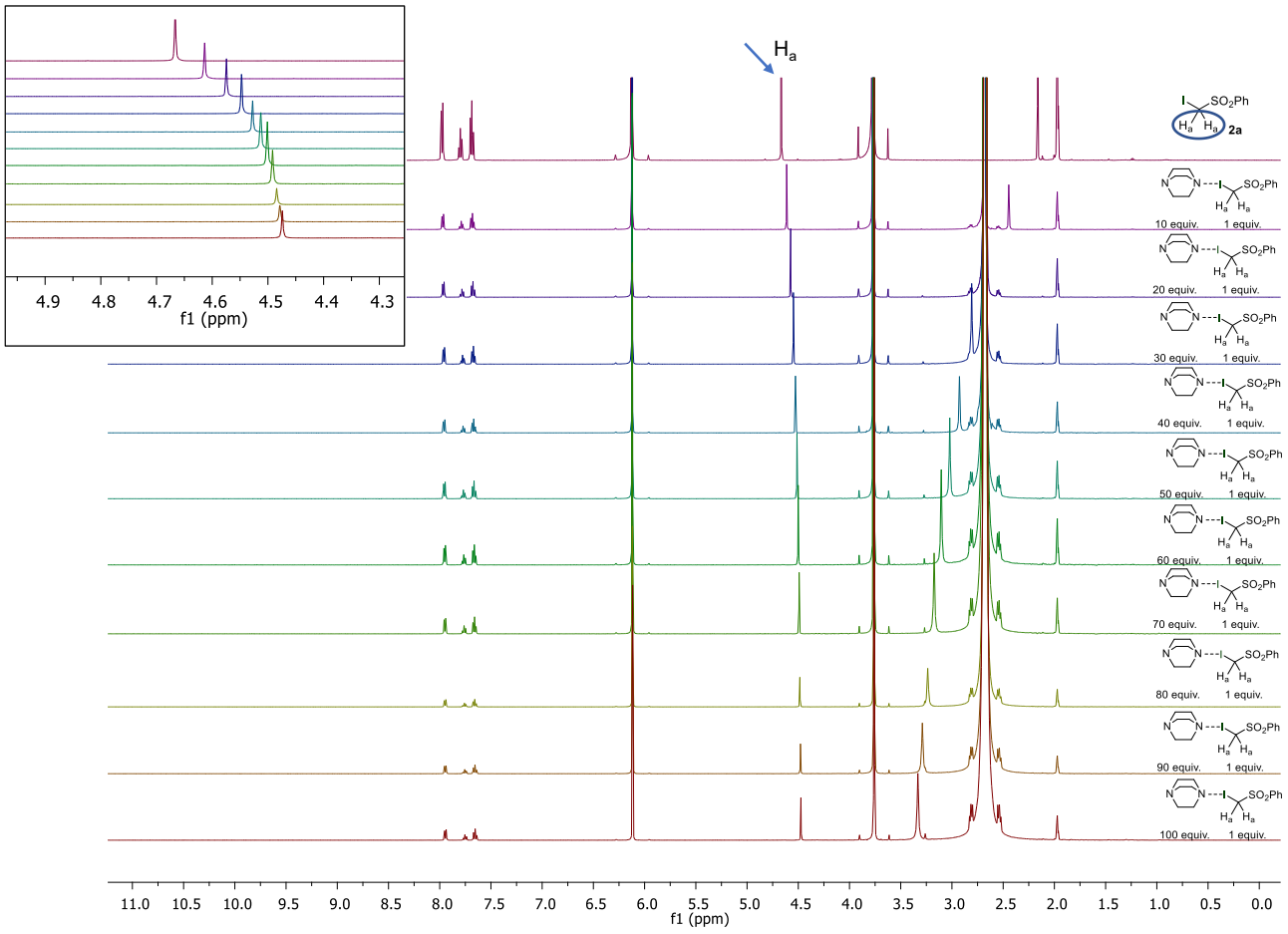

*Figure 4.9 ^{1}H-NMR spectra of titration between host **2a** and increasing quantity of DABCO until 100 equiv.*

^{19}F-NMR studies

Regarding the ^{19}F-NMR studies, a change to lower chemical shift of the diagnostic α-fluorine of **2d** was displayed upon addition of increasing amounts of DABCO, suggesting the presence of the halogen-bonding interaction. An important shift of the fluorine signal was observed confirming that the halogen-bonding interaction between **2a** and DABCO.

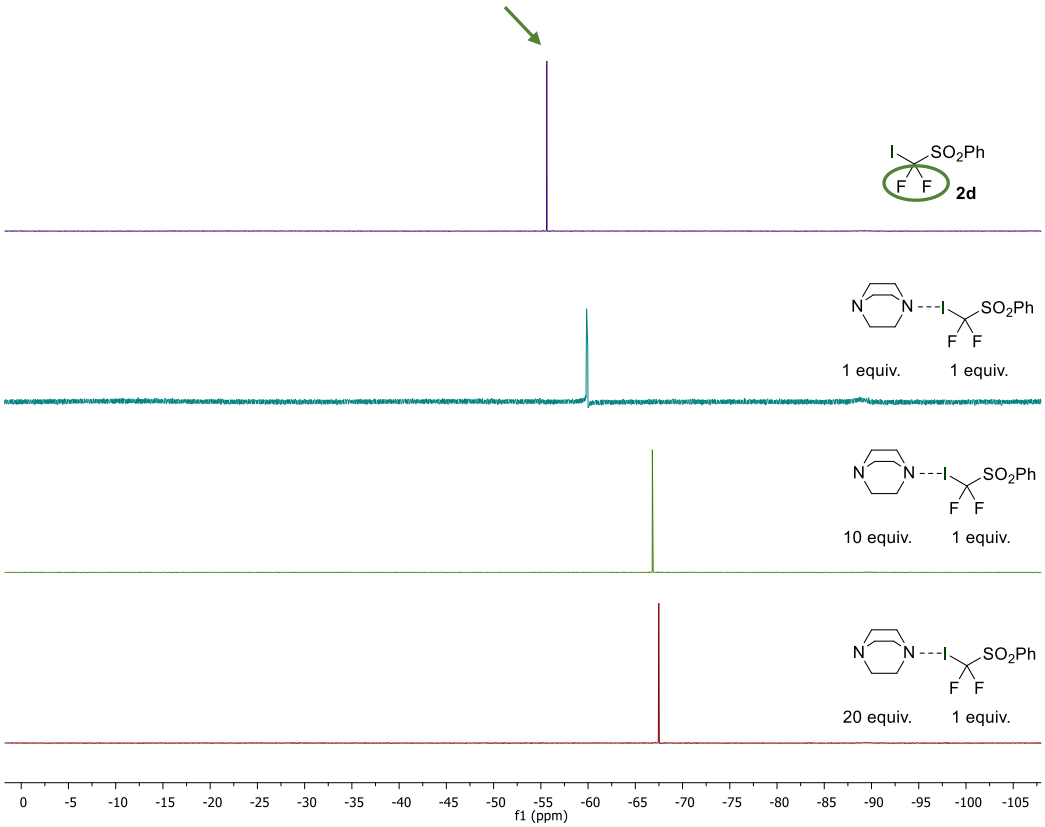

*Figure 4.10 ^{19}F NMR spectra of titration between host **2d** and increasing quantity of DABCO until 20 equiv.*

4.6 References Chapter 4

(1) Mamone, M.; Gentile, G.; Dosso, J.; Prato, M.; Filippini, G. Direct C2–H Alkylation of Indoles Driven by the Photochemical Activity of Halogen-Bonded Complexes. *Beilstein J. Org. Chem.* **2023**, *19*, 575–581. https://doi.org/10.3762/bjoc.19.42.

(2) Godula, K.; Sames, D. C-H Bond Functionalization in Complex Organic Synthesis. *Science* **2006**, *312* (5770), 67–72. https://doi.org/10.1126/science.1114731.

(3) Davies, H. M. L.; Morton, D. Recent Advances in C–H Functionalization. *J. Org. Chem.* **2016**, *81* (2), 343–350. https://doi.org/10.1021/acs.joc.5b02818.

(4) L. Davies, H. M.; Bois, J. D.; Yu, J.-Q. C–H Functionalization in Organic Synthesis. *Chemical Society Reviews* **2011**, *40* (4), 1855–1856. https://doi.org/10.1039/C1CS90010B.

(5) Zhang, L.; Ritter, T. A Perspective on Late-Stage Aromatic C–H Bond Functionalization. *J. Am. Chem. Soc.* **2022**, *144* (6), 2399–2414. https://doi.org/10.1021/jacs.1c10783.

(6) Yang, J. Transition Metal Catalyzed Meta-C–H Functionalization of Aromatic Compounds. *Org. Biomol. Chem.* **2015**, *13* (7), 1930–1941. https://doi.org/10.1039/C4OB02171A.

(7) Shang, W.; Sun, H.; Chen, W.; Liu, J. Diversification of Pharmaceutical Molecules via Late-Stage C(Sp2)–H Functionalization. *Green Synthesis and Catalysis* **2023**, *4* (2), 104–123. https://doi.org/10.1016/j.gresc.2022.12.007.

(8) Guillemard, L.; Kaplaneris, N.; Ackermann, L.; Johansson, M. J. Late-Stage C–H Functionalization Offers New Opportunities in Drug Discovery. *Nat Rev Chem* **2021**, *5* (8), 522–545. https://doi.org/10.1038/s41570-021-00300-6.

(9) Wencel-Delord, J.; Glorius, F. C–H Bond Activation Enables the Rapid Construction and Late-Stage Diversification of Functional Molecules. *Nature Chem* **2013**, *5* (5), 369–375. https://doi.org/10.1038/nchem.1607.

(10) He, J.; Wasa, M.; Chan, K. S. L.; Shao, Q.; Yu, J.-Q. Palladium-Catalyzed Transformations of Alkyl C–H Bonds. *Chem. Rev.* **2017**, *117* (13), 8754–8786. https://doi.org/10.1021/acs.chemrev.6b00622.

(11) Kuhl, N.; Hopkinson, M. N.; Wencel-Delord, J.; Glorius, F. Beyond Directing Groups: Transition-Metal-Catalyzed C□H Activation of Simple Arenes. *Angew Chem Int Ed* **2012**, *51* (41), 10236–10254. https://doi.org/10.1002/anie.201203269.

(12) Hartwig, J. F. Regioselectivity of the Borylation of Alkanes and Arenes. *Chem. Soc. Rev.* **2011**, *40* (4), 1992. https://doi.org/10.1039/c0cs00156b.

(13) Beck, E. M.; Hatley, R.; Gaunt, M. J. Synthesis of Rhazinicine by a Metal-Catalyzed C□H Bond Functionalization Strategy. *Angew Chem Int Ed* **2008**, *47* (16), 3004–3007. https://doi.org/10.1002/anie.200705005.

(14) Kar, S.; Sanderson, H.; Roy, K.; Benfenati, E.; Leszczynski, J. Green Chemistry in the Synthesis of Pharmaceuticals. *Chem. Rev.* **2022**, *122* (3), 3637–3710. https://doi.org/10.1021/acs.chemrev.1c00631.

(15) Bortolato, T.; Cuadros, S.; Simionato, G.; Dell'Amico, L. The Advent and Development of Organophotoredox Catalysis. *Chem. Commun.* **2022**, *58* (9), 1263–1283. https://doi.org/10.1039/D1CC05850A.

(16) Romero, N. A.; Nicewicz, D. A. Organic Photoredox Catalysis. *Chem. Rev.* **2016**, *116* (17), 10075–10166. https://doi.org/10.1021/acs.chemrev.6b00057.

(17) Yoon, T. P.; Ischay, M. A.; Du, J. Visible Light Photocatalysis as a Greener Approach to Photochemical Synthesis. *Nature Chem* **2010**, *2* (7), 527–532. https://doi.org/10.1038/nchem.687.

(18) Goti, G.; Manal, K.; Sivaguru, J.; Dell'Amico, L. The Impact of UV Light on Synthetic Photochemistry and Photocatalysis. *Nat. Chem.* **2024**, *16* (5), 684–692. https://doi.org/10.1038/s41557-024-01472-6.

(19) Shaw, M. H.; Twilton, J.; MacMillan, D. W. C. Photoredox Catalysis in Organic Chemistry. *J. Org. Chem.* **2016**, *81* (16), 6898–6926. https://doi.org/10.1021/acs.joc.6b01449.

(20) Marzo, L.; Pagire, S. K.; Reiser, O.; König, B. Visible-Light Photocatalysis: Does It Make a Difference in Organic Synthesis? *Angew. Chem. Int. Ed.* **2018**, *57* (32), 10034–10072. https://doi.org/10.1002/anie.201709766.

(21) Crisenza, G. E. M.; Mazzarella, D.; Melchiorre, P. Synthetic Methods Driven by the Photoactivity of Electron Donor–Acceptor Complexes. *J. Am. Chem. Soc.* **2020**, *142* (12), 5461–5476. https://doi.org/10.1021/jacs.0c01416.

(22) Yan, M.; Lo, J. C.; Edwards, J. T.; Baran, P. S. Radicals: Reactive Intermediates with Translational Potential. *J. Am. Chem. Soc.* **2016**, *138* (39), 12692–12714. https://doi.org/10.1021/jacs.6b08856.

(23) Rosokha, S. V.; Kochi, J. K. Fresh Look at Electron-Transfer Mechanisms via the Donor/Acceptor Bindings in the Critical Encounter Complex. *Acc. Chem. Res.* **2008**, *41* (5), 641–653. https://doi.org/10.1021/ar700256a.

(24) Lima, C. G. S.; De M. Lima, T.; Duarte, M.; Jurberg, I. D.; Paixão, M. W. Organic Synthesis Enabled by Light-Irradiation of EDA Complexes: Theoretical Background and Synthetic Applications. *ACS Catal.* **2016**, *6* (3), 1389–1407. https://doi.org/10.1021/acscatal.5b02386.

(25) Slama-Schwok, A.; Blanchard-Desce, M.; Lehn, J. M. Intramolecular Charge Transfer in Donor-Acceptor Molecules. *J. Phys. Chem.* **1990**, *94* (10), 3894–3902. https://doi.org/10.1021/j100373a007.

(26) Foster, R. Electron Donor-Acceptor Complexes. *J. Phys. Chem.* **1980**, *84* (17), 2135–2141. https://doi.org/10.1021/j100454a006.

(27) Kandukuri, S. R.; Bahamonde, A.; Chatterjee, I.; Jurberg, I. D.; Escudero-Adán, E. C.; Melchiorre, P. X-Ray Characterization of an Electron Donor–Acceptor Complex That Drives the Photochemical Alkylation of Indoles. *Angew Chem Int Ed* **2015**, *54* (5), 1485–1489. https://doi.org/10.1002/anie.201409529.

(28) Nappi, M.; Bergonzini, G.; Melchiorre, P. Metal-Free Photochemical Aromatic Perfluoroalkylation of α-Cyano Arylacetates. *Angew Chem Int Ed* **2014**, *53* (19), 4921–4925. https://doi.org/10.1002/anie.201402008.

(29) Arceo, E.; Jurberg, I. D.; Álvarez-Fernández, A.; Melchiorre, P. Photochemical Activity of a Key Donor–Acceptor Complex Can Drive Stereoselective Catalytic α-Alkylation of Aldehydes. *Nature Chem* **2013**, *5* (9), 750–756. https://doi.org/10.1038/nchem.1727.

(30) Marzo, L.; Wang, S.; König, B. Visible-Light-Mediated Radical Arylation of Anilines with Acceptor-Substituted (Hetero)Aryl Halides. *Org Lett* **2017**, *19* (21), 5976–5979. https://doi.org/10.1021/acs.orglett.7b03001.

(31) Zhang, H.-H.; Yu, S. Visible-Light-Induced Radical Acylation of Imines with α-Ketoacids Enabled by Electron-Donor–Acceptor Complexes. *Org. Lett.* **2019**, *21* (10), 3711–3715. https://doi.org/10.1021/acs.orglett.9b01169.

(32) Xie, S.; Li, D.; Huang, H.; Zhang, F.; Chen, Y. Intermolecular Radical Addition to Ketoacids Enabled by Boron Activation. *J. Am. Chem. Soc.* **2019**, *141* (41), 16237–16242. https://doi.org/10.1021/jacs.9b09099.

(33) Sun, X.; Wang, W.; Li, Y.; Ma, J.; Yu, S. Halogen-Bond-Promoted Double Radical Isocyanide Insertion under Visible-Light Irradiation: Synthesis of 2-Fluoroalkylated Quinoxalines. *Org. Lett.* **2016**, *18* (18), 4638–4641. https://doi.org/10.1021/acs.orglett.6b02271.

(34) Dewanji, A.; Van Dalsen, L.; Rossi-Ashton, J. A.; Gasson, E.; Crisenza, G. E. M.; Procter, D. J. A General Arene C–H Functionalization Strategy via Electron Donor–Acceptor Complex

Photoactivation. *Nat. Chem.* **2023**, *15* (1), 43–52. https://doi.org/10.1038/s41557-022-01092-y.

(35) Buzzetti, L.; Crisenza, G. E. M.; Melchiorre, P. Mechanistic Studies in Photocatalysis. *Angew Chem Int Ed* **2019**, *58* (12), 3730–3747. https://doi.org/10.1002/anie.201809984.

(36) Metrangolo, P.; Neukirch, H.; Pilati, T.; Resnati, G. Halogen Bonding Based Recognition Processes: A World Parallel to Hydrogen Bonding. *Acc. Chem. Res.* **2005**, *38* (5), 386–395. https://doi.org/10.1021/ar0400995.

(37) Bowman, W. R.; Storey, J. M. D. Synthesis Using Aromatic Homolytic Substitution—Recent Advances. *Chem. Soc. Rev.* **2007**, *36* (11), 1803. https://doi.org/10.1039/b605183a.

(38) Studer, A.; Bossart, M. Homolytic Aromatic Substitutions. In *Radicals in Organic Synthesis*; John Wiley & Sons, Ltd, 2001; pp 62–80. https://doi.org/10.1002/9783527618293.ch29.

(39) Mari, G.; De Crescentini, L.; Favi, G.; Santeusanio, S.; Mantellini, F. Metal and Oxidant Free Construction of Substituted- and/or Polycyclic Indoles: A Useful Alternative to Bischler and Related Syntheses. *European Journal of Organic Chemistry* **2020**, *2020* (33), 5411–5424. https://doi.org/10.1002/ejoc.202000845.

(40) Shao, C.; Shi, G.; Zhang, Y.; Pan, S.; Guan, X. Palladium-Catalyzed C–H Ethoxycarbonyldifluoromethylation of Electron-Rich Heteroarenes. *Org. Lett.* **2015**, *17* (11), 2652–2655. https://doi.org/10.1021/acs.orglett.5b01024.

(41) Madabhushi, S.; Jillella, R.; Sriramoju, V.; Singh, R. Oxyhalogenation of Thiols and Disulfides into Sulfonyl Chlorides/Bromides Using Oxone-KX (X = Cl or Br) in Water. *Green Chem.* **2014**, *16* (6), 3125–3131. https://doi.org/10.1039/C4GC00246F.

(42) Rosso, C.; Cuadros, S.; Barison, G.; Costa, P.; Kurbasic, M.; Bonchio, M.; Prato, M.; Dell'Amico, L.; Filippini, G. Unveiling the Synthetic Potential of Substituted Phenols as Fully Recyclable Organophotoredox Catalysts for the Iodosulfonylation of Olefins. *ACS Catal.* **2022**, *12* (8), 4290–4295. https://doi.org/10.1021/acscatal.2c00565.

(43) Cuadros, S.; Rosso, C.; Barison, G.; Costa, P.; Kurbasic, M.; Bonchio, M.; Prato, M.; Filippini, G.; Dell'Amico, L. The Photochemical Activity of a Halogen-Bonded Complex Enables the Microfluidic Light-Driven Alkylation of Phenols. *Org. Lett.* **2022**, *24* (16), 2961–2966. https://doi.org/10.1021/acs.orglett.2c00604.

(44) Filippini, G.; Silvi, M.; Melchiorre, P. Enantioselective Formal α-Methylation and α-Benzylation of Aldehydes by Means of Photo-organocatalysis. *Angew Chem Int Ed* **2017**, *56* (16), 4447–4451. https://doi.org/10.1002/anie.201612045.

(45) Nobile, E.; Castanheiro, T.; Besset, T. C–H Electrophilic (Phenylsulfonyl)Difluoromethylation of (Hetero)Arenes with a Newly Designed Reagent. *Chem. Commun.* **2021**, *57* (92), 12337–12340. https://doi.org/10.1039/D1CC04737J.

(46) Gu, Y.; Leng, X.; Shen, Q. Cooperative Dual Palladium/Silver Catalyst for Direct Difluoromethylation of Aryl Bromides and Iodides. *Nat Commun* **2014**, *5* (1), 5405. https://doi.org/10.1038/ncomms6405.

(47) Prakash, G. K. S.; Hu, J.; Wang, Y.; Olah, G. A. Nucleophilic Difluoromethylation of Primary Alkyl Halides Using Difluoromethyl Phenyl Sulfone as a Difluoromethyl Anion Equivalent. *Org. Lett.* **2004**, *6* (23), 4315–4317. https://doi.org/10.1021/ol048166i.

(48) Mi, X.; Kong, Y.; Zhang, J.; Pi, C.; Cui, X. Visible-Light-Promoted Sulfonylmethylation of Imidazopyridines. *Chinese Chemical Letters* **2019**, *30* (12), 2295–2298. https://doi.org/10.1016/j.cclet.2019.09.040.

Chapter 5.

A Logic Approach to the Photopermutation Reaction of Indazoles to Benzimidazoles

Abstract

The following chapter describes the study of the photopermutation reaction of indazole derivatives to easily afford the corresponding benzimidazoles. Few works reported the photochemical behaviour of five-membered heterocyclic compounds and their tendency to rearrange under Hg high pressure lamp. Starting from this, we first carried out an in-depth optimization of the reaction conditions for the benzimidazole formation under UV light. Subsequently, we assessed the generality of this methodology by investigating the impact of the indazole substituents on the reactivity, thus providing a comprehensive study of the generality of the photopermutation on indazoles.

This work was conducted in the Leonori group during the four-month research period at the RWTH University of Aachen. The project was supervised and conceived by *Prof. Daniele Leonori. Dr Thiago Dos Santos* and *Dr Cornelia Büttner* performed the optimization experiments and collaborated in the photochemical reactions.

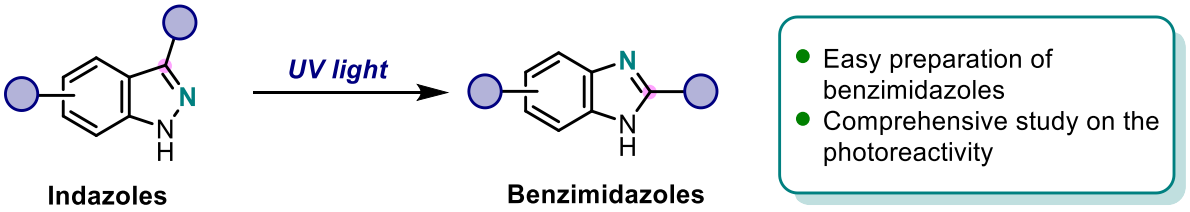

5.1 Introduction

5.1.1 Nitrogen Containing Cyclic Compounds

Heterocyclic compounds have garnered increasing attention in synthetic chemistry due to their significant roles across various chemical domains ranging from biomedical to pharmaceutical applications.[1,2] The structure of heterocyclic compounds is demonstrated to have a great influence in aspects such as target recognition and pharmacokinetic, thus they can be defined “privileged scaffolds”. Indeed, heterocyclic moieties are present in over ninety of the top 100 most frequently used cyclic scaffolds in small drugs listed in the FDA's Orange Book.[3] Specifically, nitrogen containing heterocycles, such as pyrimidine (ranked 11), imidazoline (ranked 13), and benzimidazole (ranked 22), are widely represented in a variety of available pharmaceuticals. A critical challenge in medicinal chemistry is to accelerate the synthetic processes for obtaining heterocyclic derivatives, facilitating quicker access to potential hit molecules for medicinal applications.[4–6] Therefore, the demand for accessible heterocyclic compounds, particularly five-membered rings containing nitrogen atoms, is pivotal in drug discovery.

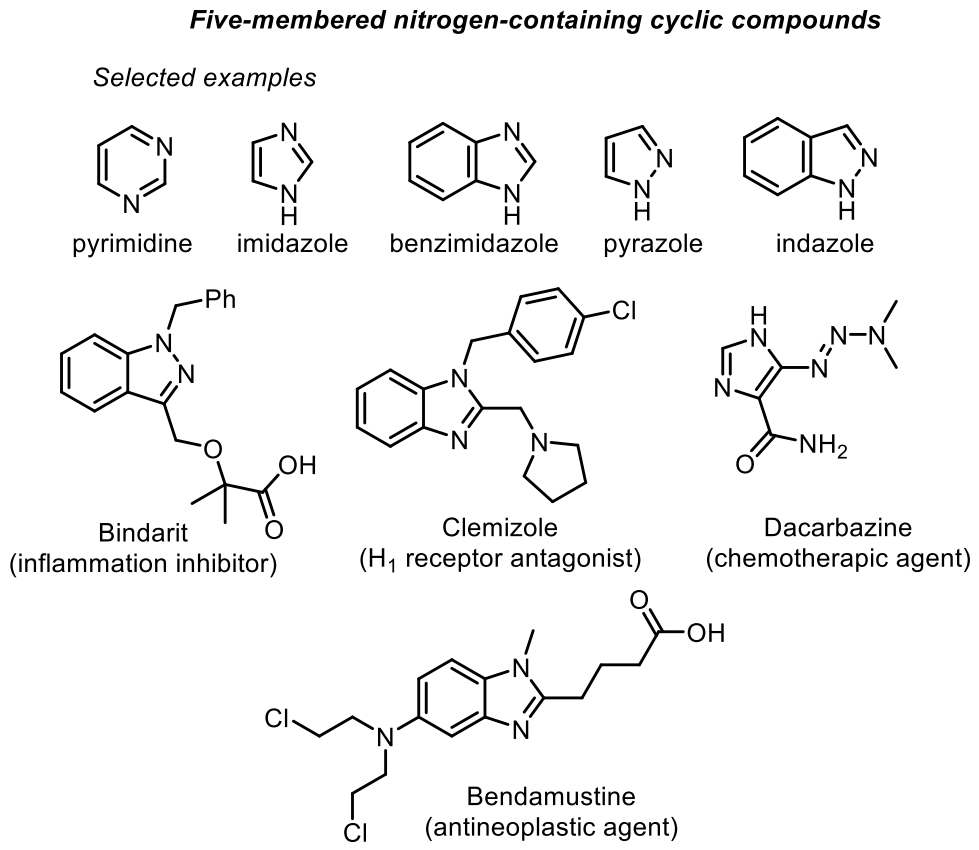

Figure 5.1 Selected five-membered nitrogen containing compounds and examples of pharmaceutic molecules

Generally, synthesizing nitrogen containing heterocycles involves multi-step preparations of suitable functionalized precursors and subsequent reactions. In literature, these synthetic processes are often described as time-consuming, involving toxic reagents or harsh reaction conditions.[4,5] Although strategies based on transition metal-catalysed C–H activation or radical intermediates have significantly simplified these synthetic efforts, they still require directing groups for targeting functionalization.[6] For example, almost all reported syntheses of benzimidazoles employ benzene derivatives possessing ortho di nitrogen atoms as starting materials, which undergo condensation reaction with carboxylic acids by heating at high temperature in toxic solvents.[7,8] The preparation of bendamustine (Figure 5.1), an approved antineoplastic agent, containing the benzimidazole scaffold, requires more than six synthetic steps, starting from nitroaniline, including hydrogenations and reflux with HCl.[9]

Among the nitrogen containing heterocycles, the structure of benzimidazole along with imidazole moiety, stands out as notable five-membered heterocycles essential to many natural products and synthetic compounds.[10] The electron-rich nature of imidazole-based derivatives allows for versatile binding with various receptors and enzymes, thereby showing broad biological activity. Indeed, several imidazole-based molecules (*e.g.* Bindarit, dacarbazine, and clemizole, depicted in Figure 5.1), exhibit high therapeutic potency and antifungal properties.[11] Therefore, new economically viable and environmentally sustainable methods are now under investigation to develop protocols for the large production of benzimidazoles or similar nitrogen containing cyclic compounds. Photochemical reactions may provide a valuable tool for delivering the desired products under mild reaction conditions.[12] Several studies have explored the photochemical behaviour of various nitrogen containing cyclic compounds, including pyrazoles, benzisoxazoles, thiazoles, and indazoles, revealing significant potential for further exploration in this field.

5.1.2 Photochemical Rearrangement Reaction on Five-Membered Heterocycles

In light of the recent interest in photochemical strategies aimed at minimizing multi-step procedures, and complex synthetic designs, rearrangement reactions promoted by light appear an interesting synthetic tool.[13] Since the mid-twentieth century, many scientists have recognized the potential of energy derived from light irradiation to affect a variety of compounds. The alteration of electronic configurations of the irradiated compounds leads to the cleavage and formation of novel chemical bonds, resulting in the migration of one or more atoms inside the molecules to gain the rearranged product.[14–16] Usually, energy transfer process can initiate these rearrangements by exploiting the

energy of the excited species. As an example, in the family of nitrogen containing five-membered cyclic compounds, the pyrazole scaffold can be transformed into the imidazole one by migration of nitrogen. Thereby, photochemical rearrangements may provide one-step synthesis for complex novel molecules. Indeed, considerable attention has been focused in the past years on the photochemistry of five-membered heterocycle ring systems. An interesting essay has identified five distinct mechanistic pathways for the photoisomerization of five-membered heterocycles.[17] The mechanisms are described as follows:

Mechanism I begin with the homolytic cleavage of the weakest bond upon light irradiation of the cyclic compound (Figure 5.2a). The resulting biradical species undergo the formation of a three-membered ring, which is in equilibrium with its rearranged product. The photostability of the species significantly affects the formation of the final isomer. This pathway, called “ring contraction-ring expansion”, is commonly proposed for many photochemical rearrangements involving cyclic compounds with two heteroatoms.

Another notable pathway is the “internal cyclization-isomerization” pathway (mechanism II) involving an initial disrotatory formation of a bicyclic isomer, followed by a [1,3] sigmatropic shift (Figure 5.2b). Then, a disrotatory ring-opening takes place affording the rearranged product. Importantly, the [1,3] sigmatropic shift may occur twice, potentially yielding a second product following the disrotatory electrocyclic reaction. However, the selectivity of the different isomer product depends on the photostability of the bicyclic intermediates.

A third general mechanistic proposal for all five-membered ring compounds is known as the Van Tamelen-Whitesides mechanism. This pathway initiates with the cleavage of the weakest single bond, forming a three-membered ring species depicted in Figure 5.2c. This intermediate may generate the five-membered ring isomer, as discussed in Mechanism I, while simultaneously establishing an equilibrium with the bicyclic isomer, leading to the formation of another isomer as a secondary product of photoisomerization.

Mechanism IV specifically addresses the photochemical rearrangements of the thiophene ring system. This mechanism proposes that the 3d orbitals of sulphur interact with the neighbouring double bond to yield a tricyclic zwitterion, which subsequently collapses into the rearranged product (Figure 5.2d).

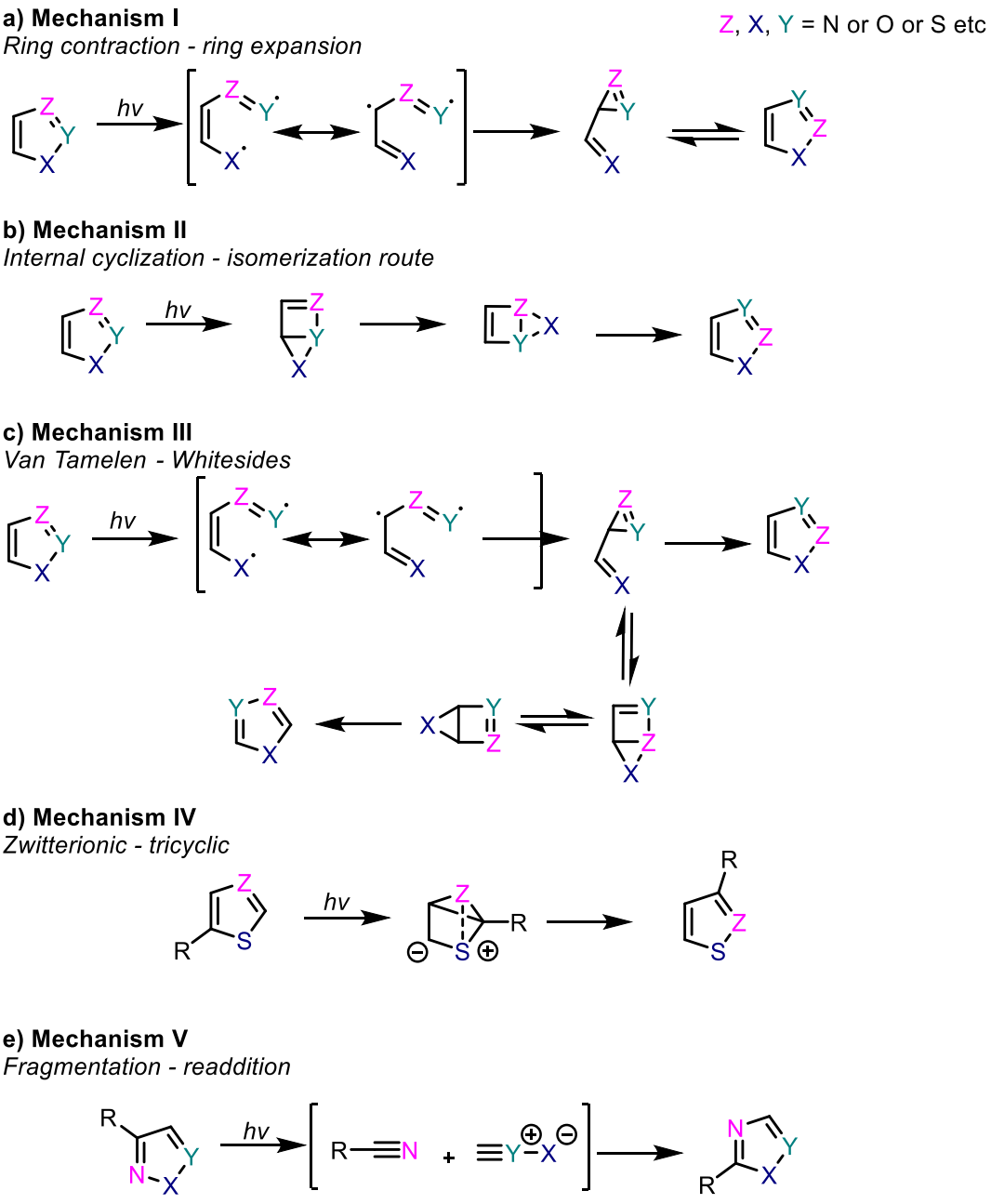

Figure 5.2 Mechanistic possibilities for photoisomerizations of five-membered heterocycles

Finally, mechanism V focuses on heterocyclic compounds containing at least one nitrogen atom, described as the "fragmentation-readdition" route (Figure 5.2e). Under light irradiation, the starting material is fragmented into a nitrile molecule and corresponding 1,3-dipole substrate. This allows the intermediates to rearrange into a new isomer.

In summary, these pathways illustrate how heteroaromatic compounds, upon light irradiation, can transform into (*i*) biradical species through cleavage of the weakest bond and (*ii*) bicyclic isomers via

internal cyclization. However, identifying the correct pathway remains a challenging issue in the field. Various studies have attempted to clarify the photochemical rearrangements of nitrogen containing five-membered cyclic compounds. Notable efforts were spent on the photoactivity of pyrazole moiety, which plays a key role in biologically active chemistry.

One of the first studies addressing the photostability of pyrazole scaffold and the formation of structural isomers was conducted by Schmid and colleagues in 1964.[18] They reported the formation of benzimidazole, using Hg high pressure lamp, from the respective indazole (Figure 5.3a). Additionally, they tested indazoles with methyl substituent in 3-, 4-, 5-, 6-, 7-position, yielding the corresponding products in low yields (10-22%). They noticed the impact of the substituent on the yields of products, albeit modest.

The same authors continued the investigation on this promising topic. In the work of 1967, they performed experiments with indazoles led to the identification of the side product *ortho*-aminobenzonitrile, likely arising from the biradical intermediate described in Mechanism I. Meanwhile, they studied also the photoisomerization of pyrazole compounds. They analysed the effects of temperature, type and concentration of the reaction solvent on the photopermutation of pyrazoles (Figure 5.3b).[19] Although their results did not yield definitive conclusions, they observed significant influences of the studied reaction parameters on product yields.

A few years later, Messer and Beak proposed a pathway for the formal photorearrangement of 1,4-dimethylimidazole.[20] They explained that the photoisomerization of various substituted *N*-methylimidazoles under a Hg high pressure lamp proceeds via a cascade of ring contraction and ring expansion (mechanism II), ultimately yielding the corresponding *N*-methylimidazole isomer. As illustrated in Figure 5.3c, the formation of the three-membered ring and the subsequent interchange of adjacent ring atoms lead to the reformation of five-membered heterocyclic compounds.

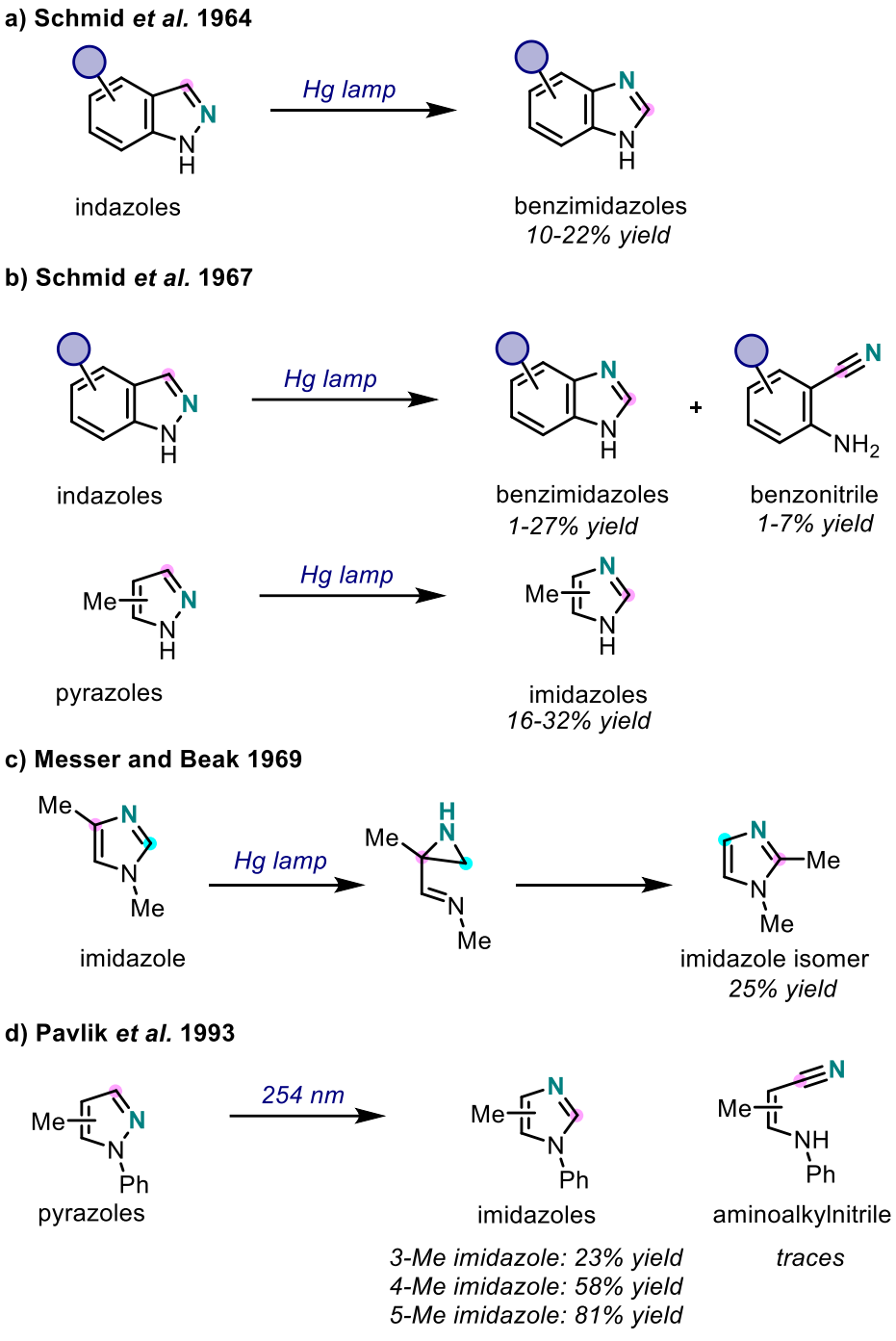

Figure 5.3 Examples of photopermutations of pyrazole and indazole to afford imidazole and benzimidazole respectively

Pavlik significantly contributed to the field of five-membered heterocyclic permutations in the late twentieth century.[21–23] In a notable work, Pavlik and colleagues conducted a detailed analysis of the photopermutation of 1-phenylpyrazole and its 3-, 4-, and 5-methyl derivatives under a 254 nm lamp (Figure 5.3d).[21] They notably observed the substantial influence of methyl substituents on the yields of the corresponding imidazole products. Specifically, the 3-methyl-1-phenylimidazole was

generated in 23% yield while the one of 5-methyl substituted was 81%. Furthermore, the mechanistic analysis revealed that these reactivities were attempted by the energy transfer process. Moreover, the formation of aminoalkylnitrile was detected in trace amounts, providing further insight into the proposed "ring contraction-ring expansion" mechanism. Later studies on CF_3-substituted pyrazoles detected photoisomerization reactivity via the internal "internal cyclization-isomerization" pathway, underscoring the critical impact of substituents on the pyrazole scaffold.

In conclusion, the existing literature in this field is limited and often unclear. Moreover, the examples studied are not exhaustive, lacking a cohesive view of the reactivity and its advantages in synthetic chemistry.

5.2 Aim of the Project

Historically, photoinduced rearrangements of heteroaromatic compounds have attracted significant interest, even if the knowledge of the subject remains unclear. In particular, photopermutation of indazoles **1** provided an efficient pathway to easily prepare valuable substituted benzimidazole derivatives **2** in one synthetic step. Therefore, we aimed to investigate the photopermutation of various indazoles to address these gaps. Our goal is to overcome several limitations associated to the synthesis of pharmaceutical valuable benzimidazoles, such as harsh reaction conditions and limited scope.

To do this, we conducted a detailed study of the optimal conditions for the photorearrangements, along with a comprehensive investigation of the scope of the reaction.

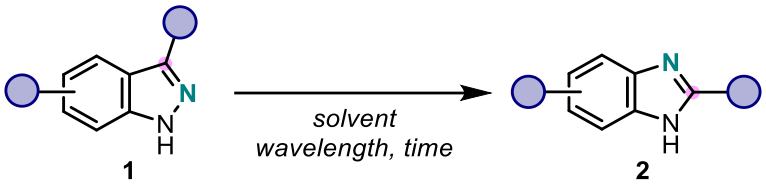

Figure 5.4 Study of the permutation of indazole derivates to overcome the strategy limitations

5.3 Results and Discussion

In previous reports it was shown that heterocyclic compounds 1H- and 2H-indazoles are unstable under UV light irradiation at around 90°C, thus generating the rearranged benzimidazole compounds.

Based on these reports, we chose 3-methyl-1H-indazole as model compound **1a** to investigate its behaviour under UV light irradiation. Preliminary results attested the formation of 2-methyl-1H-

benzimidazole as the main product from the corresponding indazole upon irradiation at 300 nm. Instead, the reaction under 254 nm UV light displayed several by-products.

*Table 5.1 Optimization study of the photopermutation of indazole **1a***

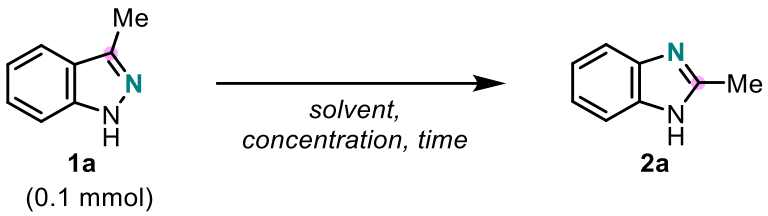

Entry	Wavelength (nm)	Solvent [M]	Time (h)	Yield **2a**[a] [%]	rsm[a] [%]
1	300	Methanol [0.05]	16	20	78
2	300	Isopropanol [0.05]	16	21	53
3	300	Isobutanol [0.05]	16	n.d.	80
4	300	H_2O [0.05]	16	n.d.	95
5	300	TFE [0.05]	16	27	71
6	300	HFIP [0.05]	16	86	n.d.
7	300	EtOAc [0.05]	16	7	93
8	300	Toluene [0.05]	16	n.d.	90
9	300	MeCN [0.05]	16	5	91
10	300	HFIP [0.025]	16	81	8
11	300	HFIP [0.075]	16	84	11
12	300	HFIP [0.1]	16	71	25
13	300	HFIP [0.2]	16	69	27
14	300	HFIP [0.05]	8	54	45
15	300	HFIP [0.05]	12	67	31

[a] Yield determined by ^{1}H-NMR spectroscopy using 1,3-dinitrobenzene as the internal standard. rsm: remaining starting material; HFIP: hexafluoroisopropanol; TFE: 2,2,2-Trifluoroethanol.

Starting from this result, we carried out an in-depth optimization of the three reaction conditions, namely solvent, concentration and time, under 300 nm light irradiation. Initially, different solvents were tested with the same concentration of **1a** (0.05 M). The photorearrangement using protic and polar solvents (Table 5.1, Entries 1-5) showed traces of **2a** but a large amount of remaining starting

material (rsm). Since carrying out the reaction in 2,2,2-Trifluoroethanol (TFE) slightly improved the yield (Table 5.1, Entry 5), the solvent hexafluoroisopropanol (HFIP), with a longer fluoroalcohol chain, was tested. Remarkably, we achieved product **2a** in 86% yield using HFIP (Table 5.1, Entry 6). Furthermore, no formation of **2a** was detected employing toluene and ethyl acetate (EtOAc) as non-polar and aprotic solvents. The same outcome was obtained with acetonitrile. Considering that HFIP gave the best results in terms of yield, we then evaluated the influence of the concentration of **1a** on the reaction. Therefore, reactions in HFIP at 0.025, 0.075, 0.1 and 0.2 M were performed (Table 5.1, Entries 10-14). We found out that 0.05 M was the optimal concentration of HFIP for the reaction, noticing a decrease in the yield of **2a** with the rise in the concentration. Finally, a short screening of the time of the photopermutation revealed lower conversation of **1a** at 8 and 12 h, thus confirming 16 h as the best time for the transformation (Table 5.1, Entry 6). After the optimization of the reaction conditions, we moved to prove the generality of the reactivity.

Indazole **1b** photopermutated smoothly affording 28% yield of benzimidazole **2b**. Reactions with substituents at 1N position of indazoles, such as methoxymethyl ether (MOM) or *tert*-butyloxycarbonyl (Boc), did not provide satisfactory results. Unfortunately, the same outcome was observed with *N*-functionalised indazoles with methyl in position 3 (**2e**-**2f**). Thus, these results indicated the lack of reactivity for indazoles with functional groups at the 1N position. Notably, indazoles with alkyl substituents at position 3 gave the corresponding benzimidazoles **2g**-**2i** in excellent yields (up to 99%). On the contrary, methyl ester group was not tolerated by this strategy resulting in almost rsm. By these results, we noticed that position 3 of the reactive indazoles needs an adjacent aliphatic carbon to yield the corresponding benzimidazoles. Accordingly, indazoles containing ester or alcohol in β position, led to the corresponding products in good yields (**2k**-**2l**).

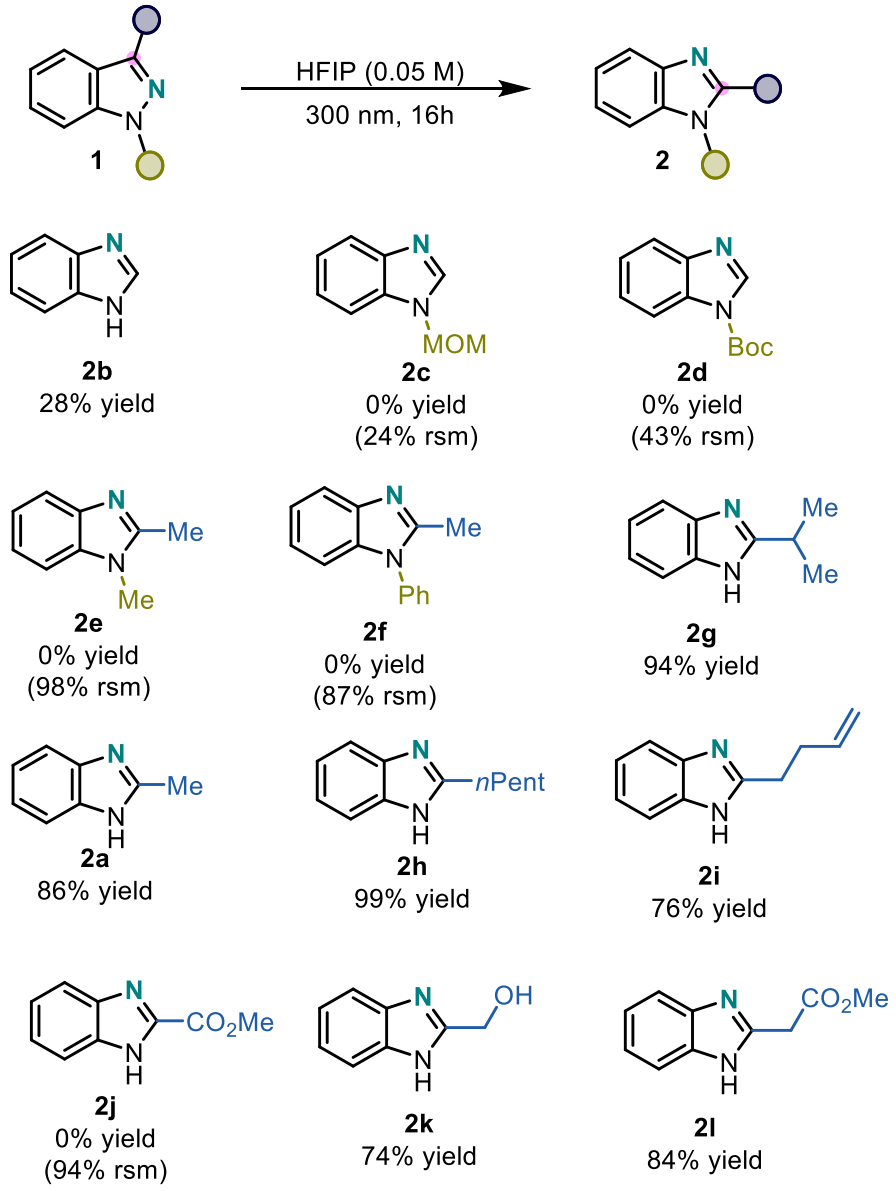

*Figure 5.5 Preliminary photopermutation reactions on indazole derivatives **1***

Considering these unsatisfying preliminary results, we reasoned that the type of substituents greatly influences the reactivity. Consequently, a series of designed experiments on photopermutations were carried out to study the effects of the different indazole substituents on the yields of the corresponding products. Hence, Figure 5.6 displayed the results of these experiments by delivering an extensive guideline to logically comprehend the reactivity. In particular, the photopermutations were performed on the model 3-methylindazole bearing, for each position, the following functional groups: methyl, phenyl, methyl ether, halogens (F, Cl, Br). The yields illustrated in Figure 5.6 correspond to the final benzimidazole derivatives.

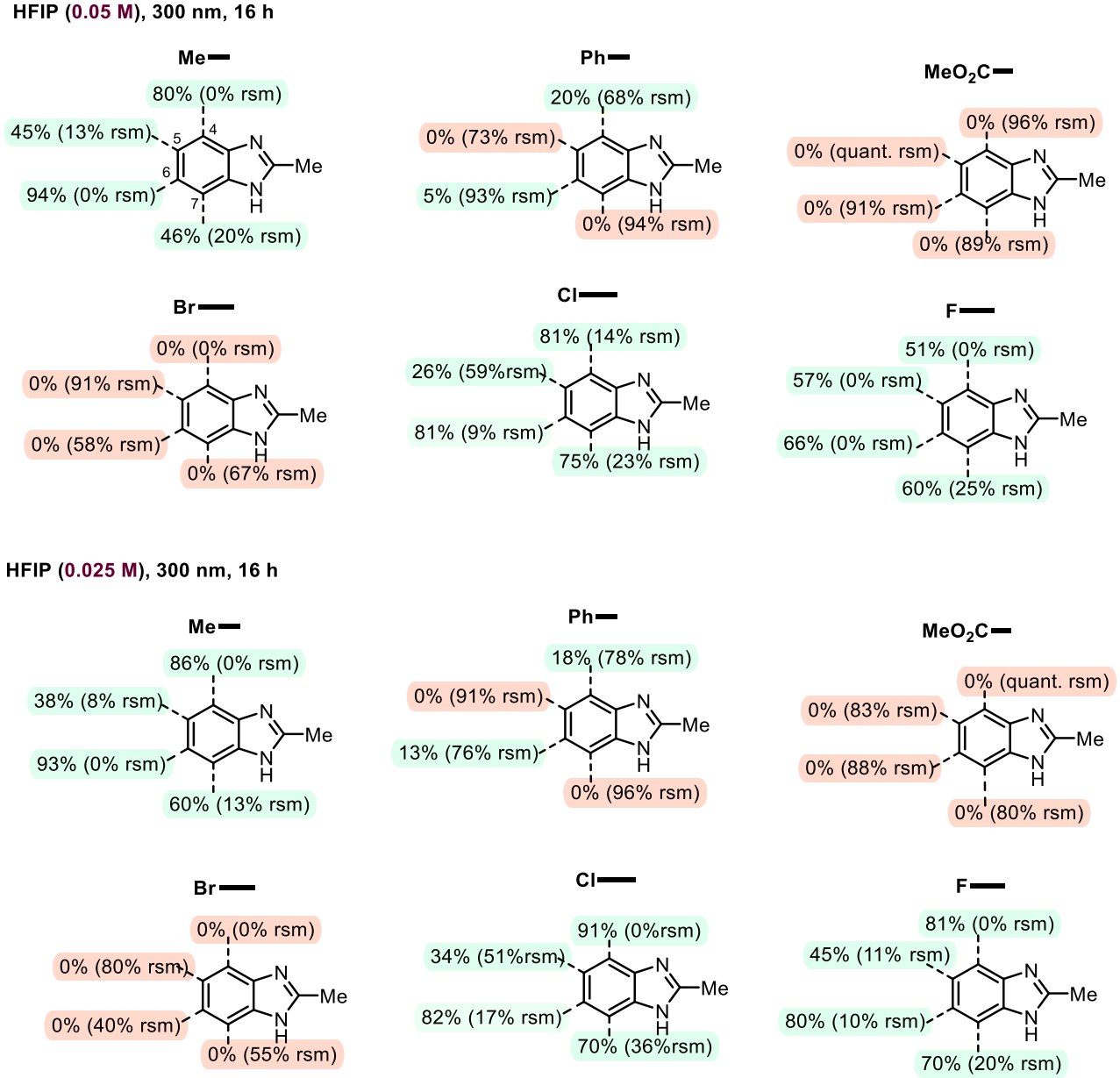

Figure 5.6 Guideline for substitution pattern indazoles containing yields of benzimidazole products

Initially, we investigated the influence on the yields of **2** using indazoles bearing methyl group at each position of the phenyl ring in 0.05M of HFIP. The corresponding benzimidazoles were achieved in very good yields: methyl group in positions 4 and 6 exhibited higher yields (up to 94%) compared to the ones with methyl in positions 5 and 7 (up to 46%). Similar results in terms of yields were obtained in a more diluted solution. Based on these tests, substituents in positions 4 and 6 activate strongly the substrates for the photorearrangements while positions 5 and 7 show reduced yields and remaining starting materials. This attitude was detected also for the substrates with phenyl

functionality. Phenyl ring in positions 4 and 6 accessed to low yields of corresponding benzimidazoles, while only starting material was recovered for indazoles with positions 5 and 7 occupied. Unfortunately, we did not observe any formation of products using indazoles with methyl ester or bromide moieties on the positions from 4 to 7. Pleasantly, indazoles bearing halogen substituents -F and -Cl in each position of the aromatic ring under 300 nm irradiation, delivered the respective benzimidazoles with remarkable results. Even in this case, the positions 4 and 6 were the more activating positions for the photopermutations, thus displaying an increased yield of the desired products.

From the guidelines outlined in Figure 5.6, several key aspects of the photochemical rearrangement of indazoles emerge. Firstly, the selectivity to achieve the desired benzimidazoles, based on their yields, depends on the type of substituents on the indazole back ring. The indazole substitutions presumably have an impact on their photostability making them low reactive if their photostability rises. The final high percentage of rsm may prove this logic, for instance using indazoles bearing methyl ester. On the other hand, low amount of both product and rsm indicated photodegradation of the reagents, notably among those Br substituted indazoles. Remarkably, the presence of functional groups at positions 4 or 6 consistently enhanced the product yields. Furthermore, we observed that the concentration of the HFIP strongly influenced the reaction outcomes in most cases.

Subsequently, considering the promising results of photopermutations on methyl substituted indazoles, we expanded the scope using different aliphatic groups on the indazole scaffold.

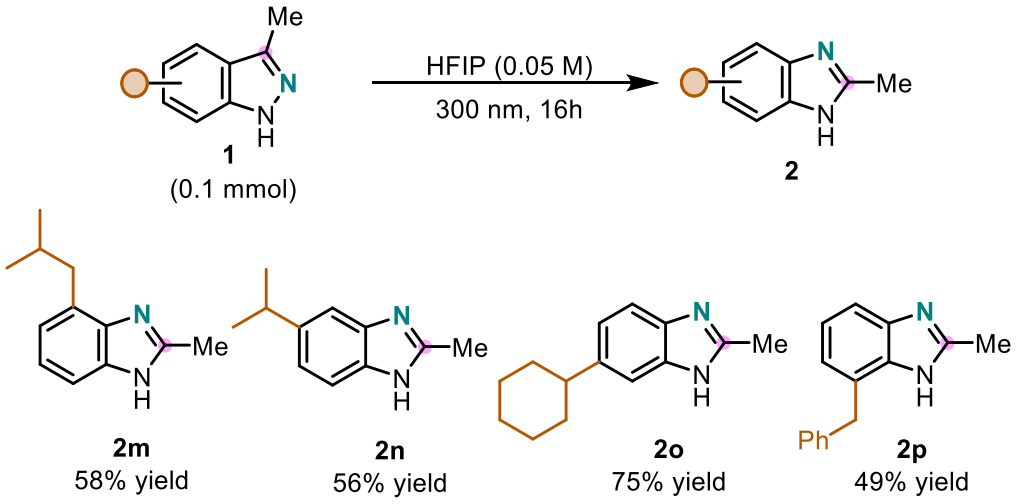

*Figure 5.7 Scope study of the photopermutation on the alkyl functionalised indazoles **1** based on the guideline table*

Once we optimised the synthesis of different indazoles, bearing secondary and tertiary aliphatic groups, following a cross-coupling reaction (details in section 5.5.2), we then evaluated their reactivity. In Figure 5.7, 4-isobutylindazole underwent photopermutation to provide product **2m** in 58% yield. Secondary alkyl substituted indazoles **1n**-**1o** reacted smoothly to afford the corresponding desired products bearing isopropyl or cyclohexyl groups in good yields (up to 75%). Furthermore, benzyl moiety in position 7 was well tolerated, while previous experiments on 7-phenylindazole did not provide any formation of the corresponding product.

5.4 Conclusion

A comprehensive study on the photopermutation reaction of indazole derivatives was accomplished. The radical process involving indazoles successfully provides benzimidazole products under UV light irradiation, achieving yields ranging from moderate to excellent (up to 99%). Specifically, we thoroughly investigated and optimized the photopermutation process paying particular attention to the effects of substituents on the scaffold of the indazole. Therefore, a series of photopermutations were carried out and summarized in a guideline table to proceed with a logic approach to the study of the reaction scope. As future perspective, detailed mechanistic studies will be carried out as well as additional examples of photopermutation involving pharmaceutical targets.

5.5 Experimental Section

5.5.1 General Information

All required fine chemicals were used directly without purification unless stated otherwise. All air and moisture sensitive reactions were carried out under nitrogen atmosphere using standard Schlenk manifold technique. All solvents were bought from Acros as 99.8% purity and degassed by N_2 bubbling. ^{1}H and ^{13}C Nuclear Magnetic Resonance (NMR) spectra were acquired at various field strengths as indicated and were referenced to $CDCl_3$ (7.27 and 77.16 ppm for 1H and 13C respectively). ^{1}H-NMR coupling constants are reported in Hertz and refer to apparent multiplicities and not true coupling constants. The spectra measurements were specified when decoupled (e.g., $^{19}F\{^{1}H\}$). Data are reported as follows: chemical shift, integration, multiplicity (s = singlet, br s = broad singlet, d = doublet, t = triplet, q = quartet, qi = quintet, sx = sextet, sp = septet, m = multiplet, dd = doublet of doublets, etc.), proton assignment (determined by 2D NMR experiments: COSY, HSQC and HMBC) where possible. High-resolution mass spectra were obtained using a JEOL JMS-700 spectrometer or a Fissions VG Trio 2000 quadrupole mass spectrometer. Spectra were obtained using electron impact ionization (EI) and chemical ionization (CI) techniques, or positive electrospray

(ESI). Analytical TLC: aluminum backed plates pre-coated (0.25 mm) with Merck Silica Gel 60 F254. Compounds were visualized by exposure to UV-light or by dipping the plates in permanganate (KMnO4) stain followed by heating. Flash column chromatography was performed using Merck Silica Gel 60 (40–63 µm). All mixed solvent eluents are reported as v/v solutions. Reactions were run in a RPR-200 Rayonet reactor using 300 nm light, with a fan placed above the photoreactor. No stirrer bars were added to the reaction mixtures. All the reactions were conducted in CEM 9 mL glass microwave tubes capped with a LABSOLUTE crimp seal with septum (PTFE/butyl) purchased from Th. Geyer.

5.5.2 General Procedures for the Preparation of Indazoles

PREPARATION OF 5-ALKYL-3-METHYL-1*H*-INDAZOLE

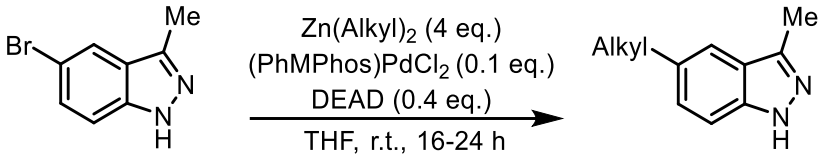

To a solution of 5-bromo-3-methyl-1*H*-indazole (211 mg, 1 mmol, 1 eq.) and [1,1'-bis(diphenylphosphino)ferrocene]dichloropalladium complex (73 mg, 0.1 mmol, 0.1 eq.) in dry THF (15 mL) *N*,*N*-dimethylethanolamin (26 µL, 0.2 mmol, 0.2 eq.) and a dialkyl zinc solution (2.0 mmol, 2 eq.) was added under argon. The yellow solution was stirred for 1 h. Then additional *N*,*N*-dimethylethanolamin (0.2 eq.) and dialkyl zinc solution (2 eq.) were added and the mixture were heated to 60°C. After 16-24 h at 60°C the solution was quenched with a saturated ammonium chloride solution. The layers were separated, and the aqueous layer was extracted with ethyl acetate (3 x 50 mL). The combined organic layers were dried ($MgSO_4$), filtered and evaporated. Purification by flash column chromatography on silica gel gave the products.[24]

Characterization data

3,5-dimethyl-1H-indazole

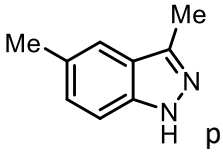

Following the general procedure for 24 h, 5-bromo-3-methyl-1H-indazole (424 mg, 2 mmol) and $Zn(Me)_2$ (2.0 M in toluene, 2 x 1 mL, 2 x 2 mmol) gave, after purification by column chromatography on silica gel eluting with Pentane–EtOAc (9:1 to 6:4), 3,5-dimethyl-1H-indazole (198 mg, 68%) as a solid. R_f 0.25 [Petroleum ether:EtOAc (4:1)].

^{1}H-NMR (600 MHz, $CDCl_3$) δ 7.44 (1H, s), 7.32 (1H, d, *J* =8.5 Hz), 7.21 (1H, d, *J* =8.5 Hz), 2.56 (3H, d, *J* =1.7 Hz), 2.47 (3H, s). **^{13}C-NMR (151 MHz, $CDCl_3$)** δ 143.1, 139.1, 129.8, 128.9, 123.3, 119.4, 109.4,

21.4, 12.1. **HRMS** (ESI): Found MH^+ 147.0917, $C_9H_{11}N_2$ requires 147.0917.

5-isopropyl-3-methyl-1H-indazole (1n)

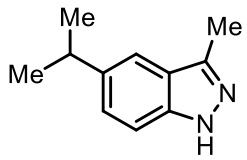

Following the general procedure for 16 h, 5-bromo-3-methyl-1H-indazole (212 mg, 1 mmol) and Zn(*i*Pr)$_2$ (1.0 M in toluene, 2 x 2 mL, 2 x 4 mmol) gave, after purification by column chromatography on silica gel eluting with DCM–EtOAc (9:1 to 8:2), 5-isopropyl-3-methyl-1H-indazole (173 mg, 99%) as a solid. R_f 0.22 [DCM:EtOAc (4:1)].

^{1}H-NMR (600 MHz, $CDCl_3$) δ 9.77 (1H, br s), 7.48 (1H, s), 7.35 (1H, d, *J* = 8.6 Hz), 7.29 (1H, dd, *J* = 8.6, 1.6 Hz), 3.04 (1H, p, *J* = 6.9 Hz), 2.59 (3H, s), 1.32 (6H, d, *J* = 7.0 Hz). **^{13}C-NMR (151 MHz, $CDCl_3$)** δ 143.1, 141.0, 139.9, 126.5, 122.9, 116.4, 109.4, 34.0, 24.4, 11.9. **HRMS** (ESI): Found MH^+ 175.1230, $C_{11}H_{15}N_2$ requires 175.1229.

PREPARATION OF ALKYL SUBSTITUTED 3-METHYL-1*H*-INDAZOLE

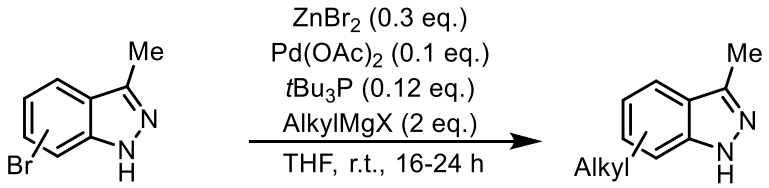

To a solution of bromo-3-methyl-1*H*-indazole (211 mg, 1 mmol, 1 eq.) and tri-tert-butylphosphonium tetrafluoroborate (0.12 mmol, 35 mg, 0.12 equiv) in dry THF (2 mL) under N_2 were added $Pd(OAc)_2$ (0.1 mmol, 23 mg, 0.1 equiv) and zinc bromide anhydrous (67 g, 0.3 mmol, 0.3 equiv). Grignard reagent (2 mmol, 2 equiv) was added slowly over 30 min at room temperature. The reaction mixture was stirred for an additional 16-24h and monitored by GCMS. The crude was cooled to 0 °C, and water (10 mL) was added slowly. The layers were separated, and the aqueous layer was extracted with ethyl acetate (3 x 50 mL). The combined organic layers were dried ($MgSO_4$), filtered and evaporated. Purification by flash column chromatography on silica gel gave the products.[25]

Characterization data

4-isobutyl-3-methyl-1H-indazole (1m)

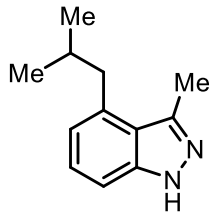

Following the general procedure for 24h, 4-bromo-3-methyl-1H-indazole (212 mg, 1 mmol) and *i*BuMgBr (1.0 M in THF, 2 mL, 2 mmol) gave, after purification by column chromatography on silica gel eluting with pentane–EtOAc–DCM (8:2:1 to 6:3:1), 4-isobutyl-3-methyl-1H-indazole (108 mg, 57%) as a solid. R_f 0.25 [pentane:EtOAc:DCM (8:2:1)].

^{1}H-NMR (600 MHz, $CDCl_3$) δ 9.89 (1H, s), 7.26 (2H, d, *J* = 4.2 Hz), 6.85 (1H, t, *J* = 4.0 Hz), 2.87 (2H, d, *J* = 7.1 Hz), 2.73 (3H, s), 1.94 (1H, hept, *J* = 6.7 Hz), 0.98 (d, *J* = 6.5 Hz, 6H). **^{13}C-NMR (151 MHz, $CDCl_3$)**

δ 143.2, 142.2, 136.4, 126.8, 121.7, 121.6, 107.5, 42.4, 30.8, 22.6, 15.3. **HRMS** (ESI): Found MH^+ 189.1386, $C_{14}H_{19}N_2$ requires 189.1383.

6-cyclohexyl-3-methyl-1H-indazole (1o)

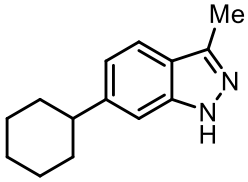

Following the general procedure for 16h, 6-bromo-3-methyl-1H-indazole (212 mg, 1 mmol) and CyhexMgBr (1.0 M in hexane, 2 mL, 2 mmol) gave, after purification by column chromatography on silica gel eluting with DCM–MeOH (99:1 to 97:3), 6-cyclohexyl-3-methyl-1H-indazole (40 mg, 18%) as a solid. R_f 0.40 [DCM:MeOH (98:2)].

^{1}H-NMR (600 MHz, $CDCl_3$) δ 10.40 (1H, s), 7.59 (1H, d, *J* = 8.4 Hz), 7.23 (1H, s), 7.04 (1H, d, *J* = 8.3 Hz), 2.70 – 2.57 (4H, m), 1.94 (2H, d, *J* = 11.9 Hz), 1.87 (2H, d, *J* = 11.1 Hz), 1.78 (1H, d, *J* = 13.4 Hz), 1.57 – 1.36 (4H, m), 1.34 – 1.19 (1H, m). **^{13}C-NMR (151 MHz, $CDCl_3$)** δ 147.5, 143.2, 141.9, 121.4, 120.7, 119.9, 106.9, 45.1, 34.8, 27.0, 26.3, 12.2. **HRMS** (ESI): Found MH^+ 215.1540, $C_{14}H_{19}N_2$ requires 215.1543.

7-benzyl-3-methyl-1H-indazole (1p)

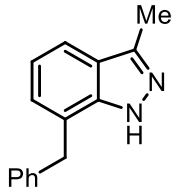

Following the general procedure for 16h, 7-bromo-3-methyl-1H-indazole (212 mg, 1 mmol) and BenzylMgCl (2.0 M in THF, 1.0 mL, 1 mmol) and gave, after purification by column chromatography on silica gel eluting with pentane–EtOAc–DCM (8:2:1 to 6:3:1), 7-benzyl-3-methyl-1H-indazole (73 mg, 33%) as a solid. R_f 0.30 [pentane:EtOAc:DCM (8:2:1)].

^{1}H-NMR (600 MHz, $CDCl_3$) δ 9.50 (1H, s), 7.59 (1H, d, *J* = 8.0 Hz), 7.32 (2H, t, *J* = 7.0 Hz), 7.28 – 7.24 (3H, m), 7.22 (1H, d, *J* = 7.0 Hz), 7.13 (1H, t, *J* = 7.5 Hz), 4.26 (2H, s), 2.58 (3H, s). **^{13}C-NMR (151 MHz, $CDCl_3$)** δ 143.9, 140.8, 139.0, 129.0, 128.8, 126.9, 126.9, 123.2, 122.8, 120.7, 118.7, 38.4, 12.2. **HRMS** (ESI): Found MH^+ 223.1224, $C_{15}H_{15}N_2$ requires 223.1229.

5.5.3 General Procedure for the Photopermutation of Indazoles (GP)

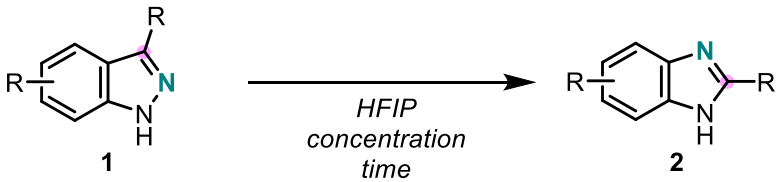

A microwave vial was charged with the 1H-indazole (1.0 equiv.) and the tube was capped with a Supelco aluminium crimp seal with septum (PTFE/butyl), evacuated and refilled with N_2 (×3). Then degassed HFIP was added, the lid sealed with parafilm, and the reaction mixture placed under 300

nm light. After the specified time, the reaction mixture was removed, a solution of 1,3-dinitrobenzene in $CDCl_3$ (1.0 equiv, 0.2 M) was added as an internal standard and the reaction analysed by ^{1}H-NMR.

Characterization data for the guideline products

Benzimidazoles with the same substituents in positions 4 and 7 are tautomers. Hence, the products characterisations below will indicate only for one of the tautomer. The same logic is applied for benzimidazoles with the same substituents in positions 5 and 6.

5- and 6- substituted benzimidazoles tautomers

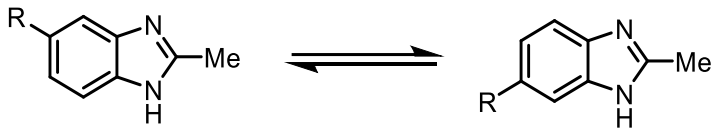

4- and 7- substituted benzimidazoles tautomers

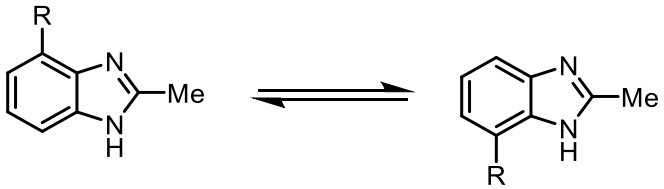

2,4-Dimethyl-1*H*-benzo[*d*]imidazole

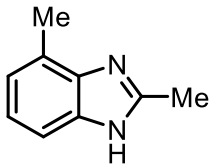

Following GP, 3,4-Dimethyl-1*H*-indazole (14.6 mg, 0.1 mmol) gave, after purification by column chromatography on silica gel eluting with EtOAc–MeOH (9:1), benzimidazole (12.6 mg, 86%) as a solid.

2,7-Dimethyl-1*H*-benzo[*d*]imidazole

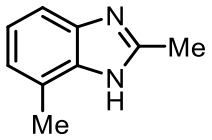

Following GP, 3,7-Dimethyl-1*H*-indazole (14.6 mg, 0.1 mmol) gave, after purification by column chromatography on silica gel eluting with EtOAc–MeOH (9:1), benzimidazole (8.8 mg, 60%) as a solid. R_f 0.47 [EtOAc:MeOH (9:1)];

^{1}H-NMR (400 MHz, $CDCl_3$) δ 7.35 (1H, d, *J* = 8.0 Hz), 7.12 (1H, t, *J* = 7.5 Hz), 7.02 (1H, d, *J* = 7.5 Hz), 2.62 (3H, s), 2.57 (3H, s); **^{13}C-NMR ($CDCl_3$, 151 MHz)** δ ^{13}C-NMR (101 MHz, $CDCl_3$) δ 150.7, 138.8, 137.8, 122.8, 122.3, 111.6, 17.2, 15.1; **HRMS** (EI): Found M^+ 146.0835, $C_9H_{10}N_2$ requires 146.0844. Data in accordance with literature.[26]

2,5-Dimethyl-1H-benzo[d]imidazole

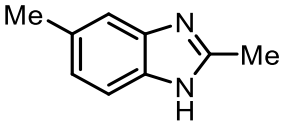

Following GP, 3,5-Dimethyl-1H-indazole (15 mg, 0.1 mmol) gave, after purification by column chromatography on silica gel eluting with pentane–EtOAc (8:2 to 0:1), benzimidazole (45%) as a solid.

2,6-Dimethyl-1H-benzo[d]imidazole

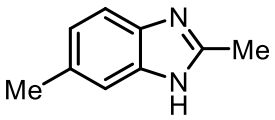

Following GP, 3,7-Dimethyl-1H-indazole (15 mg, 0.10 mmol) gave, after purification by column chromatography on silica gel, eluting with EtOAc–MeOH (1:0 to 19:1), benzimidazole (12 mg, 82%) as a solid. R_f 0.18 [EtOAc]; **^{1}H-NMR (600 MHz, $CDCl_3$)** δ 7.42 (d, *J* = 8.2 Hz, 1H), 7.31 (s, 1H), 7.04 (dd, *J* = 8.2, 1.6 Hz, 1H), 2.60 (s, 3H), 2.45 (s, 3H); **^{13}C-NMR (151 MHz, $CDCl_3$)** δ 150.7, 138.6, 137.3, 132.1, 123.8, 114.6, 114.1, 21.7, 15.2; **HRMS** (ESI): Found MH^+ 147.0913, $C_9H_{11}N_2$ requires 147.0917. Data in accordance with literature.[27]

2-Methyl-4-phenyl-1H-benzo[d]imidazole

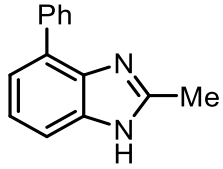

Following GP, 0.025 M, 24 h, 3-Methyl-4-phenyl-1H-indazole (21 mg, 0.10 mmol) gave, after purification by column chromatography on silica gel, eluting with pentane–EtOAc (1:1 to 0:1), benzimidazole (9 mg, 43%) as a solid. R_f 0.41 [EtOAc];

2-Methyl-6-phenyl-1*H*-benzo[*d*]imidazole

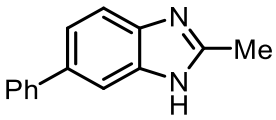

Following GP, 3-Methyl-6-phenyl-1H-indazole (20.8 mg, 0.1 mmol) gave, after purification by column chromatography on silica gel eluting with EtOAc– MeOH (8:2), benzimidazole (14.6 mg, 70%) as an oil.

^{1}HNMR (600 MHz, $CDCl_3$) δ 7.70 (d, *J* = 7.0 Hz, 2H), 7.56 (dd, *J* = 5.7, 3.4 Hz, 1H), 7.44 (t, *J* = 7.7 Hz, 2H), 7.34 (td, *J* = 7.2, 1.3 Hz, 1H), 7.31 – 7.28 (m, 2H), 2.55 (s, 3H); **^{13}CNMR (151 MHz, $CDCl_3$)** δ 151.3, 138.8, 132.2, 129.0, 128.8, 128.7, 128.5, 127.6, 122.7, 122.2, 115.3, 15.1; **HRMS** (EI): Found M^+ 208.0992, $C_{14}H_{12}N_2$ requires 208.0995.

5-chloro-2-methyl-1H-benzo[d]imidazole

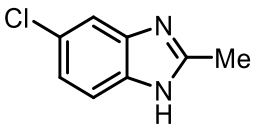

Following GP, 5-chloro-3-methyl-1H-indazole (17 mg, 0.10 mmol) gave, after purification by column chromatography on silica gel, eluting with EtOAc–MeOH (1:0 to 95:5), benzimidazole (10 mg, 59%) as a solid. R_f 0.10 [EtOAc];

6-Chloro-2-methyl-1*H*-benzo[*d*]imidazole

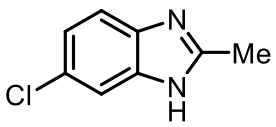

Following GP, 6-Chloro-3-methyl-1H-indazole (16.7 mg, 0.1 mmol) gave, after purification by column chromatography on silica gel eluting with EtOAc–MeOH (4:1), benzimidazole (13.7 mg, 82%) as a solid. R_f 0.34 [EtOAc:MeOH (4:1)];

^{1}H-NMR (600 MHz, $CDCl_3$) δ 7.51 (1H, s), 7.43 (1H, d, *J* = 8.5 Hz), 7.19 (1H, dd, *J* = 8.5, 1.9 Hz), 2.62 (3H, s); **^{13}C-NMR (151 MHz, $CDCl_3$)** δ 152.2, 137.2, 128.1, 123.0, 115.4, 114.7, 15.2; **HRMS** (EI): Found M^+ 166.0291, $C_8H_7ClN_2$ requires 166.0298. Data in accordance with literature.[28]

4-Chloro-2-methyl-1H-benzo[d]imidazole

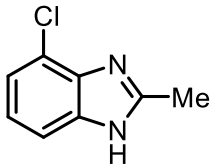

Following GP, 4-Chloro-3-methyl-1H-indazole (17 mg, 0.10 mmol) gave, after purification by column chromatography on silica gel, eluting with EtOAc–MeOH (1:0 to 98:2), benzimidazole (15 mg, 90%) as a solid. R_f 0.29 [EtOAc];

^{1}H-NMR ($CDCl_3$, 400 MHz) δ 7.43 (1H, dd, *J* = 7.9, 1.1 Hz), 7.23 (1H, dd, *J* = 7.8, 1.1 Hz), 7.14 (1H, t, *J* = 7.9 Hz), 2.66 (3H, s); **^{13}C-NMR (101 MHz, $CDCl_3$)** δ 152.1, 136.9, 123.1, 122.2, 120.0, 15.1; **HRMS** (ESI): Found MH^+ 167.0366, $C_8H_8N_2Cl$ requires 167.0371. Data in accordance with literature.[29]

7-Chloro-2-methyl-1H-benzo[d]imidazole

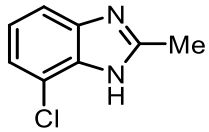

Following GP, 7-Chloro-3-methyl-1H-indazole (17 mg, 0.10 mmol) gave, after purification by column chromatography on silica gel, eluting with EtOAc–MeOH (1:0 to 9:1), benzimidazole (12 mg, 72%) as a solid.

5-Fluoro-2-methyl-1H-benzo[d]imidazole

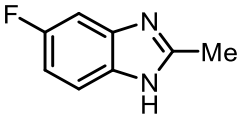

Following GP, 5-Fluoro-3-methyl-1H-indazole (15 mg, 0.1 mmol) gave, after purification by column chromatography on silica gel eluting with pentane–EtOAc (8:2 to 0:1), benzimidazole (57%) as a solid. R*f* 0.12 [pentane:EtOAc (1:9)];

^{1}H-NMR (600 MHz, $CDCl_3$) δ 7.44 (1H, dd, *J* = 8.8, 4.7 Hz), 7.21 (1H, d, *J* = 9.0 Hz), 6.97 (1H, td, *J* = 9.1, 2.4 Hz), 2.63 (3H, s); **^{13}C-NMR (151 MHz, $CDCl_3$)** δ 159.5 (d, *J* = 237.8 Hz), 152.4, 139.0, 135.2, 115.0, 110.5 (d, *J* = 25.4 Hz), 101.1, 15.2; **^{19}F-NMR (565 MHz, $CDCl_3$)** δ -120.66; **HRMS** (ESI): Found MH^+ 151.0662, $C_8H_8N_2F$ requires 151.0666; Data in accordance with literature.[30]

4-Fluoro-2-methyl-1H-benzo[d]imidazole

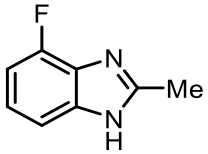

Following GP, 4-Fluoro-3-methyl-1H-indazole (15 mg, 0.1 mmol) gave, after purification by column chromatography on silica gel eluting with pentane–EtOAc (8:2 to 0:1), benzimidazole (81%) as a solid.

7-Fluoro-2-methyl-1*H*-benzo[*d*]imidazole

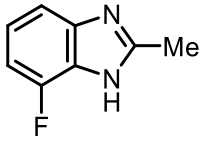

Following GP, 7-Fluoro-3-methyl-1H-indazole (13.2 mg, 0.1 mmol) gave, after purification by column chromatography on silica gel eluting with EtOAc–MeOH (4:1), benzimidazole (6.3 mg, 42%) as a solid. R_f 0.48 [EtOAc:MeOH (4:1)];

^{1}H-NMR (600 MHz, DMSO-d_6, major isomer) δ 12.47 (1H, s), 7.23 (1H, d, *J* = 7.1 Hz), 7.11 – 7.05 (1H, m), 6.92 – 6.85 (1H, m), 2.49 (3H, s); **^{1}H-NMR (600 MHz, DMSO-d_6, minor isomer)** δ 12.70 (1H, s), 7.34 (1H, d, *J* = 7.1 Hz), 7.11 – 7.05 (1H, m), 6.99 – 6.92 (1H, m), 2.49 (3H, s); **^{13}C-NMR (DMSO-d_6, 151 MHz)** δ 152.5 (*J* = 248.1 Hz), 151.9, 137.6 (*J* = 9.8 Hz), 131.6 (*J* = 16.7 Hz), 121.8 (*J* = 7.3 Hz), 107.1 (*J* = 3.5 Hz), 106.2 (*J* = 17.7 Hz), 14.5; **^{19}F-NMR (565 MHz, DMSO-d_6)** δ -129.69. **HRMS** (EI): Found M^+ 150.0584, $C_8H_7FN_2$ requires 150.0593. Data in accordance with literature.[31]

6-Fluoro-2-methyl-1*H*-benzo[*d*]imidazole

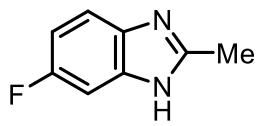

Following GP, 6-Fluoro-3-methyl-1H-indazole (15 mg, 0.1 mmol) gave, after purification by column chromatography on silica gel eluting with EtOAc–MeOH (4:1), benzimidazole (6.8 mg, 45%) as an oil.

<u>Characterization data for scope substrates</u>

2-Methyl-*1H*-benzo[*d*]imidazole (2a)

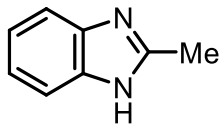

Following GP, 3-Methyl-1H-indazole (13.2 mg, 0.1 mmol) gave, after purification by column chromatography on silica gel eluting with EtOAc–MeOH (4:1), benzimidazole (11.4 mg, 86%) as a solid. R_f 0.38 [EtOAc:MeOH (4:1)];

^{1}H-NMR (400 MHz, $CDCl_3$) δ 7.55 (2H, dd, *J* = 6.0, 3.2 Hz), 7.25 – 7.19 (2H, m), 2.65 (3H, s); **^{13}C-NMR (101 MHz, $CDCl_3$)** δ 151.3, 138.8, 122.3, 114.7, 15.1; **HRMS** (ESI): Found MH^+ 133.0761, $C_8H_9N_2$ requires 133.0760. Data in accordance with literature.[32]

1*H*-Benzo[d]imidazole (2b)

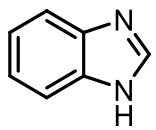

Following GP, 1H-indazole (11.8 mg, 0.1 mmol) gave, after purification by column chromatography on silica gel eluting with EtOAc–MeOH (4:1), benzimidazole (3.3 mg, 28%) as a solid. R_f 0.45 [EtOAc:MeOH (4:1)];

^{1}H-NMR (400 MHz, DMSO-d_6) δ 12.45 (1H, s), 8.21 (1H, s), 7.59 (2H, dd, *J* = 6.0, 3.3 Hz), 7.21–7.16 (2H, m); **^{13}C-NMR (101 MHz, DMSO-d_6)** δ 141.9, 138.0, 121.7, 115.3; **GC-MS** m/z (EI): 118.10 (M^+), 63.15. Data in accordance with literature.[33]

2-Isopropyl-1*H*-benzo[d]imidazole (2g)

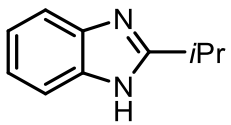

Following GP, 3-Isopropyl-1H-indazole (16, 0.10 mmol) gave, after purification by column chromatography on silica gel, eluting with pentane–EtOAc (4:2 to 1:1), benzimidazole (15 mg, 94%) as a solid. R_f 0.30 [cyclohexane:EtOAc (1:1)];

^{1}H-NMR ($CDCl_3$, 600 MHz) δ 7.49 (2H, dd, *J* = 6.0, 3.1 Hz), 7.15 (2H, dd, *J* = 6.0, 3.1 Hz), 3.19 (1H, hept, *J* = 7.0 Hz), 1.40 (6H, d, *J* = 7.0 Hz); **^{13}C-NMR (151 MHz, $CDCl_3$)** δ 159.7, 122.4, 29.1, 21.6; **HRMS** (EI): Found M^+ 160.0999, $C_{10}H_{12}N_2$ requires 160.0995. Data in accordance with literature.[34]

2-Pentyl-1*H*-benzo[d]imidazole (2h)

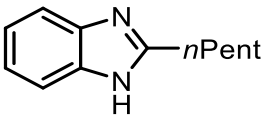

Following GP, 3-Pentyl-1H-indazole (19 mg, 0.10 mmol) gave, after purification by column chromatography on silica gel, eluting with pentane–EtOAc (4:1 to 1:1), benzimidazole (19 mg, quant.) as a solid. R_f 0.37 [pentane:EtOAc (1:1)];

^{1}H-NMR ($CDCl_3$, 600 MHz) δ 7.55 (2H, dd, *J* = 5.8, 3.1 Hz), 7.21 (2H, dd, *J* = 5.8, 3.1 Hz), 2.94 (2H, t, *J* = 7.7 Hz), 1.86 (2H, p, *J* = 7.7 Hz), 1.38 – 1.22 (4H, m), 0.83 (3H, t, *J* = 7.2 Hz); **^{13}C-NMR (151 MHz, $CDCl_3$)** δ 155.6, 138.6, 122.2, 114.7, 31.6, 29.5, 28.2, 22.5, 14.0; **HRMS** (ESI): Found MH^+ 189.1384, $C_{12}H_{17}N_2$ requires 189.1386. Data in accordance with literature.[34]

2-(But-3-en-1-yl)-1*H*-benzo[d]imidazole (2i)

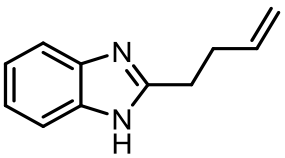

Following GP, 3-(But-3-en-1-yl)-1H-indazole (17 mg, 0.10 mmol) gave, after purification by column chromatography on silica gel, eluting with pentane–EtOAc (4:1 to 1:1), benzimidazole (13 mg, 76%) as a solid. R_f 0.34 [pentane:EtOAc (1:1)];

^{1}H-NMR (600 MHz, $CDCl_3$) δ 7.55 (2H, s), 7.22 (2H, dd, *J* = 6.0, 3.2 Hz), 5.92 (1H, ddt, *J* = 17.1, 10.3, 6.6 Hz), 5.13 (1H, dd, *J* = 17.1, 1.4 Hz), 5.07 (1H, dd, *J* = 10.3, 1.4 Hz), 3.04 (2H, t, *J* = 7.5 Hz), 2.63 (2H, q, *J* = 7.4 Hz). **^{13}C-NMR (151 MHz, $CDCl_3$)** δ 154.4, 137.0, 122.4, 116.4, 32.1, 28.8. **HRMS** (ESI): Found MH^+ 173.1070, $C_{11}H_{13}N_2$ requires 173.1073. Data in accordance with literature.[35]

(1*H*-Benzo[*d*]imidazol-2-yl)methanol (2k)

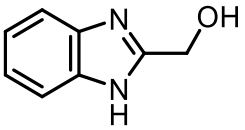

Following GP, (1H-indazole-2-yl)methanol (14.8 mg, 0.1 mmol) gave, after purification by column chromatography on silica gel eluting with EtOAc–MeOH (4:1), benzimidazole (11 mg, 74%) as a solid. R_f 0.31 [EtOAc:MeOH (4:1)];

^{1}H-NMR (600 MHz, CD_3OD) δ 7.54 – 7.50 (2H, m), 7.21 – 7.18 (2H, m), 4.83 (2H, s); **^{13}C-NMR (151 MHz, CD_3OD)** δ 156.2, 139.3, 123.3 (2C), 115.6 (2C), 58.9; **HRMS** (EI): Found M^+ 148.0631, $C_8H_8N_2O$ requires 148.0637. Data in accordance with literature.[36]

Methyl 2-(1*H*-benzo[d]imidazol-2-yl)acetate (2l)

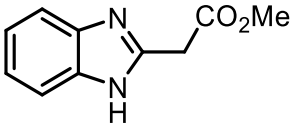

Following GP, Methyl 3-(1*H*-indazol-2-yl)acetate (19 mg, 0.10 mmol) gave, after purification by column chromatography on silica gel, eluting with pentane–EtOAc (1:1 to 0:1), benzimidazole (16 mg, 84%) as an oil. R_f 0.38 [EtOAc];

^{1}H-NMR ($CDCl_3$, 400 MHz) δ 7.58 (2H, br s), 7.26 – 7.23 (2H, m), 4.09 (2H, s), 3.79 (3H, s); **^{13}CNMR (101 MHz, $CDCl_3$)** δ 170.4, 146.9, 122.8, 52.8, 34.5; **HRMS** (ESI): Found MH^+ 191.0810, $C_{11}H_{13}O_2N_2$ requires 191.0815. Data in accordance with literature.[37]

4-isobutyl-2-methyl-1H-benzo[d]imidazole (2m)

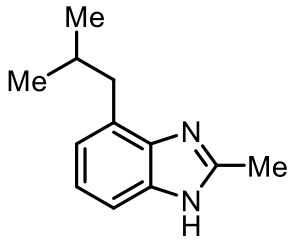

Following GP, 4-isobutyl-3-methyl-1H-indazole (17 mg, 0.1 mmol) gave, after purification by column chromatography on silica gel eluting with pentane–EtOAc (8:2 to EtOAc), benzimidazole (58%) as a solid. R_f 0.12 [pentane:EtOAc (1:9)];

^{1}H-NMR (600 MHz, $CDCl_3$) δ 7.39 (1H, d, *J* = 8.0 Hz), 7.14 (1H, t, *J* = 7.6 Hz), 7.00 (1H, d, *J* = 7.3 Hz), 2.77 (2H, d, *J* = 7.3 Hz), 2.61 (3H, s), 2.08 (1H, hept, *J* = 6.8 Hz), 0.87 (6H, d, *J* = 6.2 Hz). **^{13}C-NMR (151 MHz, $CDCl_3$)** δ 150.7, 138.9, 137.8, 128.3, 122.9, 122.1, 112.4, 41.1, 29.3, 22.7, 15.0. **HRMS** (ESI): Found MH^+ 189.1387, $C_{12}H_{17}N_2$ requires 189.1386.

5-isopropyl-2-methyl-1H-benzo[d]imidazole (2n)

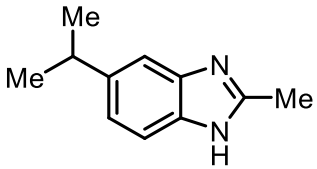

Following GP, 5-isopropyl-2-methyl-1H-indazole (15 mg, 0.1 mmol) gave, after purification by column chromatography on silica gel eluting with pentane–EtOAc (8:2 to EtOAc), benzimidazole (56%) as a solid. R_f 0.16 [pentane:EtOAc (1:9)];

^{1}H-NMR (600 MHz, $CDCl_3$) δ 7.45 (1H, d, *J* = 8.2 Hz), 7.37 (1H, s), 7.11 (1H, dd, *J* = 8.3, 1.7 Hz), 3.02 (1H, hept, *J* = 6.7 Hz), 2.61 (3H, s), 1.29 (6H, d, *J* = 6.9 Hz). **^{13}C-NMR (151 MHz, $CDCl_3$)** δ 150.7, 143.7, 131.0, 129.6, 129.0, 121.5, 114.6, 34.4, 24.7, 15.2. **HRMS** (ESI): Found MH^+ 175.1233, $C_{11}H_{15}N_2$ requires 175.1240.

6-cyclohexyl-2-methyl-1H-benzo[d]imidazole (2o)

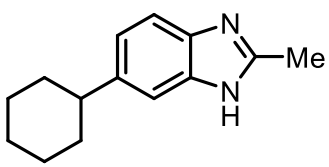

Following GP, 6-cyclohexyl-3-methyl-1H-indazole (21 mg, 0.1 mmol) gave, after purification by column chromatography on silica gel eluting with pentane–EtOAc (8:2 to EtOAc), benzimidazole (75%) as a solid. R*f* 0.12 [pentane:EtOAc (1:9)];

^{1}H-NMR (600 MHz, $CDCl_3$) δ 7.45 (1H, d, *J* = 8.2 Hz), 7.36 (1H, s), 7.09 (1H, d, *J* = 8.2 Hz), 2.64 – 2.56 (4H, m), 1.91 (2H, d, *J* = 12.0 Hz), 1.84 (2H, d, *J* = 12.1 Hz), 1.75 (1H, d, *J* = 13.3 Hz), 1.51 – 1.35 (4H, m), 1.28 – 1.23 (1H, m). **^{13}C-NMR (151 MHz, $CDCl_3$)** δ 151.0, 143.0, 142.9, 122.0 121.8, 114.4, 111.9, 44.9, 35.2, 27.2, 26.3, 15.0. **HRMS** (ESI): Found MH^+ 215.1547, $C_{14}H_{19}N_2$ requires 215.1557.

7-benzyl-2-methyl-1H-benzo[d]imidazole (2p)

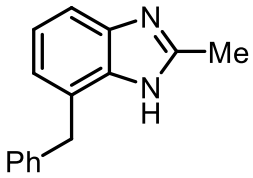

Following GP, 7-benzyl-3-methyl-1H-indazole (22 mg, 0.1 mmol) gave, after purification by column chromatography on silica gel eluting with pentane–EtOAc (8:2 to EtOAc), benzimidazole (49%) as a solid. R*f* 0.12 [pentane:EtOAc (1:9)];

^{1}H-NMR (600 MHz, $CDCl_3$) δ 7.41 (1H, d, *J* = 8.0 Hz), 7.24 – 7.22 (2H, m), 7.19 – 7.14 (4H, m), 6.99 (1H, d, *J* = 7.3 Hz), 4.29 (2H, s), 2.46 (3H, s). **^{13}C-NMR (151 MHz, $CDCl_3$)** δ 151.0, 140.1, 139.0, 137.5, 128.8, 128.5, 127.1, 126.2, 122.8, 122.3, 113.0, 37.5, 14.8. **HRMS** (ESI): Found MH^+ 223.1224, $C_{15}H_{15}N_2$ requires 223.1230.

5.6 References Chapter 5

(1) Brown, N. Bioisosterism in Medicinal Chemistry. In *Bioisosteres in Medicinal Chemistry*; John Wiley & Sons, Ltd, **2012**; pp 1–14. https://doi.org/10.1002/9783527654307.ch1.

(2) Hoffmann, N. Photochemical Reactions of Aromatic Compounds and the Concept of the Photon as a Traceless Reagent. *Photochem. Photobiol. Sci.* **2012**, *11* (11), 1613–1641. https://doi.org/10.1039/C2PP25074H.

(3) Shearer, J.; Castro, J. L.; Lawson, A. D. G.; MacCoss, M.; Taylor, R. D. Rings in Clinical Trials and Drugs: Present and Future. *J. Med. Chem.* **2022**, *65* (13), 8699–8712. https://doi.org/10.1021/acs.jmedchem.2c00473.

(4) Roughley, S. D.; Jordan, A. M. The Medicinal Chemist's Toolbox: An Analysis of Reactions Used in the Pursuit of Drug Candidates. *J. Med. Chem.* **2011**, *54* (10), 3451–3479. https://doi.org/10.1021/jm200187y.

(5) Brown, D. G.; Boström, J. Analysis of Past and Present Synthetic Methodologies on Medicinal Chemistry: Where Have All the New Reactions Gone? *J. Med. Chem.* **2016**, *59* (10), 4443–4458. https://doi.org/10.1021/acs.jmedchem.5b01409.

(6) Wu, G.; Zhao, T.; Kang, D.; Zhang, J.; Song, Y.; Namasivayam, V.; Kongsted, J.; Pannecouque, C.; De Clercq, E.; Poongavanam, V.; Liu, X.; Zhan, P. Overview of Recent Strategic Advances in Medicinal Chemistry. *J. Med. Chem.* **2019**, *62* (21), 9375–9414. https://doi.org/10.1021/acs.jmedchem.9b00359.

(7) Alaqeel, S. I. Synthetic Approaches to Benzimidazoles from *o*-Phenylenediamine: A Literature Review. *Journal of Saudi Chemical Society* **2017**, *21* (2), 229–237. https://doi.org/10.1016/j.jscs.2016.08.001.

(8) Faheem, Mohd.; Rathaur, A.; Pandey, A.; Kumar Singh, V.; Tiwari, A. K. A Review on the Modern Synthetic Approach of Benzimidazole Candidate. *ChemistrySelect* **2020**, *5* (13), 3981–3994. https://doi.org/10.1002/slct.201904832.

(9) Mishra, B. B.; Kachhadia, N. S.; Tomar, V. S.; Lahiri, S. An improved process for the preparation of bendamustine hydrochloride, *Patent WO2013046223A1*, November 16, **2016**.

(10) Tahlan, S.; Kumar, S.; Narasimhan, B. Antimicrobial Potential of 1H-Benzo[d]Imidazole Scaffold: A Review. *BMC Chemistry* **2019**, *13* (1), 18. https://doi.org/10.1186/s13065-019-0521-y.

(11) Kerru, N.; Gummidi, L.; Maddila, S.; Gangu, K. K.; Jonnalagadda, S. B. A Review on Recent Advances in Nitrogen-Containing Molecules and Their Biological Applications. *Molecules* **2020**, *25* (8), 1909. https://doi.org/10.3390/molecules25081909.

(12) Albini, A.; Fagnoni, M. Green Chemistry and Photochemistry Were Born at the Same Time. *Green Chem.* **2004**, *6* (1), 1–6. https://doi.org/10.1039/B309592D.

(13) Lefebvre, C.; Fortier, L.; Hoffmann, N. Photochemical Rearrangements in Heterocyclic Chemistry. *European Journal of Organic Chemistry* **2020**, *2020* (10), 1393–1404. https://doi.org/10.1002/ejoc.201901190.

(14) Rettig, W.; Wirz, J. Photolysis and Pyrolysis of *N* -Methyl Isoindole. *Helvetica Chimica Acta* **1978**, *61* (1), 444–448. https://doi.org/10.1002/hlca.19780610139.

(15) Ohkuma, T.; Arai, N. Construction of Unique Heterocyclic Frameworks by Photochemical Reaction of 5- and 6-Membered Heteroaromatics. *HETEROCYCLES* **2018**, *96* (6), 997. https://doi.org/10.3987/rev-18-880.

(16) Su, M.-D. A Theoretical Insight into the Reaction Mechanism of Photochemical Transposition from Pyrazole to Imidazole. *J. Phys. Chem. A* **2008**, *112* (41), 10420–10428. https://doi.org/10.1021/jp805394k.

(17) Padwa, A. Photochemical Rearrangements of Five-Membered Ring Heterocycles. In *Organic Chemistry: A Series of Monographs*; Elsevier, 1980; Vol. 42, pp 501–547. https://doi.org/10.1016/B978-0-12-481303-8.50015-9.

(18) Tiefenthaler, H.; Dörscheln, W.; Göth, H.; Schmid, H. Photoisomerisation Von Indazolen zu Benzimidazolen. *Tetrahedron Letters* **1964**, *40*, 2999-3001.

(19) Tiefenthaler, H.; Dörscheln, W.; Göth, H.; Schmid, H. Photoisomerisierung von Pyrazolen und Indazolen zu Imidazolen bzw. Benzimidazolen und 2-Amino-benzonitrilen. *Helvetica Chimica Acta* **1967**, *50* (8), 2244–2258. https://doi.org/10.1002/hlca.19670500810.

(20) Beak, P.; Messer, W. Photorearrangements of Some N-Methyl Diazoles. *Tetrahedron* **1969**, *25* (16), 3287–3295. https://doi.org/10.1016/S0040-4020(01)82860-X.

(21) Pavlik, J. W.; Connors, R. E.; Burns, D. S.; Kurzweil, E. M. Phototransposition Chemistry of 1-Phenylpyrazole. Experimental and Computational Studies. *J. Am. Chem. Soc.* **1993**, *115* (17), 7645–7652. https://doi.org/10.1021/ja00070a008.

(22) Pavlik, J. W.; Na Ayudhaya, T. I.; Pandit, C. R.; Tantayanon, S. Photochemistry of Trifluromethyl Substituted 1-Methylpyrazoles. *Journal of Heterocyclic Chemistry* **2004**, *41* (1), 61–67. https://doi.org/10.1002/jhet.5570410110.

(23) Pavlik, J. W.; Kurzweil, E. M. Phototransposition Chemistry of 1-Methylpyrazole. Deuterium, Methyl, and Fluorine Substitution. *J. Org. Chem.* **1991**, *56* (22), 6313–6320. https://doi.org/10.1021/jo00022a019.

(24) Ueberschaar, N.; Xu, Z.; Scherlach, K.; Metsä-Ketelä, M.; Bretschneider, T.; Dahse, H.-M.; Görls, H.; Hertweck, C. Synthetic Remodeling of the Chartreusin Pathway to Tune Antiproliferative and Antibacterial Activities. *J. Am. Chem. Soc.* **2013**, *135* (46), 17408–17416. https://doi.org/10.1021/ja4080024.

(25) Shu, C.; Sidhu, K.; Zhang, L.; Wang, X.; Krishnamurthy, D.; Senanayake, C. H. Palladium-Catalyzed Cross-Coupling of Cyclopropylmagnesium Bromide with Aryl Bromides Mediated by Zinc Halide Additives. *J. Org. Chem.* **2010**, *75* (19), 6677–6680. https://doi.org/10.1021/jo100983c.

(26) Kato, J.; Ito, Y.; Ijuin, R.; Aoyama, H.; Yokomatsu, T. Novel Strategy for Synthesis of Substituted Benzimidazo[1,2-a]Quinolines. *Org. Lett.* **2013**, *15* (14), 3794–3797. https://doi.org/10.1021/ol4017723.

(27) Felkin, H.; Fillebeen-Khan, T.; Gault, Y.; Holmes-Smith, R.; Zakrzewski, J. Activation of C-H Bonds in Saturated Hydrocarbons. The Catalytic Functionalisation of Cycloöctane by Means of Some Soluble Iridium and Ruthenium Polyhydride Systems. *Tetrahedron Letters* **1984**, *25* (12), 1279–1282. https://doi.org/10.1016/S0040-4039(01)80134-9.

(28) Fosu, S. C.; Hambira, C. M.; Chen, A. D.; Fuchs, J. R.; Nagib, D. A. Site-Selective C–H Functionalization of (Hetero)Arenes via Transient, Non-Symmetric Iodanes. *Chem* **2019**, *5* (2), 417–428. https://doi.org/10.1016/j.chempr.2018.11.007.

(29) Larsen, M. A.; Hartwig, J. F. Iridium-Catalyzed C–H Borylation of Heteroarenes: Scope, Regioselectivity, Application to Late-Stage Functionalization, and Mechanism. *J. Am. Chem. Soc.* **2014**, *136* (11), 4287–4299. https://doi.org/10.1021/ja412563e.

(30) Kim, J.; Kim, J.; Lee, H.; Lee, B. M.; Kim, B. H. Indium-Mediated One-Pot Benzimidazole Synthesis from 2-Nitroanilines or 1,2-Dinitroarenes with *Ortho*Esters. *Tetrahedron* **2011**, *67* (41), 8027–8033. https://doi.org/10.1016/j.tet.2011.08.017.

(31) Bonku, E. M.; Qin, H.; Odilov, A.; Abduahadi, S.; Guma, S. D.; Yang, F.; Zhu, F.; Aisa, H. A.; Shen, J. Improved and Ligand-Free Copper-Catalyzed Cyclization for an Efficient Synthesis of Benzimidazoles from o-Bromoarylamine and Nitriles. *RSC Adv.* **2024**, *14* (10), 6906–6916. https://doi.org/10.1039/D4RA00245H.

(32) Yu, B.; Zhang, H.; Zhao, Y.; Chen, S.; Xu, J.; Huang, C.; Liu, Z. Cyclization of O-Phenylenediamines by CO2 in the Presence of H2 for the Synthesis of Benzimidazoles. *Green Chem.* **2012**, *15* (1), 95–99. https://doi.org/10.1039/C2GC36517K.

(33) Shaik, B. B.; Mohite, S. B.; Partap, S.; Kumar, V.; Vangara, S.; Bala, M. D.; Singh, P.; Karpoormath, R. One-Pot Synthesis of 1,3-Diazaheterocycles via Hydroxylamine Hydrochloride Activation of Anthranilamide/Phenylenediamines and DMF Derivatives. *Tetrahedron* **2024**, *154*, 133866-. https://doi.org/10.1016/j.tet.2024.133866.

(34) Kumari, S.; Joshi, A.; Borthakur, I.; Kundu, S. Activation of Ethanol via Conjunction of a Photocatalyst and a HAT Reagent for the Synthesis of Benzimidazoles. *J. Org. Chem.* **2023**, *88* (16), 11523–11533. https://doi.org/10.1021/acs.joc.3c00674.

(35) Kljajic, M.; Puschnig, J. G.; Weber, H.; Breinbauer, R. Additive-Free Pd-Catalyzed α-Allylation of Imine-Containing Heterocycles. *Org. Lett.* **2017**, *19* (1), 126–129. https://doi.org/10.1021/acs.orglett.6b03407.

(36) Lorentz-Petersen, L. L. R.; Nordstrøm, L. U.; Madsen, R. Iridium-Catalyzed Condensation of Amines and Vicinal Diols to Substituted Piperazines. *European Journal of Organic Chemistry* **2012**, *2012* (34), 6752–6759. https://doi.org/10.1002/ejoc.201201099.

(37) Perrone, S.; Capua, M.; Cannazza, G.; Salomone, A.; Troisi, L. Synthesis of β-Enamino Acid and Heteroaryl Acetic Acid Derivatives by Pd-Catalyzed Carbonylation of α-Chloroimines and 2-Chloromethyl Aza-Heterocycles. *Tetrahedron Letters* **2016**, *57* (13), 1421–1424. https://doi.org/10.1016/j.tetlet.2016.02.035.